DRUG DESIGN AND SYNTHESIS OF COX-2 SELECTIVE INHIBITORS AS POTENTIAL NSAIDs

ABEER ABDULHADI ABDULQADER

FACULTY OF SCIENCE
UNIVERSITY OF MALAYA
KUALA LUMPUR

2016

DRUG DESIGN AND SYNTHESIS OF COX-2 SELECTIVE INHIBITORS AS POTENTIAL NSAIDs

ABEER ABDULHADI ABDULQADER

THESIS SUBMITTED IN FULFILMENT OF THE REQUIREMENTS FOR THE DEGREE OF DOCTOR OF PHILOSOPHY

FACULTY OF SCIENCE
UNIVERSITY OF MALAYA
KUALA LUMPUR

2016

UNIVERSITY OF MALAYA
ORIGINAL LITERARY WORK DECLARATION

Name of Candidate: ABEER ABDULHADI ABDULQADER

(I.C/Passport No:

Registration/Matric No: SHC120031

Name of Degree: Ph. D.

Title of Project Paper/Research Report/Dissertation/Thesis ("this Work"):

DRUG DESIGN AND SYNTHESIS OF COX-2 SELECTIVE INHIBITORS AS POTENTIAL NSAIDs

Field of Study: DRUG DESIGN AND SYNTHESIS

I do solemnly and sincerely declare that:

(1) I am the sole author/writer of this Work;
(2) This Work is original;
(3) Any use of any work in which copyright exists was done by way of fair dealing and for permitted purposes and any excerpt or extract from, or reference to or reproduction of any copyright work has been disclosed expressly and sufficiently and the title of the Work and its authorship have been acknowledged in this Work;
(4) I do not have any actual knowledge nor do I ought reasonably to know that the making of this work constitutes an infringement of any copyright work;
(5) I hereby assign all and every rights in the copyright to this Work to the University of Malaya ("UM"), who henceforth shall be owner of the copyright in this Work and that any reproduction or use in any form or by any means whatsoever is prohibited without the written consent of UM having been first had and obtained;
(6) I am fully aware that if in the course of making this Work I have infringed any copyright whether intentionally or otherwise, I may be subject to legal action or any other action as may be determined by UM.

Candidate's Signature   Date:

Subscribed and solemnly declared before,

Witness's Signature   Date:

Name:

Designation:

ABSTRACT

Cyclooxygenase (COX) is a key enzyme in the biosynthetic pathway leading to the formation of prostaglandins, which are mediators of inflammation. It exists mainly in two isoforms, COX-1 and COX-2. The conventional nonsteroidal anti-inflammatory drugs (NSAIDs) have gastrointestinal side effects because they inhibit both isoforms. Recent studies show that the inhibition of cyclooxygenase-2 can delay or prevent certain forms of cancer. Agents that inhibit COX-2 while sparing COX-1 represent a new attractive therapeutic development and offer a new perspective for a further use of COX-2 inhibitors. The present study extends the evaluation of COX activity to a series of 1,3,4-oxadiazoline derivatives (**3a-h**) following a rational approach consisting molecular modeling, synthesis, and biological tests. Based on data obtained from molecular modeling, a set of compounds with better profiles of affinity have been synthesized and tested for COX-2 inhibition *in vitro*. All compounds (**3a-h**) showed reasonable inhibitory profiles against COX-2 but not COX-1, indicating that they are selective inhibitors for COX-2. Moreover, the study showed that compound **3h** to be the best selective COX-2 inhibitor among the tested compounds with selectivity index in the range of 175, while compounds **3a, 3b, 3c** and **3d** showed moderate selectivity. Our results suggested that these novel compounds may have potential as structural templates for the design and subsequent development of the new selective COX-2 inhibitor drugs. The unique chemical structure of the compounds and their effect on COX enzyme binding and activity as well as their potency and selectivity, may prove useful in treating pain and inflammation.

ABSTRAK

Cyclooxygenase (COX) merupakan enzim yang penting di dalam laluan biosintesis pembentukkan lipid prostaglandin dimana ia adalah perantara kepada penyebab keradangan. Keseluruhannya, ia wujud dalam dua bentuk dari satu protein iaitu COX-1 dan COX-2. Ubat anti-radang bebas steroid yang lazim didapati menunjukkan kesan sampingan terhadap sistem pencernaan kerana merencat kedua-dua bentuk protein tersebut. Hasil penyelidikan terbaru menunjukkan bahawa perencetan enzim cyclooxygenase-2 ini mampu melengahkan atau menghalang beberapa jenis bentuk kanser. Agen-agen yang mampu merencat enzim COX-2 dan dalam masa yang sama tidak merencat enzim COX-1 telah menarik perhatian di dalam kaedah pembangunan rawatan dan seterusnya membuka perspektif baru dalam usaha penggunaan agen-agen ini sebagai agen perencat COX-2. Kajian ini bertujuan untuk mendalami penilaian tahap keaktifan enzim COX-2 terhadap satu siri terbitan 1,3,4-oksadiazolina melalui kaedah-kaedah permodelar molecular, sintesis dan juga ujian biologi. Berdasarkan data yang telah diperolehi dari permodelan molecular, satu set sebatian dengan profil afiniti yang lebih baik telah disintesis dan diuji sebagai agen perencat terpilih COX-2 secara "*in vitro*". Kesemua sebatian (**3a-h**) telah menunjukkan profil rencatan yang menyakinkan terhadap COX-2 tapi tidak terhadap COX-1. Ini menunjukkan bahawa terbitan-terbitan ini mampu menjadi agen perencat terpilih untuk COX-2. Hasil kajian juga menunjukkan sebatian **3h** sebagai agen perencat terpilih COX-2 yang terbaik dengan julat indeks terpilih sebanyak 175. Manakala sebatian-sebatian **3a**, **3b**, **3c** dan **3d** hanya menunjukkan julat indeks terpilih yang sederhana. Keputusan ini mencadangkan bahawa terbitan sebatian novel ini berpotensi untuk dijadikan sebagai templat dalam usaha pembangunan agen perencat terpilih COX-2. Struktur kimia yang unik, kesan aktiviti, ikatan, kebolehupayaan dan pemilihan sebatian ini terhadap enzim COX mampu menjadi alat yang berguna dalam usaha merawat kesakitan dan keradangan.

ACKNOWLEDGEMENTS

milestone. There is no substitute for the love and affection bestowed on me by him which gave me a sense of relief after hours of tedious work during my research.

My final, and most heartfelt, acknowledgment must go to, my children, Eatiman, Abdulhadi, Teamar, Afnan, and my sister Dr. Farkaad Abdulhadi. They have worked diligently, and successfully. Their support, encouragement, and companionship have turned my journey through graduate school into a pleasure. For all that, and for being everything I am not, they have my everlasting love

TABLE OF CONTENTS

LIST OF FIGURES

LIST OF TABLES

LIST OF SCHEMES

LIST OF SYMBOLS AND ABBREVIATIONS

ΔG_{dock} : Estimated mean free energy of binding

1D : One dimensional

^1H : Proton

2D-QSAR : 2-Dimensional quantitative structure-activity relationships

3D : Three dimensional

Å : Angstrom

AD4 : AutoDock

ADMET : Absorption, distribution, metabolism, excretion & toxicity

ALogP98 : Atom-type partition coefficient

Arg : Arginine

BBB : Blood brain barrier

COX : Cyclooxygenase enzyme

CYPs : Cytochromes P450

dH_2O : Distilled water

DMSO : Dimethylsulfoxide

DNA : Deoxyribonucleic acid

DuP-697 : 5-Bromo-2-[4-fluorophenyl]-3-[4-(methylsulfonyl)phenyl]thiophene

EGF : Epidermal growth factor

ER : Endoplasmic reticulum

FDA : Food and drug administration

GA : Genetic algorithm

Gln : Glutamine

H_1 : Histamine antagonists

HCl : Hydrochloric acid

HIA	:	Human intestinal absorption
His	:	Histidine
HREIMS	:	High resolution electron ionization mass spectral
IC_{50}	:	Half maximal inhibitory concentration
Ile	:	Isoleucine
kDa	:	Kilodaltons
$K_{i\,dock}$	:	Estimated inhibition constant
Leu	:	Leucine
LGA	:	Lamarkian genetic algorithm
Log P	:	Octanol/water partition coefficient
LS	:	Local search
LT5	:	Leukotrienes
LT5	:	leukotrienes
MBD	:	Membrane binding domain
Mw	:	Molecular weight
NMR	:	Nucler magnetic resonance
NS-398	:	N-[2-(Cyclohexyloxy)-4-nitrophenyl]methanesulfonamide
NSAIDs	:	Non-steroidal anti-inflammatory drugs
NumCl	:	Number in cluster
ORTEP	:	Oak ridge thermal ellipsoid plot program
PAF	:	Platelet-activating factor
PDB	:	Protein data bank
PES	:	Prostaglandin endoperoxide synthetase
PGE2	:	Prostaglandin E2
PGG_2	:	Hydroperoxy endoperoxide prostaglandin G_2
PGH_2	:	Prostaglandin H_2

PGI2	:	Prostacyclin
PGs	:	Prostaglandins
Phe	:	Phenylalanine
PHS	:	Prostaglandin synthase
PKKB	:	Pharmaco kinetics knowledge base
PSA 2D	:	2D Polar surface area
PTGS	:	Prostaglandin-endoperoxide synthase
RMSD	:	Root mean square deviation
RO5	:	Rule of Five
SAR	:	Structure-activity relationships
SC-558	:	4-[5-(4-bromophenyl)-3-(trifluoromethyl)-1h-pyrazolyl]benzene sulfonamide
Ser	:	Serine
TLC	:	Thin layer chromatography
TXB2	:	Thromboxane B2
Tyr	:	Tyrosine
Val	:	Valine

LIST OF APPENDICES

CHAPTER 1: INTRODUCTION

1.1   Background

Inflammation is an immune system's response to infection or injury. It has been concerned in the pathogeneses of arthritis, cancer, and stroke, in addition to neurodegenerative and cardiovascular diseases. Intrinsically, inflammation is useful since it leads to removal of the offending factors and restoration of tissue structure and physiological function (Ricciotti & FitzGerald, 2011).

Cyclooxygenase (COX) is an enzyme, which is responsible for the formation of prostanoids as important biological mediators, including prostaglandin, prostacyclin and thromboxane. The relief from symptoms of pain and inflammation can be provided from pharmacological inhibition of COX. There are three known COX isoenzymes; COX-1, COX-2, and COX-3. COX-1 and COX-2 can be shown at various levels through different tissues while COX-3 is a splice variant of COX-1, which possesses intron one and a frame shift mutation. Although COX-1 and COX-2 basically act in a similar fashion, selective inhibition can make a difference in their side-effects. COX-1 is considered a constituent enzyme, found in most mammalian cells. However, COX-2 is an inducible enzyme and undetectable in most normal tissues but becomes abundant in activated macrophages and other cells at sites of inflammation. More recently, COX-2 has been shown to be upregulated in several cancerous diseases and play the central role in tumorigenesis.

COX-1 and COX-2 are of similar molecular weights, approximately 70 and 72 kDa, respectively, and have about 65% amino acid sequence homology and near-comparable catalytic sites. The substitution of isoleucine at site 523 in COX-1 with valine in COX-2 is the most significant variation between the isoenzymes, which allows for its selective

inhibition. The smaller Val523 residue in COX-2 allows inhibitors better access into its hydrophobic side-pocket compared to the larger Ile523 in COX-1.

COX-1 has been recorded to play an important role in protecting the gastric mucosal lining. Inhibiting COX-1 enzyme can lead to stomach irritation and ulcer, development as observed in some patients taking Non-Steroidal Anti-inflammatory Drugs (NSAIDs). To control arthritic and other painful symptoms, however, it is more important for a drug to block COX-2 activities, which is responsible for causing inflammation in the body. So, COX-2 enzyme seems to be a suitable target for the anti-inflammatory effects of NSAIDs.

On the other hand, the acidity of some NSAIDs may cause additional damage to the gastrointestinal tract. The wide range of side-effects of NSAIDs in the gastrointestinal tract and especially, the large intestine, can be due to the inhibition of these two isoenzymes (Jackson & Hawkey, 1999). Classical COX inhibitors are not selective and therefore inhibit all types of COX enzymes. COX-2 selective inhibitor, such as coxibs, is a class of NSAID which directly targets the COX-2 enzyme (Sánchez-Pernaute *et al.*, 2004). However, several COX-2 inhibitors have been withdrawn from the market, others have been labelled with warnings on increased risk of thrombosis (Cairns, 2007). Inspired by the above observations, this study aims to design new inhibitors that could be applied to selectively inhibit COX-2 rather than COX-1.There are several questions that we will try to answer during the course of this study. They are: (i) Would docking lead to better models than manually constructed or restrained starting pose? (ii) Would the designed model give satisfactory ADMET properties? (iii) Would the designed model be selective for COX-2 only? (iv) Would the designed model contribute to new lead for COX-2 inhibitors?

To begin the design for selective inhibitors, one should first understand the difference in the active site of the protein that resulted in their activities. This difference could be studied *in silico* through the models of the active pockets of the enzymes. These models provide various informations including factors and parameters such as ligand-protein interaction that affect the inhibition of the enzymes such as in COX-1 versus COX-2. With these informations, one could design inhibitors at the active site that would be selective towards one enzyme over the other.

1.2   Problem Statement

COX-1 enzyme is present in most tissues. Its function is to convert arachidonic acid to prostaglandins, which in turn, stimulate body functions such as stomach mucous production, kidney water excretion and platelet formation.

In contrast, COX-2 is not normally present in cells. Its existence is induced, but its expression can be increased dramatically by the action of macrophages, the scavenger cells of the immune system. COX-2 plays a very important role in inflammation (Gupta *et al.*, 2010).

One of the most versatile drug and most commonly used to inhibit the COX enzymes is aspirin. Studies have also shown that inhibition of COX-1 and COX-2 enzymes by aspirin and other NSAIDs to have a wide range of side-effects in the gastrointestinal tract (Jackson & Hawkey, 1999). In addition, these drugs, including aspirin are not selective to either COX enzymes.

However, there are several drugs that have been reported to be selective towards only COX-2 enzyme. One group of such compounds is Coxibs (Figure 1.1) and they have been shown to have adverse effects, like increased risk for myocardial infarction, stroke, heart failure, and hypertension (Antman *et al.*, 2007). These adverse effects pose highest

risk in patients with prior history of cardiovascular diseases (Martinez-Gonzalez & Badimon, 2007).
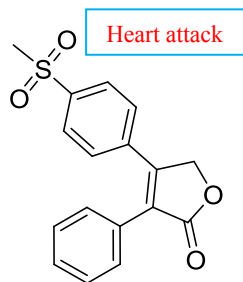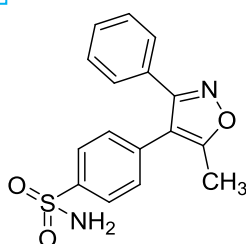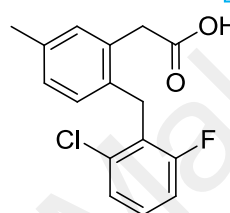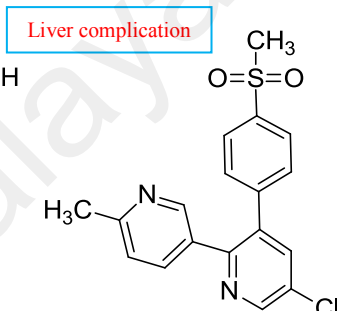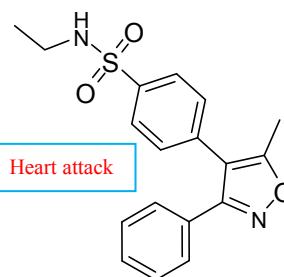
Figure 1.1: COX-2 selective drugs (Coxibs)

To minimize the adverse effects of NSAIDs, there is a need to develop new COX-2 selective inhibitors with better pharmacological profile and lesser side effects than current available NSAIDs.

1.3   **Aim of Study**

1. To design and analyze (*in silico*) a new class of diaryheterocyclic compounds as COX-2 selective inhibitors.

2. To predict the absorption, distribution, metabolism, excretion and toxicity properties of a new class of COX-2 inhibitors using ADMET software.

3. To synthesis a new class of diaryheterocyclic compounds as potential COX-2 selective inhibitors.

4. To evaluate COX-1/COX-2 selectivity and potency of a new class of COX-2 selective inhibitors using an enzyme immune (EIA) kit.

1.4   Research Project Workflow

The general workflow of this study is illustrated in Figure 1.2.
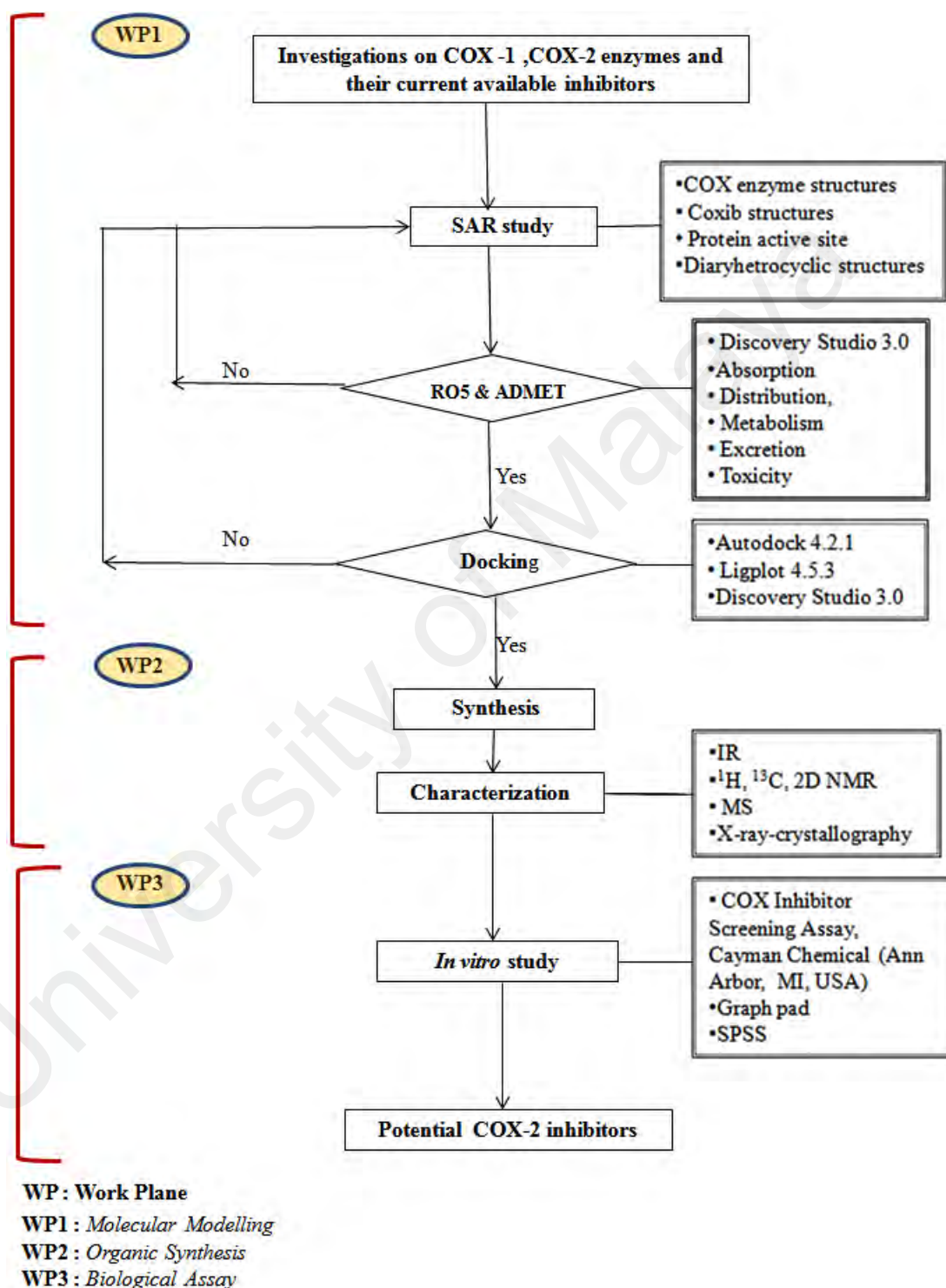
Figure 1.2: Workflow of overall research project.

CHAPTER 2: LITERATURE REVIEW

2.1   Inflammation

The discharge of chemicals from tissues and migrating cells results in inflammation. Most intensely involved chemicals are the prostaglandins (PGs), leukotrienes (LTs), histamine, bradykinin, and lately, platelet-activating factor (PAF) and interleukin-1. The indication for the chemicals' implication derives from researches with receptors and inhibitors having competitive antagonists of their synthesis. H1 histamine antagonists are efficient for high fever and some skin allergies, for instance, urticaria, which shows the significance of histamine in these states. The power of aspirin as an anti-inflammatory drug, which inhibits, the cyclooxygenase (COX) enzymes and decrease the synthesis of prostanoids, leads to the relief of rheumatoid arthritis symptoms. Corticosteroids avoid the creation of both PGs and LTs generating lipocortin, which, by the inhibition of phospholipase A2, decreases the arachidonic acid discharge (Vane & Botting, 1967).

For many years, the willow tree (Figure 2.1) and salicin (extracted from bark of the willow tree) had been used to relive pain and fever.

Salicylic acid has been found to be the compound of the willow bark extract responsible for the bioactivity in relieving pain and fever. This compound became the bases of the discovery of aspirin or acetylsalicylic acid (Stone, 1763). Salicylic acid has also exhibited to have phyto (medicinal plants) and chemotherapeutic activities as analgesic drugs (Mahdi *et al.*, 2006).

Figure 2.1: Willow tree

Historically, early civilizations, specifically in Mesopotamia, around 6000 years ago used the Willow (*Salix sp.*) as a source of drugs (Barrett *et al.*1999). For instance, archaeologists discovered leaf clay tablets made by the Assyrians during the Sumerian age (3500–2000 B.C), illustrating the function of Willow's leaves for such situations (Levesque & Lafont, 2000). The Babylonians had made use of the Willow tree extracts to medicate normal fever, ache and inflammation. As well as in the herbal remedies, in the Ebers Papyrus of ancient Egypt, the use of Willow tree has been recorded (Levesque & Lafont, 2000). In the Chinese and Greek civilizations more than 2000 years ago, the Willow bark were used to relieve fever and aches (Riddle, 1999). The ingredient that is responsible for the remedy in Willow tree was later identified as salicin (Figure 2.2). This compound then became the basis for the discovery of aspirin in the 18th century. Edward Stone's letter to the president of the Royal Society in London defined his results

from the treatment of his patients suffering from ague, with powdered Willow bark immersed in water. After one hundred and thirteen years, a Scottish physician, Thomas MacLagan, treated himself and his patients with Willow powder extract for ailments related to acute rheumatism (Maclagan, 1876).
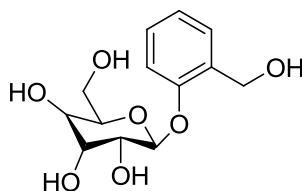
Figure 2.2: Structure of Salicin

Aspirin (acetyl salicylic acid), acetyl salicylate, was synthesized as a prodrug for salicylate, a derivative of salicin (Figure 2.3). In 1899, Bayer introduced its use to treat pain, fever, and inflammation (Vane, 2000). In low doses, aspirin had also been reported to reduce the incidence of heart attacks by an antithrombotic effect (Gum *et al.*, 2001). In 1982, Sir John Vane received the Nobel Prize in Medicine for the elucidation of the mechanism of aspirin as an inhibitor of prostaglandin synthetase (Levesque & Lafont, 2000).
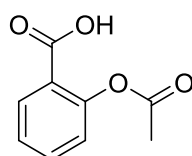
Figure 2.3: Aspirin

2.2   Cyclooxygenase (COX) Enzymes

In the 1990s, researchers discovered that two different cyclooxygenase (COX) enzymes existed, currently known as COX-1 and COX-2 (Taketo, 1998), which are stimulated by different mechanisms. COX-1 is stimulated continuously by normal body

physiology. Most tissues possess COX-1 enzyme, which is constituent, thus its concentration in the body sustained stable. COX-1 enzyme changes arachidonic acid to prostaglandins (Figure 2.4) which are responsible in the improvement of body functions like stomach mucous production, kidney water excretion and platelet formation (Habeeb *et al.*, 2001a).

The COX-2 enzyme, on the other hand, is an induced enzyme which does not usually exist in cells. However, its production can be increased significantly due to the activity of macrophages, the scavenger cells of the immune system. COX-2 takes a vital role in inflammation since it is implicated in generating prostaglandins as an inflammatory response. While COX-1 is stimulated continually, COX-2 is stimulated just as a part of an immune reaction (Habeeb *et al.*, 2001a).

Latest studies have indicated that the link between the two isoforms of enzymes is not as straight forward. COX-2 is thought to contribute to the inflammatory processes while COX-1 is constitutively expressed in different tissues and organs like brain, kidneys (Ferreri *et al.*, 1999) and reproductive tract (Yamagata *et al.*, 1993) (Figure 2.4)
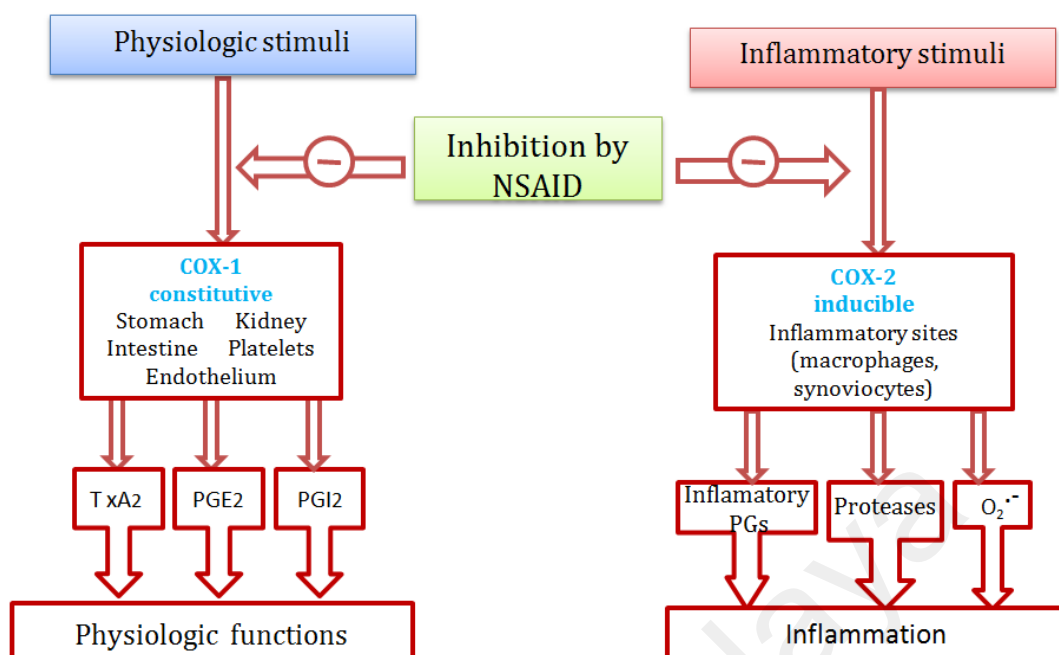
Figure 2.4: Schematic presentation of the actions of COX-1 & COX-2

2.3   Differences in the Structures of COX-1 and COX-2

The COX isoenzymes are membrane-bound enzymes in the endoplasmic reticulum (ER). In 1971, the three dimensional structure of the ovine COX-1 was first reported (Vane, 1971), followed by the crystal structures of human and murine COX-2 in the early 1990s. COX functions as a homodimer. Thus far, all efforts to create monomeric species only presented inactive enzymes. The COX monomer is composed of three structural domains: an N-terminal epidermal growth factor (EGF), a membrane binding domain (MBD) of about 48 amino acids in length which anchors the protein to one leaflet of the lipid bilayer; and a large C-terminal globular catalytic domain which contains the COX active site, which adjusts the substrate and the peroxidase, which consist of the heme cofactor. These sites are distinct but functionally and structurally connected (Garavito *et al.*, 2002) (Figure 2.5).
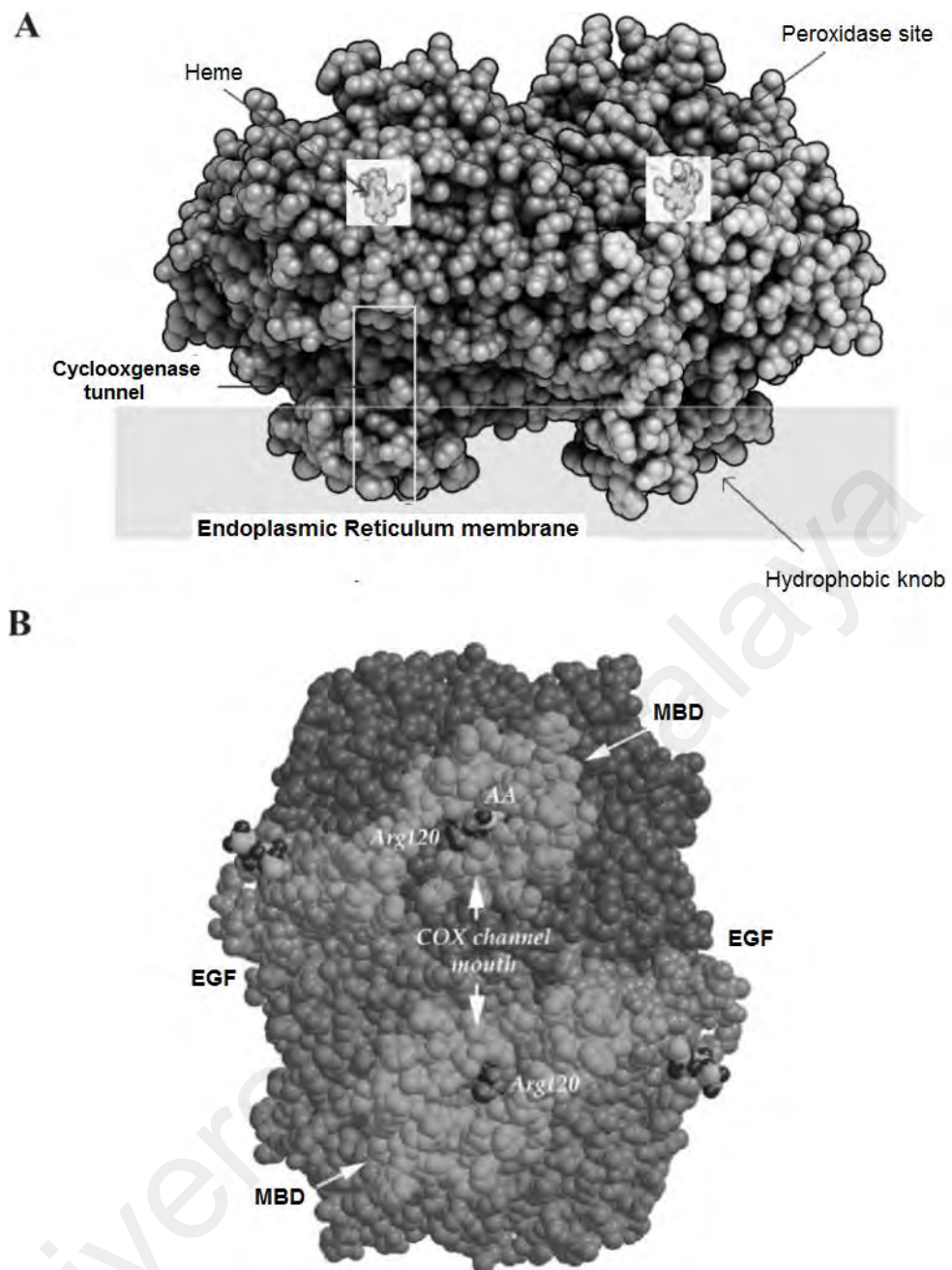
Figure 2.5: (A) Space-filling model of COX-2 energy along with a schematic presentation of the different parts of the cyclooxygenase enzyme. (B) A space-filling model of the COX-1 dimer, viewed from the membrane plane. Arg120, which is part of the channel aperture, defines the beginning of the COX active site. Within one COX channel, a buried AA (arachidonic acid) is shown (Zarghi & Arfaei, 2011).

The long hydrophobic channel is a cyclooxygenase active site, as well as the (NSAIDs) binding site, which extends from the membrane-binding domain to the core of the catalytic domain (Picot *et al.*, 1994; Kurumbail *et al.*, 2001). In the upper half of

the channel, the arachidonate binding site is placed from Arg120 to near Tyr385. Ser530, placed in the middle of the channel, is the site of acetylation by aspirin (Loll *et al.*, 1995). The change of a valine (Val) at position of 523 in COX- 2 with a relatively bulky Ile residue in COX-1 at the same place of the active site of the enzyme, resulted in a structural change of the enzymes as well as better entry to an additional side pocket in COX-2 enzyme, which is necessary for COX-2 drug selectivity (Figure 2.6). In COX-1, entry to this side pocket is somewhat restricted. In addition, the change of residue 434 from Ile to Val in COX-2 allows the neighboring Phe518 residue to swing out of the path, expanding further entry to the side space. Additionally and importantly, an amino acid difference between the two isoforms is around the side pockets of the enzymes where the residue in COX-2 is Arg513 in place of the His513 in COX-1. However, this alteration does not change the conformation of the drug-binding site but affects the chemical surroundings of the binding site where the arginine residue can have a better binding interaction with polar moieties of substrate entering the pocket. These variations between the COX enzymes' active sites (Figure 2.6) place important significance towards the development of COX-2 selective inhibitors (Charlier & Michaux, 2003; Dannhardt & Kiefer, 2001; Kurumbail *et al.*, 1996).
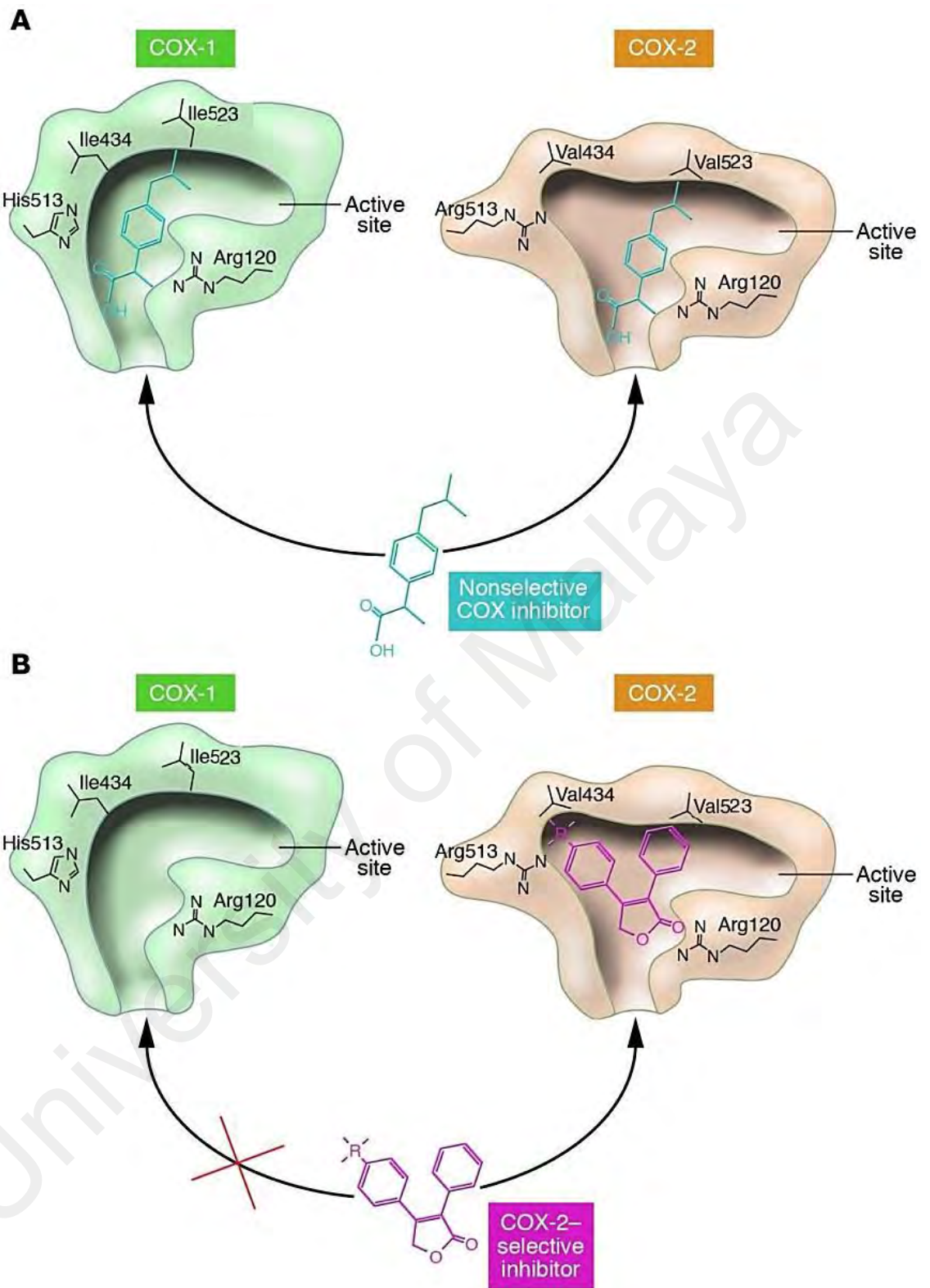
Figure 2.6: Structural differences between the substrate-binding channels (active sites) of COX-1 and COX-2 (Grosser *et al.*, 2006).

In 2002, Daniel Simmons and his co-workers identified and duplicated a COX enzyme from a dog brain which was sensitive to inhibition by paracetamol

(acetaminophen). This COX enzyme was found to be different from COX-1 and COX-2. In actual fact, it was found to be a variant of COX-1 enzyme, derived by alternative splicing of the COX-1 gene. It was subsequently designated as COX-3, with the only difference observed between these variants was that COX-3 enzyme retained an intron 1 of the COX-1 gene and participates around 5% of overall COX-1, as well as the action of cyclooxygenase of COX-3 is around 80% lower than that of COX-1. This seems to suggest that retained intron 1 may adjust the shape of the active site. Better code of COX-3 in the brain and heart has been recorded (Chandrasekharan *et al*., 2002; Shaftel *et al*., 2003). The distinguishing feature of COX-3 is its greater sensitivity to acetaminophen than that of COX-1 and COX-2. Acetaminophen has been reported to show low sensitivity to both COX-1 and COX-2 when examined in *in-vitro* experimental methods (Botting, 2000). However, it is a powerful selective inhibitor of COX-3 and most probably shows analgesic activities by inhibiting this enzyme (Botting, 2003). Likewise, NSAIDs, such as diclofenac or ibuprofen, have also shown to be strong inhibitors of COX-3. However, due to their very polar nature, NSAIDs may probably not be able to reach COX-3 in the brain in effective concentrations. COX-3 has been thought to play an important function in the biosynthesis of prostanoids, which are significant mediators in ache and fever.

2.4   Types of COX-2 Inhibitors

At least seven major structural classes of COX-2 selective inhibitors have been recognised. They include the diarylheterocyclics (or tricyclics), acidic sulfonamides, and 2,6-di-*tert*-butyl phenols, as well as the derivatives of the nonselective inhibitors which include zomepirac, indomethacin, piroxicam, and aspirin. The most different class of these inhibitors, and the first to be authorized for human use, comprises diarylheterocyclic compounds related to DuP697 & celecoxib (Figure 2.7) (DeWitt, 1999).
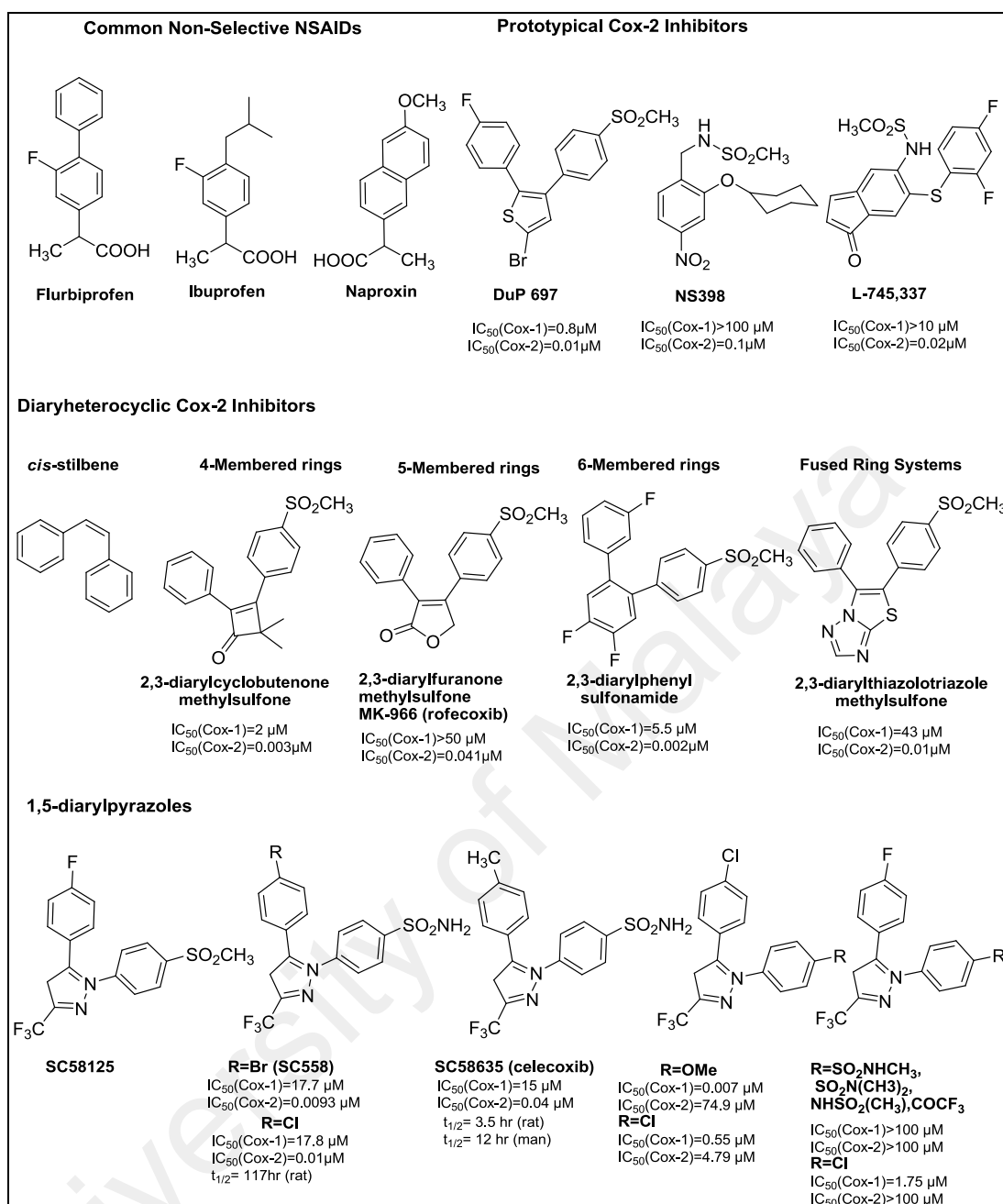
Figure 2.7: Structures of representative nonselective and COX-2-selective NSAIDs (DeWitt, 1999).

2.5 The Role of Non-Steroidal Anti-Inflammatory Drugs (NSAIDs)

NSAIDs have become among the most extensively used therapeutics due to their recorded anti-inflammatory, anti-pyretic and analgesic activities. They have been used to treat different inflammatory diseases like arthritis, rheumatism and alleviating the common aches. Aspirin (Figure 2.8) was the first NSAID with therapeutic advantages that has been used for more than 100 years (Donnelly & Hawkey, 1997).
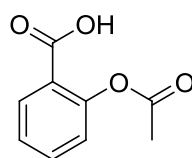
Figure 2.8: Aspirin

In 1971, Vane recognised the COX enzyme as the therapeutic target of NSAIDs, indicating that these anti-inflammatory substances block the biosynthesis of prostaglandins (PGs) that contribute to different physiological and pathophysiological roles (Vane, 1971).

Arachidonic acid converts to prostaglandin H_2 (PGH$_2$), the precursor of the series-2 prostanoids (prostacyclins, prostaglandins & thromboxanes) by COX enzyme (Figure 2.9) which contains two active sites: a heme with peroxidase activity which takes the responsibility of reducing PGG$_2$ to PGH$_2$, and a cyclooxygenase site, where arachidonic acid is changed into the hydroperoxy endoperoxide prostaglandin G_2 (PGG$_2$). The reaction proceeds through a hydrogen atom abstraction from arachidonic acid by a tyrosine radical produced from the peroxidase active site. Two molecules of oxygen react with the arachidonic acid radical to create PGG$_2$ (Chandrasekharan *et al*., 2002).
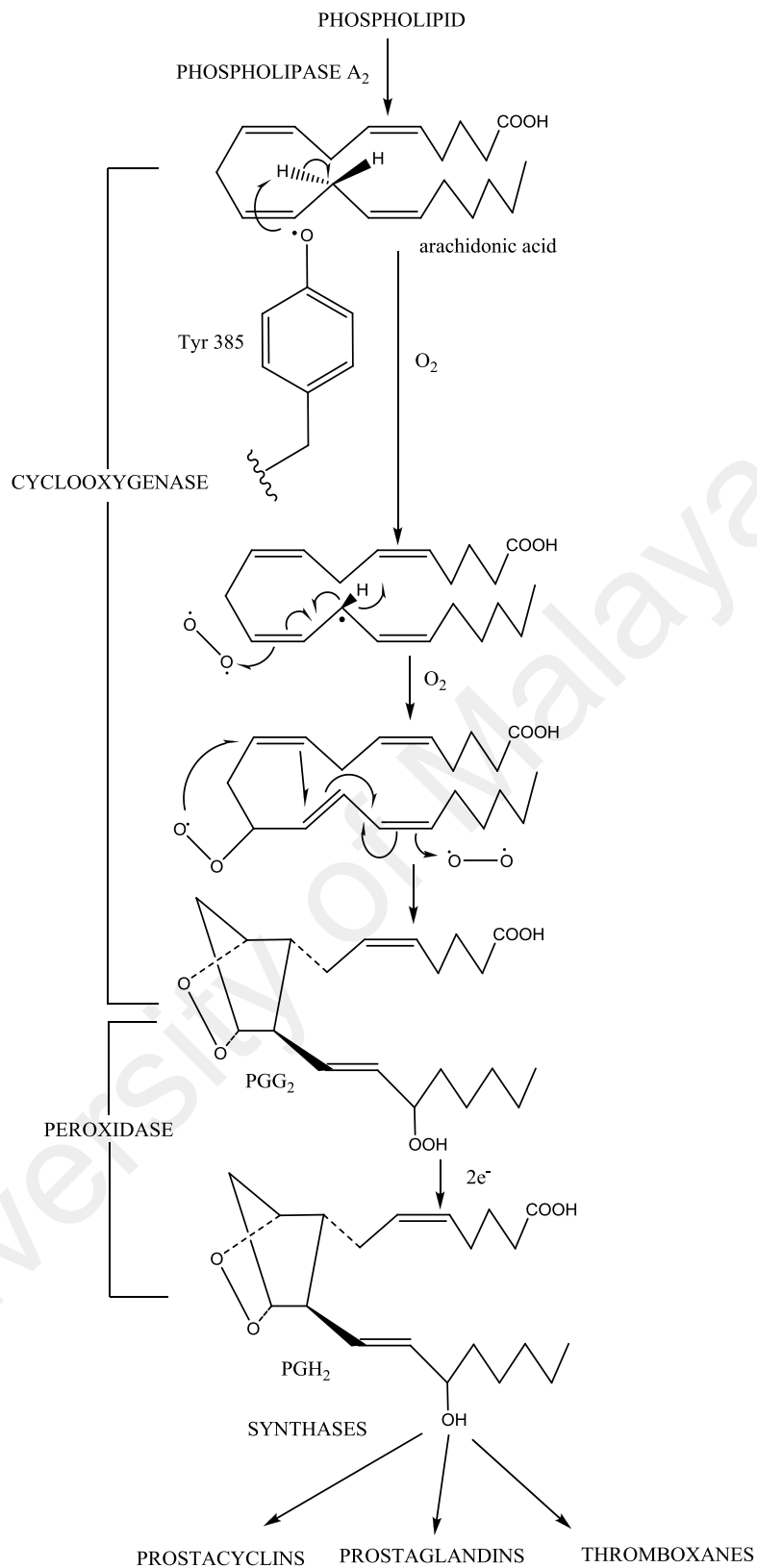
Figure 2.9: Biosynthesis of prostanoids (Chandrasekharan *et al*., 2002).

2.6   Side Effects of NSAIDs

Therapies involving COX inhibitors are often correlated with numerous after effects such as gastrointestinal erosions, renal and hepatic insufficiencies (Burdan, 2004). NSAIDs are associated with gastrointestinal tract (GIT) toxicity which has become the most common and serious problem (Sung *et al.*, 2000). NSAIDs may also lead to an increase in serum creatine levels and stimulate hypercalcemia, interstitial nephritis, proteinuria, and acute renal dysfunction (renal toxicity) (Ruiz & Lowenthal, 1997), (Shah *et al.*, 2001; Simon, 2001; Wallace, 1999). Due to decrease forming of PGs, such as PGI2, PGE2 which concerned about the regulation of renal blood circulation, the ratio of glomerular filtration is decreased. This is particularly important in patients with lower renal functions that cause water retention, hypertension and renal failure. Due to inhibition of COX enzymes in thrombocytes, the production of thromboxane A2 is reduced, leading to inhibition of platelet aggregation and prolongs the bleeding time (Dannhardt & Kiefer, 2001). NSAIDs have also been reported to increase liver enzymes levels (Kallings, 1993; Bort *et al*., 1999). Broncho-constriction with asthmatic attacks is another reaction of NSAIDs (Szczeklik & Stevenson, 2003).

2.7   Selective COX-2 Inhibitors

Several inhibitors that are selective towards COX-2 are discussed below. Meloxicam (Figure 2.10) is one inhibitor which has a more effective inhibition activity of COX-2 than COX-1 (Schattenkirchner, 1997). In addition, it is tolerated by patients, as well as, it has shown to have a good safety profile (Hawkey *et al.*, 1998). It has also been shown to be as active as other NSAIDs in the treatment of rheumatoid inflammation, osteoarthritis, and ankylosing spondylitis (Lund *et al*., 1998). However, at higher dosage, the selectivity of meloxicam towards COX-2 decreases but increases towards COX-1 (Engelhardt, 1996).
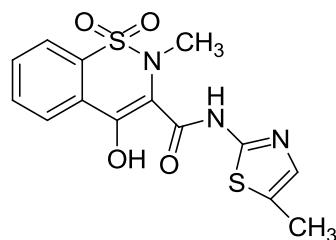
Figure 2.10: Meloxicam

Another inhibitor selective towards COX-2 is nimesulide (Figure 2.11), often used as analgesic, anti-pyretic and anti-inflammatory drug (Kataoka *et al.*, 2000). Studies had shown that nimesulide, particularly at lower dosage, was more potent to inhibit COX-2 *in vitro* than COX-1 (Cullen *et al.*, 1998). At higher dosage, however, COX-1 inhibition became more effective than COX-2 (Halter *et al.*, 2001). The anti-pyretic property of nimesulide is dependent on the inhibition of prostaglandin synthesis (Chandra & Bhatnagar, 2002), while its pain reducing effect has been found, in part, to result from the inhibition of cytokines (Ferreira, 2002). Unlike aspirin, nimesulide had been shown to not to incite gastric harm, even during the time which it was administered with the steroidal anti-inflammatory drug, prednisolone (Kataoka *et al.*, 2000). In addition, nimesulide was also reported to have anti-oxidant properties (Maffei *et al.*, 1992).
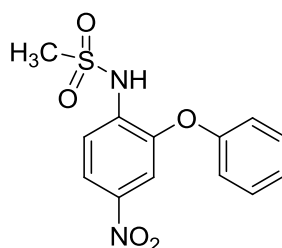
Figure 2.11: Nimesulide

Celecoxib and rofecoxib are highly selective COX-2 inhibitory drugs and they possess analgesic, antipyretic and anti-inflammatory properties (Schnitzer *et al.*, 1999). Like nimesulide, celecoxib and rofecoxib had been reported to not induce damage to the stomach tissue (Buttgereit *et al.*, 2001). Latest studies, however, have explained that

these drugs could affect thrombotic cardiovascular difficulties (Mukherjee, 2002). Thus new coxibs such as etoricoxib, valdecoxib, parecoxib and lumiracoxib (Figure 1.1, p. 4), possessing raised COX-2 selectivity have been developed. Valdecoxib (Figure 1.1, p. 4), for example, has an improving gastrointestinal safety profile, which may be due to the indication of higher selectivity than celecoxib. Parecoxib (Figure 1.1, p. 4), is an injectable selective COX-2 inhibitor which is a prodrug of valdecoxib, while etoricoxib shows slightly enhanced COX-2 selectivity than rofecoxib. Lumiracoxib is the most selective COX-2 inhibitor *in vitro* and the only acidic coxib. All the above NSAIDs are recommended to have related effect to the non-selective NSAIDs in treating osteoarthritis, rheumatoid arthritis and serious pain. However, they show related renal reverse effects in some randomized clinical reports. The obvious dose confidence level of renal toxicity may bind the usage of these new coxibs in high dosages for bettered effect (Tacconelli *et al.*, 2004). Because selective COX-2 inhibitors do not block thromboxane A2, the occurrence of bleeding is decreased. COX-2 enzyme generates PGs at inflammatory locations, and PGI2, which is a vasodilator and an inhibitor of blood platelet accumulation (Bertolini, 2001).

Using these drugs in the medication of rheumatoid arthritis, osteoarthritis, and inflammatory illnesses (Bertolini, 2001; Bianchi & Broggini, 2002; Bjorkman, 1999; Simon & Yocum, 2000) may lead to blood pressure problems and other cardio-renal difficulties in patients with high blood pressure. Various reports had shown that edema growth and high diastolic blood pressure were monitored in patients with high blood pressure taking rofecoxib and celecoxib. In celecoxib-treated patients, impairments of edema and blood pressure were less frequent than in patients taking rofecoxib (Whelton *et al.*, 2001). In latest research, rofecoxib was reported to markedly enhance the systolic blood pressure, whereas celecoxib did not boost it (White *et al.*, 2002). In addition,

rofecoxib has been shown to have a higher renal toxicity in comparison with celecoxib and historic NSAIDs (Zhao *et al.*, 2001).

2.8   The Relationship between Amino Acid Profile of COX-2 Enzyme and Inhibition Mechanism

The larger active site of COX-2 compared to that of COX-1 plays a great role in the development of selective drugs for COX-2. This makes it possible for researchers in drug design to design molecules that would be large enough to fit into the COX-2 active site but not COX-1. As Val523 is a less bulky residue in COX-2 than Ile523 in COX-1, the volume of the active site in COX-2 is increased (Ermondi *et al.*, 2004). Substitution of Ile434 (COX-1) with Val434 (COX-2) causes the side-chain of Phe518 in COX-2 to move back and make some additional space in the active site, which then allows for interactions of inhibitors with Arg513, which is a replacement for His513 (COX-1), as well as is thought to be a key residue for diaryl heterocycle inhibitors such as the coxibs. At the upper side of the receptor channel into the active site of COX-1, the side-chain of Leu384 is oriented far from the active site in COX-2 and creating more space at the top of the binding site. COX-2 inhibitors like celecoxib and rofecoxib are prevented from entering the COX-1 channel, due to the existence of the bulky sulfonamide group in these molecules. A 4-methylsulfonylphenyl bound, usually to an unsaturated five-membered ring with a vicinal lipophilic group (rofecoxib), is required, in order to obtain the optimal activity and selectivity of the coxibs. When the lipophilic pocket is occupied by an optionally substituted phenyl ring or a bulky alkoxy substituent (celecoxib), SO_2NH_2 can replace SO_2CH_3, the oxygen of the sulfonamide (or sulfone) group interacts with His90, Arg513, and Gln192 and creates hydrogen bonds, inside the hydrophilic side-pocket of COX-2. Hydrophobic and electrostatic interactions occur due to the interaction of the substituted phenyl group at the top of the channel with the side-chains of amino acid residues. Since the degree of freedom is essential for the binding,

the central ring of the coxibs affects the orientation of the aromatic rings, and as a result, affects the binding of the drugs to COX enzyme. The high lipophilicity of the active site needs low polarity of the central scaffold of the coxibs (Ermondi *et al*., 2004) (Figure 2.12).
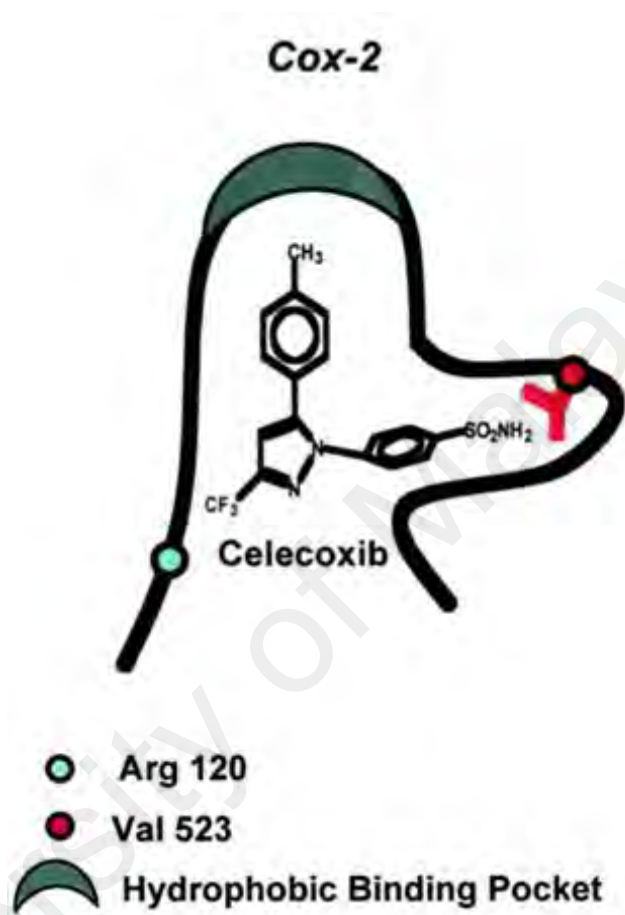
Figure 2.12: COX-2 receptor site with celecoxib in the binding site

2.9   *In Silico* **Studies**

2.9.1   **Molecular Docking**

One of the computational approaches which plays a vital role in predicting protein–ligand interactions is molecular docking. This approach has significant contributions to drug discovery research, as it has been widely implemented for hit discovery and lead optimization (Kitchen *et al*., 2004). Docking includes conformational sampling element for generating theoretical conformations in the binding pocket, and a binding affinity related scoring element for ranking theoretical conformations (Cross *et al*., 2009).

23

Protein flexibility is considered to have an impact on the reliability of molecular docking (Kitchen *et al.*, 2004). The rigidity of protein is presumed in traditional docking approaches, thus the degree of accuracy of this computation is slightly limited. However, Emil Fischer, a Dutch organic chemist, showed that enzyme and substrate fit together more like 'a lock and key'. Subsequently, there have been many experimental evidences to show proteins undergoing significant conformational changes upon ligand binding (Heh *et al.*, 2013). Current docking methods treat protein as rigid forms so as to decrease the space of searching for the most favorable structures of the complexes and to find the best spatial and energetic fit to the protein binding site (Halperin *et al.*, 2002; Wodak & Janin, 1978).

2.9.1.1 AutoDock

Computational tools, like the AutoDock software, offer the useful feature of providing new drug candidates in a faster and cheaper way (Gilbert, 2004; Warren *et al.*, 2006). The interaction of a molecule with the target protein is the key to understanding the essential part of biology. The goal of AutoDock is to provide computational tools to aid researchers in defining biomolecular complexes. AutoDock integrate two approaches to attain rapid grid-based energy rating and effective search of torsional freedom.

The default search algorithm in AutoDock 4.2 (AD4) is the Lamarkian Genetic Algorithm (LGA), a hybrid genetic algorithm with local optimization that utilizes a parameterized free-energy scoring feature to evaluate binding energy (Morris *et al.*, 2009; Goodsell *et al.*, 1996). To conduct a ligand-receptor docking experiment, the software accepts, as inputs, ligand and macromolecule coordinates, and then uses the LGA to output ligand positions and lessen binding energies, utilizing pre-calculated pairwise potential grid maps (Morris *et al.*, 1998). Each docking includes a multiple

independent implementations of the LGA, restricted to a user fixed number of energy evaluations (ga_evals) or generations (ga_num_generations). The particular LGA implementations (ga_runs) are grouped and ranked for generating the final docking output.

Three separated programs are included in the AutoDock package: AutoTors, AutoGrid and AutoDock. AutoTors allows the determination of bonds that will be dealt as rotatable in the ligand (Morris *et al*., 1998). While AutoGrid pre-calculates these grids producing one map for each type of atom in the ligand and produces analogical result of the macromolecular file with the extension molecule.glg. The docking parameter file is used to guide the AutoDock on the movement of the ligand, by using of the map files. AutoDock's search methods involve the Monte Carlo simulated annealing (SA) approach, genetic algorithm (GA), local search (LS), and the hybrid genetic algorithm with local search (GA-LS). GA-LS is also known as the Lamarckian genetic algorithm (LGA) because off springs are allowed to receive the local search adaptations of their parents, and this was the selected algorithm used in the current study (Morris *et al*., 1998). AutoDock performs docking of the ligand to a set of grids illustrating the target protein.

2.9.1.2 Docking of Standard Inhibitors Involving COX Enzymes

The active site for COX-2 complexed with flurbiprofen, indomethacin and SC-558, have been reported (Kurumbail *et al*., 1996). Of these compounds, only SC-558 is selective towards COX-2. These structures gave insights into the structural basis for the selective inhibition of COX-2, and showed some of the conformational variations related to time-dependent inhibition. Kurumbai *et al* (1996) found that Arg120, the guanidinium group of which stabilized the carboxylate of classical NSAIDs, was one of the few charged residues in the hydrophopic COX channel. The carboxylate group of

SC-558 could be a significant component for selectivity towards COX-2. Another selective COX-2 inhibitor is nimesulide (Fabiola *et al.*,1998). This drug is found to be more selective towards COX-2 than SC-558. Molecular modeling studies carried out on complexes of nimesulide with COX-2 suggested that the methyl sulphonamide in nimesulide is responsible for the better selective to COX-2 compared to SC-558.

In another study, the binding conformations and free energies of 1,5-diarylpyrazole compounds to COX-2 and COX-1 using the LGA algorithm of AutoDock had been reported (Liu *et al.*, 2002) (Figure 2.13). Results indicated that the binding energies of 1,5-diarylpyrazole compounds computed by this method to be well correlated with the reported inhibitory activities against COX-2 and COX-1. Jashim and co-workers (2003) designed a group of celecoxib analogues in which the *para* SO_2NH_2 substituent on the N^1–phenyl ring was substituted by a *para*-sulfonylazido (SO_2N_3), or a *meta* SO_2N_3 substituent, for estimation as selective COX-2 inhibitors. *In vitro* inhibition experiments showed that celecoxib with *para*-SO_2N_3 to be selective for COX-1 inhibitor, while celecoxib with a *meta*-SO_2N_3 was a selective COX-2 inhibitor (Uddin *et al.*, 2003).
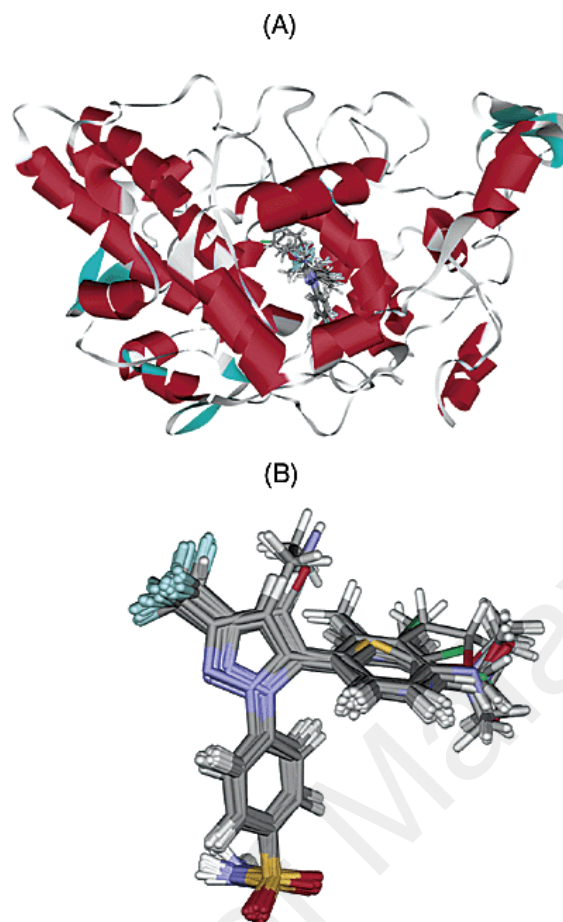
Figure 2.13: (**A**) Three-dimensional structural model of 1,5-diarylpyrazole compounds/COX-2 complex.(**B**) Probable binding conformations of 1,5-diarylpyrazole compounds and their alignment in the binding site of COX-2 (Liu *et al.*, 2002).

The study of the intermolecular interactions between four groups of anti-inflammatory inhibitors (oxazoles, pyrazoles, pyrroles and imidazoles) and COX-2 receptor was recorded (Chen *et al*., 2004). Docking results recommended that they had similar interactions. The most active compounds out of these four groups of inhibitors could form many hydrogen bonds with the residues His90, Arg513, Leu352 and Arg120, and create hydrophobic interaction with residues Phe518, Leu352 and Leu359. This outcome was consistent with the investigation published by (Kurumbail *et al*., 1996).

Selvam (2004) reported a new compound, indigocarpan (1) (Figure 2.14), and a known compound, mucronulatol (2) (Figure 2.14), which were isolated from chloroform extracts of *Indigofera aspalathoides* and estimated for COX-1 and COX-2 inhibition as well as antioxidant activities. Compound (1) showed significant COX-1 inhibition, and its *in vivo* anti-inflammatory activity was found to be similar to that of ibuprofen. Molecular docking studies showed the binding orientations of compound 1 to be in the active locations for both COX-1 and COX-2 (Selvam *et al.*, 2004).
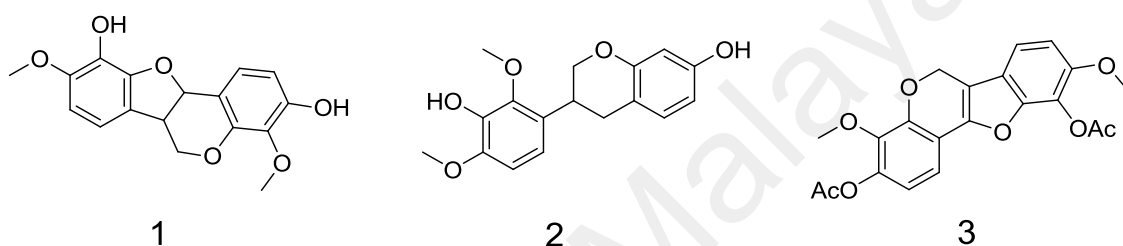
Figure 2.14: Chemical structures of indigocarpan (1), mucronulatol (2) and indigocarpan diacetate (3).

Praveen Rao and co-workers (2003) found six-membered pyran-2-one ring systems (Figure 2.15) to be an appropriate central modle to design selective COX-2 inhibitors (Praveen *et al.*, 2003).
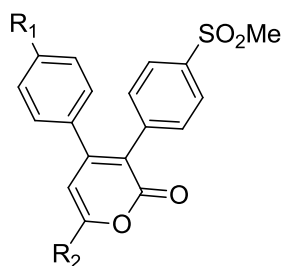
Figure 2.15: Structure of 6-alkyl(alkoxy or alkylthio)-4-aryl-3-(4-methanesulfonylphenyl)pyran-2-ones as selective COX-2 inhibitors

In another study, new models of 4,5-diaryl-4*H*-1,2,4-triazole (Figure 2.16), owning C-3 thio and alkylthio (SH, SMe or SEt) substituents, were designed and synthesized for

the assessment of selective COX-2 inhibitors with *in vitro* and *in vivo* anti-inflammatory activity. The compound 3-ethylthio-5-(4-fluorophenyl)-4-(4-methylsulfonylphenyl)-4*H*-1,2,4-triazole have been shown to exhibit a high *in vitro* selectivity (COX-1 IC_{50} = 20.5 nM; COX-2 IC_{50} = 1.8 nM; selective index (SI) = 11.39) comparative to the reference drug celecoxib (COX-1 IC_{50} = 3.7 nM; COX-2 IC_{50} = 2.2 nM; SI = 1.68), as well as, exhibited good anti-inflammatory activity compared to celecoxib, in a carrageenan-induced rat paw edema assay (Navidpour *et al.*, 2006)

R$_1$:H, Me, Et
R$_2$: H, F, Cl, Br, OMe, Me
R$_3$: H, F, Me
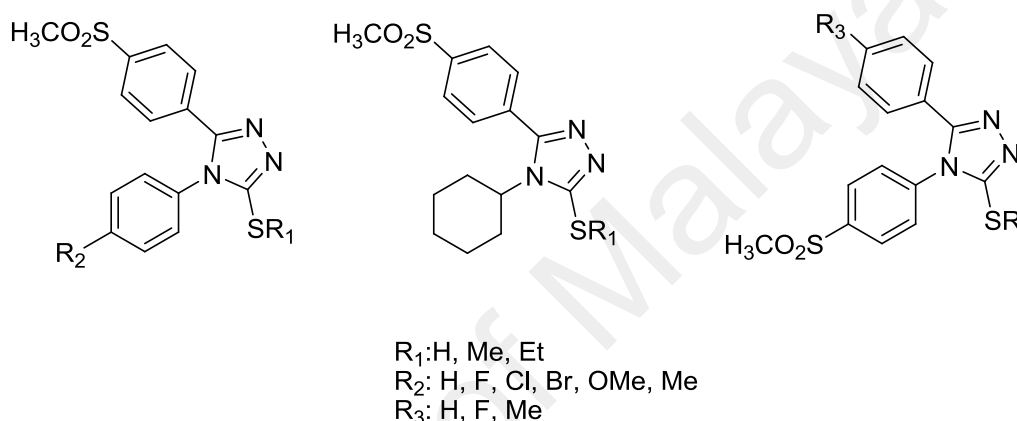
Figure 2.16: A new type of 4,5-diaryl-4*H*-1,2,4-triazoleas as selective COX-2 inhibitors (Navidpour *et al.*, 2006).

The design, synthesis, and *in vitro* COX enzyme inhibitory activities of several 4-phenyl-5-pyridin-4-yl-2,3-dihydro-3*H*-1,2,4-triazole-3-thiones possessing N-2 Mannich bases or S-alkyl substituents have been reported. Several of these compounds exhibited low nanomolar COX enzyme inhibition activities, COX-2 IC_{50} (0.8 -7.8 nM) and COX-1 IC_{50} (3.5-7.5 nM) (Radwan & Kamal, 2013).

Molecular docking studies of thiophene derivatives and their azetidinone forms as selective COX-2 inhibitors have been carried out using Autodock 4.2.1 version (Naresh, 2013).

Celecoxib and rofecoxib analogues, in which the corresponding SO_2NH_2 and SO_2Me hydrogen-bonding pharmacophores were substituted by a dipolar azido bioisosteric substituent (Figure 2.17), were inspected, and docking studies revealed that the azido substituent of these two analogues were introduced deep into the secondary pocket of the human COX-2 binding site where it endured electrostatic interaction with Arg513. The azido analogue of rofecoxib was the most effective and selective inhibitor of COX-2 (COX-1 IC_{50} = 159.7 μM; COX-2 IC_{50} = 0.196 μM; COX-2 SI = 812), showing good oral anti-inflammatory and analgesic activities (Habeeb *et al.*, 2001).

Figure 2.17: The azido analogues of celecoxib and rofecoxib

A group of regioisomeric 1-(methylsulfonylphenyl)-2-phenylacetylenes possessing a COX-2 SO_2Me pharmacophore at the *para*, *meta* or *ortho* position of the C-1 phenyl ring, in conjunction with a C-2 phenyl or substituted-phenyl ring substituent (3-F, 3-OMe, 3-OH, 3-OAc, 4-Me), were designed (Figure 2.18), synthesized, modelled and studied *in vitro* on COX-1/COX-2 inhibition assay. The compound 1-(3-methylsulfonylphenyl)-2-(4-methylphenyl) acetylene was obtained to be effective COX-2 inhibitor (IC_{50} = 0.32 μM) with a high COX-2 selectivity index (SI > 320) corresponding to the reference compound rofecoxib (COX-2 IC_{50} = 0.50 μM; COX-2 SI > 200). Structure–activity data showed that the acetylene moiety comprised an appropriate scaffold to design novel acyclic 1,2-diarylacetylenes with selective COX-2,

or dual COX-1/COX-2, inhibitory activities (Q.-H. Chen, Praveen Rao, & Knaus, 2005).

$$R_1 = H, F, OMe, OH, OAc$$
$$R_2 = H, Me$$
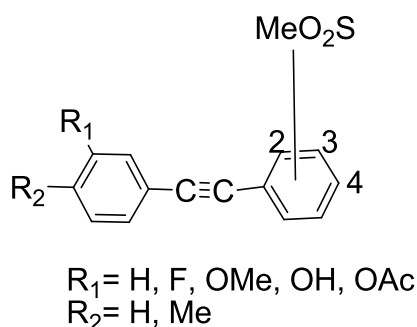
Figure 2.18: Linear 1-(4-, 3- or 2-methylsulfonylphenyl)-2-phenylacetylenes

2.9.2 Lipinski's Rule of Five

The Lipinski's rule of Five, also known as the Pfizer's rule of Five or the Rule of Five (RO5), is a rule of thumb to assess drug likeness or dictate if a chemical compound with a specific pharmacological or biological activity has properties that would make it a reasonable orally effective drug in humans. The rule was created by Christopher A. Lipinski in 1997, following to the findings that most medication drugs were correspondingly small and lipophilic molecules (Lipinski *et al*., 1997).

The original RO5 deals with orally active compounds and clarifies four simple physicochemical parameter ranks which are connected with 90% of orally active drugs that have completed phase II clinical status. The parameters are: MW $\leq$ 500 daltons, log $P \leq$ 5, number of H-bond donors $\leq$ 5, number of H-bond acceptors $\leq$ 10. These physicochemical parameters are connected with adequate aqueous solubility and intestinal permeability and include the first phases in oral bioavailability. The RO5 was intentionally formulated to be a conservative predictor in a time where medicinal and combinatorial chemistry offered too many compounds with very poor physicochemical properties. The aim was to change the chemical conduct in the desirable direction. If a

compound fails the RO5, there is a high probability that oral activity problems will be faced. Anyhow, passing the RO5 is no warranty that a compound is drug-like. Furthermore, the RO5 expresses nothing about particular chemistry structural characteristics found in drugs or non-drugs (Lipinski, 2004).

2.9.3 ADMET Studies

The first step to start most studies on ADMET (absorption, distribution, metabolism, excretion, and toxicity) is by emphasizing the role of these properties in the rates of failure of drug discovery and the consequent increasing cost of delivering a new drug to the market. For the time being, the number of marketed drug cancellations carries on increasing, mostly because of fundamental ADMET problems that were not discovered earlier (Waterbeemd & Gifford, 2003). Various solutions are recommended for detecting and directing these problems before any leading compound progresses to the clinical phases (Li, 2001). It has been reported that, the function of early screening of ADMET properties with computational methods (*in silico*) have been greatly satisfying (Valerio, 2009; Butina *et al.*, 2002). Hou and group (2006) have performed broad researches on *in silico* modeling of different ADMET-correlated properties, among them are the blood–brain barrier, Caco-2 permeability, human intestinal absorption (HIA), oral absorption, oral bioavailability, and P-glycoprotein inhibition. In current research, they observed a combined information-based PKKB (Pharmaco Kinetics Knowledge Base) (Chou *et al.*, 2013), gathering structures, pharmacological information, significant experimental or predicted physiochemical properties, and experimental ADMET information for 1685 drugs. This data base plays as an effective resource for bench marking pharmacokinetic researches, confirming the accuracy of present ADMET predictive models, and making new predictive models reliable.

CHAPTER 3: DRUG DESIGN

3.1 Design & Structure-Activity Relationships (SAR)

3.1.1 Introduction

Generation of lead compounds is one of the most significant phases in a drug discovery approach. In a modern drug discovery research, structure-activity relationships (SAR) are widely applied in detecting new leads and scaffold generation for the optimization of receptor or enzyme affinity, as well as the study of pharmacokinetic and physicochemical properties. SAR is often used to optimize leads through a continuous, multi-step process and, depending upon the knowledge gained at each stage, in the design of selective, potent, small-molecule for drug candidates (Andricopulo & Montanari, 2005).

3.1.2 Methods

Protein-ligand interactions play important roles in structure-based drug design (SBDD). In our research work, structure-based drug design method was applied to identify hit compounds for the COX enzyme. Here, the commercially available NSAID, celecoxib, was docked into the COX receptor enzyme. Several modifications were made to the functional groups that interacted with the amino acid residues at the binding site of the receptor protein. Analogues of celecoxib were prepared using the Chemdraw software and docked onto the active site of COX enzymes using the Autodock software. Modifications were carried out at the docked celecoxibe to obtain better steric compatibility and the ADMET properties following the method of (Shankar *et al*., 2012).

In silico design was done based on the celecoxib structure docked in the COX enzymes by changing various functional groups in celecoxib which interact with various amino acid residues at the active sites for both COX-1 and CO-2.

3.2   *In Silico* Studies

3.2.1   Introduction

In 1960s, computational molecular modelling was developed, and since it has become more and more common and is now frequently used in the molecular design area. Earlier researches have described the application of computational molecular modelling softwares for creating new molecule models (Kitchen *et al.*, 2004) in the advancement of new drugs like selective inhibition of COX-2, drugs (Kurumbail *et al.*, 1996), anti-fungal drugs (Baginski *et al.*, 2005), and anti-cancer agents (Bartulewic *et al.,* 2000).

3.2.2   Methods

Prediction of druggability of the designed molecules was performed based on Lipinski's rule of Five, and ADMET effects were predicted using ADMET descriptors in Discovery Studio 3.0 (Accelrys, San Diego, CA, USA). Autodock 4.2.1 program was employed to perform the molecular docking studies on a python script. Chemdraw Ultra 12 program was used to draw the two-dimensional structures of the molecules. Chemdraw 3D was used to convert the 2D structures into 3D. Energy minimization for the structures was carried out with Hyperchem Pro 6.0 software (Hyper-cube Inc.), with PM3 Semi-empirical method by applying the steepest descent and conjugate gradient procedures (termination conditions set to a maximum of 500 cycles or 0.1 kcal/Å mol rms gradient). Discovery Studio 3.0 visualiser was used as visualization tools to view and locate the active site of the enzyme and binding interactions. The Ligplot

programme was also used to check the hydrogen bonding and hydrophobic interactions between receptor and ligand's atoms.

3.2.3 Docking of Standard Ligand

Crystal structures of COX-1 & 2 enzymes (Pdb code: 1CQE & 1CX2, respectively) (Picot *et al*., 1994; Kurumbail *et al*., 1996; Sperandio da Silva *et al*., 2005), were downloaded from the Brookhaeven Protein Data Bank (PDB; http://www.rcsb.org/pdb/). The protein PDBid: 1CQE is the crystal structure of COX-1 enzyme co-crystallized with flurbiprofen NSAID. The protein PDBid: 1CX2 is the crystal structure of COX-2 enzyme co-crystallized with SC-558, which is a potent and selective inhibitor of COX-2. The active sites of 1CQE & 1CX2 were located, the inhibitor molecules were carefully removed from the active sites, and the resulting protein crystal structures were used for docking study.

3.2.4 Automated Flexible-Ligand Docking

Autodock 4.2.1 software was employed to prepare the protein pdb extended format by adding polar hydrogens and Gasteiger charges. A three-dimensional affinity grid box was set from the center of the inhibitor molecules. The proposed docking methodology was validated by re-docking the inhibitor SC-558 into the active site of 1CX2. A Lamarckian genetic algorithm was employed for the conformational searching. A population size of 150 and 250,000 energy assessments were used for 100 search runs. The grid box, with grid spacing of 0.375 Å and dimension of $190 \times 218 \times 198$ points along the x, y, and z axes, was centered on the macromolecule. After the docking searches were achieved, clustering histogram analyses were carried out based on an rmsd (root-mean-square deviation) of not more than 1.5 Å. The conformation with the lowest docked energy was selected from the most populated cluster (Othman *et al.*,

2008). Re-docking of the inhibitor flurbiprofen into the active site of 1CQE was performed using the same protocol described above. The designed structures (**3a-h**) (Figure 3.1) were then docked into the active sites of 1CX2 & 1CQE using the same procedure. Result analyses were done by studying the binding interactions, binding poses and binding energies of the docked structures from the docking log file of each compound.
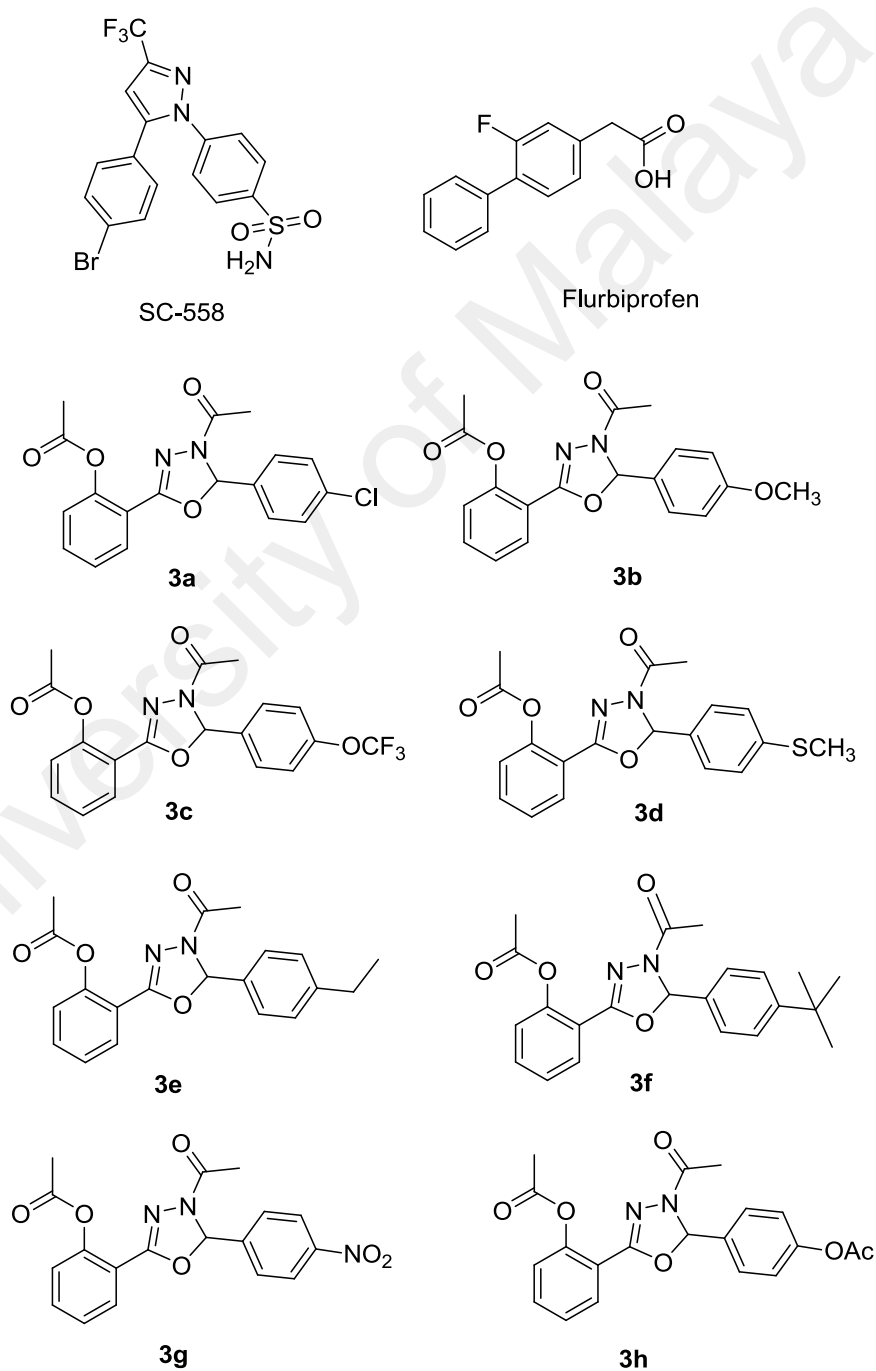
Figure 3.1: Designed Structures

3.2.5 **Running AutoGrid 4 and AutoDock 4.2**

AutoGrid 4 and AutoDock 4.2 softwares were installed in Ubuntu 10.04 Linux operating system of the workstation. AutoGrid 4 was run following instructions in the "AutoDock version 4.2" user's manual (Morris *et al*., 2010) using the command line:

autogrid4 –p protein.gpf –l protein.glg

and AutoDock 4.2 was run using the command line:

autodock4 –p ligand.dpf –l ligand.dlg

where protein.gpf is the input file (grid parameter file) for the protein molecule, protein.glg is the grid log file (protein as output file to generate maps and grid data file), ligand.dpf is the docking parameter file (input file) for the ligand, ligand.dlg is the ligand output file as docking log file

3.2.6 **Analyses of Results**

At the completion of the docking jobs, the compounds were ranked based on the lowest estimated mean free energy of binding (ΔG_{bind}) coupled with the largest NumCl (for more details, see Appendix A). ΔG_{dock} was calculated by applying Autodock 4.2 software, while the inhibition constant ($K_{i\,dock}$) was calculated using the formula (Morris *et al*., 1998).

$$K_{i\,dock} = e^{\Delta Gdock/RT}$$

$$\Delta G_{dock} = R\,T\,ln\,K_i$$

$$\Delta G_{bind} = - R\,T\,ln\,K_i$$

where R is the gas constant, 1.987 cal K^{-1} mol^{-1}, and T is the absolute room temperature, 298.15 K.

The number of different conformations that were grouped into the same cluster (NumCl) was used to indicate the probability of a specific conformer to interact with the target macromolecule, where the higher NumCl value refers to an increased possibility of interaction. The docked conformational cluster with the largest NumCl was selected as the best binding conformation. In the case where there were two or more clusters with comparable values for the largest NumCl, the cluster that displayed lower ΔG_{dock} was selected for additional analysis (see Appendix A). All the best binding conformations were then submitted for interaction analyses using the Ligplot 4.5.3 software.

3.3 Results & Discussion

3.3.1 Design & SAR Study

1,3,4-oxadizoline structure was observed to be favourable molecular template as selective inhibitor for COX-2 enzyme due to their similarity to the celecoxib's pyrazole core (Figure 3.2). To validate this observation, several 1,3,4-oxadiazoline derivatives were docked onto the active sites of the COX-2 and COX-1 enzymes.
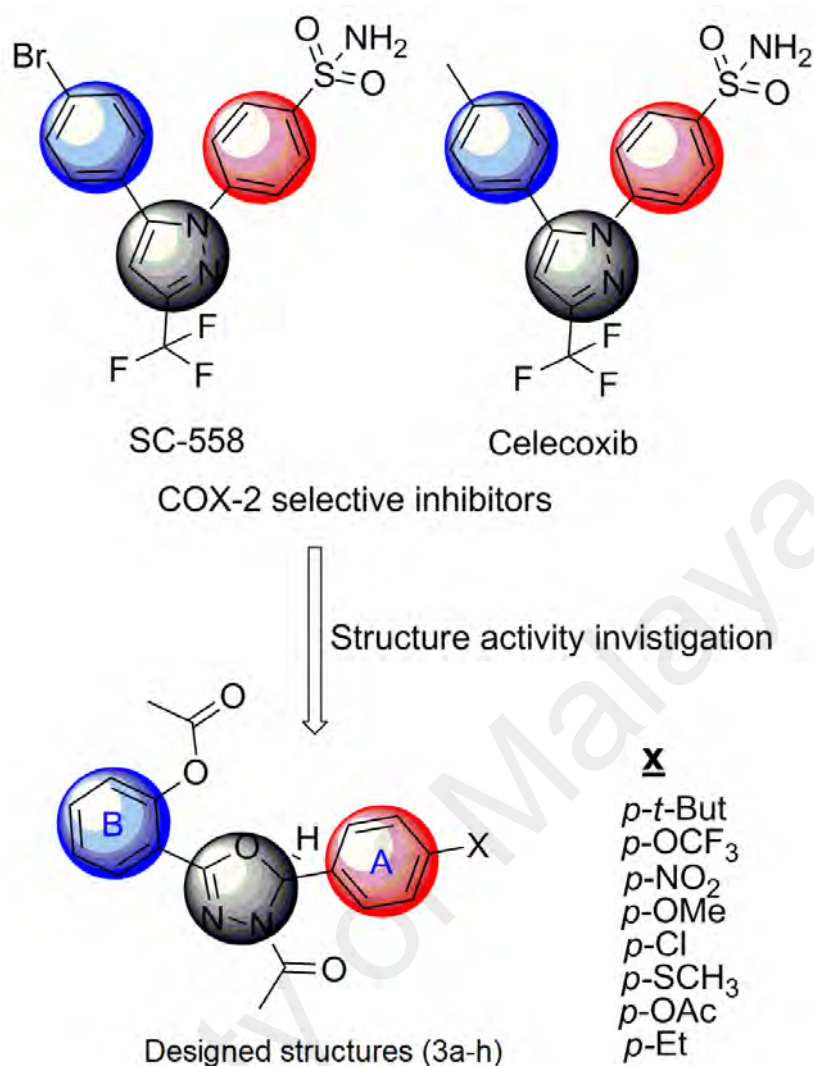
Figure 3.2: Representative examples of selective COX-2 inhibitors and the designed 1,3,4-oxadiazoline derivatives (**3a-h**)

The structure of 1,3,4-oxadiazoline possesses the essential criteria of a selective COX-2 inhibitor, which are the adjacent aryl groups attached to a heterocyclic core as in the structure of celecoxib (Figure 3.2). Different substituents were used in place of celecoxib's SO_2NH_2 group on the phenyl ring (A). A bulky acetyl group on the oxadiazoline scaffold replaced the CF_3 group on the imidazolone of celecoxib. All structures (**3a-h**) (Figure 3.2) contained an acetyl group on the *ortho* position of the second aryl group (B) to enhance their effectiveness relative to the natural anti-inflammatory salicylic acid. Plausibly, this provided a pharmacokinetic advantage to the structures, as in aspirin, by forming a covalent bond between acetyl group with the

Ser530 residue in the COX enzyme's active site and blocks the synthesis of prostaglandin (Brune & Hinz, 2004; Dovizio *et al.*, 2012).

3.3.2 Lipinski's Rule of Five and ADMET Properties

Most drug failures in the drug development were due to poor pharmacokinetic properties and toxicity. To minimise this problem, the structures (**3a-h**) were predicted for the drug-likeness / druggability according Lipinski's rule of Five and ADMET properties.

Lipinski's rule of Five is used to predict the oral bioavailability, but not the pharmacological activity, of a compound using the molecular weight (Mw), octanol/water partition coefficient (Log P), hydrogen bond acceptors and hydrogen bond donors as its criteria (Veber *et al.*, 2002). Compounds with molecular weight less than 500, hydrogen bond acceptor less than 10, hydrogen bond donor less than 5, and a log P value of less than 5 were considered to be orally bioavailable. In the current study, all the parameters of the compounds **3a-h** were consistent with the Rule of Five 5 as shown in Table 3.1. According to the Lipinski's rule of Five, three violations in the compounds **3a-h** are allowed in the molecular docking studies except all violations are in compound **3a** (Ekins *et al.*, 2005; Lipinski, *et al.*, 2001; Valasani *et al.*, 2014). Docking studies and the Lipinski's Rule of Five facilitate drug development by reducing expensive post clinical experiments.

Table 3.1: Molecular descriptors for designed structures (**3a-h**), SC-558, celecoxib and flurbiprofen in the prediction of the Lipinski's rule of 5

Compound	No.	MW	log P	No. H-Acceptor	No. H-Donor	No. of criteria met
		<500	<5	<10	<5	at least 3
SC-558	*	446.242	4.69	3	1	All
Celecoxib	*	381.372	4.43	3	1	All
Flurbiprofen	*	243.253	2.21	2	0	3
3f	1	380.437	4.1	7	0	3
3c	2	408.328	4.81	6	0	3
3g	3	369.328	2.6	7	0	3
3b	4	402.421	2.22	5	0	3
3a	5	358.776	3.35	7	1	All
3d	6	370.422	3.23	5	0	3
3h	7	382.367	2.46	5	0	3
3e	8	352.384	3.63	7	0	3

* Standard drug, MW; moleculer waight, log P; polar surface area, No. H-Acceptor; number of hydrogen bond acceptor, No.H-Donor; number of hydrogen bond donor

ADMET study was performed on compound **3a-h** using ADMET descriptor algorithm of Accelrys Discovery Studio 3.1, based on aqueous solubility (AS), human intestinal absorption (HIA), blood-brain barrier (BBB), cytochrome P450 2D6 (CYP2D6), plasma protein binding (PPB), and hepatotoxicity (HT) descriptors.

Table 3.2 shows the classification of ADMET descriptors for the chemical structure of the molecules based on the accessible drug information: ADMET absorption level predicts human intestinal absorption (HIA) after oral administration. HIA was based on the Alog P (ADMET Alog P98) and polar surface area (PSA-2D) calculations. The absorption levels are defined by 95% and 99% confidence ellipses. In the ADMET-PSA-2D planes ADMET aqueous solubility level predicts the solubility of each compound in water at 25°C. ADMET blood brain barrier (BBB) descriptor predicts the blood-brain penetration of a molecule after oral administration (Egan & Lauri, 2002). This model was developed from a quantitative linear regression model for the prediction of blood-brain penetration, as well as 95% and 99% confidence ellipses in the ADMET

PSA 2D and ADMET AlogP98 plane (Ponnan *et al.*, 2013). ADMET plasma protein binding (PPB) model predicts whether a compound is likely to be highly bound to carrier proteins in the blood and it is a significant descriptor that controls a drug's effectiveness as only the unbound part is responsible for pharmacological properties (Leong *et al.*, 2014). The lipophilicity and the ionization conditions of a molecule are significant for plasma protein binding and take part to the various conducts of acidic and basic drugs in the plasma. Additionally, the presence of aromatic rings and H-bonds may lead to an increase the in PPB capabilities of the molecules (Zhivkova & Doytchinova, 2012). There are two levels of binding: values more than 90% are classified as binders (true), and values less than 90% are classified as non-binders (false) (Votano *et al.*, 2006). ADMET CYP2D6 binding predicts inhibition by cytochrome P450 2D6 (CYP2D6) enzyme by exploiting the 2D chemical structures as input, as well as a probability estimate for the prediction (Susnow & Dixon, 2003). CYP2D6 involves a type of enzyme which stimulates the oxidative metabolism of drugs in the liver. It can either metabolize a drug from its effective form into its inefficient metabolites or transform an inefficient drug into its effective metabolites. ADMET hepatotoxicity predicts the potential human hepatotoxicity compounds. Predictions are based on an ensemble recursive partitioning model of training compounds known to exhibit liver toxicity or to trigger dose-related elevated aminotransferase levels in more than 10% of the human population (Cheng & Dixon, 2003).

Most of drug failures at the early stage are due to unwanted pharmacokinetics and toxicity issues. If these problems could be confronted even earlier, it would be really useful for the drug discovery development. Consequently, the use of *in silico* system to calculate ADMET properties is considered as an initial step in this orientation to study the novel chemical structures in order to avoid wasting resourceful time on lead

candidates that would be toxic or metabolized by the body into inactive metabolites and unable to cross membranes.

Table 3.2: ADMET descriptors and their rules/keys**.**

ADMET absorption level (human intestinal absorption) HIA	
Level	**Description**
0	Good absorption
1	Moderate absorption
2	Low absorption
3	Very low absorption

ADMET aqueous solubility level		
Level	**Value**	**Description**
0	$\log (S_m) < -8.0$	Extremely low
1	$-8.0 < \log (S_m) < -6.0$	No, very low, but possible
2	$-6.0 < \log (S_m) < -4.0$	Yes, low
3	$-4.0 < \log (S_m) < -2.0$	Yes, good
4	$-2.0 < \log (S_m) < 0.0$	Yes, optimal
5	$0.0 < \log (S_m)$	No, too soluble
6	-1000	Warning: molecules with one or more unknown AlogP98 types

ADMET (blood brain barrier penetration level) BBB	
Level	**Description**
0	Very High
1	High
2	Medium
3	Low
4	Undefined
5	Warning molecules with one or more unknown AlogP calculation

ADMET CYP2D6	
Predicted class	**Value**
False	Noninhibitor
True	Inhibitor

ADMET hepatotoxicity	
Predicted class	**Value**
False	Nontoxic
True	Toxic

ADMET (plasma protein binding level) PPB		
Predicted class	**Value**	**Description**
False	Unbinding	Binding is <90%
True	Highly bound	Binding is ≥90%

S_m = Molar solubility.

Herein Table 3.3 together with a bi-plot (Figure3.3) summarizes the pharmacokinetic profile of all the molecules (**3a-h**) obtained from the ADMET studies.

Table 3.3: Prediction of ADMET properties of the designed 1,3,4-oxadiazoline analogues using Discovery Studio 3.1

Compound	No.	Absorption level (HIA)	Solubility level	BBB level	PSA-2D*	AlogP98*	Hepatotoxicity Prediction	CYP2D6 Prediction	PPB Prediction
SC-558	*	good	1	1	77.75	4.69	true	false	true
Celecoxib	*	good	1	2	77.75	4.43	true	false	true
Flurbiprofen	*	good	3	2	34.6	2.21	true	true	true
3f	1	good	2	1	67.137	4.09	true	false	true
3c	2	good	2	1	67.1	4.8	true	false	true
3g	3	good	3	4	109.96	2.58	true	false	true
3b	4	good	3	3	101.73	2.216	true	false	true
3a	5	good	2	2	67.137	3.354	true	true	true
3d	6	good	2	2	67.137	3.232	true	false	true
3h	7	good	3	3	93.368	2.458	true	false	true
3e	8	good	2	2	67.137	3.632	true	false	true
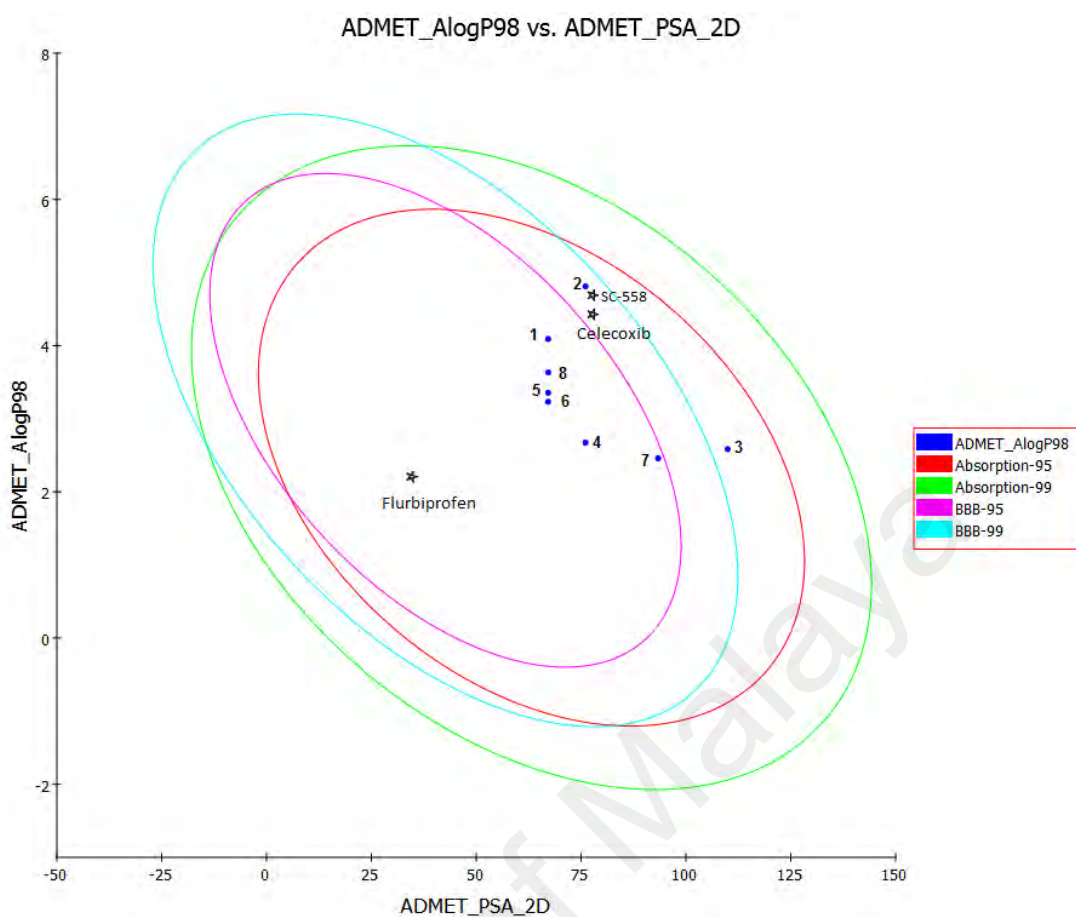
Figure 3.3: A biplot showing the results obtained for the prediction of drug absorption for the designed compounds 3a-h considered for selective COX-2 inhibitions. Discovery studio 3.1 ADMET Descriptors, atom-type partition coefficient (ALogP98) is plotted for each compound against their corresponding calculated 2D polar surface area (PSA 2D) in A^2. The numbers 1, 2, 3, 4, 5, 6, 7 and 8 are the temporary code names for **3f**, **3c**, **3g**, **3b**, **3a**, **3d**, **3h** and **3e**, respectively. The area surrounded by the ellipse is a prediction of good absorption with no violation of ADMET properties. The 95% and 99% confidence limit ellipses related to the Blood Brain Barrier (BBB) and Intestinal Absorption (HIA) models are based on the absorption model of Egan *et al.*, 2000.

The bi-plot in Figure 3.3 shows the two analogous 95% and 99% confidence ellipses corresponding to HIA and BBB models. The upper limit of PSA_2D value for the 95% confidence ellipsoid is at 131.62, while the upper limit of PSA_2D value for the 99% confidence ellipsoid is at 148.12 (Egan *et al.*, 2000).

PSA was shown to have a reverse correlation with percent human intestinal absorption and consequently cell wall permeability (Palm *et al.*, 1997). The fluid mosaic form of cell membrane shows that the membrane phospholipid bilayer has the capability

of hydrophobic and hydrophilic interactions and because of that, lipophilicity is also recognized as an essential property for drug design. Lipophilicity could be considered as the log of the partition coefficient between n-octanol and water (log P). Although log P is commonly used to assess a compound's lipophilicity, the reality that log P is a proportion elevates a concern about the use of log P to estimate hydrophilicity and hydrophobicity. Therefore, the data of H-bonding features as acquired by calculating PSA could be taken into account along with log P calculation (Egan *et al.*, 2000). Therefore, to accurately predict the cell permeability of the compounds under study, a model containing the descriptors AlogP98 and PSA 2D with a bi-plot involving 95% and 99% confidence ellipses was used (Ponnan *et al.*, 2013). The 95% confidence ellipse represents the region of chemical space where it can be expected to find well absorbed compounds ($\geq 90\%$) 95 out of 100 times. The 99% confidence ellipse represents the region of chemical space with compounds having excellent absorption through the cell membrane. The 99% confidence ellipse is bigger than the 95% confidence ellipse (Figure 3.3) because, to increase the possibility that the ellipse contains more compounds, the space enclosed by the ellipse must increase (Ponnan *et al.*, 2013). According to the model for a compound to have an optimum cell permeability, the following criteria should be followed (PSA $< 1 0$ ^{2} and AlogP98 $<$ 5) (Egan *et al.*, 2000). All the compounds showed polar surface area (PSA) < 140 ^{2} and AlogP98 < 5 (Table 3.3).

Table 3.3 shows that majority of the compounds have high, medium, low, and undefined values for BBB penetration levels (levels 1, 2, 3 and 4 as mentioned in Table 3.2). In the bi-plot for BBB descriptor (Figure 3.3), structures **3a**, **3b**, **3d**, **3e**, **3f** and **3h** seem to fall inside the 95% ellipse, while structure **3c** is within the 99% ellipse, indicating that all the structures would be able to penetrate the BBB, with moderate to

high BBB penetration. However, structure **3g** falls outside the 99% ellipse indicating that structure **3g** have undefined value for BBB penetration.

Additionally, the low solubility and low permeability for drugs lead to their the poor oral bioavailability (Savjani *et al*., 2012). So, adequately aqueous solubility and human intestinal absorption (HIA) are significant change for better delivery of the drugs in the human body. As can be seen in Table 3.3, compounds **3a-h** showed low to good aqueous solubility levels (levels 2 and 3 as mentioned in Table 3.2), and good absorption (HIA). Compounds **3a-h** fall within the 95% ellipse (Figure 3.3), showing evidence that they could be valid candidates for oral drugs. In the meantime, in spite of showing good HIA values, molecules **3a**, **3c**, **3d**, **3e** and **3f** exhibit low aqueous solubility.

The model classifies the hepatotoxicity prediction of the compounds as either "toxic" (true) or "nontoxic" (false) (Table 3.2). Our results indicate that all compounds **3a-h** are toxic to the liver (prediction true, Table 3.3) similar to most common NSAIDs that are associated with drug-induced liver injury (Aithal & Day, 2007). It is therefore, recommended that experiments should be carried out to seek the actual hepatotoxic influence of the compounds **3a-h**, as well as to ascertain their favorable therapeutic doses. Recent studies suggested many genetic factors that play vital roles in the formation and accumulation of diclofenac metabolite with increased vulnerability to hepatotoxicity (Aithal & Day, 2007). However, there are no specific markers currently available to recognize those at risk of NSAID-induced hepatotoxicity, or those likely to develop liver failure. Hence, it is highly important to be cautious on the hepatotoxic potential of any NSAID. With raised awareness, surveillance and reporting of any case will lead to a better understanding of the risk factors and the pathophysiology of NSAID-induced hepatotoxicity (O'connor *et al*., 2003).

However, except compound **3a**, all compounds (**3b-h**) are predicted to be satisfactory with respect to CYP2D6 liver (with reference to Table 3.2), suggesting that **3b-h** are non-inhibitors of CYP2D6 enzyme, and indicating that compounds **3b-h** are well metabolized in Phase-I metabolism (Table 3.3). Finally, as presented in Table 3.3, the ADMET plasma protein binding (PPB) property prediction indicates that all of compounds **3a-h** are probable to be highly bound ($\geq$ 90%) to carrier proteins in the blood, in which case, high doses might then be essential to obtain therapeutic concentrations in treatments.

3.3.3 Ligand Binding Interaction

Insights into the differences between the binding sites of COX-1 and COX-2 obtained from X-ray crystal structure data (Kurumbail *et al*., 1996; Meade *et al*., 1993) provided useful guidelines that facilitated the design of the selective COX-2 inhibitors (Figure 2.6, p. 14). For instance, the COX-2 binding site has two extra pockets that are absent in the COX-1 binding site. This information is extremely significant and useful for designing COX-2 selective inhibitors. The difference in the COX-2 binding pocket arises due to a conformational alteration at Tyr355, that is attributed to the existence of Ile523 in COX-1 as compared to Val523 in COX-2 which has a smaller side chain (Meade, Smith, & DeWitt, 1993). In addition, it has been reported that the replacement of His513 in COX-1 by Arg513 in COX-2 plays a key role with relation to the H-bond network in the COX-2 binding site. Entry of ligands to the two pockets of COX-2 is regulated by His90, Gln192 and Tyr355 (Llorens, 1999). The interaction of Arg513 with the bound drug is a requirement for time dependent inhibition of COX-2 (Figure 3.4) (Garavito & DeWitt, 1999).
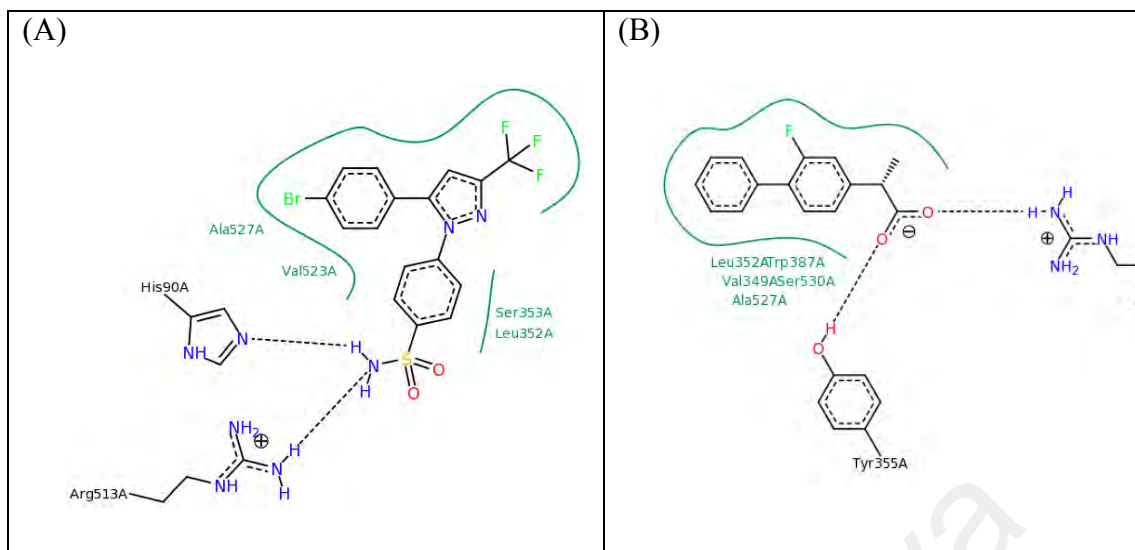
Figure 3.4: The active site of crystal structures of COX-1 & COX-2, (A); Interactions between drug (SC-558) and amino acids in the binding site of COX-2 (PDBid: 1CX2 (Kurumbail *et al.*, 1996). (B); Interactions between drug Flurbiprofen and amino acids in the binding site of COX-1 (PDBid: 1CQE (Picot *et al.*, 1994). Black dashed lines represent hydrogen bonds; green solid lines represent hydrophopic interactions.

AutoDock program was used to dock the structures **3a-h** into the active site of the COX-2 enzymes. The orientation of docked conformation of SC-558 (standard drug used in this study) was reproduced (Figures 3.5 & 3.6) with similar binding interaction as that of its original conformation in the crystal structure (Figure 3.5). In addition the *p*-sulfonyl moiety was observed to form hydrogen bonds with Arg513 and His90 (Figures 3.6).
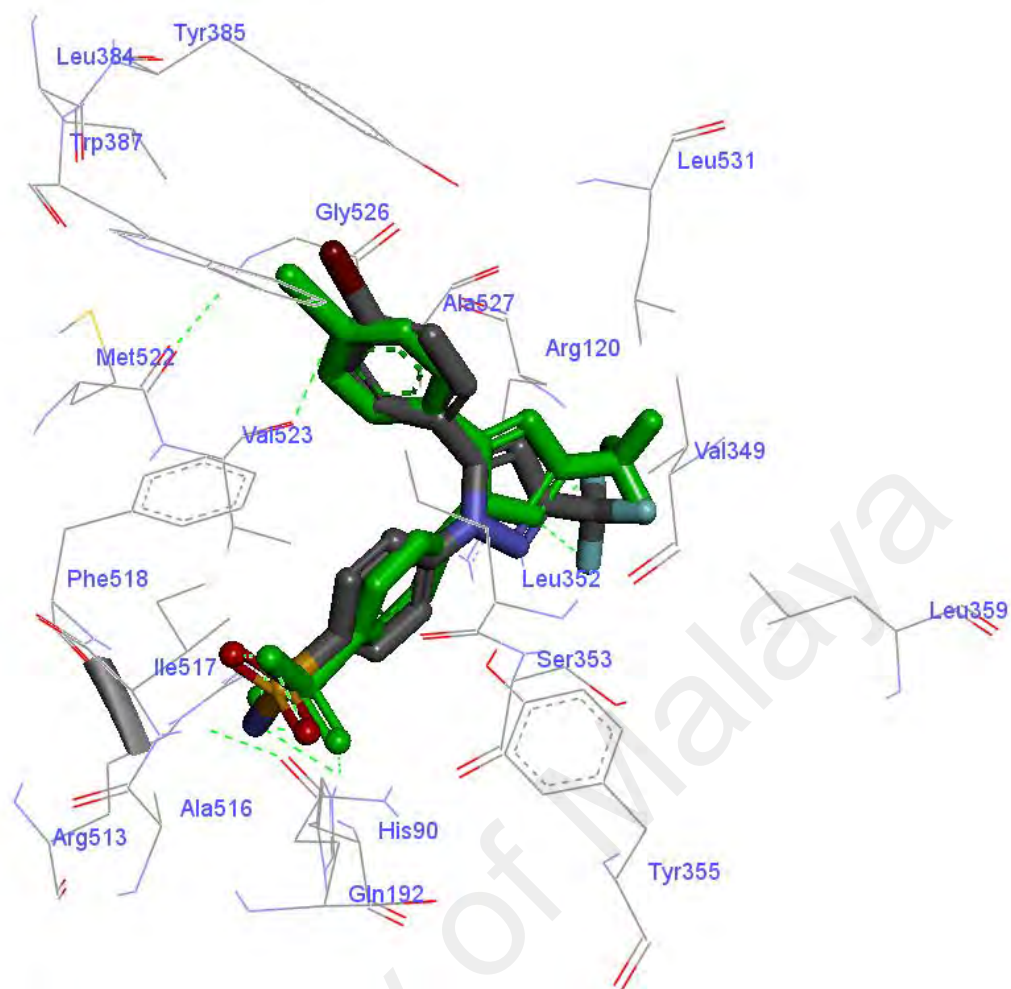
Figure 3.5: Diagram showing the superimposed poses of the re-docked SC-558 (green ball and stick model) and SC-558 co-crystallized with COX-2 (PDBid: 1CX2) (gray ball and stick model). The same positions of the drug reveals the accuracy of docking protocol used in this study.
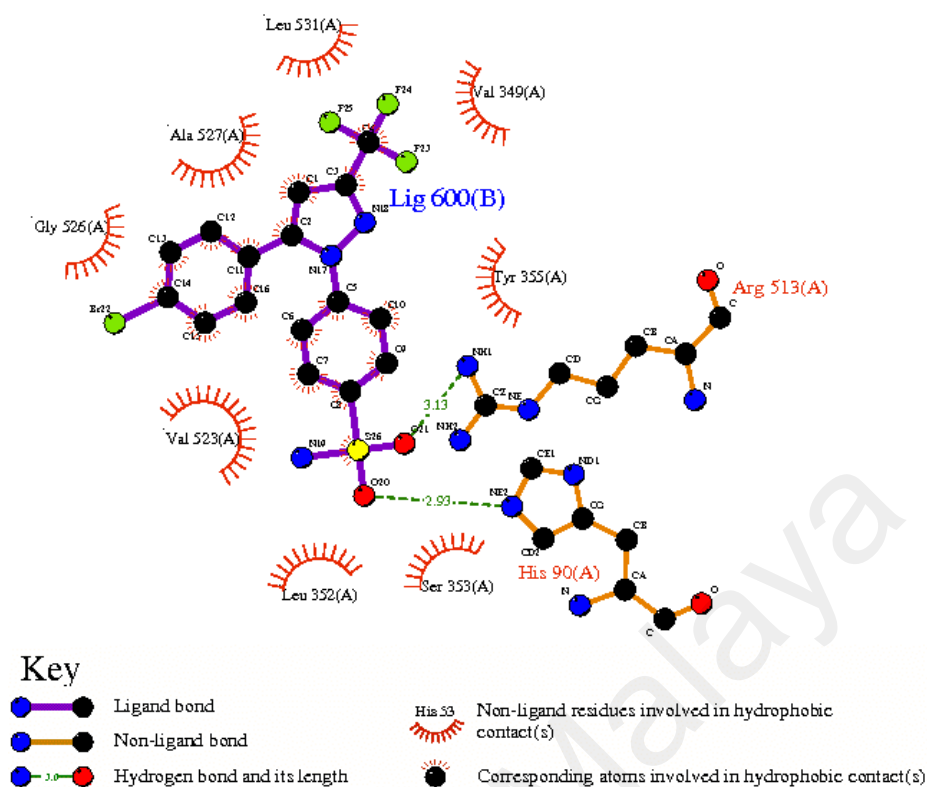
Figure 3.6: Hydrogen bonding and hydrophobic interactions between COX-2 and SC-558, Lig 600(B) is the temporary code name for ligand. (A) represents the amino acids belong to COX-2 enzyme.

Celecoxib, mostly interacts with COX-2 enzyme through hydrogen bonds between the carbonyl group and Arg513 and His90, and an arene-cation interaction with Arg120. Meanwhile, SC-558 only shows hydrogen bond interactions, with (Figure 3.5). It is worthy to mention that site-directed mutation study has demonstrated Tyr385 and Ser530 to be crucial residues for enzyme action and they play important roles in interaction between inhibitors and enzyme. Our docking results seemed to confirm this fact and are in agreement with that reported by Rowlinson (2003).

The designed compounds in the current study were found to have excellent binding affinity to COX-2 enzyme (Figure 3.7). The most stable docking model was chosen for each enzyme according to the lowest binding energy value (Appendix A). Docking results illustrated that all structures, except for structure **3g**, are in the appropriate position within the active site of COX-2 (Figure 3.7).

A (**3a**)
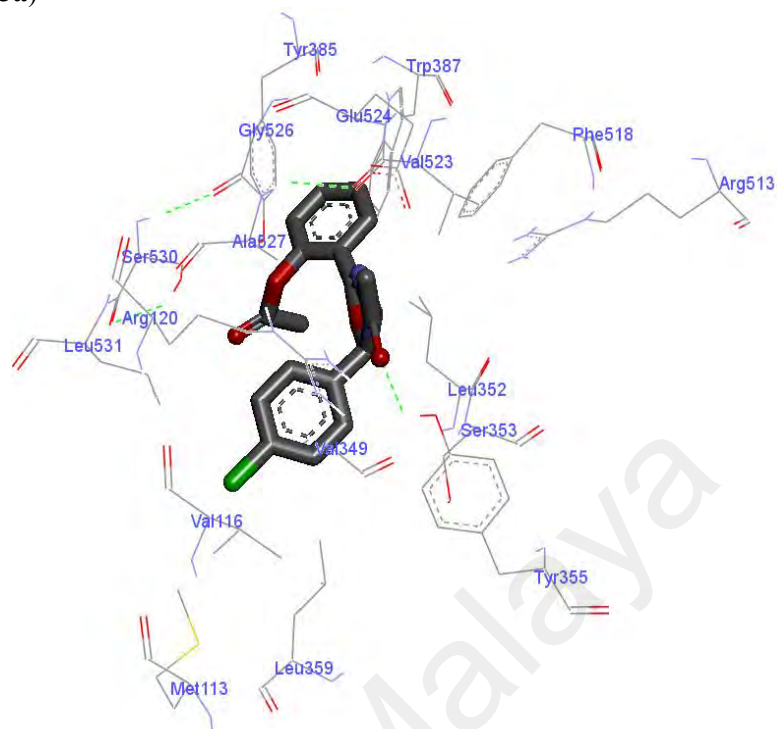
A"
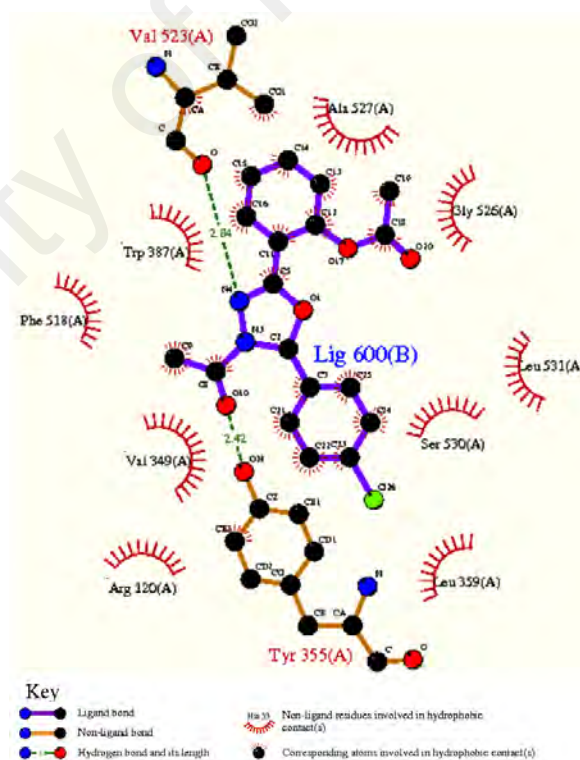
Figure 3.7: (A, B, C, D, E, F, G): Binding conformations generated by Discovery studio 3.1 of compounds 3a-h and their interactions with amino acid residues of COX-2 (PDBid: 1CX2). The hydrogen bonds are represented by the green dotted lines. (A", B", C", D", E", F", G"): Graphical results generated by Ligplot 4.5.3 software. It illustrates the hydrogen bond and hydrophobic interactions between 3a-h conformation and amino acid residues of ICX2. Lig 600(B) is the temporary code name for ligand. (A) is the temporary code name for protein.

B (3b)
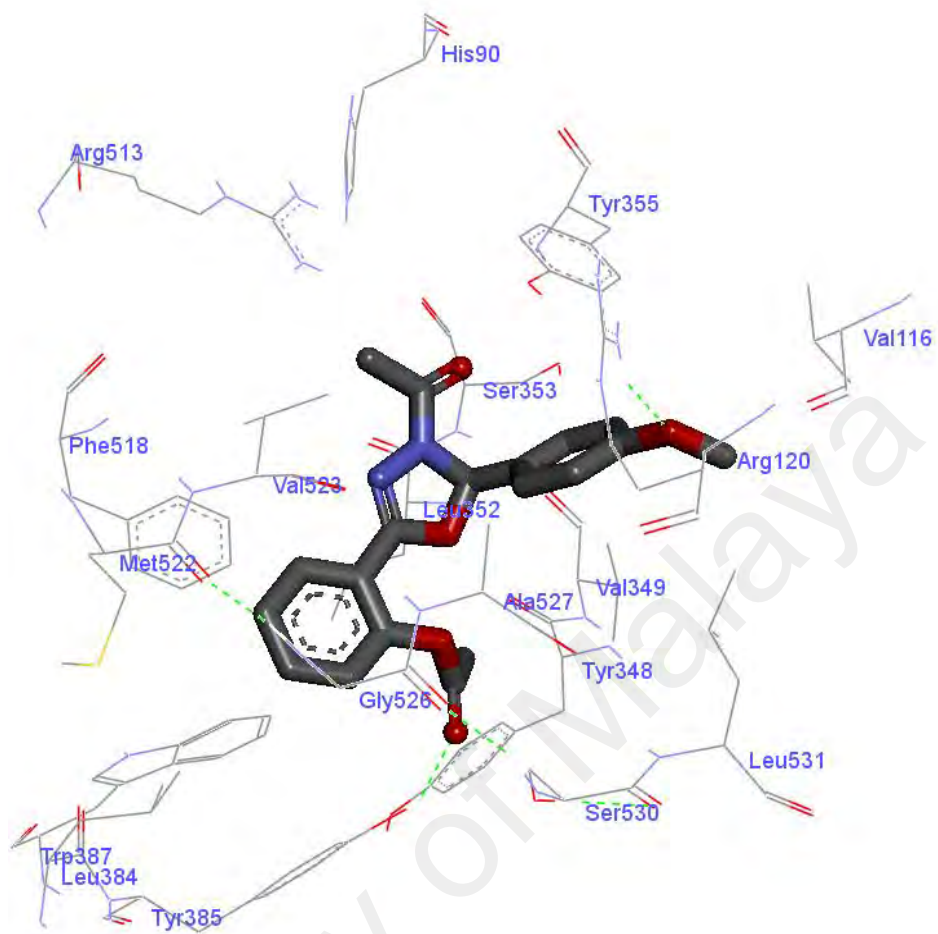
Figure 3.7, continued

B"
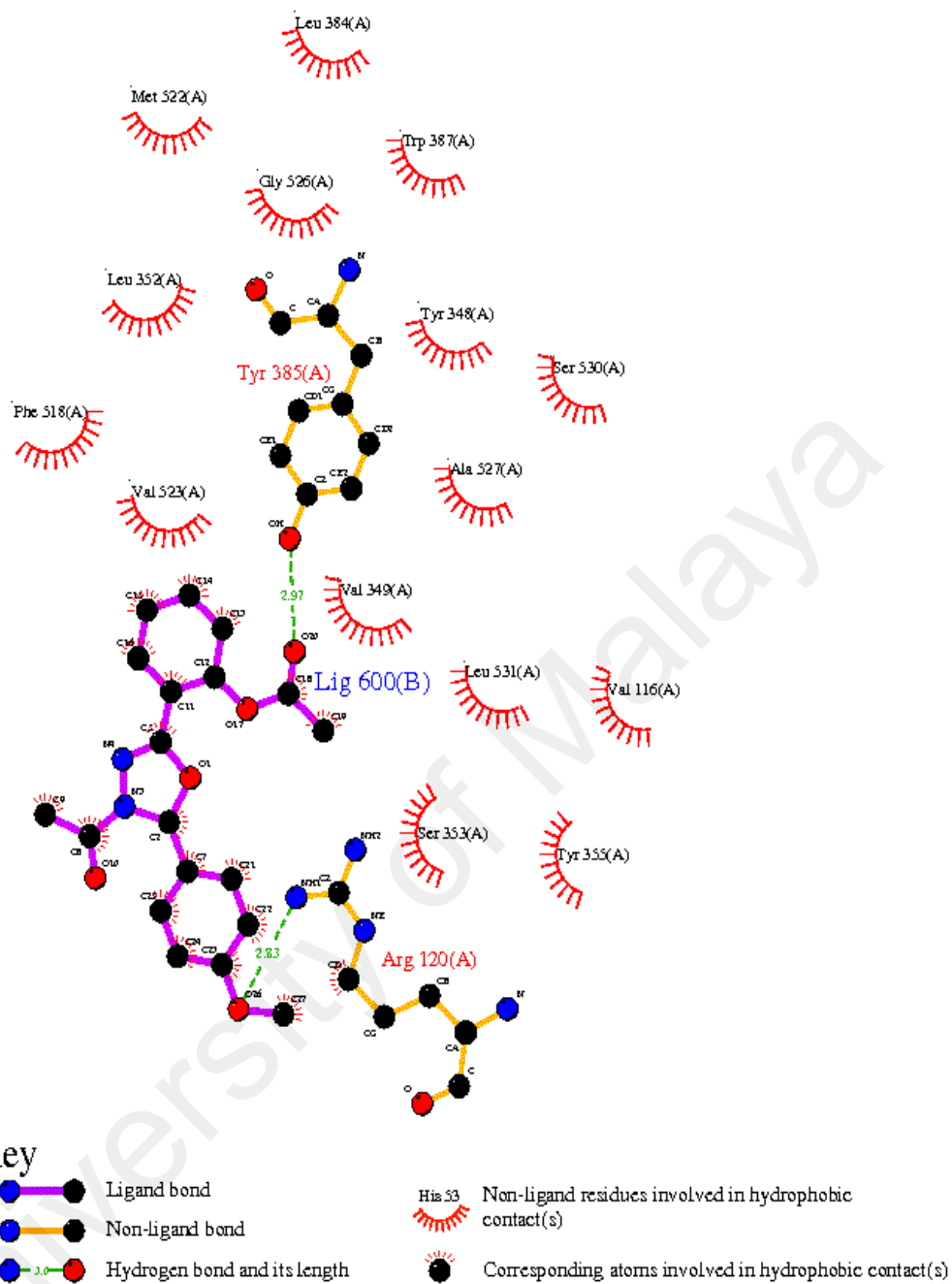
Figure 3.7, continued

C (3c)
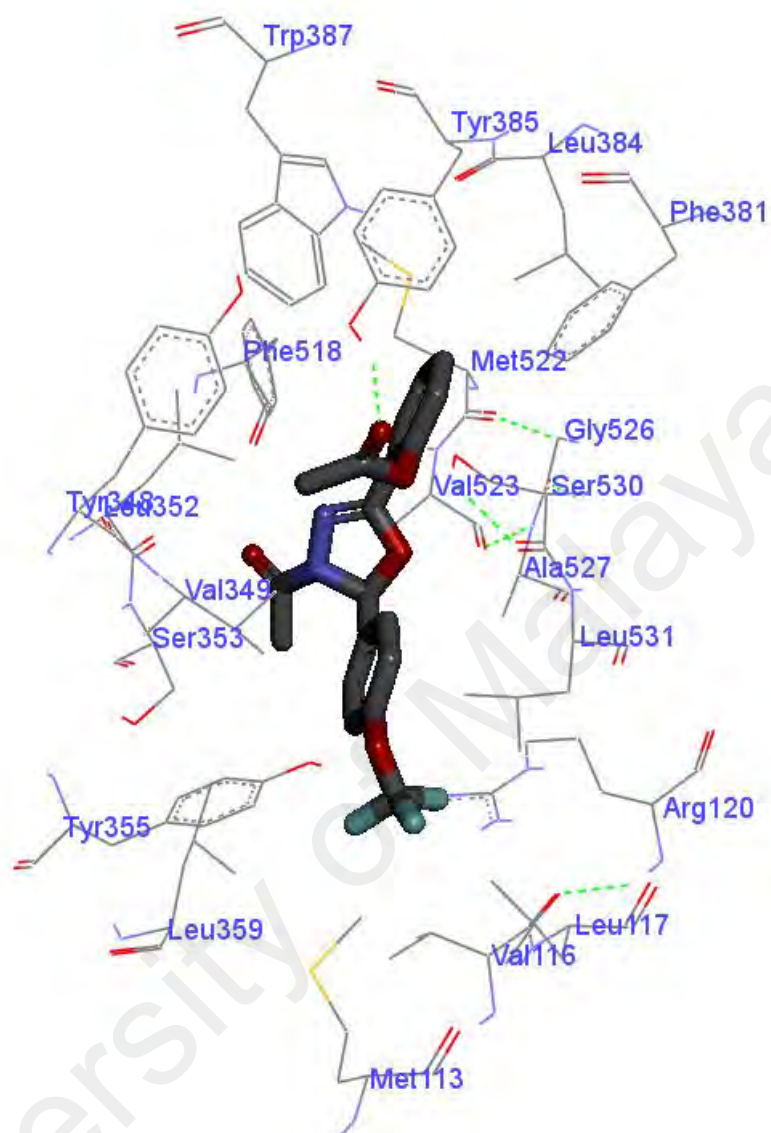
Figure 3.7, continued

C"
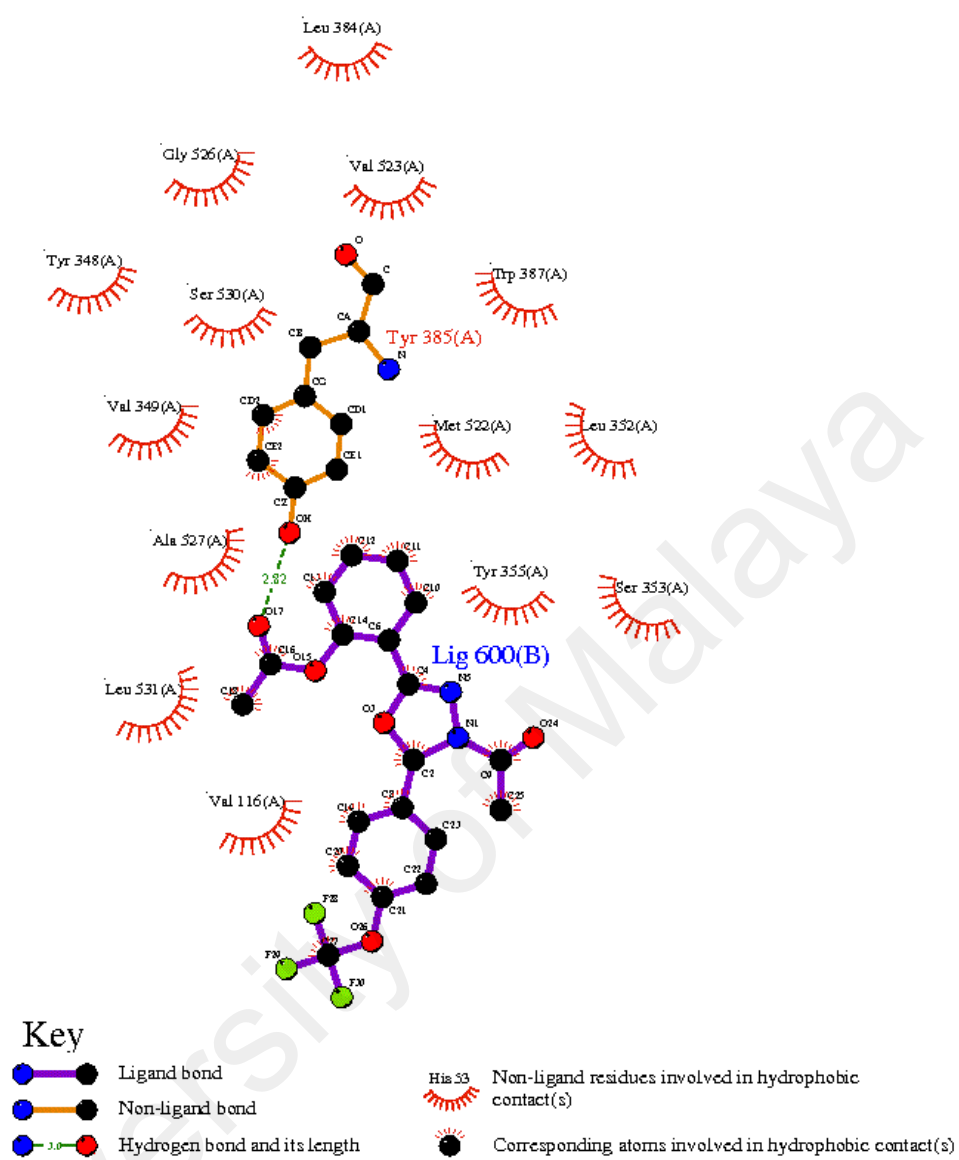
Figure 3.7, continued

D (3d)
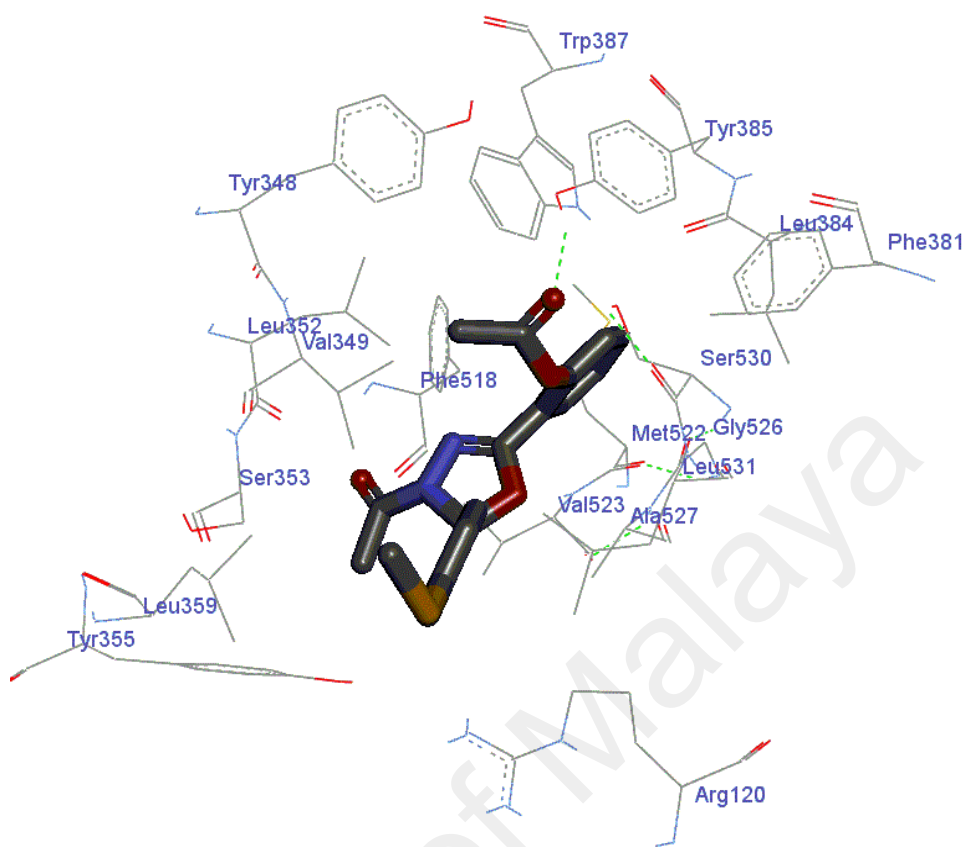
Figure 3.7, continued

D"
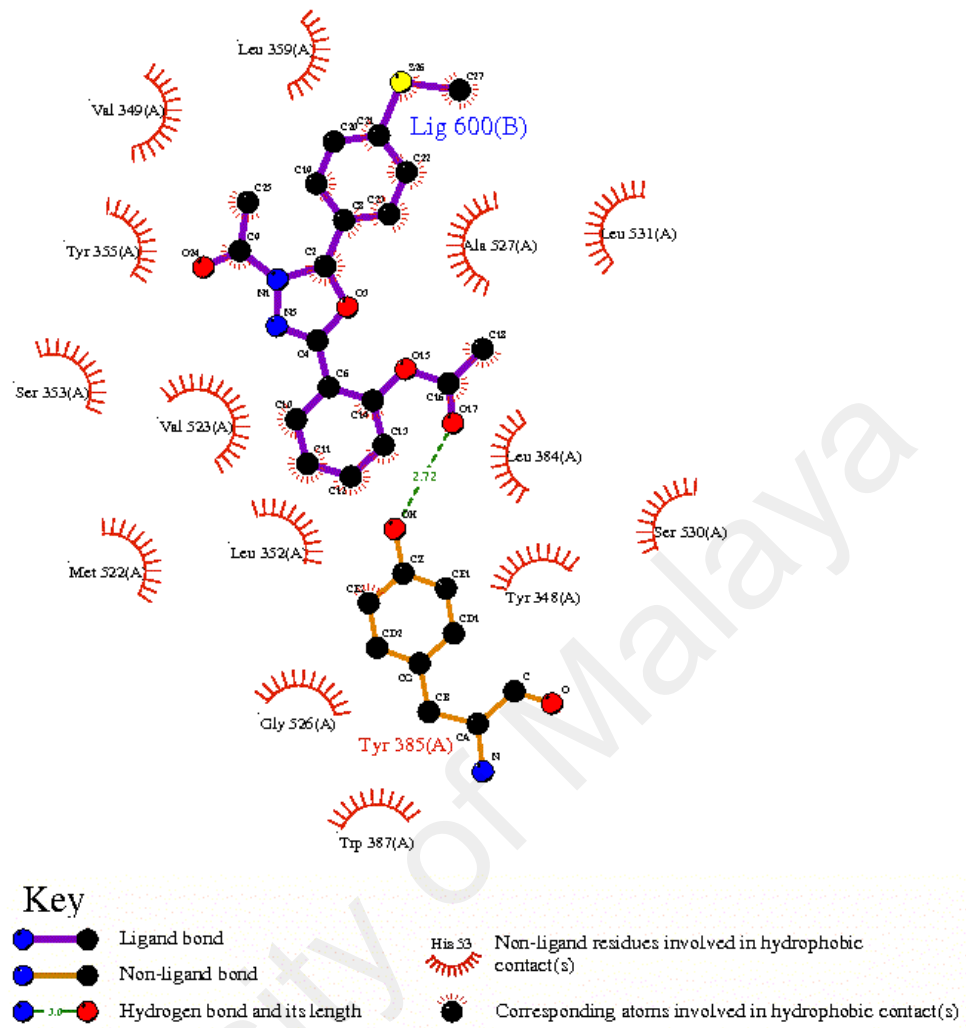
Figure 3.7, continued

E (3e)

Figure 3.7, continued

E"
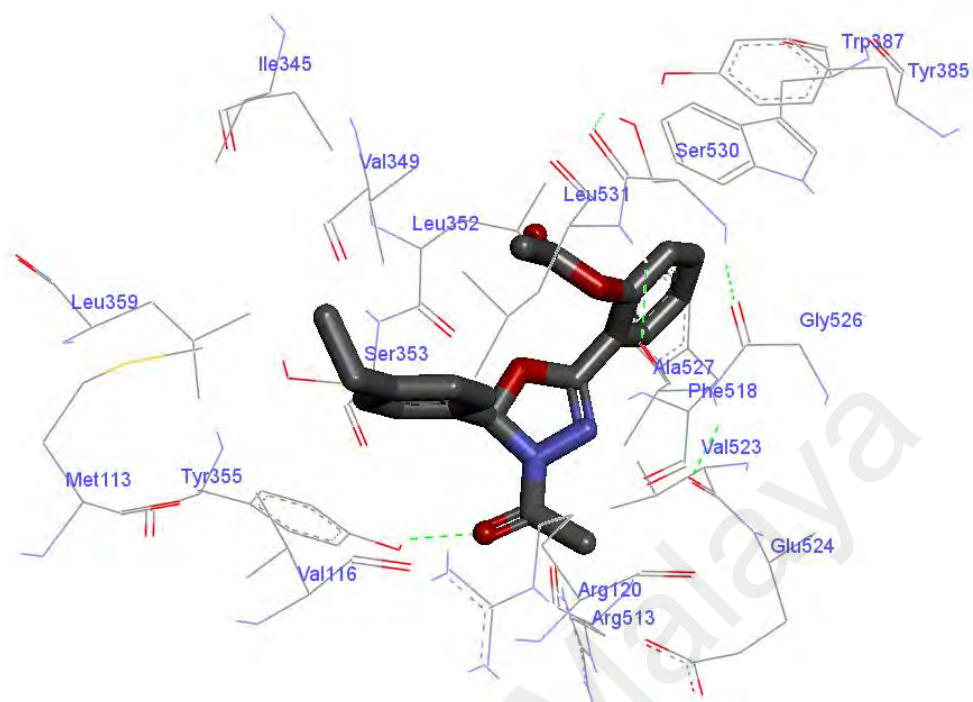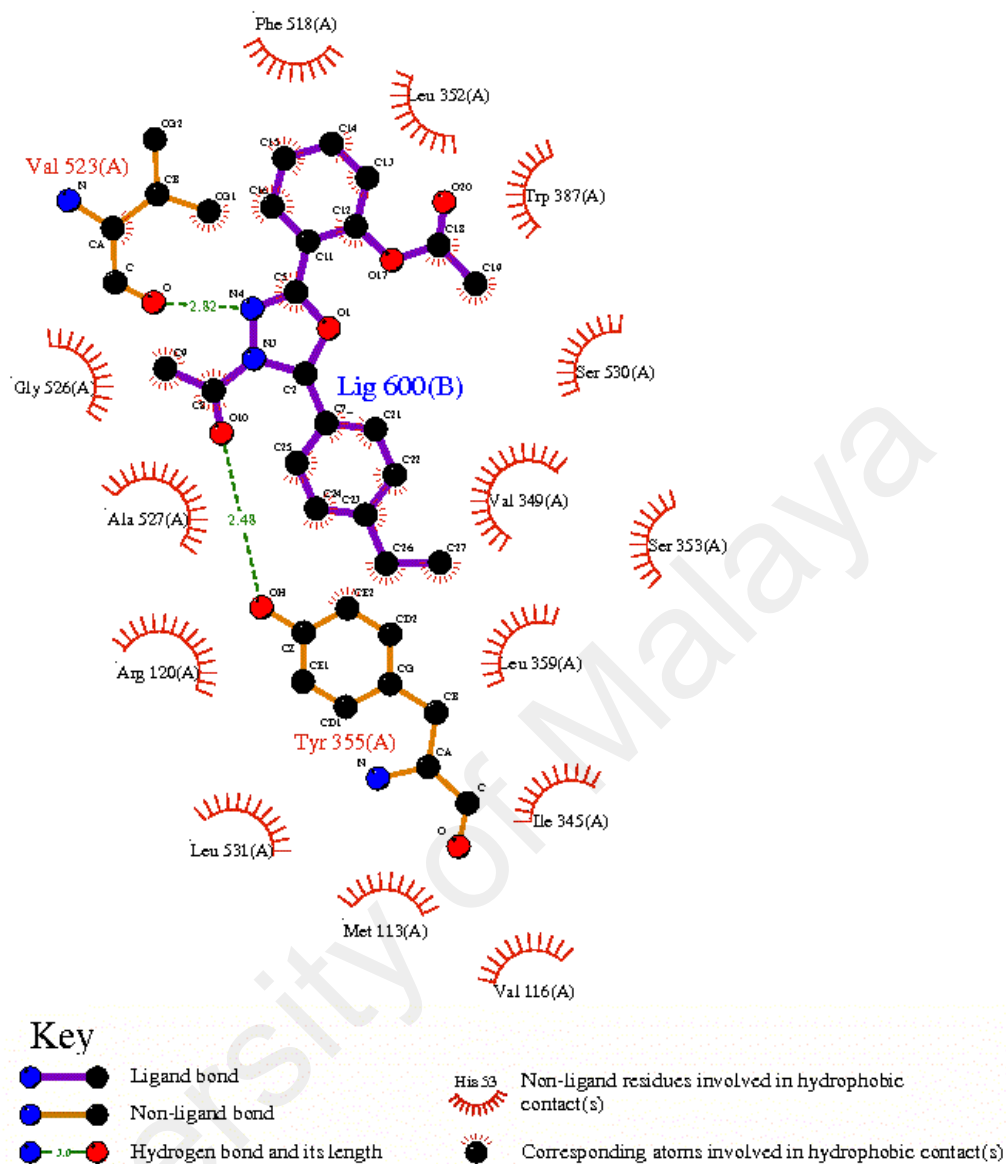
Figure 3.7, continued

F (3f)
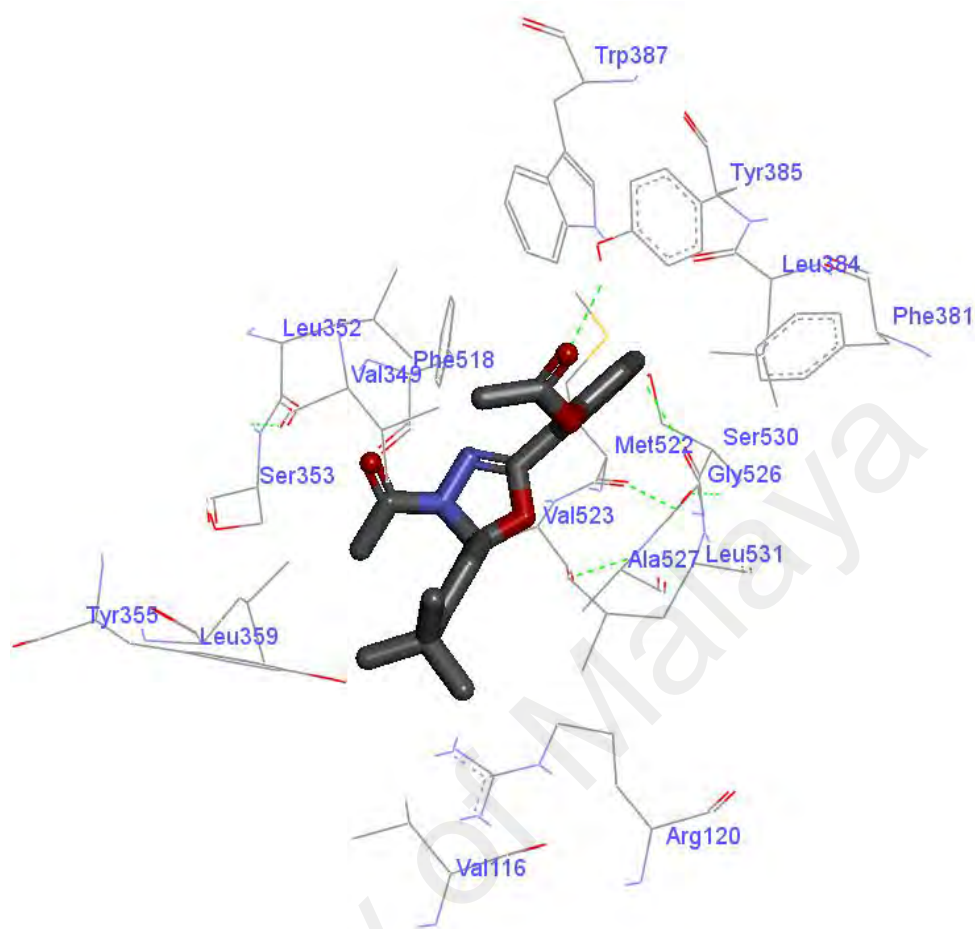
Figure 3.7, continued

F''
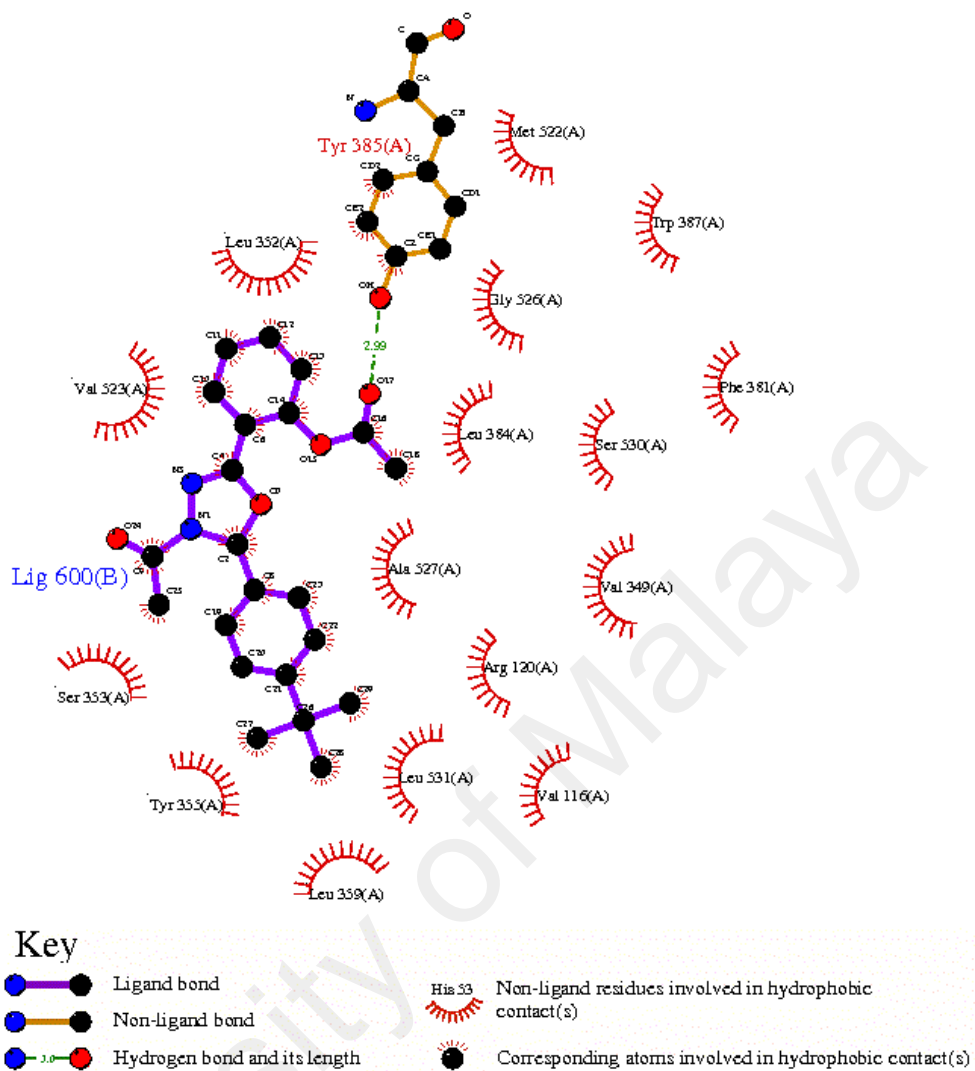
Figure 3.7, continued

G (3h)
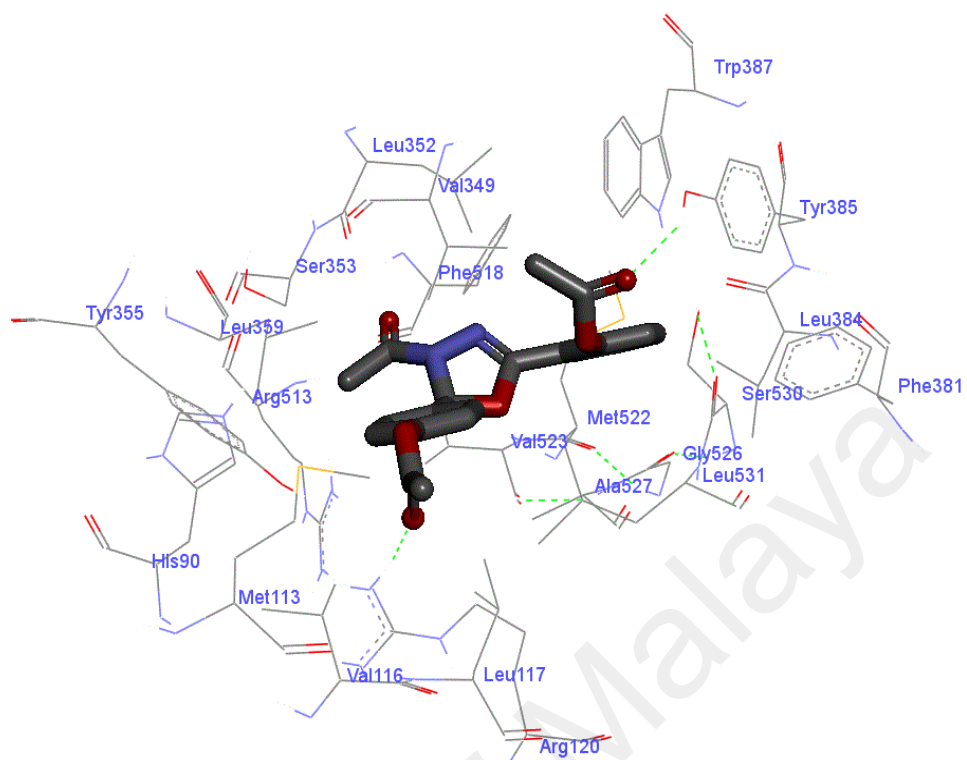
Figure 3.7, continued

G"
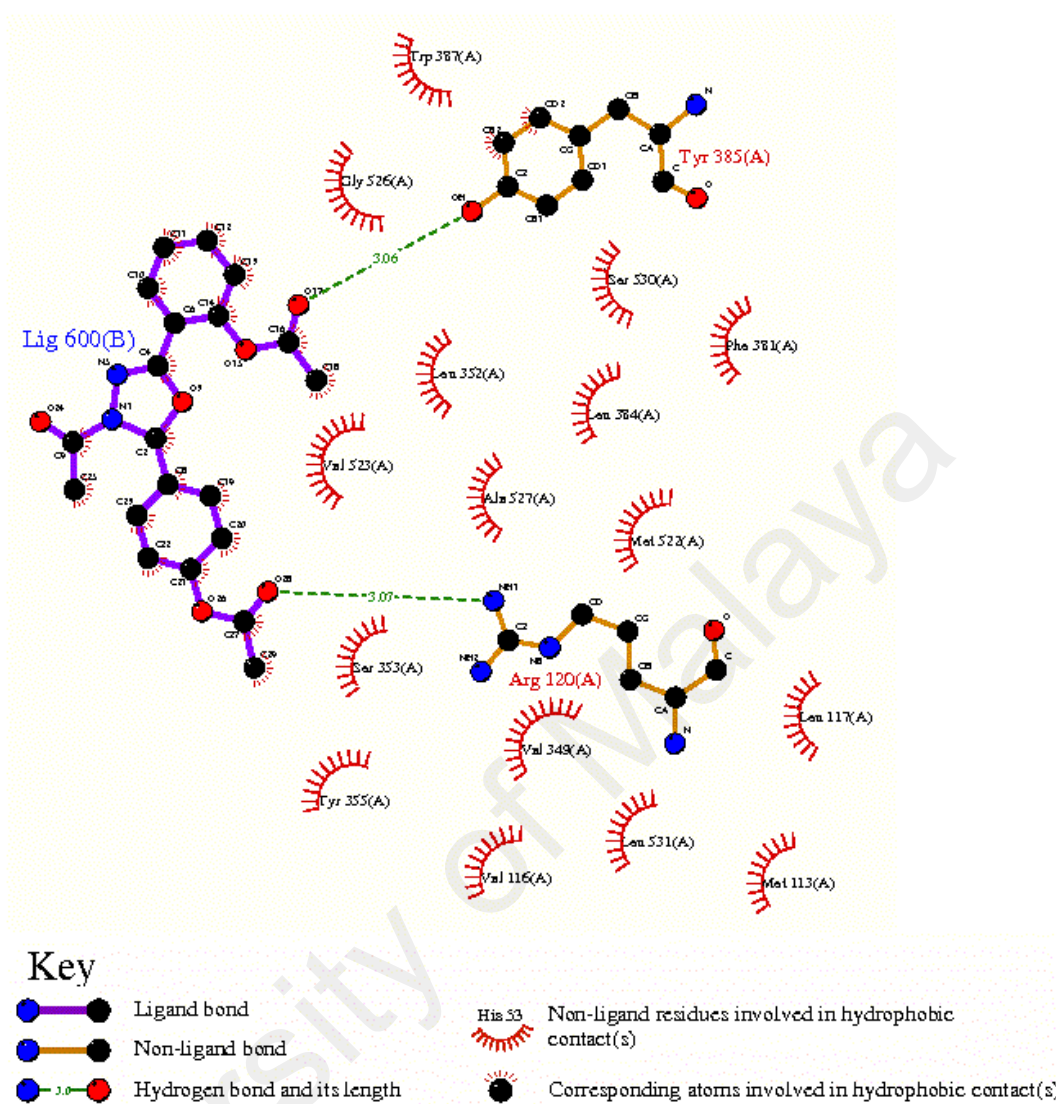
Figure 3.7, continued

Hydrogen bonds between the carbonyl oxygen with Tyr385, Tyr355 and Arg120 residues, as well as an arene-cation interaction with the aromatic ring, were observed in all compounds (Figure 3.7 & Table 3.4). As a result of docking it was proven that hydrogen bonds between ligands and COX-2 are crucial in COX-2 selectivity of the ligands. Binding energies and estimated inhibition constant values $K_{i\ dock}$ of compounds **3a-h** are summarized in Table 3.4.

Table 3.4: Results obtained from docking of 1,3,4-Oxadiazoline derivatives (**3a-h**).

Compounds	No.	Best Lowest binding energy in to COX-2 (Kcal Mol^{-1})	Residues that interaction via H-bond	Best Lowest binding energy in to COX-1 (Kcal Mol^{-1})	Residues that interaction via H-bond	Ki/ COX-2	Ki/ COX-1
SC-558	*	-7.95	Arg513, His90	Nil	Nil	1.50 μM	Nil
Flurbiprofen	*	-7.26	Arg120,Tyr355	-8.01	Arg120, Arg120	4.74μM	1.33μM
3f	1	-7.64	Tyr385	Nil	Nil	2.50 μM	Nil
3c	2	-6.89	Tyr385	-8.92	Pi-Pi & Pi-Sigma	8.80μM	289.5 nM
3g	3	Nil	Nil	Nil	Nil	Nil	Nil
3b	4	-6.74	Arg120, Tyr385	Nil	Nil	6.98 μM	Nil
3a	5	-6.50	Tyr355	Nil	Nil	17.10 μM	Nil
3d	6	-7.38	Tyr385	Nil	Nil	3.87 μM	Nil
3h	7	-7.46	Arg120, Tyr385	Nil	Nil	3.40 μM	Nil
3e	8	-6.33	Arg513	Nil	Nil	22.70μM	Nil

*: Standard drug
Nil: Molecules do not fit in this active site
Ki: Estimated inhibition constant

The orientation of the docked conformation of Flurobiprofen **(**Figures 3.8 and 3.9**)** was reproduced with similar binding interactions to that of its original conformation in the crystal structure (Figures 3.8) using the similar procedure explained above.
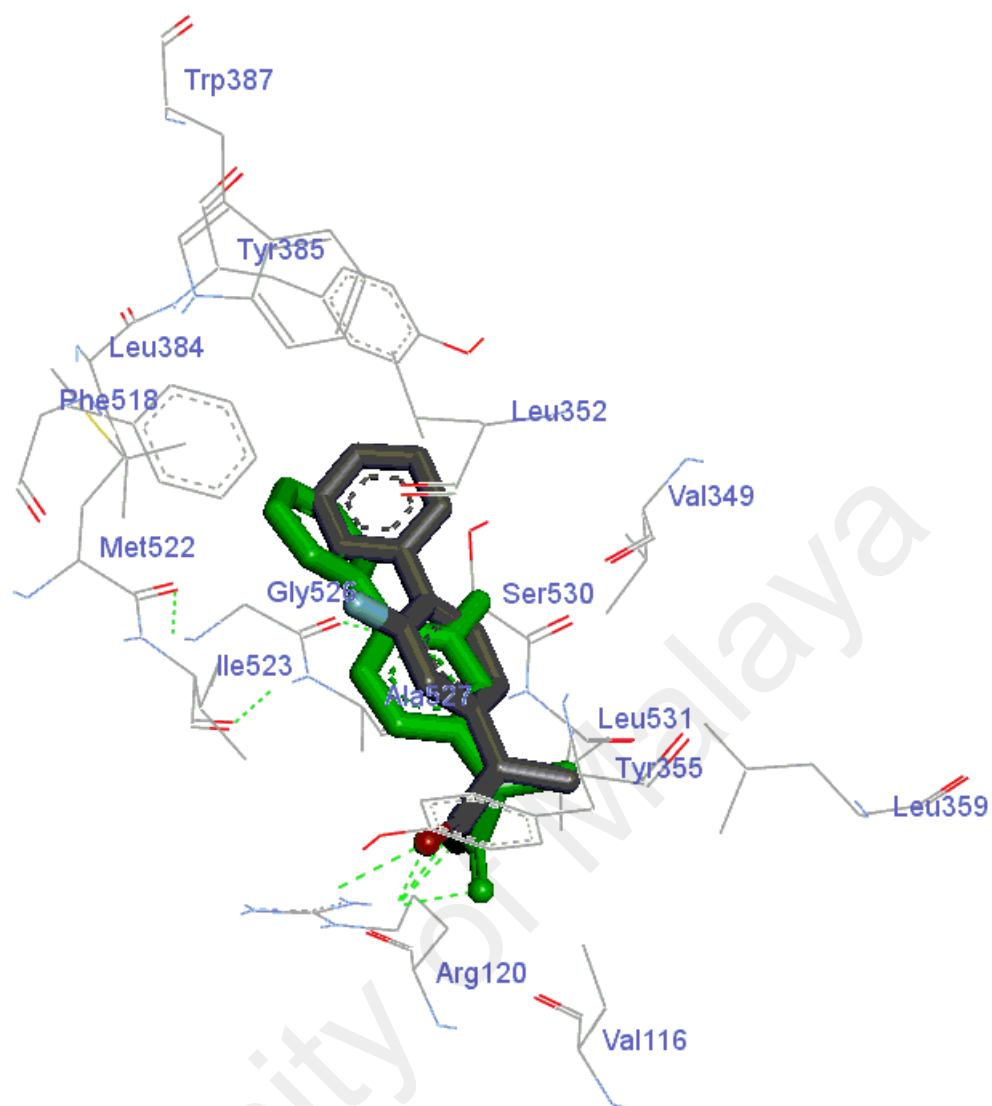
Figure 3.8: Diagram showing the superimposed poses of the re-docked flurobiprofen (green ball and stick model) and flurobiprofen co-crystallized with COX-1 (PDBid: 1CQE) (gray ball and stick model). The same positions of the drug reveals the accuracy of docking protocol used in this study.
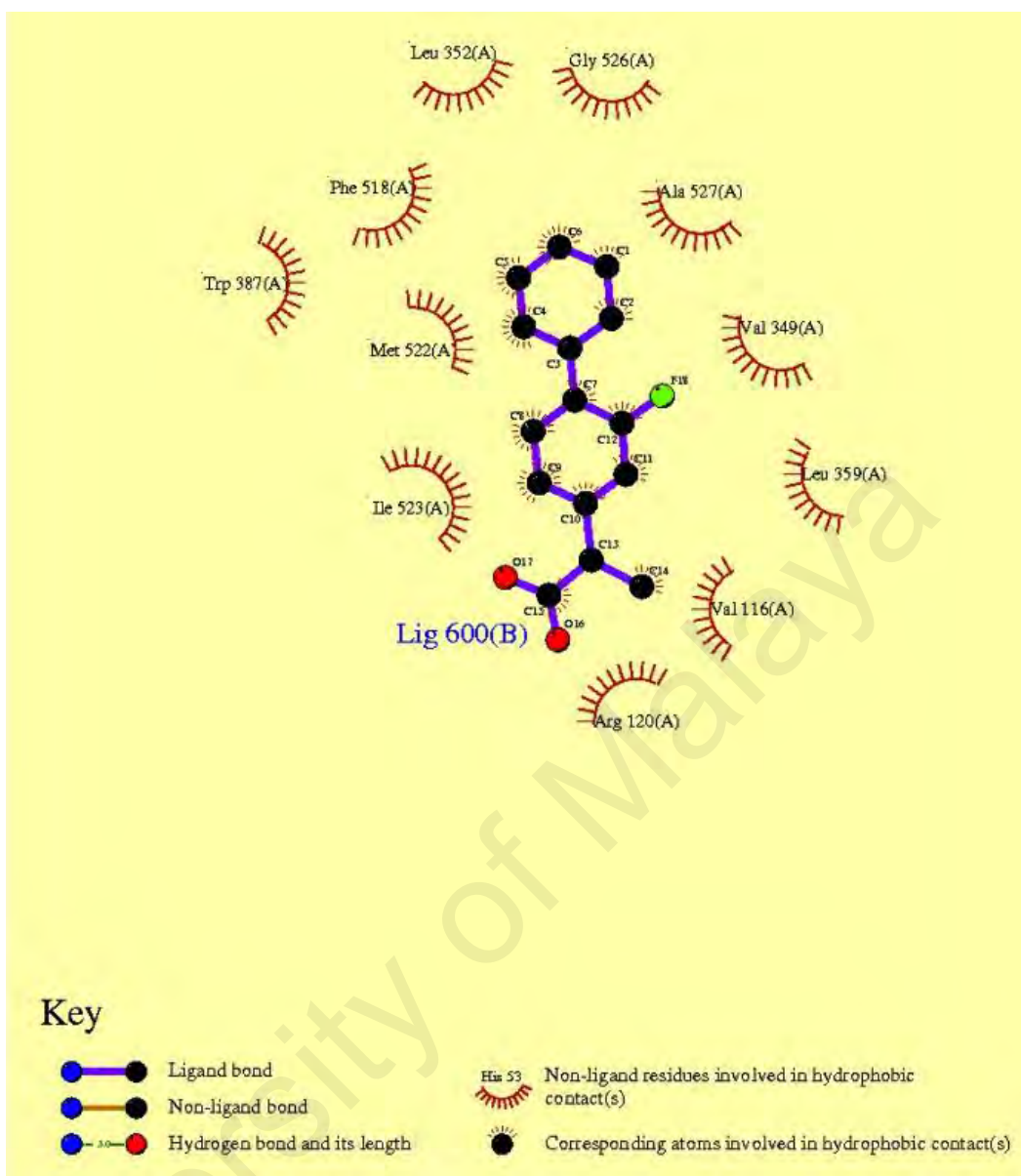
Figure 3.9: Hydrogen bonding and hydrophobic interactions between COX-1 and flurobiprofen, Lig 600(B) is the temporary code name for flurobiprofen. (A) represents the amino acids belong to COX-1 enzyme.

All structures **3a-h** were also modeled onto the functioning location of COX-1 enzyme and could not fit into the active site of COX-1 except structure **3c** which appeared to be binding to the active site with *pi-pi* and *pi-sigma* interactions, but no hydrogen bonding (Figure 3.10, Figure 3.11 & Table 3.4).
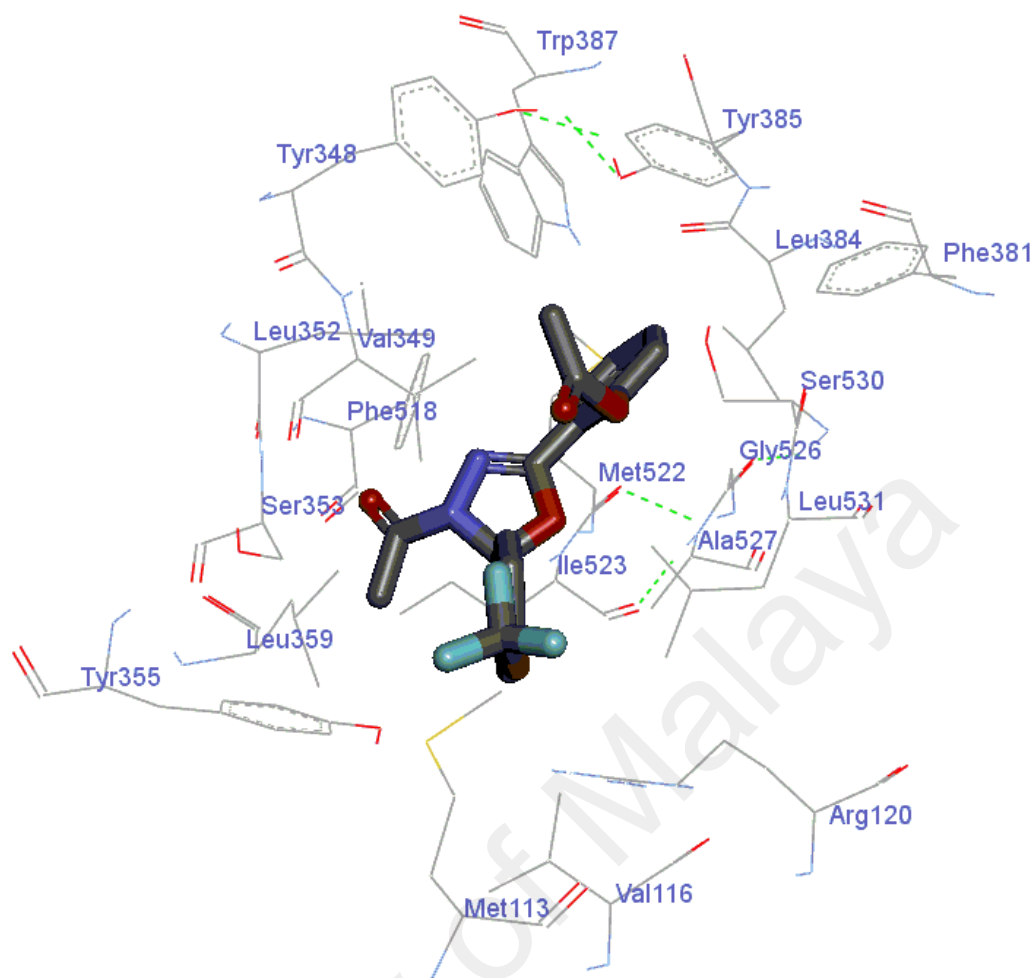
Figure 3.10: Binding conformations generated by Discovery studio 3.1 of compounds **3c** and its interactions with amino acid residues of COX-1 (PDBid: 1CQE). The hydrogen bonds are represented by the green dotted lines.
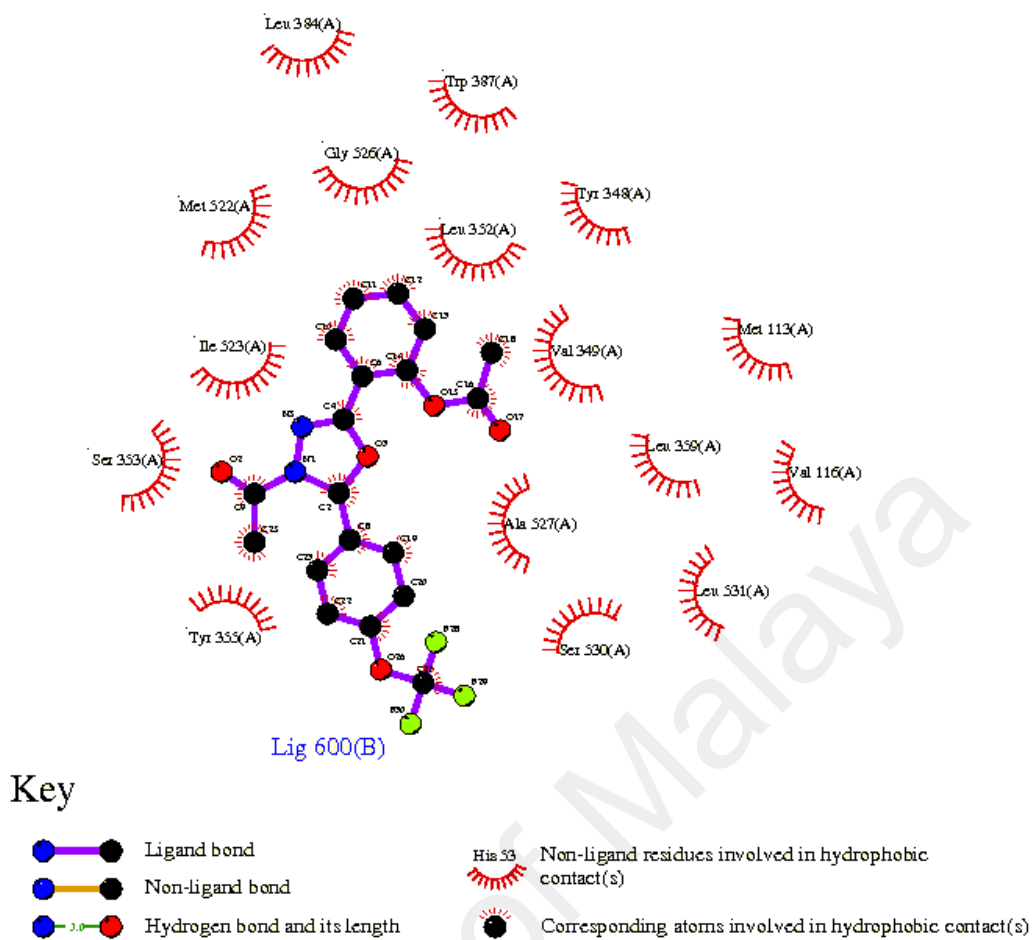
Figure 3.11: Graphical results generated by Ligplot 4.5.3 software. It illustrates the hydrogen bond and hydrophobic interactions between **3c** conformation and amino acid residues of 1CQE. Lig 600(B) is the temporary code name for **3c**. (A) is the temporary code name for protein.

CHAPTER 4: SYNTHESIS OF DESIGNED STRUCTURES

4.1   Introduction

Many diarylheterocycles and central ring pharmacophore templates were produced as a research attempts in the discovery of selective COX-2 inhibitors (Patel *et al.*, 2010; Sakya *et al.*, 2006; Lehmann & Beglinger, 2005). This chapter deals with the synthesis and structural elucidation of 1,3,4-Oxadiazoline Derivatives and of 5-Oxobenzo[f][1,3,4]Oxadiazepine Derivatives. Oxadiazolines and oxadiazepines are important compounds for both chemical and biological purposes (Yang *et al.*, 2011; El-Badry & Taha, 2011). They have been used extensively as synthons in various organic syntheses such as for the preparation of spiro-fused b-lactam oxadiazolines (Zoghbi & Warkentin, 1993) and of fused oxadiazepines used as gamma secretase modulators for the treatment of Alzheimer's disease (Li *et al.*, 2013). In addition, oxadiazolines and oxadiazepines have been reported to exhibit diverse pharmacological properties (Ke *et al.*, 2009), which include antimicrobial (Fuloria *et al.*, 2009), cytotoxic (Manojkumar *et al.*, 2009), antifungal, and anticancer activities (Daeniker & Druey, 1957). Various aldehyde and ketone acyl hydrazones have been cyclized to give 3-acyl-1,3,4-oxadiazolines under acylating conditions (Somogyi, 2007; Arora *et al.*, 2013). However, there are only three reports on acylhydrazones with a hydroxyl group at the ortho position of the benzene ring being cyclized to give 3-acyl-1,3,4-oxadiazolines (Yehye *et al.*, 2010). In the case of oxadiazepines, several methods have been reported for their synthesis, all of which are multi-step in nature (Fuloria *et al.*, 2009; Oe *et al.*, 1977; Souldozi *et al.*, 2007) For example, El Badry and Taha, reported that the diazotization of ethyl 1-aminotetrazole-5-carboxylate in the presence of water resulted in the formation of ethyl 1-hydroxytetrazole-5-carboxylate. Condensation of ethyl 1-hydroxytetrazole-5-carboxylate with bromoacetone and/or phenacyl bromide in absolute

ethanol in the presence of anhydrous potassium carbonate provided acetyloxy and 2-oxyacetophenone compounds, which were then reacted with various 4-substituted anilines in the presence of acetic anhydride/ acetic acid to give 7-methyl(phenyl)-8-aryltetrazolo[1,5-b]-1,2,5-oxadiazepin-9-ones in three steps (Fuloria *et al.*, 2009). Herein, we report novel, one-step intramolecular oxidative cyclization of a variety of substituted benzaldehyde acylhydrazones **2** with a free hydroxyl group at the ortho position to give the oxadiazolines **3**. In some cases, when the cyclization reactions of **1** were carried out at 50–60 °C in acetic anhydride/acetic acid solution, 1,3,4-oxadiazepines **4** were obtained instead of 1,3,4-oxadiazolines **3.** The structures were determined using a combination of spectroscopic methods; 1D-NMR (^{1}H, ^{13}C, DEPT), 2D-NMR (COSY, HMQC, and HMBC), IR, MS (HRMS) as well as X-ray diffraction analysis.

4.2   **Materials & Methods**

All melting points were taken on a Mel & Temp II melting point instrument. Infra Red (IR) spectra were recorded on a Thermo Scientific Nicolet 6700 Fourier IR spectrometer (ATIR). Nuclear magnetic resonance (NMR) spectra were obtained using a Jeol ECA 400 (400 MHz) NMR spectrometer with TMS as the internal standard. All measurements were accomplished in solution in DMSO-*d^6* or CDCl$_3$. All chemical shifts are reported in ppm. Analytical thin layer chromatography (TLC) was carried out on Merck precoated aluminium silica gel sheets (Kieselgel 60 F & 254). Visualization was accomplished under UV light or iodine vapour. Most products were found to be homogeneous by TLC and 400 MHz ^{1}H NMR analyses, but when needed, heterogenous products were readily purified by silica gel column chromatography using a hexane/chloroform eluent. All target compounds were characterized by IR, ^{1}H, ^{13}C, 2D NMR, high resolution electron ionization mass spectral (HRMS) (ESI) analyses and X-ray Crystallographic Data Collection. The X-ray diffraction measurements were

obtained from University of Malaya, Malaysia. Single crystal X-ray diffraction data collection of selected compounds were performed on a Burker Apex II CCD diffractometer at 100 K employing graphite-monochromated Mo Kα radiation (λ =0.71073Å). The intensities were collected using the ω-2θ scan mode, in the range 2.4 < θ < 27.0. All structures were solved by direct method by using SHELXS-97 (Sheldrick, 2008) and refined by full matrix least–square methods on F^2 with the use of the SHELXS-97 (Sheldrick, 2008) program package (semi-empirical absorption corrections were applied using SADABS program). Other anhydrous solvents and reagents were purchased from Merck.

4.2.1 General Procedure For Preparation of Hydrazones 1a-h

R= Cl, SCH$_3$, OMe, Et, *t*-Bu, OCF$_3$, OAc & NO$_2$
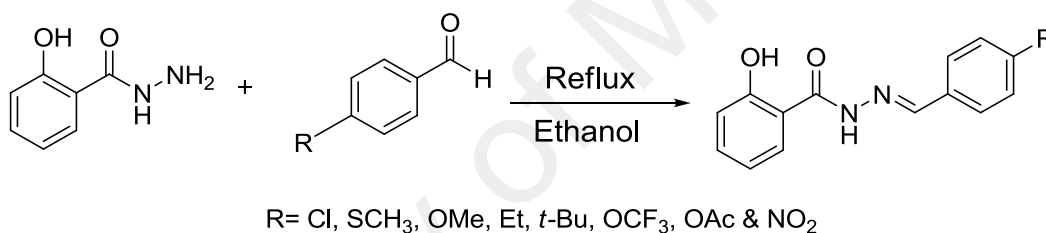
Scheme 4.1: Synthesis of **1a-h**

2-hydroxybenzohydrazide (0.30 g, 2 mmol) and various *para*-substituted benzaldehyde derivatives (0.2 g, 2 mmol) were refluxed in ethanol (20 ml) for 5 h (Scheme 4.1). The solvent was removed by evaporation and the resulting product was white solid powder for compounds **1a-h**, except for compound **1b** which was yellow solid powder (Jablonski *et al*., 2012).

4.2.2 General Procedure For Synthesis of 1,3,4-Oxadiazoline Derivatives 3a-h
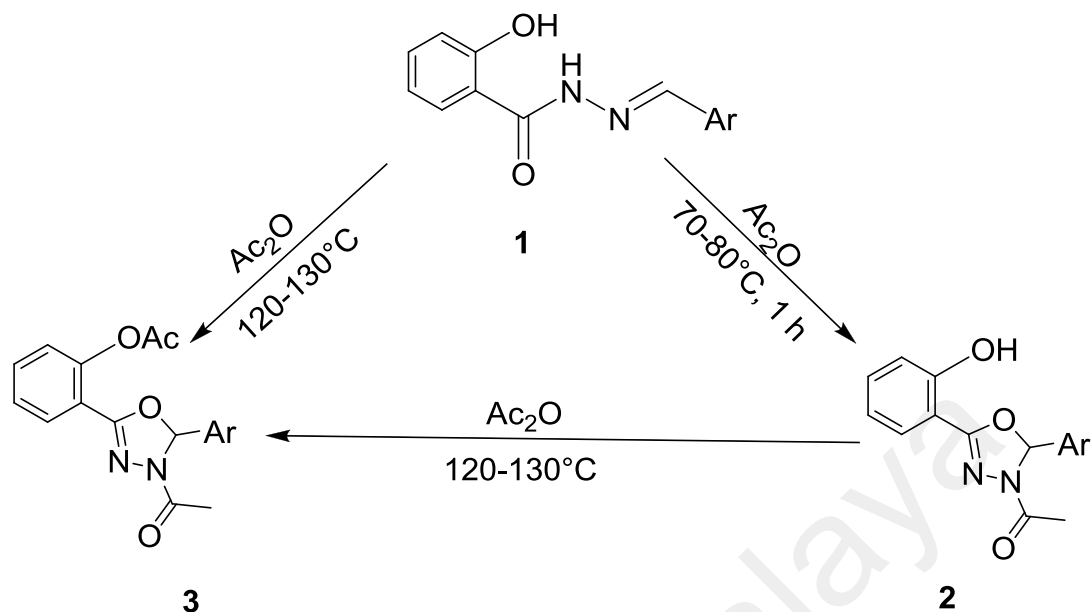
Scheme 4.2: Synthesis of 1,3,4-oxadiazoline derivatives **3a-h**

A mixture of each compound **1a-h** (0.3 g, 1.58 mmol) and acetic anhydride (6 ml) was refluxed for 2 h under vigorous stirring. The solution was cooled and then poured into crushed ice and stirred vigorously. A precipitate was formed which was then washed with distilled water to remove the acetic anhydride. The obtained solid was further purified by recrystallization with an appropriate solvent (Arora *et al.*, 2013; Somogyi, 2007).

4.2.3 General Procedure For Synthesis of 5-Oxobenzo[f][1,3,4]Oxadiazepine Derivatives
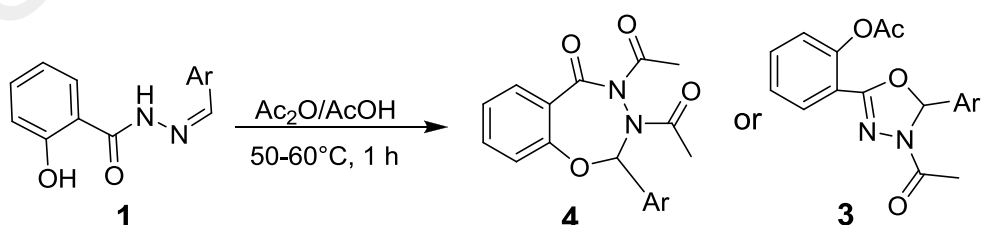
Scheme 4.3: Synthesis of 1,3,4- oxadiazepines 4 &1,3,4- oxadiazolines 3

Compounds **4a, 4d, 4e** and **4f** were obtained from the reaction of acetic anhydride in acetic acid (6 ml) with the respective hydrazone (**1a**, **1d**, **1e**, and **1f**) (0.3 g, 2 mmol), and the resulting solution was stirred vigorously for 1 h at 50-60°C. The structures of the products were elucidated using IR, ^{1}H, ^{13}C, 2D NMR and MS.

4.3 Results

4.3.1 *N*-(4-chlorobenylidene)-2-hydroxbenzohydrazide (1a)
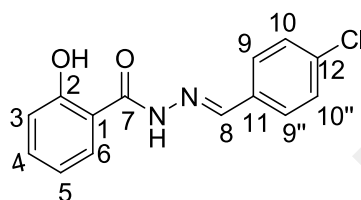
(Yield: 90%), mp = 262°C. IR (ATIR): 3448 hydroxyl (O-H), 3248 N-H, 1655 (C=O), 1629 (C=N) cm^{-1}. ^{1}H NMR (DMSO-d6, 400 MHz), δ, ppm: 6.90-6.95 (m, 2H, H3,H5), 7.41 (t, J = 7.7 Hz, 1H, H4), 7.50 (d, J = 8.6Hz, 2H, H10,10"), 7.73 (d, J = 8.7 Hz, 2H, H9,9"), 7.84 (d, J = 7.7 Hz, 1H, H6), 8.41 (s,1H, C-H), 11.74 (s, 1H, CONH), 11.85 (s, 1H, Ar-OH). ^{13}C NMR (DMSO-d6, 100 MHz), δ, ppm: 165.21 (C=O; C7), 159.35 (C-OH; C2), 147.80 (C=N; C8), 135.25 (C12), 134.37 (C4), 133.59 (C11), 129.52 (C9,9"), 129.40 (C10,10"), 129.21 (C6), 119.51 (C5), 117.78 (C1), 116.54 (C3). HRMS (ESI) calculated for C$_{14}$H$_{11}$ClN$_2$NaO$_2$: 297.0411 [M+Na]$^+$, found: 297.0401 [M+Na]$^+$.

4.3.2 2-Hydroxy-*N*-(4-methoxybenzylidene)benzohydrazide (1b)
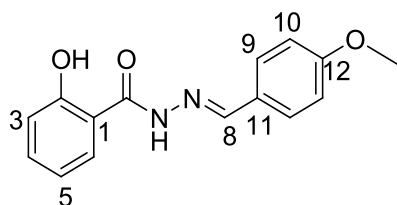
(Yield: 90%), mp = 250°C. IR (ATIR): 3245 (N-H), 1652, (C=O), 1627 (C=N) cm^{-1}. ^{1}H NMR (DMSO-d6, 400 MHz), δ, ppm: 2.45(s, 3H, OCH$_3$), 6.89-6.95 (m, 2H,

H3, H5), 6.99 (d, J = 9.1 Hz, 2H, H10, 10''), 7.40 (t, J = 9.6 Hz, 1H, H4), 7.66 (d, J = 7.3 Hz, 2H, H9, 9''), 7.86 (d, J = 8.7 Hz, 1H, H6), 8.37 (s, 1H, =C-H), 11.71 (s, 1H, CONH), 11.92 (s, 1H, Ar-OH). ^{13}C NMR (DMSO-d6, 100 MHz), δ, ppm: 165.19 (C=O; C7), 161.53 (C-OH; C2), 159.65 (C=N; C8), 149.21 (C12), 134.25 (C4), 129.40 (C9,9''), 128.91 (C6), 127.17 (C11), 119.45 (C5), 117.80 (C3), 116.28 (C1), 114.85 (C10,10''), 55.82 (OCH$_3$). HRMS (ESI) calculated for C$_{15}$H$_{14}$N$_2$NaO$_3$: 293.0904 [M+Na]$^+$, found: 293.0897 [M+Na]$^+$.

4.3.3 2-Hydroxy-*N*-(4-(trifloromethoxy)benzylidene)benzohydrazide (1c)
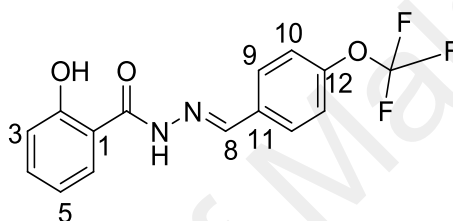
(Yield: 85%), mp = 243°C. IR (ATIR): 3250 (N-H), 1655 amide (C=O), 1626 (C=N) cm^{-1}. ^{1}H NMR (DMSO-d6, 400 MHz), δ, ppm: 6.89-6.96 (m, 2H, H3, H5), 7.38-7.44 (m, 4H, H4, H6, H9,9''), 7.8 (d, J = 7.8 Hz, 2H, H10,10''), 8.44 (s, 1H, C-H), 11.73 (s, 1H, Ar-OH), 11.86 (s, 1H, CONH). ^{13}C NMR (DMSO-d6, 100 MHz), δ, ppm: 165.24 (C=O; C7), 159.35 (C-OH; C2), 149.92 (C12), 147.51 (C=N; C8), 134.37 (C11), 133.92 (C4), 129.60 (C9,9''), 129.25 (C6), 121.83 (C10,10''), 119.56 (C5), 117.77 (C3), 116.58 (C1). HRMS (ESI) calculated for C$_{15}$H$_{11}$F$_3$N$_2$NaO$_3$: 347.0621 [M+Na]$^+$, found: 347.0614 [M+Na]$^+$.

4.3.4 2-Hydroxy-*N'*-(4-(methylthio)benzylidene)benzohydrazide (1d)
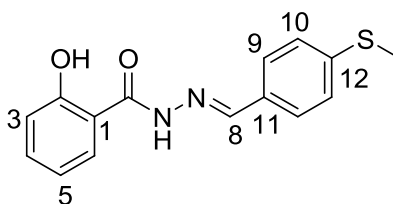
(Yield: 90%), mp = 230°C. IR (ATIR): 3379 hydroxyl (O-H), 3247 N-H, 1653 (C=O), 1626 (C=N) cm^{-1}. ^{1}H NMR (DMSO-d6, 400 MHz), δ, ppm: 2.48 (s, 3H, SCH$_3$), 6.85-6.95 (m, 2H, H3,H5), 7.30 (d, J = 8.2Hz, 2H, H10,10''), 7.35-7.43 (m, 1H, H4), 7.64 (d, J = 8.2 Hz, 2H, H9,9''), 7.76 (d, J = 7.8 Hz, 1H, H6), 7.85 (d, J = 7.3 Hz, 1H, C-H), 8.37 (s, 1H, CONH), 11.77 (s, 1H, Ar-OH). ^{13}C NMR (DMSO-d6, 100 MHz), δ, ppm: 165.25 (C=O) (C7), 159.60 (C-OH; C2), 149.30 (C=N; C8), 146.91 (C12), 134.31 (C4), 132.17 (C11), 128.99 (C6), 128.84 (C9,9''), 127.84 (C10,10''), 119.46 (C5), 117.77 (C1), 116.39 (C3), 15.80 (CH$_3$). HRMS (ESI) calculated for C$_{15}$H$_{14}$N$_2$NaO$_2$S: 309.0680 [M+Na]$^+$, found: 309.0668 [M+Na]$^+$.

4.3.5 *N'*-(4-ethylbenzylidene)-2-hydroxybenzohydrazide (1e)
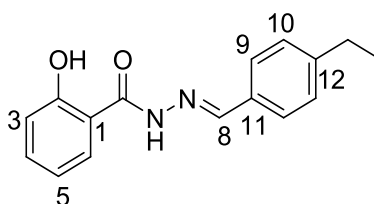
(Yield: 90%), mp = 220°C. IR (ATIR): 3247 (N-H), 1652 (C=O), 1627 (C=N) cm^{-1}. ^{1}H NMR (DMSO-d6, 400 MHz), δ, ppm: 1.14 (t, J = 8.0 Hz, CH$_3$), 2.58 (q, J = 7.3 Hz, 2H, CH$_2$), 6.89-6.95 (m, 2H, H3, H5), 7.25 (d, J = 7.7 Hz, 2H, H10,10''), 7.39 (t, J = 7.7 Hz, 1H, H4), 7.62 (d, J = 7.3 Hz, 2H, H9,9''), 7.84 (d, J = 7.7 Hz, 1H, H6), 8.38 (s, 1H, C-H), 11.77 (s, 1H, CONH), 11.86 (s, 1H, Ar-OH). ^{13}C NMR (DMSO-d6, 100 MHz), δ, ppm: 165.30 (C=O; C7), 159.58 (C-OH; C2), 149.33 (C=N; C8), 146.93 (C12), 134.32 (C4), 132.17 (C11), 129.02 (C6), 128.83 (C9,9''), 127.87 (C10,10''), 119.36 (C5),

117.85 (C3),116.35 (C1), 28.52 (CH$_2$), 15.72 (CH$_3$). HRMS (ESI) calculated for C$_{16}$H$_{16}$N$_2$NaO$_2$: 291.1112 [M+Na]$^+$, found : 291.1104 [M+Na]$^+$.

4.3.6 *N'*-(4-(tert-butyl)benzylidene)-2-hydroxybenzohydrazide (1f)
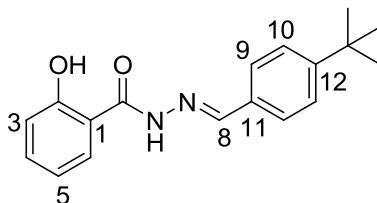
(Yield: 90%), mp = 215°C. IR (ATIR): 3271 (N-H), 1631 (C=O), 1610 (C=N) cm^{-1}. ^{1}H NMR (DMSO-d6, 400 MHz), δ, ppm: 1.25 (s, 9H, 3CH$_3$), 6.89-6.95 (m, 2H, H3, H5), 7.40 (t, J = 7.5 Hz, 1H, H4), 7.46 (d, J = 8.0 Hz, 2H, H10, 10"), 7.64 (d, J = 8.2 Hz, 2H, H9,9"), 7.85 (d, J = 7.8 Hz, 1H, H6), 8.39 (s, 1H, C-H), 11.76 (s, 1H, CONH), 11.83 (s, 1H, Ar-OH). ^{13}C NMR (DMSO-d6, 100 MHz), δ, ppm: 165.24 (C=O; C7), 159.55 (C-OH; C2), 153.68 (C12), 149.22 (C=N; C8), 134.30 (C4), 131.88 (C11), 128.99 (C6), 127.59 (C9, 9"), 126.23 (C10,10"), 119.44 (C5), 117.78 (C3), 116.42 (C1), 35.16 (C- *tert*-But), 31.49 (*t*-Bu). HRMS (ESI) calculated for C$_{18}$H$_{20}$N$_2$NaO$_2$: 319.1430 [M+Na]$^+$, found: 319.1417 [M+Na]$^+$.

4.3.7 2-Hydroxy-*N*-(4-nitrobenzylidene)benzohydrazide (1g)
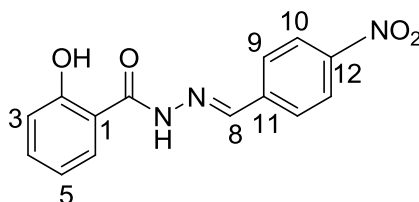
(Yield: 94%), mp = 260°C. IR (ATIR): 3440 hydroxyl (O-H), 3245 (N-H), 1650 (C=O), 1622 (C=N) cm^{-1}. ^{1}H NMR (DMSO-d6, 400 MHz), δ, ppm: 6.90-6.97 (m, 2H, H3, H5), 7.41 (t, J = 7.3 Hz, 1H, H4), 7.83 (d, J = 7.3 Hz, 1H, H6), 7.96 (d, J = 8.2 Hz, 2H, H9,9"), 8.26 (d, J = 8.2 Hz, 2H, H10,10"), 8.51 (s, 1H, C-H), 11.60 (s, 1H, Ar-OH), 12.01 (s, 1H, CONH). ^{13}C NMR (DMSO-d6, 100 MHz), δ, ppm: 165.20 (C=O; C7),

159.04 (C-OH; C2), 148.39 (C12), 146.48 (C=N; C8), 140.96 (C11), 134.50 (C4), 129.46 (C6), 128.65 (C9,9"), 124.59 (C10,10"), 119.63 (C5), 117.71 (C3), 116.81 (C1). HRMS (ESI) calculated for $C_{14}H_{11}N_3NaO_4$: 286.0826 $[M+Na]^+$, found: 286.0822 $[M+Na]^+$.

4.3.8 4-((2-(2-Hydroxybenzoyl)hydrazono)methyl)phenyl acetate (1h)
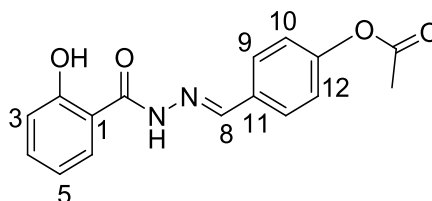
(Yield: 92%), mp = 220°C. IR (ATIR): 3240 (N-H), 1759 (acetyl; C=O), 1634 (C=O), 1602 (C=N) cm^{-1}. ^1H NMR (DMSO-d6, 400 MHz), δ, ppm: 2.26 (s, 3H, CH₃), 6.90-6.96 (m, 2H, H3, H5), 7.20 (d, J = 9.16Hz, 2H, H10,10"), 7.40 (t, J = 10.76 Hz, 1H, H4), 7.76 (d, J = 8.2 Hz, 2H, H9,9"), 7.85 (d, J = 9.6 Hz, 1H, H6), 8.43 (s, 1H, CONH), 11.84 (s, 1H, =C-H). ^{13}C NMR (DMSO-d6, 100 MHz), δ, ppm: 169.56 (C=O; OAc) 165.28 (C=O; C7), 159.42 (C-OH; C2), 152.46 (C12), 148.24 (C=N; C8), 134.44 (C4), 132.37 (C11), 129.19 (C6), 129.00 (C9,9"), 122.85 (C10,10"), 119.62 (C5), 117.58 (C3), 116.22 (C1), 21.36 (CH₃). HRMS (ESI) calculated for $C_{16}H_{15}N_2O_4$: 299.1023 $[M+H]^+$, found: 299.1026 $[M+H]^+$.

4.3.9 2-(4-Acetyl-5-(chlorophenyl)-4,5-dihydro-1,3,4-oxadiazol-2-yl)phenyl acetate (3a)
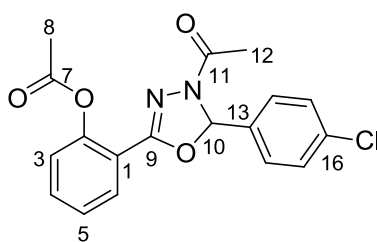
(Yield: 78%), mp = 119–120°C. IR (ATIR): 1759 (acetyl; C=O), 1695 (C=O), 1617 (C=N) cm^{-1}. ^1H NMR (CDCl₃, 400 MHz), δ, ppm: 2.31 (s, 3H, H8), 2.36 (s, 3H, H12), 6.99 (s, 1H, H10), 7.19 (d, J = 7.76 Hz, 1H, H3), 7.34-7.44 (m, 5H, H5, H14, H14",

H15, H15"), 7.56 (t, J = 11.44 Hz, J = 5.84 Hz, J = 5.96, Hz 1H, H4), 7.91 (d, J = 6.8 Hz, 1H, H6). ^{13}C NMR (CDCl$_3$, 100 MHz), δ, ppm: 169.36 (C=O; C7), 167.73 (C=O; C11), 152.93 (C9), 148.99 (C16), 136.09 (C2), 134.82 (C13), 132.92 (C4), 129.68 (C6), 129.17 (C14,14"), 128.24 (C15, 15"), 126.58 (C5), 124.02 (C3), 117.93 (C1), 90.87 (C10), 21.70 (C12), 21.19 (C8). HRMS (ESI) calculated for C$_{18}$H$_{15}$ClN$_2$NaO$_4$: 381.0624 [M+Na]$^+$, found: 381.0613 [M+Na]$^+$.

4.3.10 1-(2-(4-Chlorophenyl)-5-(2-hydroxyphenyl)-1,3,4-oxadiazol-3(2H)-yl)ethanone (2a)
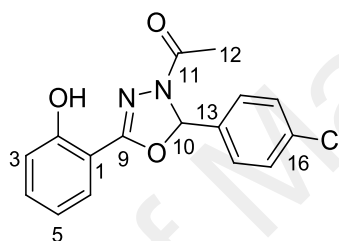
Compound **2a** was synthesized by the addition of acetic anhydride (6mL) to hydrazone (0.3 g, 0.0002 mmol) and the resulting solution was heated to 70-80°C for 1h. The reaction mixture was poured into ice water and the resulting solid product was filtered and washed with copies amounts of water, drying under air. Compound **2a** was isolated as a white solid. (Yield: 70%), mp = 130-137°C. IR (ATIR): 1759 (acetyl; C=O), 1657, (C=O), 1610 (C=N) cm^{-1}. ^{1}H NMR (CDCl$_3$, 400 MHz), δ, ppm: 2.33 (s, 3H, H12), 6.96 (t, J = 7.7 Hz, 1H, H4), 7.06 (d, J = 9.6 Hz, 2H, H10, H3), 7.36-7.07 (m, 5H, H15, H15", H14, H14", H5), 7.62 (d, J = 8 Hz, 1H, H6), 9.08 (s, 1H, OH). ^{13}C NMR (CDCl$_3$, 100 MHz), δ, ppm: 167.61 (C=O; C11), 157.38 (C16), 156.22 (C2), 136.31 (C9), 134.24 (C13), 133.93 (C6), 129.22 (C14,14"), 128.07 (C15,15"), 127.54 (C5), 120.12 (C4), 117.11 (C3), 108.67 (C1), 90.64 (C10), 21.63 (C12). HRMS (ESI) calculated for C$_{16}$H$_{14}$ClN$_2$O$_3$: 317.0682 [M+H]$^+$, found : 317.1285 [M+H]$^+$.

4.3.11 2-(4-Acetyl-5-(4-(methoxyphenyl)-4,5-dihydro-1,3,4-oxadiazol-2-yl)phenyl acetate (3b)
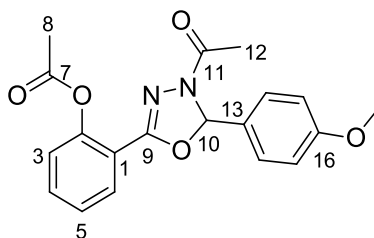
White solid (Yield: 70%), mp = 130°C. IR (ATIR): 1764 (acetyl; C=O), 1663 (C=O), 1608 (C=N) cm^{-1}. ^{1}H NMR (DMSO-d6, 400 MHz), δ, ppm: 2.46 (s, 3H, H8), 3.30 (s, 3H, H12), 3.72 (s, 3H, OCH$_3$), 6.95 (d, J = 8.2 Hz, 1H, H3), 7.04 (s, 1H, H10), 7.26 (d, J = 8.2 Hz, 2H, H15, H15″), 7.32 (d, J = 8.7 Hz, 2H, H14, H14″), 7.38 (t, J = 7.8 Hz, 1H, H5), 7.60 (t, J = 7.8 Hz, 1H, H4), 7.77 (d, J = 7.7 Hz, 1H, H6). ^{13}C NMR (DMSO-d6, 100 MHz), δ, ppm: 169.48 (C=O; C7), 167.05 (C=O; C11), 160.92 (C9), 152.27 (C16), 149.01 (C2), 133.53 (C13), 129.59 (C4), 129.15 (C6), 128.56 (C14,14″), 127.18 (C5), 124.68 (C15, 15″), 118.15 (C3), 114.65 (C1), 91.44 (C10), 55.80 (OCH$_3$), 21.89 (C12), 21.25 (C8). HRMS (ESI) calculated for C$_{19}$H$_{18}$N$_2$NaO$_5$: 377.1121 [M+Na]$^+$, found : 377.1108 [M+Na]$^+$.

4.3.12 1-(5-(2-Hydroxyphenyl)-2-(4-methoxyphenyl)-1,3,4-oxadiazol-3(2H)-yl)ethanone (2b)
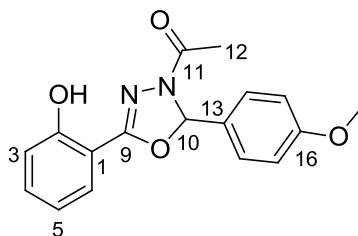
Compound **2b** was synthesized by the addition of acetic anhydride (6mL) to hydrazone **1b** (0.3 g, 0.0002 mmol) and the resulting solution was heated to 70-80°C for 2h. The reaction mixture was poured into ice water and the resulting solid product was filtered and washed with copies amounts of water, drying under air. Compound **2b** was

isolated as a white solid. (Yield: 66%), mp = 132°C. IR (ATIR): 1759 amid (C=O), 1657 (C=N) cm^{-1}. ^{1}H NMR (CDCl$_3$, 400 MHz), δ, ppm: 2.33 (s, 3H, OCH$_3$), 3.79 (s, 3H, H12), 6.91 (d, J = 8.2 Hz, 2H, H15, H15"), 6.89-6.96 (m, 1H, H3), 7.03-7.07 (m, 2H, H10, H4), 7.40 (d, J = 8.2 Hz, 2H, H14, H14"), 7.39-7.43 (m, 1H, H5), 7.62 (d, J = 7.7 Hz, 1H, H6), 9.18 (s, 1H, OH). ^{13}C NMR (CDCl$_3$, 100 MHz), δ, ppm: 167.38 (C=O; C11), 161.08 (C16), 157.37 (C2), 156.18 (C9), 133.72 (C6), 128.16 (C14,14"), 127.98 (C13), 127.59 (C5), 120.02 (C4), 117.02 (C3), 114.23 (C15,15"), 108.67 (C1), 91.45 (C10), 55.45 (OCH$_3$), 21.67 (C12). HRMS (ESI) calculated for C$_{17}$H$_{17}$N$_2$O$_4$: 313.1190 [M+]$^+$, found : 313.1183 [M+]$^+$.

4.3.13 2-(4-Acetyl-5-(4-trifluoromethoxy)phenyl)-4,5-dihydro-1,3,4-oxadiazol-2-yl)phenyl acetate (3c)
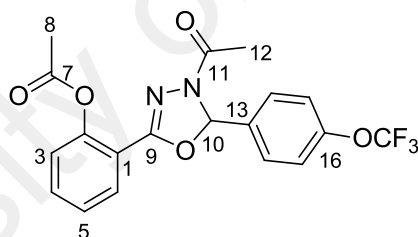
White solid (Yield: 70%), mp = 84°C. IR (ATIR): 1766 (acetyl; C=O), 1676 (C=O), 1624 (C=N) cm^{-1}. ^{1}H NMR (CDCl$_3$, 400 MHz), δ, ppm: 2.28 (s, 3H, H8), 2.32 (s, 3H, H12), 6.99 (s, 1H, H10), 7.15 (d, J = 8.24 Hz, 1H, H3), 7.23 (d, J= 9.6 Hz, 1H, H15, H15"), 7.33 (t, J = 8 Hz, 1H, H4), 7.49-7.56 (m, 3H, H14, H14", H6), 7.88 (d, J = 8.2 Hz, 1H, H6). ^{13}C NMR (CDCl$_3$, 100 MHz), δ, ppm: 169.33 (C=O; C7), 167.79 (C=O; C11), 152.88 (C9), 150.33 (C16), 148.94 (C2), 134.84 (C13), 132.92 (C4), 129.65 (C6), 128.45 (C14,14", OCF$_3$), 126.55 (C5), 123.98 (C3), 121.26 (C15, 15"), 117.82 (C1), 90.61 (C10), 21.61 (C12), 21.19 (C8). HRMS (ESI) calculated for C$_{19}$H$_{15}$F$_3$N$_2$NaO$_5$: 431.0837 [M+Na]$^+$, found : 431.0825 [M+Na]$^+$.

4.3.14 2-(4-Acetyl-5-(4-(methylthio) phenyl)-4,5-dihydro-1,3,4-oxadiazol-2 yl)phenyl acetate (3d)
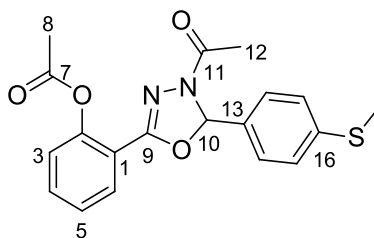
White solid (Yield: 65%), mp = 127°C. IR (ATIR): 1768 (acetyl; C=O), 1655 (C=O), 1621 (C=N) cm^{-1}. ^{1}H NMR (CDCl$_3$, 400 MHz), δ, ppm: 2.28 (s, 3H, H8), 2.31 (s, 3H, H12), 2.45 (s, 3H, SCH$_3$), 6.94 (s, 1H, H10), 7.15 (d, J = 8.7 Hz, 1H, H3), 7.24 (d, J = 7.7 Hz, 2H, H15, H15"), 7.32 (t, J = 15.5 Hz, , J = 7.7 Hz, J = 7.8 Hz, 1H, H4), 7.36 (d, J = 8.7 Hz, 2H, H14, H14"), 7.52 (t, J = 15.5 Hz, J = 7.3 Hz, J = 8.2 Hz, 1H, H4), 7.87 (d, J = 7.8 Hz, 1H, H6). ^{13}C NMR (CDCl$_3$, 100 MHz), δ, ppm: 169.38 (C=O; C7), 167.57 (C=O; C11), 152.93 (C9), 148.92 (C16), 141.05 (C2), 132.81 (C13), 129.68 (C4), 127.16 (C6, C14, 14"), 126.50 (C5), 126.38 (C15, 15"), 123.93 (C3), 118.02 (C1), 91.33 (C10), 21.68 (C12), 21.13 (C8), 15.41 (CH$_3$). HRMS (ESI) calculated for C$_{19}$H$_{18}$N$_2$NaO$_4$S: 393.0891 [M+Na]$^+$, found : 393.0879 [M+Na]$^+$.

4.3.15 2-(4-Acetyl-5-(4-(ethylphenyl)-4,5-dihydro-1,3,4-oxadiazol-2-yl)phenyl acetate (3e)
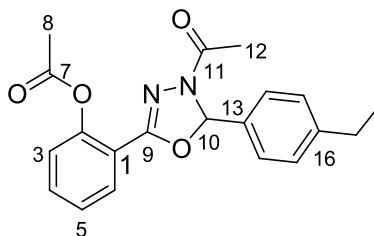
White solid (Yield: 60%), mp = 92°C. IR (ATIR): 1764 acetyl (C=O), 1656 (C=O), 1622 (C=N) cm^{-1}. ^{1}H NMR (CDCl$_3$, 400 MHz), δ, ppm: 1.20 (t, J = 7.3 Hz, 3H, CH$_3$) 2.27 (s, 3H, H8), 2.31 (s, 3H, H12), 2.63 (q, J = 7.6 Hz, 2H, CH$_2$), 6.96 (s, 1H, H10), 7.14 (d, J = 8.2 Hz, 1H, H3), 7.21 (d, J = 7.76 Hz, 2H, H15, H15"), 7.31 (t, J = 15.5 Hz,

J = 7.8 Hz, J = 7.7 Hz, 1H, H4), 7.36 (d, J = 7.3 Hz, 2H, H14, H14"), 7.51 (t, J = 15.5 Hz, J = 7.8 Hz, J = 7.7 Hz, 1H, H4), 7.88 (d, J = 8.2 Hz, 1H, H6). ^{13}C NMR (CDCl$_3$, 100 MHz), δ, ppm: 167.54 (C=O; C7), 167.49 (C=O; C11), 154.15 (C9), 148.98 (C16), 146.58 (C2), 133.60 (C13), 132.67 (C4), 129.86 (C6), 128.39 (C14, 14"), 126.70 (C15, 15"), 126.47 (C5), 123.09 (C3), 118.07 (C1), 91.64 (C10), 28.78 (CH$_2$), 21.70 (C12), 21.25 (C8), 15.50 (CH$_3$). HRMS (ESI) calculated for C$_{20}$H$_{20}$N$_2$NaO$_4$: 375.1324 [M+Na]$^+$, found : 375.1315 [M+Na]$^+$.

4.3.16 2-(4- Acetyl-5-(4-(tert-butyl)phenyl)-4,5-dihydro-1,3,4-oxadiazol-2-yl)phenyl acetate (3f)
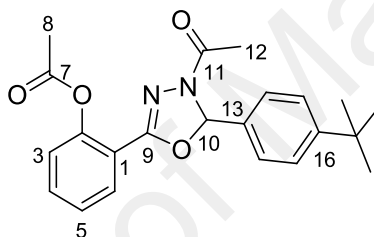
White solid (Yield: 58%), mp = 85°C. IR (ATIR): 1760 (acetyl; C=O), 1651 (C=O), 1613 (C=N) cm^{-1}. ^{1}H NMR (CDCl$_3$, 400 MHz), δ, ppm: 1.28 (s, 9H, *tert*-But) 2.27 (s, 3H, H8), 2.32 (s, 3H, H12), 6.98 (s, 1H, H10), 7.14 (d, J = 8.2 Hz, 1H, H3), 7.32 (t, J = 7.8Hz, 1H, H5), 7.36-7.42 (m, 4H, 4H, H15, H15", H14, H14"), 7.52 (t, J = 7.8 Hz, 1H, H4), 7.88 (d, J = 8.2 Hz, 1H, H6). ^{13}C NMR (CDCl$_3$, 100 MHz), δ, ppm: 169.31 (C=O; C7), 167.57 (C=O; C11), 153.17 (C9), 152.96 (C16), 148.92 (C2), 133.27 (C13), 132.67 (C4), 129.73 (C6), 126.47 (C5), 126.40 (C14,14"), 125.84 (C15,15"), 123.89 (C3), 118.16 (C1), 91.53 (C10), 34.83 (C-*tert*-But), 31.31 (*tert*-But), 21.71 (C12), 21.11 (C8). HRMS (ESI) calculated for C$_{22}$H$_{24}$N$_2$NaO$_4$: 403.1630 [M+Na]$^+$, found : 403.1628 [M+Na]$^+$.

4.3.17 2-(4-Acetyl-5-(4-nitrophenyl)-4,5-dihydro-1,3,4-oxadiazol-2-yl)phenyl acetate (3g)
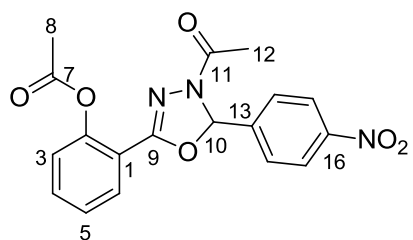
(Yield: 85%), mp = 115–119°C. IR (ATIR): 1750 (acetyl; C=O), 1690 (C=O), 1615 (C=N) cm^{-1}. ^{1}H NMR (CDCl$_3$, 400 MHz), δ, ppm: 2.30 (s, 3H, H8), 2.32 (s, 3H, H12), 7.05 (s, 1H, H10), 7.17 (d, J = 8.24 Hz, 1H, H3), 7.35 (t, J = 16.0 Hz, J = 7.8 Hz, J = 8.2 Hz, 1H, H5), 7.55 (t, J = 16.4 Hz, J = 8.2 Hz, J = 8.2 Hz, 1H, H4), 7.66 (d, J = 8.7 Hz, 2H, H14, H14"), 7.88 (d, J = 7.3 Hz, 1H, H6), 8.24 (d, J = 9.1 Hz, 2H, H15, H15"). ^{13}C NMR (CDCl$_3$, 100 MHz), δ, ppm: 169.27 (C=O; C7), 168.00 (C=O; C11), 152.91 (C9), 148.98 (C16), 148.84 (C2), 142.54 (C13), 133.16 (C4), 129.59 (C6), 127.94 (C14,14"), 126.64 (C5), 124.15 (C15, 15"), 124.06 (C3), 117.58 (C1), 89.98 (C10), 21.61 (C12), 21.19 (C8). HRMS (ESI) calculated for C$_{18}$H$_{15}$N$_2$NaO$_6$: 392.0856 [M+Na]$^+$, found: 392.0853 [M+Na]$^+$.

4.3.18 4-(5-(2-Acetoxyphenyl)-3-acetyl-2,3-dihydro-1,3,4-oxadiazol-2 yl) phenyl acetate (3h)
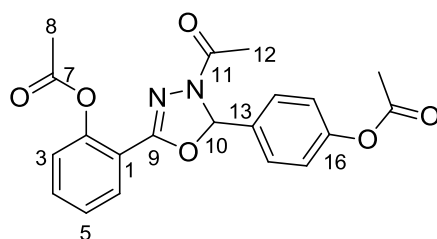
White solid (Yield: 70%), mp = 108–110°C. IR (ATIR): 1766, 1749 (2 acetyl; C=O), 1660 (C=O), 1623 (C=N) cm^{-1}. ^{1}H NMR (CDCl$_3$, 400 MHz), δ, ppm: 2.15 (s, 3H, H8"), 2.27-2.33 (m, 6H, H8, H12), 6.99 (s, 1H, H10), 7.11 (d, J = 8.6 Hz, 2H, H15, H15"), 7.15 (d, J = 8.2 Hz, 1H, H3), 7.33 (t, J = 7.7 Hz, 1H, H5), 7.48 (d, J = 8.4 Hz, 2H, H14,

H14"), 7.76 (t, J = 7.3 Hz, 1H, H4), 7.88 (d, J = 7.7 Hz, 1H, H6). ^{13}C NMR (CDCl$_3$, 100 MHz), δ, ppm: 169.38 (C=O; C7), 169.27 (C=O; C7"), 167.70 (C=O; C11), 152.93 (C9), 151.85 (C16), 149.01 (C2), 133.83 (C13), 132.83 (C4), 129.69 (C6), 128.15 (C14,14"), 126.48 (C5), 123.94 (C3) 122.10 (C15, 15"), 117.95 (C1), 90.87 (C10), 21.69 (C12), 21.22 (C8), 21.13 (C8"). HRMS (ESI) calculated for C$_{20}$H$_{18}$N$_2$NaO$_6$: 405.1067 [M+Na]$^+$, found: 405.1057 [M+Na]$^+$.

4.3.19 1,1"-(2-(4-Chlorophenyl)-5-oxobenzo[f][1,3,4]oxadiazepine-3,4 (2H,5H)-diyl) diethanone (4a)
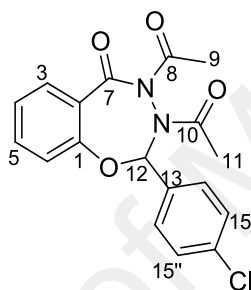
White solid (Yield: 63%), mp = 120°C. IR (ATIR): 2 (acetyl; C=O), 1757, 1737, 2 (C=O), 1699, 1661 cm^{-1}. ^{1}H NMR (CDCl$_3$, 400 MHz), δ, ppm: 1.86 (s, 3H, H9), 2.42 (s, 3H, H11), 7.22 (d, J = 7.7 Hz, 1H, H3), 7.31 (s, 1H, H12), 7.32-7.35 (m, 3H, H5, H14, H14"), 7.49 (d, J= 8.2 Hz, H15, H15"), 7.62 (t, J = 7.7 Hz, 1H, H4) 7.83 (d, J= 8.2 Hz, 1H, H6). ^{13}C NMR (CDCl$_3$, 100 MHz), δ, ppm: 172.05 (C=O; C8), 169.90 (C=O; C10), 169.02 (C7), 153.43 (C1), 135.83 (C16), 135.44 (C13), 133.46 (C5), 130.89 (C3), 128.68 (C14,14"), 128.03 (C15, 15"), 126.42 (C2), 125.94 (C4), 122.60 (C6), 86.88 (C12), 25.03 (C11), 20.61 (C9). HRMS (ESI) calculated for C$_{18}$H$_{15}$ClN$_2$NaO$_4$: 381.0619 [M+Na]$^+$, found: 381.0613 [M+Na]$^+$.

4.3.20 1,1"-(2-(4-Methylthio)phenyl)-5-oxobenzo[f][1,3,4]oxadiazepine 3,4(2*H*,5*H*)-diyl)diethanone (4d)
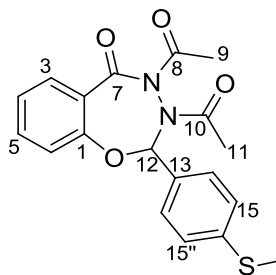
White solid (Yield: 75%), mp = 138°C. IR (ATIR): 1741, 1708, 2 acyl; C=O), 2 (C=O), 1686, 1599 cm^{-1}. ^{1}H NMR (CDCl$_3$, 400 MHz), δ, ppm: 1.89 (s, 3H, (S-CH$_3$), 2.43 (s, 3H, H9), 2.50 (s, 3H, H11, 7.25 (d, J = 8.2Hz, 2H, H14, H14" 7.24-7.28 (m, 1H, H3), 7.34-7.37 (m, 3H, H5, H12), 7.47 (d, J= 8.7 Hz, H15, H15"), 7.64 (t, J = 7.7 Hz, 1H, H4) 7.82 (d, J = 7.8 Hz, 1H, H6). ^{13}C NMR (CDCl$_3$, 100 MHz), δ, ppm: 172.01 (C=O; C8), 169.98 (C=O; C10), 169.04 (C7), 153.62 (C1), 140.38 (C16), 135.75 (C13), 131.37 (C5), 130.87 (C3), 127.02 (C14,14"), 126.35 (C2), 125.89 (C15,15"), 125.72 (C4), 122.61 (C6), 87.22 (C12), 25.06 (C11), 20.70 (C9), 15.45 (CH$_3$). HRMS (ESI) calculated for C$_{19}$H$_{18}$N$_2$NaO$_4$S: 393.0890 [M+Na]$^+$, found: 393.0879 [M+Na]$^+$.

4.3.21 1,1"-(2-(4-Ethylphenyl)-5-oxobenzo[f][1,3,4]oxadiazepine-3,4(2*H*,5*H*)-diyl)diethanone (4e)
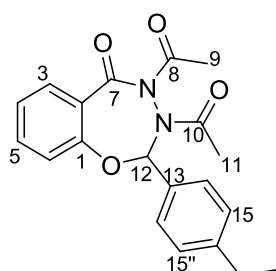
White solid (Yield: 60%), mp = 98°C. IR (ATIR): (2 acetyl; C=O), 1739, 1700, 2 (C=O), 1688, 1601 cm^{-1}. ^{1}H NMR (CDCl$_3$, 400 MHz), δ, ppm: 1.22 (t, J = 7.7 Hz, 3H, (CH$_3$), 1.86 (s, 3H, H9), 2.37 (s, 3H, H11), 2.65 (q, J = 7.6 Hz, (CH$_2$), 7.20 (m, 3H, H3, H14,H14"), 7.30 (t, J =7.5 Hz, 1H, H5), 7.34 (S, 1H, H12) 7.43 (d, J= 8.2 Hz, H15,

H15"), 7.60 (t, J = 7.7 Hz, 1H, H4) 7.82 (d, J = 7.8 Hz, 1H, H6). ^{13}C NMR (CDCl$_3$, 100 MHz), δ, ppm: 171.97 (C=O; C8), 170.06 (C=O; C10), 169.06 (C7), 153.77 (C1), 145.76 (C16), 135.71 (C13), 132.10 (C5), 130.89 (C3), 127.97 (C14,14"), 126.60 (C15, 15"), 126.25 (C2), 125.54 (C4), 122.62 (C6), 87.48 (C12), 28.73 (CH$_2$), 24.97 (C11), 20.71 (C9), 15.53 (CH$_3$). HRMS (ESI) calculated for C$_{20}$H$_{20}$N$_2$NaO$_4$: 375.1329 [M+Na]$^+$, found: 375.1315 [M+Na]$^+$.

4.3.22 1,1"-(2-(4-(tert-butyl)phenyl)-5-oxobenzo[f][1,3,4]oxadiazepine-3,4(2*H*,5*H*)-diyl)diethanone (4f)
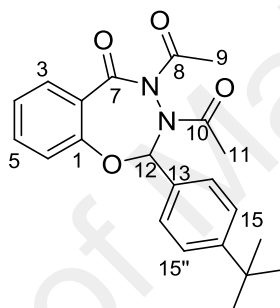
White solid (Yield: 55%), mp = 90°C. IR (ATIR): (2 acetyl; C=O), 1730, 1695, 2 (C=O), 1685, 1600 cm^{-1}. ^{1}H NMR (CDCl$_3$, 400 MHz), δ, ppm: 1.30 (s, 9H, (CH$_3$)$_3$), 1.86 (s, 3H, H9), 2.35 (s, 3H, H11), 7.20 (d, J = 7.8 Hz, 1H, H3), 7.31 (t, J =8.0 Hz, 1H, H5), 7.34 (S, 1H, H12) 7.38 (d, J = 8.6 2H, H14, H14"), 7.44 (d, J = 8.2 Hz, H15, H15"), 7.61 (t, J = 8.0 Hz, 1H, H4), 7.83 (d, J = 7.8 Hz, 1H, H6). ^{13}C NMR (CDCl$_3$, 100 MHz), δ, ppm: 172.00 (C=O; C8), 170.05 (C=O; C10), 169.07 (C7), 153.79 (C1), 152.72 (C16), 135.72 (C13), 131.80 (C5), 130.93 (C3), 126.36 (C14,14"), 126.09 (C2), 125.47 (C4), 125.39 (C15, 15"), 122.60 (C6), 87.46 (C12), 34.78 (C-*tert*-But), 31.35 (*tert*-But), 24.94 (C11), 20.71 (C9) HRMS (ESI) calculated for C$_{22}$H$_{24}$N$_2$NaO$_4$: 403.1638 [M+Na]$^+$, found: 403.1628 [M+Na]$^+$.

4.4   Discussion

4.4.1   Spectroscopic Features of (1a-h), (2a, 2b), (3a-h) & (4a, 4f, 4e, 4d)

The positions of IR bands provided significant indication for the formation of compounds **1a-h**, **2a**, **2b**, **3a-h**, **4a**, **4f**, **4e**, and **4d**. The bands on the IR spectra of these compounds were mainly due to the C=N, C=O and C-O-C functional groups. A strong band at 1677-1645 cm^{-1} could be assigned to C=O stretching, which had actually undergone shifting to a lower wave number due to the conjugated system in the compounds. The absorption bands at 1577-1504 cm^{-1} were attributed to the C=N stretching vibrations. Compounds **1a-h** showed sharp bands in the region 3271-3240 cm^{-1} from N-H stretching vibrations. In addition, the absorption bands at 1231-1219 cm^{-1} were attributed to the C-O-C, stretching which confirmed the formation of the desired oxadiazoline ring in compounds **2a, 2b** and **3a-h**. In addition, the band due to *v* N-H stretching was not observed. Compounds **4a**, **4d**, **4e** and **4f** showed two absorption bands in the region 1757-1695 cm^{-1} due to the stretching vibrations of two acetyl (C=O) groups.

Further evidence for the formation of compounds **1a-h**, **2a**, **2b**, **3a-h, 4a**, **4d**, **4e** and **4f** were obtained by ^{1}H NMR spectroscopy, which provided information for the positions of the protons. In the ^{1}H NMR spectra, phenyl protons were observed at the expected chemical shifts and appropriate integral values in all compounds. The single peak at 8.43-12.01 ppm was assigned to the amino proton, N-H peak in all compounds **1a-h,** while the H-C=N proton showed single peak at 7.3-11.84 ppm (see ^{1}H NMR spectrum of **1a-h** in Appendix B. 1-8). In the ^{13}C NMR spectra, phenyl carbons were observed at the expected chemical shifts with appropriate integral values for all compounds **1a-h** and the C=N carbon of compounds found at 146.48-159.65 ppm. In addition, the peak for the carbonyl carbon was found to be at 165.21-165.30 ppm (see ^{13}C NMR spectrum of **1a-h** in Appendix B. 23-29). As for the compounds **3a-h, 2a** and

88

2b, no peaks for N-H and H-C=N proton were observed. Presumably, these peaks disappeared following the ring closure. The peak for the proton in the oxadiazoline ring was observed with the expected chemical shift at 6.9-7.04 ppm. In addition, the two single peaks at 2.27-2.24 ppm and 2.28-2.45 ppm were due to the six protons of the acetyl group (See ^{1}H NMR spectrum of **3a-h, 2a** and **2b** in Appendix B. 9-17). For compounds **4a**, **4d**, **4e** and **4f**, the peaks of N-H and H-C=N protons were not observed after the ring closure. The proton of the oxadiazepine ring was observed with peak at the expected chemical shift of 7.31-7.43 ppm. Similarly, the two single peaks at 1.86-2.43 ppm and 2.35-2.50 ppm were due to six protons of the acetyl groups (see ^{1}H NMR spectrum of **4a, 4d, 4e** and **4f**, in Appendix B. 18-21). In the ^{13}C NMR spectra, the greatest differences observed between the compounds **1a-h** and compounds **3a-h** were in the peaks for the C=N carbon (C8) of compounds **1a-h** found at 146.48- 159.65 ppm, while the peaks for the C10 carbon belonging to the oxadiazoline ring in the ^{13}C NMR spectra for **3a-h** were observed at the expected chemical shift of 89.98-91.64 ppm. (See ^{13}C NMR spectrum of **1a-h** and **3a-h** in Appendix B. 22-36). Compounds **4a**, **4d**, **4e** and **4f** showed similar differences from **1a-h** and **3a-h**, where the signals for the three carbonyl carbons (C7, C8 and C10) were observed at 169.02-169.07 ppm, 171.97-172.05 ppm and 169.90-170.06 ppm, respectively (see ^{13}C NMR spectrum of **4a**, **4d**, **4e** and **4f** in Appendix B. 37-40). In addition, the signals for the C10 carbon belonging to the oxadiazoline ring in the ^{13}C NMR spectra for **3a-h** and **4a**, **4d**, **4e** and **4f** were observed at the expected chemical shift of 89.98-91.64 ppm while the signals for carbon C12 for the oxadiazapine compounds **4a**, **4d**, **4e** and **4f** were observed at the expected chemical shift of 86.88-87.48 ppm.
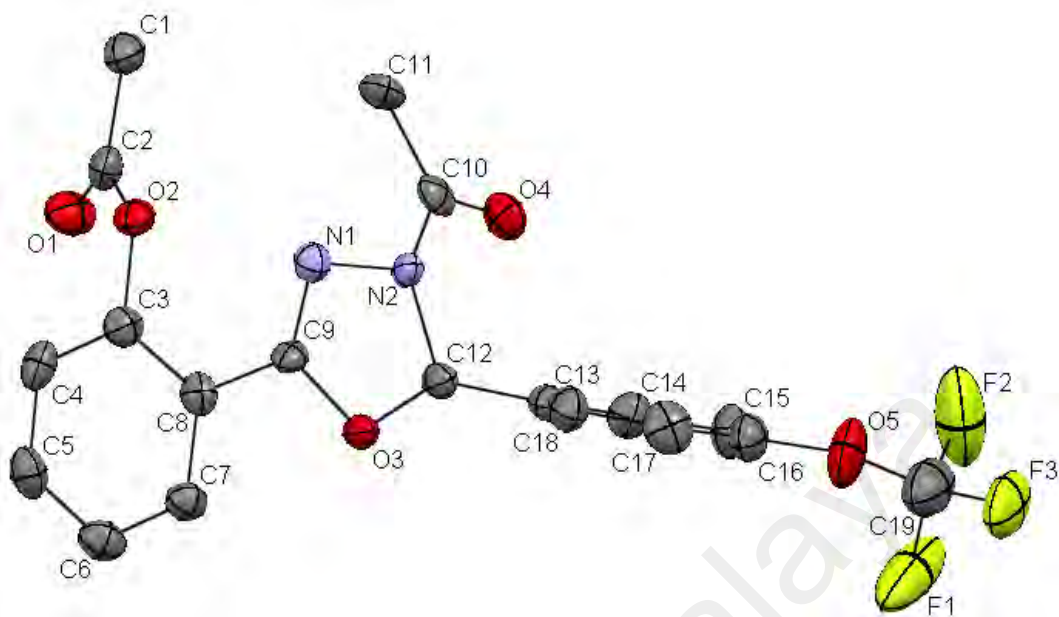
Figure 4.1: The molecular structure of **3c** with atoms shown at 50% probability level

Figure 4.1 shows the Oak ridge thermal ellipsoid plot program for crystal structure illustrations (ORTEP) diagram for the structure of molecule **3c** which is twisted about the C12—C13 bond. Within the five-membered oxadiazoline ring, there is a formal C9=N1 double bond (1.282 (3) Å). The bond distance of C9—O3 (1.37 (2) Å) is considerably shorter than that of C12—O3 bond (1.443 (2) Å), suggesting some delocalization of π-electron density over the O3—C9—N1 chromophore via the presence of a *pi* bond with an adjacent atom bearing lone pairs of electrons. Furthermore, the acyl group is coplanar with the oxadiazoline ring [O—C—N—C torsion angle = -12.81 (3)°]. (For more details, see Appendix C. 1)
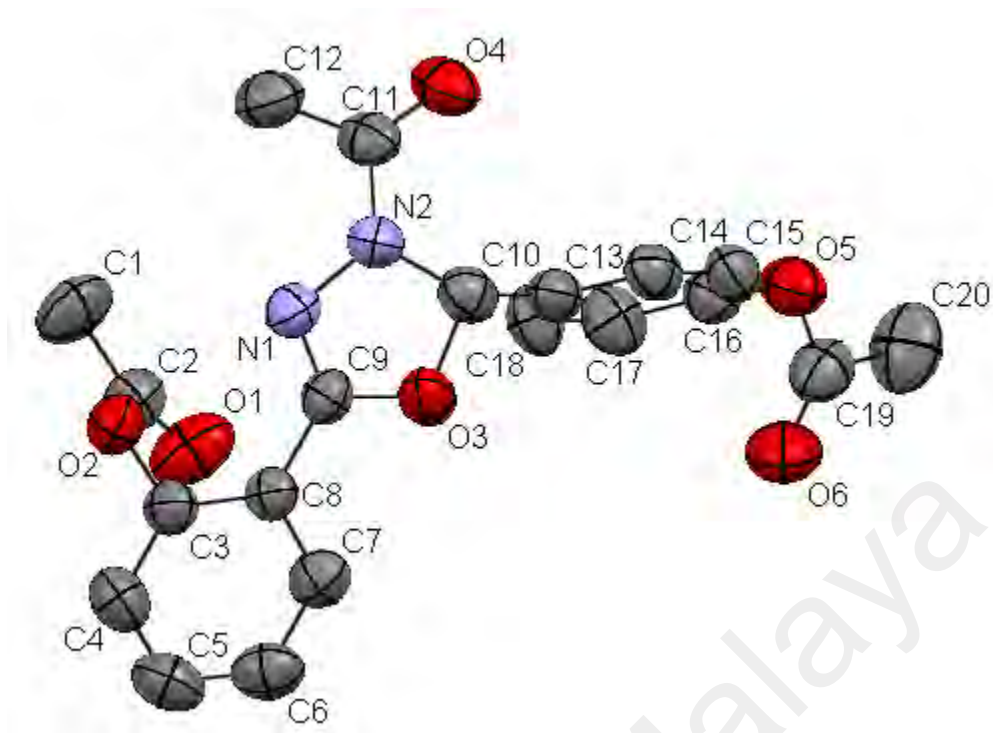
Figure 4.2: The molecular structure of **3h** with atoms shown at 70% probability level

Figure 4.2 is the ORTEP diagram for the structure of molecule **3h,** which is twisted about the C10—C13 bond. Within the five-membered oxadiazoline ring, there is a formal C9=N1 double bond (1.279 (3) Å). The bond distance of C9—O3 (1.366 (2) Å) is considerably shorter than C10—O4 bond (1.448 (2) Å), suggesting some delocalization of π-electron density over the O3—C9—N1 chromophore. Furthermore, the acyl group is coplanar with the oxadiazoline ring [O—C—N—C torsion angle = 0.54 (3) Å]. (For more details, see Appendix C. 2)
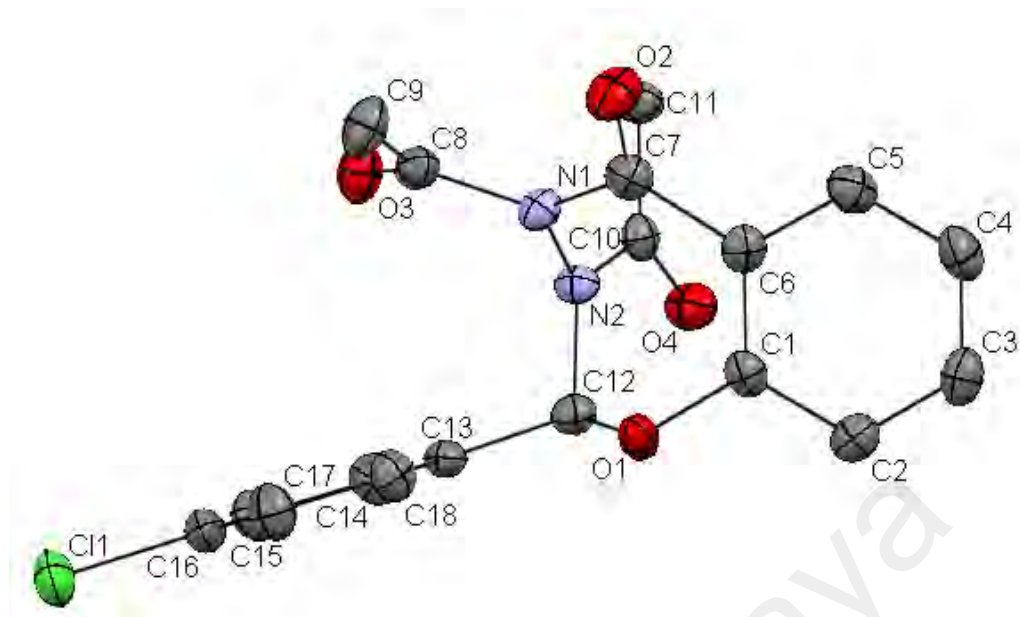
Figure 4.3: The molecular structure of **4a** with atoms shown at 50% probability level

Figure 4.3 is an ORTEP diagram showing the structure of molecule **4a** which is twisted about the C12—C13 bond. The atom O1 lies near to the mean plane of the aromatic ring to which it is bonded (deviation: 1.378(2) A). Furthermore, the acyl group is coplanar to the oxadizepine ring [O4—C10—N2—C12 torsion angle = 3.25 (3) Å], while the other acyl group is perpendicular to the oxadizepine ring [O3—C8—N1—C7 torsion angle= 159.21 (3) Å]. The chloro-substituted phenyl ring is almost orthogonal to the oxadizepine ring, the dihedral angle between them being 108.17°. (For crystal data and structure refinement, see Appendix C. 3)
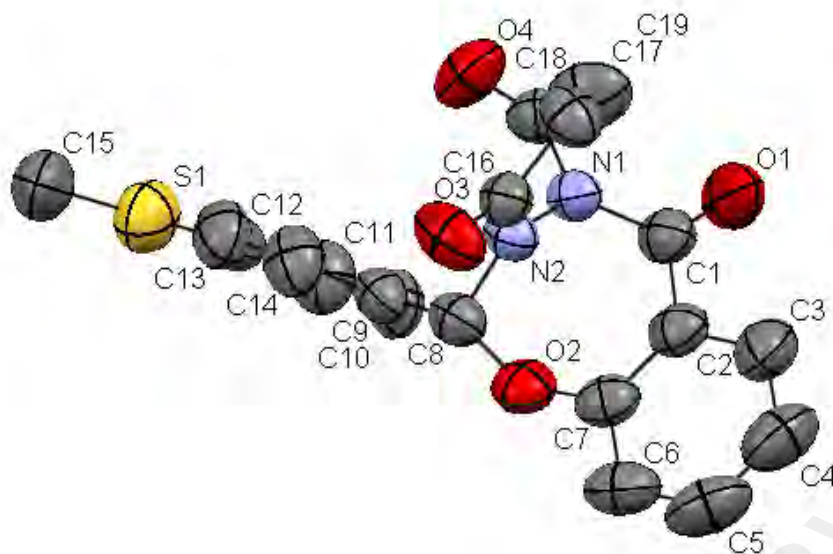
Figure 4.4: The molecular structure of **4d** with atoms shown at 50% probability level

Figure 4.4 shows the ORTEP diagram for the structure of molecule **4d** which is twisted about the C8—C9 bond. Atom O2 lies near the mean plane of the aromatic ring to which it is bonded [deviation: 1.382 (2) Å]. Furthermore, the acyl group is coplanar with the oxadizepine ring [O3—C16—N2—C8 torsion angle= -4.99 (3)°], while the other acyl group is perpendicular with the oxadiazepine ring [O4—C18—N1—C1 torsion angle = 160.10 (3) Å]. The thiomethyl-substituted phenyl ring is almost orthogonal with the oxadiazepine ring, the dihedral angle between them being 108.88°. (For more details, see Appendix C. 4).
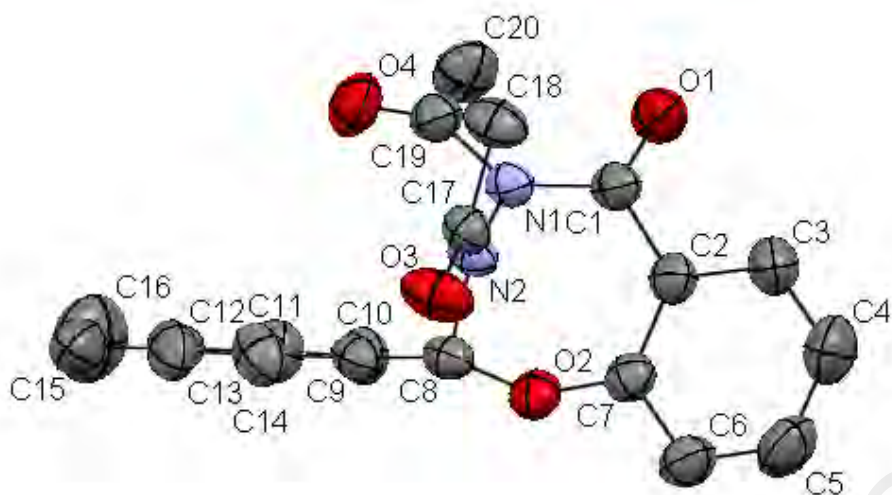
Figure 4.5: The molecular structure of **4e** with atoms shown at 50% probability level

Figure 4.5 is an ORTEP diagram showing the structure of molecule 4e which is twisted about the C8—C9 bond. Atome O2 lies near the mean plane of the aromatic ring to which it is bonded [deviation: 1.369 (2) Å]. Furthermore, the acyl group is coplanar with the oxadiazepine ring [O3—C17—N2—C8 torsion angle = -2.47 (3) Å], while the other acyl group is perpendiculur with the oxadiazepine ring [O4—C19—N1—C1 torsion angle = 160.18 (3) Å]. (For more details, see Appendix C. 5)

4.4.3 Formation of 1,3,4-Oxadiazoline and 1,3,4-Oxadiazepine Through Acetylation of Salicylic Hydrazones

The syntheses of 1,3,4-oxadiazoline and oxadiazapine compounds began with the reaction between hydroxybenzohydrazide with various *para*- substituted benzaldehyde derivatives to produce hydrazones **1a-h** (Scheme 4.1, p. 72). Reactions of substituted benzaldehyde acylhydrazones **1a-h** in acetic anhydride at 120-130°C resulted in the cyclised products **3a-h** (Scheme 4.2, p. 73). The reactions proceeded smoothly with no side products observed. Under these acylation conditions, compounds **1a-h**, possessing either electron-donating or electron-withdrawing substituents on the aryl ring cyclised to give 1,3,4-oxadiazolines **3a-h** in 58-85% yields (Table 4.1). The presence of an electron-withdrawing substituent on the phenyl ring tended to give better yields, with

the best yield obtained with a nitro substituent, and the lowest with a *t*-butyl substituent. This is to be expected since a strong electron-withdrawing group such as NO$_2$ on the aryl ring would enhance the electrophilicity of the iminium carbon, whilst an electron-donating group would decrease the electrophility.

Table 4.1: Structures and yields of synthesized compounds **3a-h**
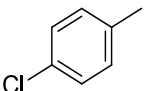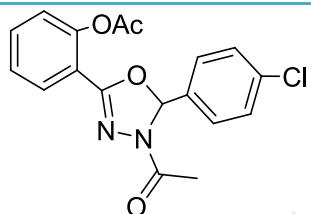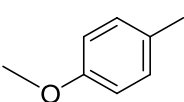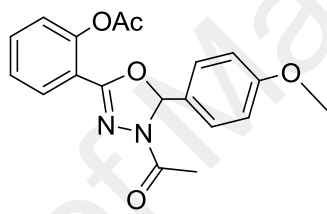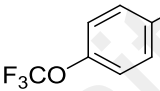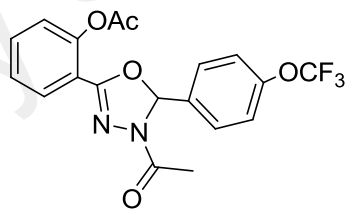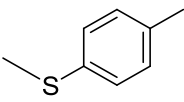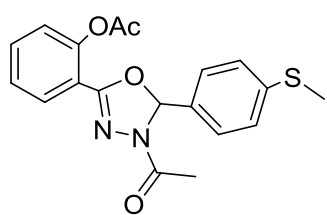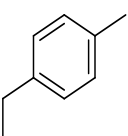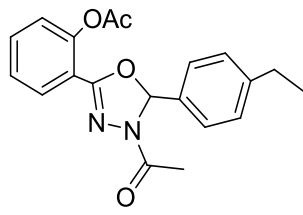
Entry	Ar	Product [a]	Yield [c]
1		**3a** [b]	78%
2		**3b**	70%
3		**3c** [b]	70%
4		**3d**	65%
5		**3e**	60%
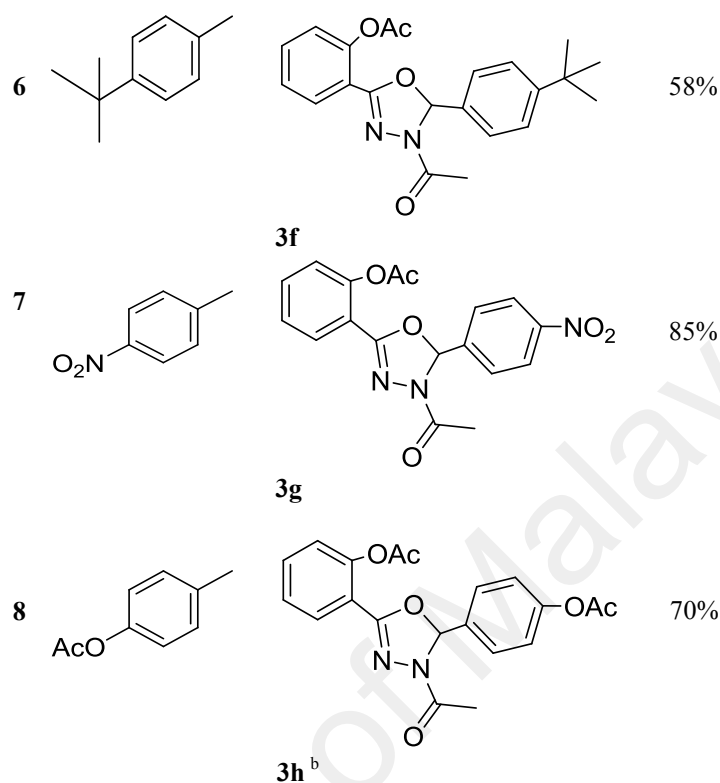
| 6 | | 58% |

3f

| 7 | | 85% |

3g

| 8 | | 70% |

3h [b]

When the cyclization reactions of **1a-h** were carried out at 50-60°C in acetic anhydride/acetic acid solution, 1,3,4-oxadiazepines **4a**, **4d**, **4e** and **4f** were obtained instead of the 1,3,4-oxadiazoline analogs, in some cases (Scheme 4.3, p. 73). Table 4.2 summarizes the products of the cyclization reactions of compounds **1** using the Ac₂O-AcOH conditions. Presumably, the acidic conditions influenced the reaction in some manner to form the seven-membered oxadiazepines.

Table 4.2: Structures and yields of compounds **4(a**, **d**, **e**, **f)** and **3(b**, **c**, **g**, **h)**
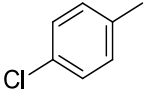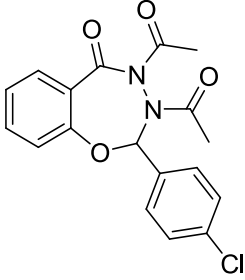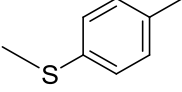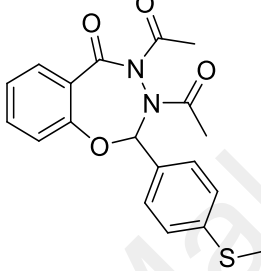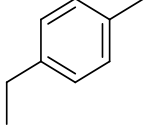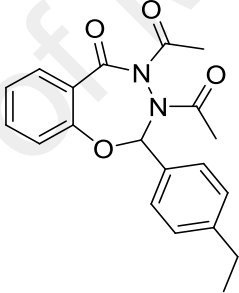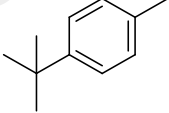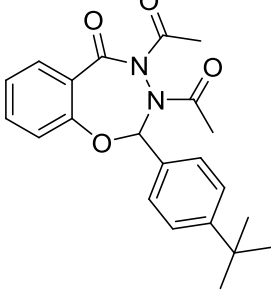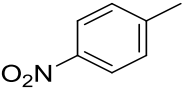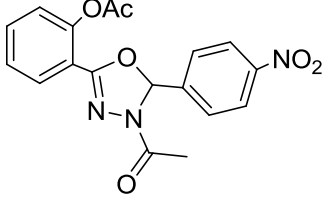
Entry	Ar	Product	yield[c]
10		**4a[b]**	63%
11		**4d[b]**	75%
12		**4e[b]**	66%
13		**4f**	55%
14		**3g**	70%

Table 4.2, continued

15   65%

3c

16   65%

3b

17   63%

3h
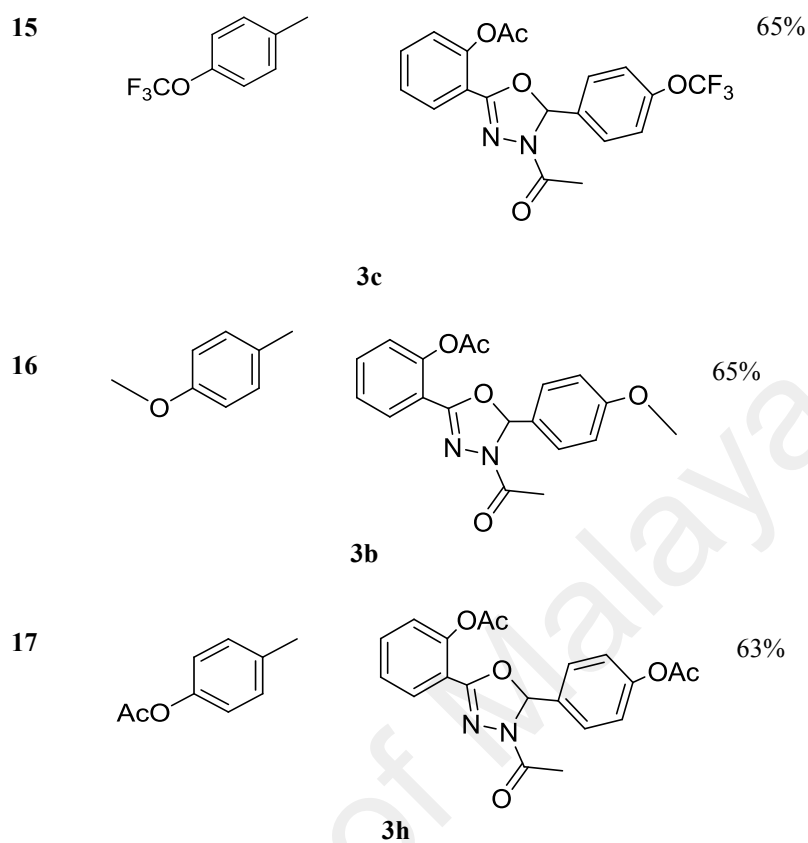
^b Structure was confirmed by X-crystallograph
^c Isolated yield after recrystallization

In this study two pathways have been proposed leading to the formation of the oxadiazolines **3** (Scheme 4.4). One pathway involves acetylation of the free hydroxyl group on the benzene ring to form **5** that undergoes subsequent intramolecular cyclization to form **3** (Pathway A). An alternative pathway involves an intramolecular cyclization of **1** to first produce **2a** and **2b,** followed by acylation of the phenol to form **3** (Pathway B).
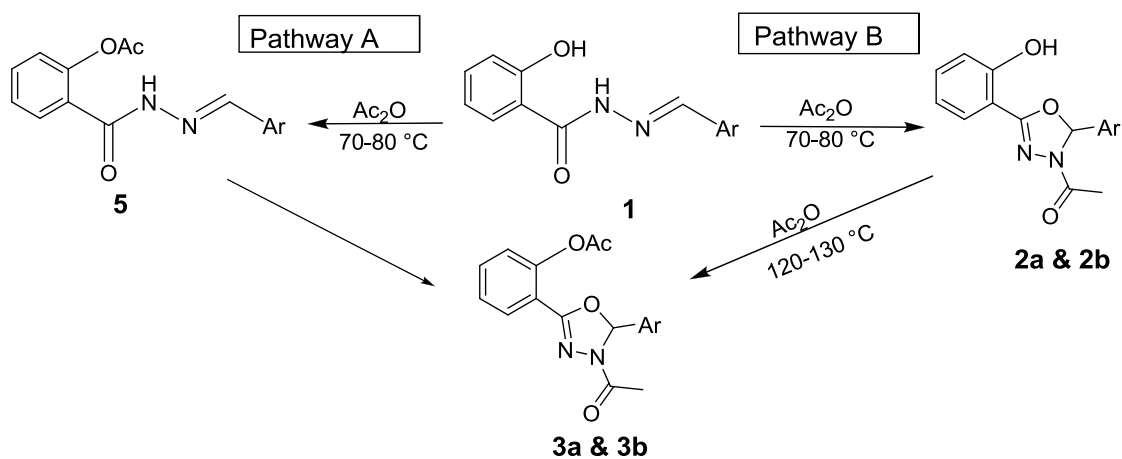
Scheme 4.4: Pathways cyclization of **1**

However, since only the oxadiazolines **2a** and **2b** were isolated with a free *ortho* phenolic group and no product **5** was observed in this reaction, it could be concluded that the cyclization of compound **1** went through pathway B. In this pathway, compounds **2a** and **2b** were first formed, which then underwent acetylation to produce **3a** and **3b** (Scheme 4.4).

It has been well-established that compound **1** can undergo keto-enol tautomerisation as shown in Figure 4.6 (Lin *et al*., 1999).
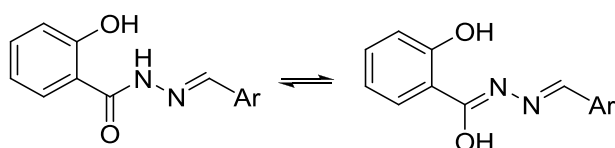
Figure 4.6: Tautomerisation of compound **1**

Hence, in this study, it is proposed that the mechanism for the oxidative cyclization reactions leading to **2a** and **2b** involves the attack of the enolic oxygen of the enol tautomer at the azomethine imine moiety as shown in Scheme 4.5.
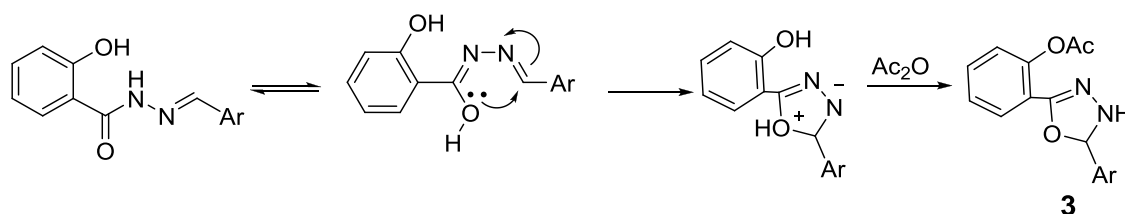
Scheme 4.5: A plausible mechanism for the formation of compounds **3a-h**

In the case of the seven membered oxadiazepines, it is proposed that the mechanism of formation occurs via nucleophilic attack of the phenolic oxygen on the iminium carbon, as shown in Scheme 4.6. Here, the iminium carbon acted as a carbonyl analogue and participated in an intramolecular nucleophilic addition reaction (Dewick, 2006; Jiang & Chen, 2011) with the *ortho* phenolic group. Subsequently, the oxadiazepines underwent acetylation to give the diacetylated product **4** (Scheme 4.6).
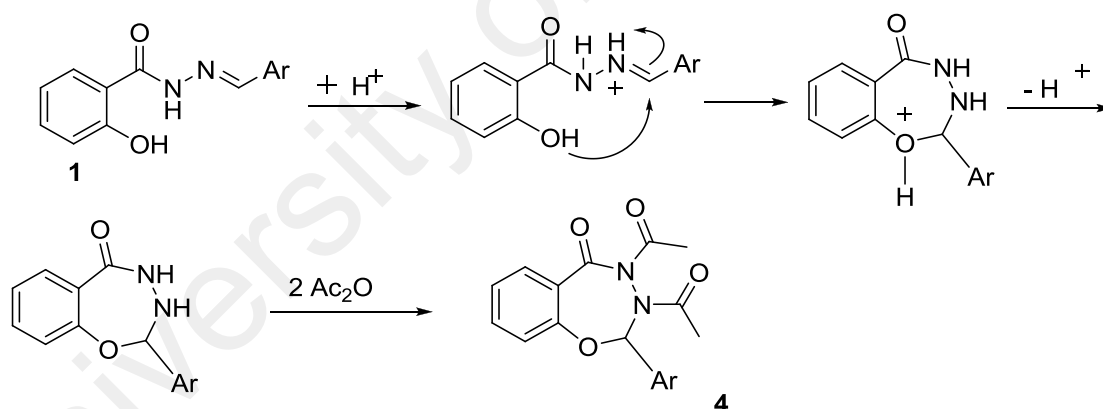
Scheme 4.6: A plausible mechanism for the formation of compounds **4(a**, **d**, **e** & **f)**

CHAPTER 5: *IN VITRO* COX ENZYME INHIBITION STUDIES

5.1   Introduction

There are several types of assays that can be utilized to evaluate the COX-2 selectivity. Previously, *in vitro* assays that utilised animal enzymes or cell lines were used. Even though *in vitro* human whole blood assay is criticised for its inherent limitation which may not give accurate reflection of the COX inhibition in target tissues (e.g gastric mucosa), it has been used for COX-2 selectivity evaluation (Goei The *et al*. , 1997). More recently, human target cells such as gastric mucosal cells, chondrocytes and synoviocytes have been used to prepare *in vitro* assays. *Ex vivo* assays which measure COX-2 selectivity by the relative inhibition of TXB2 in monocytes and macrophages, platelet accumulation and renal PGE2 synthesis, have also been used.

5.2   Materials

The COX Inhibitor Screening Assay Kit was purchased from Cayman Chemical (Ann Arbor, MI, USA). The materials included in the kit are Prostaglandin (PG) screening enzyme immunoassay (EIA) antiserum, PG screening Acetylcholinesterase (AchE) tracer, PG Screening EIA Standard, EIA buffer, wash buffer, tween 20, mouse anti-rabbit immunoglobulin (IgG) coated plate, 96-well cover sheet, Ellman's reagent, reaction buffer, COX-1 (ovine), COX-2 (human recombinant), heme, arachidonic acid, potassium hydroxide, hydrochloric acid and stannous chloride. Celecoxib was purchased from Sigma Aldrich (St. Louis, MO, USA). Ultra pure water was used to prepare all the EIA reagents and buffers.

5.3   **Methods**

COX inhibitory activity was measured using an enzyme immunoassay (EIA) Screening Assay Kit (Catalog No 560131) from Cayman Chemicals, Ann Arbor, Michigan, U.S.A. The kit was used to measure the COX-1 and COX-2 derived Prostaglandin H_2 (PGH_2) produced in the COX kit reaction. The prostanoid product was quantified using a broadly specific antiserum that bound to all major prostaglandins. All samples and positive controls were added as DMSO solutions to assay solutions. All procedures were performed as indicated in the assay kit instructions. The control consisted of 475 µl of 100 mM Tris-HCl buffer pH 8.0, 5 µl heme, 5 µl of COX-1 or COX-2 and 10 µl of 100 mM Tris-HCl buffer pH 8.0 containing 0.5% DMSO. The background was similar to the control except that the enzyme was heat inactivated. Each COX sample was assayed in triplicate.

5.4   **Data Analysis**

IC_{50} values were calculated with GraphPad Prism software version 5.02 from dose-response curves generated. All data are expressed as mean ± S.E.M in triplicate. Statistical significance was assessed using the Student's t-test in Excel (Microsoft). The level of significance was set at $^*P < 0.05$, indicating statistically significant. Percent inhibitory activity of each compound was derived using the following equation:

$$\text{Percentage inhibition} = \frac{[(Abs_{control} - Abs_{background}) - (Abs_{sample} - Abs_{background})]}{(Abs_{control} - Abs_{background})} \times 100\%$$

where $Abs_{control}$ = absorbance of control mixture at 100% initial activity; Abs_{sample} = absorbance of sample mixture; and $Abs_{background}$ = absorbance of background.

5.5   Results and Discussion

5.5.1   Determination of the Concentration of Prostaglandin

The % B/B_o (% Bound / Maximum Bound) on the prostaglandin standard curve was calculated, and the harmonious values on the x-axis were recorded to identify the production amount of prostaglandin (Figure 5.1). As soon as the production amount of prostaglandin has been confirmed, the percentage inhibition can be calculated.
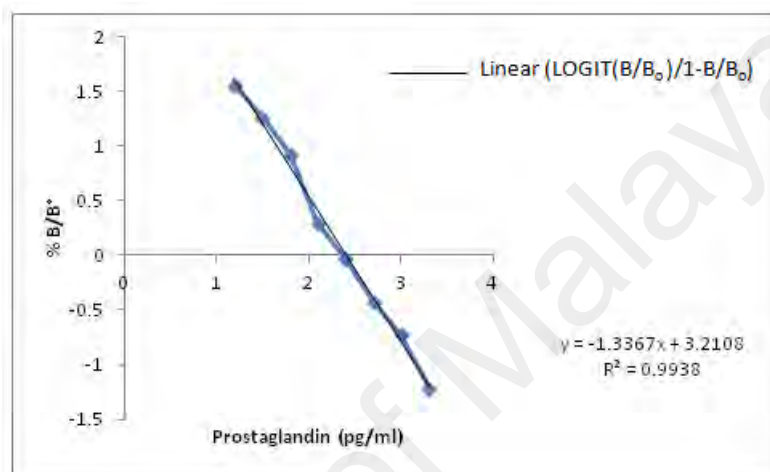
Figure 5.1: Prostaglandin standard curve, where % B/B_o; is the ratio of the absorbance of a paticular sample or standard to that from solution with the maximum binding (B_o); and 1-B/B_o is prostaglandin concentration (pg/mL).

5.5.2   Effects of Compounds (3a-h) on COX-1 and COX-2 Enzymes

Compounds **3a-h** were assayed at graded concentrations ranging from 1.56 μM to 50 μM, and activities were compared to the standard reference drug, celecoxib (1.56 μM to 25 μM). As shown in Figure 5.2, celecoxib displayed a dose dependent inhibition of COX-1 and COX-2 activities. The findings were analogous to those reported by (Uddin *et al*., 2004; Habeeb *et al*., 2001; Praveen Rao *et al*., 2003). The COX 2 inhibitory activity was observed to increase with the increase in the concentration of the compounds.
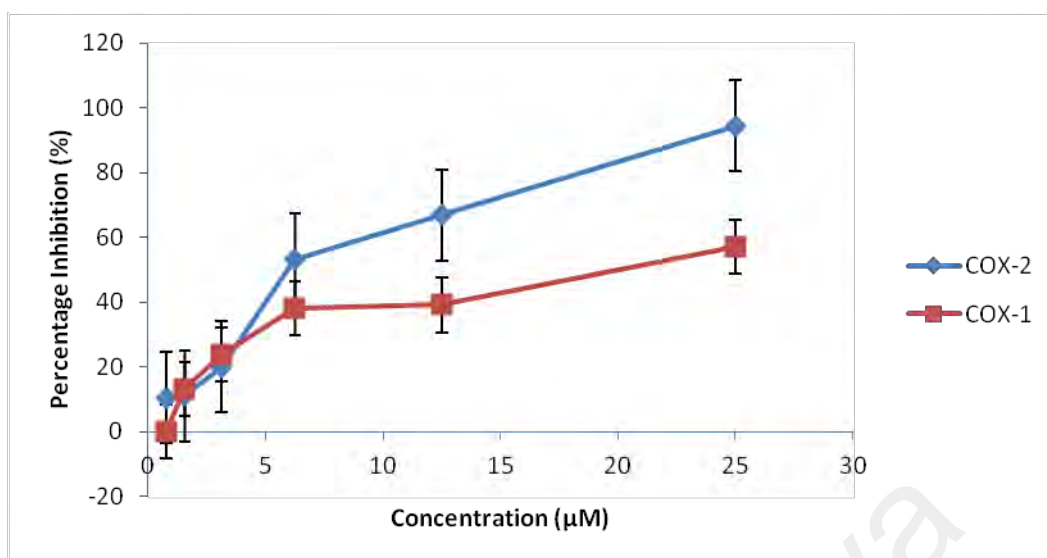
Figure 5.2: Percentage inhibition of celecoxib on COX-1 and COX-2 activities

As shown in Figure 5.3, the maximal COX-2 inhibition at a concentration of 50 μM for each compounds were 82% (**3h**), 80% (**3a**), 76% (**3c**), 59% (**3g**), 54% (**3d**), 52% (**3b**), 52% (**3f**) and 51% (**3e**), respectively. The standard reference, celecoxib, demonstrated an inhibition of 94.4% of COX-2 at 25 μM concentrations.
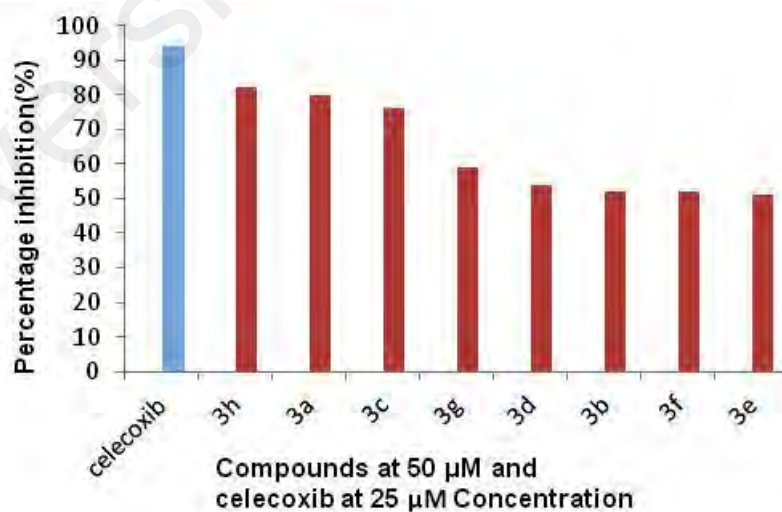
Figure 5.3: Percentage inhibition of compounds **3a-h** and celecoxib on COX-2 activity

As shown in Figure 5.4 maximal COX-1 inhibition of 54%, 52%, 51.2%, 51%, 18.6%, 7.3%, 7% and 6.5%, were observed at a concentration of 50 μM of compounds **3c**, **3a**, **3h**, **3g**, **3f**, **3e**, **3d** and **3b,** respectively. The standard reference, celocoxib, demonstrated an inhibition of 56.9 % of COX-1 at 25 μM.
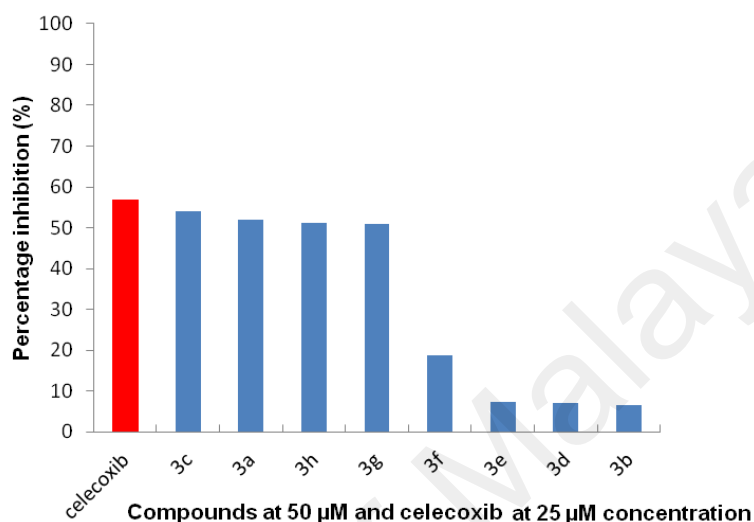
Figure 5.4: Percentage inhibition of compounds **3a-h** and celecoxib on COX-1 activity

The IC$_{50}$ values for compounds **3a-h** and celecoxib are listed in Table 5.1. These values are the dose-response inhibition of **3a-h** on ovine COX-1 and human recombinant COX-2, and were calculated using the GraphPad Prism software.

Table 5.1: IC_{50} values of compounds tested as inhibitors of COX-1 and COX-2

| Compounds | NO. | IC_{50}^{a} (μM) ± S.E.M [c] | | Selectivity index[b] |
		COX-1	COX-2	IC_{50} COX-1 / IC_{50} COX-2
Celecoxib	*	23 ± 0.05	0.10±0.001	230
3h	7	35 ± 3	0.19±0.005	175
3c	2	37±0.7	0.29 ± 0.01	124
3a	5	35 ±2.6	0.33 ± 0.01	106
3g	3	37 ±0.6	0.90 ±0.01	41
3b	4	>50 [d]	0.70±0.05	86
3d	6	>50 [d]	0.70±0.005	83
3e	8	>50 [d]	1.20±0.1	52
3f	1	>50 [d]	48±2.3	3.3

[*]Standard drug
[a] The *in vitro* test compound concentration required to produce 50% inhibition of ovine COX-1 or human recombinant COX-2, which was determined by nonlinear regression analysis, using GraphPad Prism software. The result (IC_{50}, μM) is the mean of three determinations and the deviation from the mean is < 10% of the mean value. Statistical significance of differences was assessed by using the Student's *t*-test in Excel (microsoft). The level of significance was set at [*]$P < 0.05$.
[b] *In vitro* COX-2 selectivity index (COX-1 IC_{50}/COX-2 IC_{50}).[c] S.E.M: standard error of the mean. [d] No inhibition of COX-1 up to 50 μM and precipitation of compounds observed beyond this concentration.

5.5.3 Discussion

In the enzyme inhibitory assay study, celecoxib had shown in high potency and selectivity towards COX-2 with IC_{50} values of 0.1 μM for COX-2 and 23 μM for COX-1, which is in the same range as previously reported, (Habeeb *et al*., 2001). The effectiveness of the tested compounds were evaluated as the concentration of compounds resulting in 50% enzyme inhibition (IC_{50}) (Table 5.1). Compounds **3a-h** showed appreciable results on the activity as COX-2 inhibitors that depend on the type of substituents at the *para*-position of one of the aryl rings. Compounds **3a-h** displayed only low or no inhibition against COX-1 enzyme in the range of 35 μM to ≤ 50 μM. Compounds **3b**, **3d**, **3e** and **3f** having large electron-donating substituents (OCH$_3$, SCH$_3$, CH$_3$CH$_2$, *t*-But, respectively), showed low inhibition against COX-2 enzyme, as indicated by the IC_{50} values in the μM range (0.7 μM to 48 μM). Additionally, strong

electron-withdrawing substituents such as OAc, OCF_3, and Cl in compounds **3h**, **3c** and **3a** respectively, led to IC_{50} values in the submicro molar range (0.19 - 0.33 μM) and SI values of 175, 124, and 106, respectively. This is evidence of the selectivity and efficacy of these compounds as COX-2 inhibitors. Compound **3g** with NO_2 substituent, however, showed low inhibition against COX-2 as exhibited by an IC_{50} value of 0.9 μM.

One of the major challenges that can be seen in drug discovery is selectivity (therapeutic) index. A reasonable number of drug candidates fail, even though there is surge in spending in the research and development of new drugs. This is due to the small therapeutic effect at nano toxic concentrations required. This is especially the case for the treatment of cancer, metabolic, and inflammatory disorders (Lehar *et al.*, 2009). The selectivity indices of the compounds towards COX-2 were determined and compared with that of celecoxib. In the assay, the IC_{50} values of celecoxib towards COX-1 and COX-2 were calculated to be 23 and 0.1 μM, respectively, indicating celecoxib to be a highly selective COX-2 inhibitor, while **3a**, **3b**, **3c**, **3d**, and **3h** showed moderate selectivity towards COX-2, lower than that of celecoxib. The involvement of less number of hydrogen bonding in ligand-protein interaction resulted in the reduced selectivity of the compounds in comparison to celecoxib. Despite the low rates of gastrointestinal unfavorable effects of selective COX-2 inhibitors, the high selectivity of COX-2 inhibitors results in increase of cardiovascular side effects by tipping the balance of prostacyclin and thromboxane toward vasoconstriction and thrombosis (James *et al.*, 2007; Dajani & Islam, 2008). Plausibly, the synthesized compounds **3a**, **3b**, **3c** and **3h** with moderate selectivity may have less cardiovascular side effects.

These results, COX-2 inhibitory potency and selectivity with IC_{50} findings support the suggestion the significance of electronic influence on hydrazone derivatives, special

design around the oxadiazoline core and increasing the size of the *para* substituent, enhanced COX-2 inhibiting activity (Portevin *et al*., 2000).

Structure-activity relationship (SAR) study performed on compounds **3a-h** in the order of COX-2 inhibitory potency and selectivity is depended on the substituent on ring and follows the order: $OAc > OCF_3 > Cl > NO_2 > OCH_3 > SCH_3 > CH_3CH_2 > t$-But. The acetyl moiety (OAc), as known in aspirin, is liable for acetylation and blocking the COX enzyme by acetylating the protein. In medicinal chemistry, single fluorine atom, trifluoromethyl or trifluoromethoxy groups are usually used to tailor the pKa values of the lead compound and to assist cell membrane penetration and improve its metabolic stability of compounds. These advantages of fluorine contribute to the critical "bioavailability" of therapeutically active compounds. The increasing interest and use of the trifluoromethoxy substitutent in drugs and agrochemical products show challenging synthetic strategies, which are highly being implemented in industrial and academic research programmes. Trifluoromethoxy group is more electron-withdrawing and more lipophilic in nature than its methoxy analogue, so it results in increasing the metabolic stability of a compound (Leroux *et al*., 2008). Additionally, the findings of compounds **3a-h** as COX-2 selective inhibitors are also supported by a number of studies on tricycle syntheses possessing two vicinal aryl moieties on the central heterocyclic ring arrangement (Singh & Mittal, 2008).

CHAPTER 6: CONCLUSION

In our efforts to generate new selective COX-2 enzyme inhibitors, the following approaches were employed in this study: a structural based drug design (SBDD), SAR study, ADMET prediction, RO5 prediction, design of compounds, syntheses and biological evaluations.

Using diaryl heterocyclic compounds as template for a new class of COX-2 selective inhibitors, a total of eight 1,3,4-oxadiazoline derivatives **3a-h** were designed and docked onto the active sites of COX-1 and COX-2 enzymes to investigate their binding affinities. Results obtained were compared to that of SC-558 (celecoxib) as the standard drug of use. Ligand binding interactions that contributed to enzyme inhibition activity were studied and the ADMET properties and RO5 compliance were predicted.

Based on the SAR, binding interactions, ADMET and RO5 studies, we suggested a potential lead structure as selective COX-2 enzyme inhibitor. Compounds **3a-h** were then synthesized through a one-step intramolecular cyclization reaction of a variety of substituted benzaldehyde acylhydrazones with free hydroxyl group at the *ortho* position of the phenyl ring in the acylhydrazone. Based on 1,3,4-oxadiazolines or 1,3,4-oxadiazepines obtained in some cases, when the reactions were carried under acid-catalysed conditions. This method will allow future researchers to carry out studies to prepare 1,3,4-oxadiazepine compounds. Bioassay studies on compounds **3a-h** indicated that the presence of electron-withdrawing groups such as OAc, OCF_3 & Cl in the compounds favoured selectivity towards COX-2 over COX-1 enzyme.

6.1 **Future Studies**

The potential lead compounds **3a-h** (Figure 3.2) could be used in the future drug design research for COX-2 selective inhibitors, starting by synthesizing new compounds with the proposed features for *in vitro* assay investigation. Furthermore, compounds **3a-**

109

h could also be used for future studies for antioxidant activity. *In vivo* testing using the carrageenan–induced rat paw oedema model can be performed depending on the results achieved from the *in vitro* analysis of a COX-2 inhibitor to study acute local inflammation, cancer and arthritis. Additionally, compounds **3a-h** could be used in further *in vitro* studies such as cell bioassay to confirm their inhibition activities as well as toxicity at the cellular level.

6.2 **Limitations of Study**

One of the limitations of this study is that, the lowest binding energy computed by AutoDock software which, cannot be used directly to defined the real binding energy of a compound. That is mostly because the AutoDock software uses implied water environment, with only parameters amended for water environment, rather than uses explicit water environment where certain water molecules will be combined for calculation. However, eventhough this method might be more accurate, it consumes a lot of time and computer power. Furthermore, AutoDock software uses semi empirical force fields for energy calculation rather quantum mechanic force field with more accuracy and so on, this technique is time and computer power consuming. So, AutoDock software with faster calculating time was used in spite of it is less accuracy.

In addition, the purchasable of chemicals and solvents for the syntheses of compounds **3a-h,** and the Kit (Catalog No 560131) from Cayman Chemicals using an enzyme immunoassay (EIA) Screening Assay were quite costly.

REFERENCES

Aithal, G. P., & Day, C. P. (2007). Nonsteroidal anti-inflammatory drug–induced hepatotoxicity. *Clinics in Liver Disease, 11*(3), 563-575.

Andricopulo, A. D., & Montanari, C. A. (2005). Structure-activity relationships for the design of small-molecule inhibitors. *Mini-Reviews in Medicinal Chemistry, 5*(6), 585-593.

Antman, E. M., Bennett, J. S., Daugherty, A., Furberg, C., Roberts, H., & Taubert, K. A. (2007). Use of nonsteroidal antiinflammatory drugs: An update for clinicians: A scientific statement from the american heart association. *Circulation, 115*(12), 1634-1642.

Arora, P., Mittal, A., Kaur, G., & Chauhan, A. (2013). Synthesis of some novel oxadiazole based chalcone derivatives as anti-bacterial agents. *International Journal of Pharmaceutical Sciences and Research, 4*(1), 419-424.

Baginski, M., Sternal, K., Czub, J., & Borowski, E. (2005). Molecular modelling of membrane activity of amphotericin B, a polyene macrolide antifungal antibiotic. *Acta biochimica Polonica, 52*(3), 655-658.

Barrett, B., Kiefer, D., & Rabago, D. (1999). Assessing the risks and benefits of herbal medicine: An overview of scientific evidence. *Alternative Therapies*, *Health* and *Medicine, 5*(4), 40-49.

Bartulewic, D., Markowska, A., Wolczynski, S., Dabrowska, M., & Rozanski, A. (2000). Molecular modelling, synthesis and antitumour activity of carbocyclic analogues of netropsin and distamycin--new carriers of alkylating elements. *Acta biochimica Polonica, 47*(1), 23-35.

Bertolini, A. O., A.; Sandrini, M. (2001). Dual acting anti-inflammatory drugs: A reappraisal. *Pharmacological Research, 44*(6).

Bianchi, M., & Broggini, M. (2002). Anti-hyperalgesic effects of nimesulide: Studies in rats and humans. *International Journal of Clinical Practice. Supplement* (128), 11-19.

Bjorkman, D. J. (1999). Current status of nonsteroidal anti-inflammatory drug (NSAID) use in the United States: Risk factors and frequency of complications. *The American Journal of Medicine, 107*(6), 3-8.

Bort, R., Ponsoda, X., Jover, R., Gómez-Lechón, M. J., & Castell, J. V. (1999). Diclofenac toxicity to hepatocytes: A role for drug metabolism in cell toxicity. *Journal of Pharmacology and Experimental Therapeutics, 288*(1), 65-72.

Botting, R. (2003). COX-1 and COX-3 inhibitors. *Thrombosis Research, 110*(5-6), 269-272.

Botting, R. M. (2000). Mechanism of action of acetaminophen: Is there a cyclooxygenase 3? *Clinical Infectious Diseases, 31* (Supplement 5), S202-S210.

Brune, K., & Hinz, B. (2004). The discovery and development of antiinflammatory drugs. *Arthritis & Rheumatism, 50*(8), 2391-2399.

Burdan, F., Szumilo, J., Klepacz, R., Dudka, J., Korobowicz, A., Tokarska, E., Cendrowska-Pinkosz, M., Madej, B., Klepacz, L. (2004). Gastrointestinal and hepatic toxicity of selective and non-selective cyclooxygenase-2 inhibitors in pregnant and non-pregnant rats. *Pharmacological Research, 50*(5), 533-43.

Butina, D., Segall, M. D., & Frankcombe, K. (2002). Predicting ADME properties in silico: Methods and models. *Drug Discov Today, 7*(11), S83-88.

Buttgereit, F., Burmester, G. R., & Simon, L. S. (2001). Gastrointestinal toxic side effects of nonsteroidal anti-inflammatory drugs and cyclooxygenase-2–specific inhibitors. *The American journal of medicine, 110*(3), 13-19.

Cairns, J. A. (2007). The coxibs and traditional nonsteroidal anti-inflammatory drugs: A current perspective on cardiovascular risks. *The Canadian Journal of Cardiology*, *23*(2), 125–131.

Chandra, J., & Bhatnagar, S. K. (2002). Antipyretics in children. *The Indian Journal of Pediatrics, 69*(1), 69-74.

Chandrasekharan, N. V., Dai, H., Roos, K. L. T., Evanson, N. K., Tomsik, J., Elton, T. S., & Simmons, D. L. (2002). COX-3, a cyclooxygenase-1 variant inhibited by acetaminophen and other analgesic/antipyretic drugs: Cloning, structure, and expression. *Proceedings of the National Academy of Sciences, 99*(21), 13926-13931.

Charlier, C., & Michaux, C. (2003). Dual inhibition of cyclooxygenase-2 (COX-2) and 5-lipoxygenase (5-LOX) as a new strategy to provide safer non-steroidal anti-inflammatory drugs. *European Journal* of *Medicinal Chemistry, 38*(7-8), 645-659.

Chen, H., Li, Q., Yao, X., Fan, B., Yuan, S., Panaye, A., & Doucet, J. P. (2004). CoMFA/CoMSIA/HQSAR and docking study of the binding mode of selective cyclooxygenase (COX-2) inhibitors. *QSAR & Combinatorial Science, 23*(1), 36-55.

Chen, Q.-H., Praveen Rao, P. N., & Knaus, E. E. (2005). Design, synthesis, and biological evaluation of linear 1-(4-, 3- or 2-methylsulfonylphenyl)-2-phenylacetylenes: A novel class of cyclooxygenase-2 inhibitors. *Bioorganic & Medicinal Chemistry, 13*(23), 6425-6434.

Cheng, A., & Dixon, S. (2003). In silico models for the prediction of dose-dependent human hepatotoxicity. *Journal of Computer-Aided Molecular Design, 17*(12), 811-823.

Chou, C.-H., Lin, F.-M., Chou, M.-T., Hsu, S.-D., Chang, T.-H., Weng, S.-L., Shrestha, S., Hsiao1, C.-C., Hung, J.-H., Huang, H.-D. (2013). A computational approach for identifying microRNA-target interactions using high-throughput CLIP and PAR-CLIP sequencing. *BMC Genomics, 14*(1), 1-11.

Cross, J. B., Thompson, D. C., Rai, B. K., Baber, J. C., Fan, K. Y., Hu, Y., & Humblet, C. (2009). Comparison of several molecular docking programs: Pose prediction and virtual screening accuracy. *Journal of Chemical Information and Modeling, 49*(6), 1455-1474.

Cullen, L., Kelly, L., Connor, S. O., & Fitzgerald, D. J. (1998). Selective cyclooxygenase-2 inhibition by nimesulide in man. *Journal of Pharmacology and Experimental Therapeutics, 287*(2), 578-582.

Daeniker, H. U., & Druey, J. (1957). Heilmittelchemische Studien in der heterocyclischen Reihe. 18. Mitteilung. Über Polymethylen-bis-sydnone und Polymethylen-bis-hydrazine. *Helvetica Chimica Acta, 40*(4), 918-932.

Dajani, E. Z., & Islam, K. (2008). Cardiovascular and gastrointestinal toxicity of selective cyclo-oxygenase-2 inhibitors in man. *Journal of Physiology* and *Pharmacology, 2*, 117-133.

Dannhardt, G., & Kiefer, W. (2001). Cyclooxygenase inhibitors - Current status and future prospects. *European Journal of Medicinal Chemistry, 36*(2), 109-126.

Dewick, P. M. (2006). *Essentials of organic chemistry*: *For students of pharmacy, medicinal chemistry and biological chemistry*. *Wiley*, p. 369. 1st ed.).

DeWitt, D. L. (1999). Cox-2-selective inhibitors: The new super aspirins. *Molecular Pharmacology, 55*(4), 625-631.

Donnelly, M. T., & Hawkey, C. J. (1997). Review article: COX-II inhibitors—a new generation of safer NSAIDs? *Alimentary Pharmacology & Therapeutics, 11*(2), 227-235.

Dovizio, M., Tacconelli, S., Sostres, C., Ricciotti, E., & Patrignani, P. (2012). Mechanistic and pharmacological issues of aspirin as an anticancer agent. *Pharmaceuticals, 5*(12), 1346-1371.

El-Badry, S. M. , & Taha, M. A. M. (2011). Novel and Efficient Synthesis of Tetrazolo[1,5-b]-1,2,5-oxadiazepines as Antibacterial Activities from Ethyl 1-aminotetrazole-5-carboxylate. *Journal of the Korean Chemical Society, 55* (6) Korean Chemical Society.

Egan, W. J., & Lauri, G. (2002). Prediction of intestinal permeability. *Advanced Drug Delivery Reviews, 54*(3), 273-289.

Egan, W. J., Merz Jr, K. M., & Baldwin, J. J. (2000). Prediction of drug absorption using multivariate statistics. *Journal of Medicinal Chemistry, 43*(21), 3867-3877.

Ekins, S., Nikolsky, Y., & Nikolskaya, T. (2005). Techniques: Application of systems biology to absorption, distribution, metabolism, excretion and toxicity. *Trends in Pharmacological Sciences, 26*(4), 202-209.

Engelhardt, G. (1996). Pharmacology of Meloxicam, A New Non-Steroidal Anti-Inflammatory Drug with an Improved Safety Profile Through Preferential Inhibition of COX-2. *Rheumatology, 35*(suppl 1), 4-12.

Ermondi, G., Caron, G., Lawrence, R., & Longo, D. (2004). Docking studies on NSAID/COX-2 isozyme complexes using contact statistics analysis. *Journal of Computer-Aided Molecular Design, 18*(11), 683-696.

Fabiola, G. F., Pattabhi, V., & Nagarajan, K. (1998). Structural basis for selective inhibition of COX-2 by nimesulide. *Bioorganic & Medicinal Chemistry, 6*(12), 2337-2344.

Ferreira, S. (2002). Peripheral analgesic sites of action of anti-inflammatory drugs. *International Journal of clinical practice. Supplement*(128), 2-10.

Ferreri, N. R., An, S. J., & McGiff, J. C. (1999). Cyclooxygenase-2 expression and function in the medullary thick ascending limb. *American Journal of Physiology, 277*(3 Pt 2), F360-368.

Fiorucci, S., Meli, R., Bucci, M., & Cirino, G. (2001). Dual inhibitors of cyclooxygenase and 5-lipoxygenase. A new avenue in anti-inflammatory therapy? *Biochemical Pharmacology, 62*(11), 1433-1438.

Fuloria, N. K., Singh, V., Shaharyar, M., & Ali, M. (2009). Synthesis and Antimicrobial Evaluation of Some New Oxadiazoles Derived from Phenylpropionohydrazides. *Molecules, 14*(5), 1898.

Garavito, R. M., & DeWitt, D. L. (1999). The cyclooxygenase isoforms: structural insights into the conversion of arachidonic acid to prostaglandins. *Biochimica et Biophysica Acta (BBA), 23*, 2-3.

Gilbert, D. (2004). Bioinformatics software resources. *Briefings in Bioinformatics, 5*(3), 300-304.

Goei The, H. S., Lund, B., Distel, M. R., & Bluhmki, E. (1997). A double-blind, randomized trial to compare meloxicam 15 mg with diclofenac 100 mg in the treatment of osteoarthritis of the knee. *Osteoarthritis and Cartilage, 5*(4), 283-288.

Goodsell, D. S., Morris, G. M., & Olson, A. J. (1996). Automated docking of flexible ligands: applications of AutoDock. *Journal of Molecular Recognition, 9*(1), 1-5.

Grosser, T., Fries, S., & FitzGerald, G. A. (2006). Biological basis for the cardiovascular consequences of COX-2 inhibition: Therapeutic challenges and opportunities. *Journal of Clinical Investigation, 116*(1), 4-15.

Gum, P. A., Kottke-Marchant, K., Poggio, E. D., Gurm, H., Welsh, P. A., Brooks, L., Sapp, S. K., Topol, E. J. (2001). Profile and prevalence of aspirin resistance in patients with cardiovascular disease. *The American Journal of Cardiology, 88*(3), 230-235.

Gupta, M. R., Kapoor, R., Sudheesh, M., & Patil, U. (2010). An applauded novel drug delivery system for arthritis using NSAIDS by microencapsulation technique - A *Scholars Research Library, 2*, 335-345.

Habeeb, A. G., Praveen Rao, P. N., & Knaus, E. E. (2001a). Design and synthesis of 4,5-diphenyl-4-isoxazolines: Novel inhibitors of cyclooxygenase-2 with analgesic and antiinflammatory activity. *Journal of Medicinal Chemistry, 44*(18), 2921-2927.

Habeeb, A. G., Praveen Rao, P., & Knaus, E. E. (2001). Design and synthesis of celecoxib and rofecoxib analogues as selective cyclooxygenase-2 (COX-2) inhibitors: Replacement of sulfonamide and methylsulfonyl pharmacophores by an azido bioisostere. *Journal of Medicinal Chemistry, 44*(18), 3039-3042.

Halperin, I., Ma, B., Wolfson, H., & Nussinov, R. (2002). Principles of docking: An overview of search algorithms and a guide to scoring functions. *Proteins: Structure, Function, and Bioinformatics, 47*(4), 409-443.

Halter, F., Tarnawski, A., Schmassmann, A., & Peskar, B. (2001). Cyclooxygenase 2 - implications on maintenance of gastric mucosal integrity and ulcer healing: Controversial issues and perspectives. *Gut, 49*(3), 443-453.

Hawkey, C., Kahan, A., Steinbruck, K., Alegre, C., Baumelou, E., Begaud, B., Dequeker, J., Isomaki, H., Littleiohn, G., Mau, J., Papazoglou, S. (1998). Gastrointestinal tolerability of meloxicam compared to diclofenac in osteoarthritis patients. international MELISSA study group. meloxicam large-scale international study safety assessment. *British Journal of Rheumatology, 37*(9), 937-945.

Heh, C. H., Othman, R., Buckle, M. J., Sharifuddin, Y., Yusof, R., & Rahman, N. A. (2013). Rational discovery of dengue type 2 non-competitive inhibitors. *Chemical Biology & Drug Design, 82*(1), 1-11.

Hou, H., Leung, K. C., Lanari, D., Nelson, A., Stoddart, J. F., & Grubbs, R. H. (2006). Template-directed one-step synthesis of cyclic trimers by ADMET. [Research Support, U S Gov't, Non-P H S]. *Journal of the American Chemical Society, 128*(48), 15358-15359.

IAAAS. (1986). Risks of agranulocytosis and aplastic anemia: A first report of their relation to drug use with special reference to analgesics. *Journal of the American Medical Association, 256*(13), 1749-1757.

Jablonski, J. J., Basu, D., Engel, D. A., & Geysen, H. M. (2012). Design, synthesis, and evaluation of novel small molecule inhibitors of the influenza virus protein NS1. *Bioorganic & Medicinal Chemistry, 20*(1), 487-497.

Jackson, L. M., & Hawkey, C. J. (1999). Gastrointestinal effects of COX-2 inhibitors. *Expert Opinion on Investigational Drugs, 8*(7), 963-971.

James, M. J., Cook-Johnson, R. J., & Cleland, L. G. (2007). Selective COX-2 inhibitors, eicosanoid synthesis and clinical outcomes: A case study of system failure. *Lipids, 42*(9), 779-785.

Jiang, L., & Chen, Y.-C. (2011). Recent advances in asymmetric catalysis with cinchona alkaloid-based primary amines. *Catalysis Science & Technology, 1*(3), 354-365.

Kallings, P. (1993). Nonsteroidal anti-inflammatory drugs. *The Veterinary Clinics of North America. Equine Practice, 9*(3), 523-541.

Kataoka, H., Horie, Y., Koyama, R., Nakatsugi, S., & Furukawa, M. (2000). Interaction between NSAIDs and steroid in rat stomach. *Digestive Diseases and Sciences, 45*(7), 1366-1375.

Ke, S., Liu, F., Wang, N., Yang, Q., & Qian, X. (2009). 1,3,4-Oxadiazoline derivatives as novel potential inhibitors targeting chitin biosynthesis: Design, synthesis and biological evaluation. *Bioorganic & Medicinal Chemistry Letters, 19*(2), 332-335.

Kitchen, D. B., Decornez, H., Furr, J. R., & Bajorath, J. (2004). Docking and scoring in virtual screening for drug discovery: methods and applications. *Nature Reviews Drug discovery, 3*(11), 935-949.

Kurumbail, R. G., Kiefer, J. R., & Marnett, L. J. (2001). Cyclooxygenase enzymes: Catalysis and inhibition. *Current Opinion in Structural Biology, 11*(6), 752-760.

Kurumbail, R. G., Stevens, A. M., Gierse, J. K., McDonald, J. J., Stegeman, R. A., Pak, J. Y., Gildehaus, D., Miyashiro, J. M., Penning, T. D., Seibert, K., Isakson, P.C., Stallings, W. C. (1996). Structural basis for selective inhibition of cyclooxygenase-2 by anti-inflammatory agents. *Nature, 384*(6610), 644-648.

Lehar, J., Krueger, A. S., Zimmermann, G. R., & Borisy, A. A. (2009). Therapeutic selectivity and the multi-node drug target. *Discovery medicine, 8*(43), 185-190.

Lehmann, F. S., & Beglinger, C. (2005). Impact of COX-2 inhibitors in common clinical practice a gastroenterologist's perspective. [Review]. *Current Topics* in *Medicinal Chemistry, 5*(5), 449-464.

Leong, S. W., Faudzi, S. M., Abas, F., Aluwi, M. F., Rullah, K., Wai, L. K., Bahari, M. N., Ahmad, S., Tham, C.L., Shaari, K., Lajis, N. H. (2014). Synthesis and SAR study of diarylpentanoid analogues as new anti-inflammatory agents. *Molecules, 19*(10), 16058-16081.

Leroux, F. R., Manteau, B., Vors, J.-P., & Pazenok, S. (2008). Trifluoromethyl ethers–synthesis and properties of an unusual substituent. *Beilstein Journal of Organic Chemistry, 4*(1), 13.

Levesque, H., & Lafont, O. (2000). Aspirin throughout the ages: A historical review. *La Revue de Médecine Interne, 21 Suppl 1*, 8s-17s.

Li, A. P. (2001). Screening for human ADME/Tox drug properties in drug discovery. *Drug Discovery Today, 6*(7), 357-366.

Li, H.; Qin, J.; Dhondi, P.; Zhou, W.; Vicarel, M.; Bara, T.; Cole, D.; Josien, H.; Pissarnitski, D.; Zhu, Z.; Palani, A.; Aslanian, R.; Clader, J.; Czarniecki, M.;

Greenlee, W.; Cohen-Williams, M.; Hyde, L.; Song, L.; Zhang, L.; Chu, I.; Huang, X. (2013). The discovery of fused oxadiazepines as gamma secretase modulators for treatment of Alzheimer's disease. *Bioorganic & Medicinal Chemistry Letters, 23*(2), 466-471.

Lin, S.-T., Yang, M.-L., & Tien, H.-J. (1999). Reactions of 4-Hydrazinocarbonylmethylene 3-Arylsydnones and 3-(4-Hydrazinocarbonylphenyl) sydnones. *Journal of the Chinese Chemical Society, 46*(1), 63-68.

Lipinski, C. A. (2004). Lead- and drug-like compounds: The rule-of-five revolution. *Drug Discovery Today: Technologies, 1*(4), 337-341.

Lipinski, C. A., Lombardo, F., Dominy, B. W., & Feeney, P. J. (1997). Experimental and computational approaches to estimate solubility and permeability in drug discovery and development settings. *Advanced Drug Delivery Reviews, 23*(1–3), 3-25.

Lipinski, C. A., Lombardo, F., Dominy, B. W., & Feeney, P. J. (2001). Experimental and computational approaches to estimate solubility and permeability in drug discovery and development settings. *Advanced Drug Delivery Reviews, 46*(1-3), 3-26.

Liu, H., Huang, X., Shen, J., Luo, X., Li, M., Xiong, B., Chen, G., Shen, J., Yang, Y., Chen, K., Jiang, H. (2002). Inhibitory mode of 1, 5-diarylpyrazole derivatives against cyclooxygenase-2 and cyclooxygenase-1: Molecular docking and 3D QSAR analyses. *Journal of Medicinal Chemistry, 45*(22), 4816-4827.

Llorens, O. P., Juan J.; Palomer, Albert.; Mauleon, David. (1999). Structural basis of the dynamic mechanism of ligand binding to cyclooxygenase. *Bioorganic & Medicinal Chemistry Letters, 9*(19), 2779-84.

Loll, P. J., Picot, D., & Garavito, R. M. (1995). The structural basis of aspirin activity inferred from the crystal structure of inactivated prostaglandin H2 synthase. *Nature Structural & Molecular Biology, 2*(8), 637-643.

Lund, B., Distel, M., & Bluhmki, E. (1998). A double-blind, randomized, placebo-controlled study of efficacy and tolerance of meloxicam treatment in patients with osteoarthritis of the knee. *Scandinavian Journal of Rheumatology, 27*(1), 32-37.

Maclagan, T. (1876). The treatment of acute rheumatism by salicin. *The Lancet, 107*(2740), 342-343.

Maffei, F. R., Carini, M., Aldini, G., Saibene, L., & Macciocchi, A. (1992). Antioxidant profile of nimesulide, indomethacin and diclofenac in phosphatidylcholine liposomes (PCL) as membrane model. *International Journal of Tissue Reactions, 15*(6), 225-234.

Mahdi, J. G., Mahdi, A. J., Mahdi, A. J., & Bowen, I. D. (2006). The historical analysis of aspirin discovery, its relation to the willow tree and antiproliferative and anticancer potential. *Cell Proliferation, 39*(2), 147-155.

Manojkumar, P., Ravi, T., & Subbuchettiar, G. (2009). Synthesis of coumarin heterocyclic derivatives with antioxidant activity and in vitro cytotoxic activity against tumour cells *Acta Pharmaceutica 59*(2), 159–170.

Martinez-Gonzalez, J., & Badimon, L. (2007). Mechanisms underlying the cardiovascular effects of COX-inhibition: benefits and risks. [Research Support, Non-U S Gov't Review]. *Curr Pharm Des, 13*(22), 2215-2227.

Meade, E. A., Smith, W. L., & DeWitt, D. L. (1993). Differential inhibition of prostaglandin endoperoxide synthase (cyclooxygenase) isozymes by aspirin and other non-steroidal anti-inflammatory drugs. *Journal of Biological Chemistry, 268*(9), 6610-6614.

Morris, G. M., Goodsell, D. S., Halliday, R. S., Huey, R., Hart, W. E., Belew, R. K., & Olson, A. J. (1998). Automated docking using a Lamarckian genetic algorithm and an empirical binding free energy function. *Journal of Computational Chemistry, 19*(14), 1639-1662.

Morris, G. M., Goodsell, D. S., Pique, M. E., Lindstrom, W. L., Huey, R., Forli, S., Hart, W. E., Halliday, S., Belew, R., & J., O. A. (2010). AutoDock Version 4.2 - Automated Docking of Flexible Ligands to Flexible Receptors.

Morris, G. M., Huey, R., Lindstrom, W., Sanner, M. F., Belew, R. K., Goodsell, D. S., & Olson, A. J. (2009). AutoDock4 and AutoDockTools4: Automated docking with selective receptor flexibility. *Journal of Computational Chemistry, 30*(16), 2785-2791.

Mukherjee, D. (2002). Selective cyclooxygenase-2 (COX-2) inhibitors and potential risk of cardiovascular events. *Biochemical Pharmacology, 63*(5), 817-821.

Naresh K, S. K., Nishitha D, Ramya K, Jagadeeshwar K. (2013). Molecular docking studies of novel azetidinone and schiff bases of thiophene derivatives as selective cyclooxygenase-2 inhibitors. *Journal of Pharmaceutical Research Inventions and Innovations 1*, 10-15.

Navidpour, L., Shafaroodi, H., Abdi, K., Amini, M., Ghahremani, M. H., Dehpour, A. R., & Shafiee, A. (2006). Design, synthesis, and biological evaluation of substituted 3-alkylthio-4, 5-diaryl-4H-1, 2, 4-triazoles as selective COX-2 inhibitors. *Bioorganic & Medicinal Chemistry, 14*(8), 2507-2517.

O'connor, N., Dargan, P. I., & Jones, A. L. (2003). Hepatocellular damage from non-steroidal anti-inflammatory drugs. *Quarterly Journal of Mathematics, 96*(11), 787-791.

Oe, K., Tashiro, M., & Tsuge, O. (1977). Photochemistry of heterocyclic compounds. 5. Photochemical reaction of 2,5-diaryl-1,3,4-oxadiazoles with indene. *The Journal of Organic Chemistry, 42*(9), 1496-1499.

Othman, R., Kiat, T. S., Khalid, N., Yusof, R., Irene Newhouse, E., Newhouse, J. S., Alam, M., Rahman, N. A. (2008). Docking of noncompetitive inhibitors into

dengue virus type 2 protease: understanding the interactions with allosteric binding sites. *Journal of Chemical Information and Modeling, 48*(8), 1582-1591.

Palm, K., Stenberg, P., Luthman, K., & Artursson, P. (1997). Polar molecular surface properties predict the intestinal absorption of drugs in humans. *Pharmaceutical Research, 14*(5), 568-571.

Patel, C. K., Rami, C., Panigrahi, B., & Patel, C. (2010). Synthesis and Biological Evaluation of (4-Substituted Benzylidene)-3-Methyl-1-(Substituted Phenyl Sulfonyl and Substituted Benzoyl)-1H-Pyrazol-5 (4H)-one As Anti-inflammatory Agent. *Journal of Chemical and Pharmaceutical Research, 2*(1), 73-78.

Picot, D., Loll, P. J., & Garavito, R. M. (1994). The X-ray crystal structure of the membrane protein prostaglandin H2 synthase-1. *Nature, 367*(6460), 243-249.

Ponnan, P., Gupta, S., Chopra, M., Tandon, R., Baghel, A. S., Gupta, G., Prasad, A. K., Rastogi, R. C., Bose, M., Raj, H. G. (2013). 2d-qsar, docking studies, and *in silico* admet prediction of polyphenolic acetates as substrates for protein acetyltransferase function of glutamine synthetase of mycobacterium tuberculosis. *International Scholarly Research Notices Structural Biology, 2013,* 12.

Portevin, B., Tordjman, C., Pastoureau, P., Bonnet, J., & De Nanteuil, G. (2000). 1, 3-Diaryl-4, 5, 6, 7-tetrahydro-2 H-isoindole derivatives: A new series of potent and selective COX-2 inhibitors in which a sulfonyl group is not a structural requisite. *Journal of Medicinal Chemistry, 43*(24), 4582-4593.

Praveen Rao, P. N., Amini, M., Li, H., Habeeb, A. G., & Knaus, E. E. (2003). Design, synthesis, and biological evaluation of 6-substituted-3-(4-methanesulfonylphenyl)-4-phenylpyran-2-ones: a novel class of diarylheterocyclic selective cyclooxygenase-2 inhibitors. *Journal of Medicinal Chemistry, 46*(23), 4872-4882.

Radwan, A. A., & Kamal, E. (2013). Synthesis and *in-silico* studies of some diaryltriazole derivatives as potential cyclooxygenase inhibitors. *Archives of Pharmacal Research, 36*(5), 553-563.

Ricciotti, E., & FitzGerald, G. A. (2011). Prostaglandins and inflammation. *Arteriosclerosis, Thrombosis, and Vascular Biology, 31*(5), 986-1000.

Riddle, J. M. (1999). Historical data as an aid in pharmaceutical prospecting and drug safety determination. *Journal of Alternative and Complementary Medicine, 5*(2), 195-201.

Rowlinson, S. W., Kiefer, J. R., Prusakiewicz, J. J., Pawlitz, J. L., Kozak, K. R., Kalgutkar, A. S., Stallings, W. C., Kurumbail, R. G., Marnett, L. J. (2003). A novel mechanism of cyclooxygenase-2 inhibition involving interactions with Ser-530 and Tyr-385. *Journal of Biological Chemistry, 278*(46), 45763-45769.

Ruiz, J. G., & Lowenthal, D. T. (1997). NSAIDS and nephrotoxicity in the elderly. *Geriatric Nephrology and Urology, 7*(1), 51-57.

Sakya, S. M., Lundy DeMello, K. M., Minich, M. L., Rast, B., Shavnya, A., Rafka, R. J., Koss, D. A., Cheng, H., Li, J., Jaynes, B.H., Ziegler, C.B., Mann, D.W., Petras, C.F., Seible, S.B., Silvia, A.M., George, D.M., Lund, L.A., Denis, S.S., Hickman, A., Haven, M.L.,Lynch, M. P. (2006). 5-Heteroatom substituted pyrazoles as canine COX-2 inhibitors. Part 1: Structure–activity relationship studies of 5-alkylamino pyrazoles and discovery of a potent, selective, and orally active analog. *Bioorganic & Medicinal Chemistry Letters, 16*(2), 288-292.

Sánchez-Pernaute, R., Ferree, A., Cooper, O., Yu, M., Brownell, A.-L., & Isacson, O. (2004). Selective COX-2 inhibition prevents progressive dopamine neuron degeneration in a rat model of Parkinson's disease. *Journal of Neuroinflammation, 1*(1), 1-11.

Savjani, K. T., Gajjar, A. K., & Savjani, J. K. (2012). Drug solubility: Importance and enhancement techniques. *International Scholarly Research Notices Pharmaceutics, 2012*.

Schattenkirchner, M. (1997). Meloxicam: A selective COX-2 inhibitor non-steroidal anti-inflammatory drug. *Expert Opinion on Investigational Drugs, 6*(3), 321-334.

Schnitzer, T. J., Truitt, K., Fleischmann, R., Dalgin, P., Block, J., Zeng, Q., Bolognese, J., Seidenberg, B., Ehrich, E. W. (1999). The safety profile, tolerability, and effective dose range of rofecoxib in the treatment of rheumatoid arthritis. *Clinical Therapeutics, 21*(10), 1688-1702.

Selvam, C., Jachak, S. M., Thilagavathi, R., Chakraborti, A. K., & Bhutani, K. K. (2004). A new cyclooxygenase (COX) inhibitory pterocarpan from indigofera aspalathoides: Structure elucidation and determination of binding orientations in the active sites of the enzyme by molecular docking. *Tetrahedron Letters, 45*(22), 4-4.

Shaftel, S. S., Olschowka, J. A., Hurley, S. D., Moore, A. H., & O'Banion, M. K. (2003). COX-3: A splice variant of cyclooxygenase-1 in mouse neural tissue and cells. *Molecular Brain Research, 119*(2), 213-215.

Shah, A., Thjodleifsson, B., Murray, F., Kay, E., Barry, M., Sigthorsson, G., Gudjonsson, H., Oddsson, E., Price, A. B., Fitzgerald, D. J., Bjarnason, I. (2001). Selective inhibition of COX-2 in humans is associated with less gastrointestinal injury: A comparison of nimesulide and naproxen. *Gut, 48*(3), 339-346.

Shankar, M., Gowrishankar, N. L., Narendiran, S., & Sudhakar, K. (2012). Denovo design of the Lead against cyclo-oxygenase receptor. *Asian Journal of Research in Chemistry, 5*(1), 38-43.

Sheldrick, G. M. (2008). A short history of SHELX. *Acta Crystallographica Section A: Foundations of Crystallography, 64*(1), 112-122.

Simon, L., & Yocum, D. (2000). New and future drug therapies for rheumatoid arthritis. *Rheumatology, 39*, 36-42.

Simon, L. S. (2001). COX-2 inhibitors: Are they nonsteroidal anti-inflammatory drugs with a better safety profile? *Gastroenterology Clinics of North America, 30*(4), 1011-1026.

Singh, P., & Mittal, A. (2008). Current status of COX-2 inhibitors. *Mini-Reviews in Medicinal Chemistry, 8*(1), 73-90.

Somogyi, L. (2007). Synthesis, oxidation and dehydrogenation of cyclic N,O- and N,S-acetals. Part III. Transformation of N,O-acetals: 3-acyl-1,3,4-oxadiazolines. *Journal of Heterocyclic Chemistry, 44*(6), 1235-1246.

Souldozi, A., Ramazani, A., Bouslimani, N., & Welter, R. (2007). The reaction of (N-isocyanimino)triphenylphosphorane with dialkyl acetylenedicarboxylates in the presence of 1,3-diphenyl-1,3-propanedione: a novel three-component reaction for the stereoselective synthesis of dialkyl (Z)-2-(5,7-diphenyl-1,3,4-oxadiazepin-2-yl)-2-butenedioates. *Tetrahedron Letters, 48*(14), 2617-2620.

Sperandio da Silva, G. M., Lima, L. M., Fraga, C. A. M., Sant'Anna, C. M. R., & Barreiro, E. J. (2005). The molecular basis for coxib inhibition of p38α MAP kinase. *Bioorganic & Medicinal Chemistry Letters, 15*(15), 3506-3509.

Stone, E. (1763). An Account of the Success of the Bark of the Willow in the Cure of Agues. In a Letter to the Right Honourable George Earl of Macclesfield, President of R. S. from the Rev. Mr. Edmund Stone, of Chipping-Norton in Oxfordshire. *Philosophical Transactions (1683-1775),* 195-200.

Sung, J., Russell, R. I., Nyeomans, Chan, F. K., Chen, S., Fock, K., Goh, K.L., Kullavanijaya, P., Kimura, K., Lau, C., Louw, J., Sollano, J., Triadiafalopulos, G., Xiao, S., Brooks, P. (2000). Non-steroidal anti-inflammatory drug toxicity in the upper gastrointestinal tract. *Journal of Gastroenterology and Hepatology, 15*(68), G58-68.

Susnow, R. G., & Dixon, S. L. (2003). Use of robust classification techniques for the prediction of human cytochrome P450 2D6 inhibition. *Journal of Chemical Information and Modeling, 43*(4), 1308-1315.

Szczeklik, A., & Stevenson, D. D. (2003). Aspirin-induced asthma: Advances in pathogenesis, diagnosis, and management. *Journal of Allergy and Clinical Immunology, 111*(5), 913-921.

Tacconelli, S., Capone, M., & Patrignani, P. (2004). Clinical pharmacology of novel selective COX-2 inhibitors. *Current pharmaceutical design, 10*(6), 589-601.

Taketo, M. M. (1998). Cyclooxygenase-2 Inhibitors in Tumorigenesis (Part I). *Journal of the National Cancer Institute, 90*(20), 1529-1536.

Tarlow, M. (1986). Reye's syndrome and aspirin. *British Medical Journal (Clinical research ed.), 292*(6535), 1543.

Uddin, M. J., Praveen Rao, P., McDonald, R., & Knaus, E. E. (2004). A new class of acyclic 2-alkyl-1, 1, 2-triaryl (Z)-olefins as selective cyclooxygenase-2 inhibitors. *Journal of Medicinal Chemistry, 47*(24), 6108-6111.

Uddin, M. J., Rao, P. N. P., & Knaus, E. E. (2003). Design and synthesis of novel celecoxib analogues as selective cyclooxygenase-2 (COX-2) inhibitors: Replacement of the sulfonamide pharmacophore by a sulfonylazide bioisostere. *Bioorganic & Medicinal Chemistry, 11*(23), 5273-5280.

Valasani, K. R., Vangavaragu, J. R.; Day, V. W.; Yan, S. S. (2014). Structure based design, synthesis, pharmacophore modeling, virtual screening, and molecular docking studies for identification of novel cyclophilin D inhibitors. *Journal of Chemical Information and Modeling, 54*(3), 902-912.

Valerio, L. G., Jr. (2009). *In silico* toxicology for the pharmaceutical sciences. *Toxicology and Applied Pharmacology, 241*(3), 356-370.

van de Waterbeemd, H., & Gifford, E. (2003). ADMET *in silico* modelling: Towards prediction paradise? *Nature Reviews Drug Discovery, 2*(3), 192-204.

Vane, J., & Botting, R. (1987). Inflammation and the mechanism of action of anti-inflammatory drugs. *The Federation of American Societies for Experimental Biology Journal, 1*(2), 89-96.

Vane, J. R. (1971). Inhibition of prostaglandin synthesis as a mechanism of action for aspirin-like drugs. *Nature New Biology, 231*(25), 232-235.

Vane, S. J. (2000). Aspirin and other anti-inflammatory drugs. *Thorax, 55*(Suppl 2), S3-S9.

Veber, D. F., Johnson, S. R., Cheng, H.-Y., Smith, B. R., Ward, K. W., & Kopple, K. D. (2002). Molecular properties that influence the oral bioavailability of drug candidates. *Journal of Medicinal Chemistry, 45*(12), 2615-2623.

Votano, J. R., Parham, M., Hall, L. M., Hall, L. H., Kier, L. B., Oloff, S., & Tropsha, A. (2006). QSAR modeling of human serum protein binding with several modeling techniques utilizing structure-information representation. *Journal of Medicinal Chemistry, 49*(24), 7169-7181.

Wallace, J. L. (1999). Distribution and expression of cyclooxygenase (COX) isoenzymes, their physiological roles, and the categorization of nonsteroidal anti-inflammatory drugs (NSAIDs). *The American Journal of Medicine, 107*(6), 11-16.

Warren, G. L., Andrews, C. W., Capelli, A. M., Clarke, B., LaLonde, J., Lambert, M. H., Lindvall, M., Nevins, N., Semus, S. F., Senger, S., Tedesco, G., Wall, I. D., Woolven, J. M., Peishoff, C. E., Head, M. S. (2006). A critical assessment of docking programs and scoring functions. *Journal of Medicinal Chemistry, 49*(20), 5912-5931.

Whelton, A., Fort, J. G., Puma, J. A., Normandin, D., Bello, A. E., Verburg, K. M., & Group, S. V. S. (2001). Cyclooxygenase-2-specific inhibitors and cardiorenal function: a randomized, controlled trial of celecoxib and rofecoxib in older hypertensive osteoarthritis patients. *American Journal of Therapeutics, 8*(2), 85-95.

White, W. B., Whelton, A., & Fort, J. G. (2002). Rofecoxib but not celecoxib increases systolic blood pressure in hypertensive patients treated with ace inhibitors and beta-blockers. *Journal of the American College of Cardiology, 39*, 249.

Willoughby, D. A., Moore, A. R., & Colville-Nash, P. R. (2000). COX-1, COX-2, and COX-3 and the future treatment of chronic inflammatory disease. *The Lancet, 355*(9204), 646-648.

Wodak, S. J., & Janin, J. (1978). Computer analysis of protein-protein interaction. *Journal of Molecular Biology, 124*(2), 323-342.

Yamagata, K., Andreasson, K. I., Kaufmann, W. E., Barnes, C. A., & Worley, P. F. (1993). Expression of a mitogen-inducible cyclooxygenase in brain neurons: Regulation by synaptic activity and glucocorticoids. *Neuron, 11*(2), 371-386.

Yehye, W. A., Ariffin, A., Rahman, N. A., & Ng, S. W. (2010). 2-[4-Acetyl-5-(biphenyl-4-yl)-4, 5-dihydro-1, 3, 4-oxadiazol-2-yl] phenyl acetate. *Acta Crystallographica Section E: Structure Reports Online, 66*(4), o878-o878.

Zarghi, A., & Arfaei, S. (2011). Selective COX-2 inhibitors: A review of their structure-activity relationships. *Iranian Journal of Pharmaceutical Research, 10*(4), 655-683.

Zhao, S. Z., Reynolds, M. W., Lefkowith, J., Whelton, A., & Arellano, F. M. (2001). A comparison of renal-related adverse drug reactions between rofecoxib and celecoxib, based on the World Health Organization/Uppsala Monitoring Centre safety database. *Clinical Therapeutics, 23*(9), 1478-1491.

Zhivkova, Z., & Doytchinova, I. (2012). Quantitative structure--plasma protein binding relationships of acidic drugs. *Journal of Pharmaceutical Sciences, 101*(12), 4627-4641.

Zoghbi, M., & Warkentin, J. (1993). Spiro-fused β-lactam oxadiazolines by formal [2+2] cycloaddition of 2-imino-Δ3-1,3,4-oxadiazolines to ketenes. *Canadian journal of chemistry, 71*(6), 912-918.

LIST OF PUBLICATIONS AND PAPERS PRESENTED

1. Alhadi, A. A., Othman, R., Yehye, W. A., & Rahman, N. A. (2015). Formation of 1,3,4-oxadiazolines and 1,3,4-oxadiazepines through acetylation of salicylic hydrazones. *Tetrahedron Letters, 56*(4), 573-576.

2. Ariffin, A., Rahman, N. A., Yehye, W. A., Alhadi, A. A., & Kadir, F. A. (2014). PASS-assisted design, synthesis and antioxidant evaluation of new butylated hydroxytoluene derivatives. *European Journal of Medicinal Chemistry, 87*(0), 564-577.

3. Alhadi, A. A., Othman, R., Yehye, W. A., & Rahman, N. A. Hoong, L. K. 1,3,4-Oxadiazoline Derivatives as Potential COX-2 Selective Inhibitors. *In preparation.*

4. Alhadi, A. A., Othman, R., Yehye, W. A., & Rahman, N. A. (2014, 19 Apr -21 May). Rational Design and Biological Evaluations of 1,3,4-Oxadiazoline and their Derivatives as Potential COX-2 Selective Inhibitors. The International Startup Symposium of Cutting-Edge Organic Chemistry in Asia (III), Chiba University, Taiwan, (International)

5. Alhadi, A. A., Othman, R., Yehye, W. A., & Rahman, N. A. (2013, 25-28, November). Studies Of Oxadiazole Derivatives As Potential Cox-2 Selective Inhibitor. The IICCEOCA-8 and NICCEOCA-4 joint conference. Osaka, Japan. *(poster presentation).*

6. Alhadi, A. A., Othman, R., Yehye, W. A., & Rahman, N. A. (2012, 16-18 May). Drug Design, Docking and Drug-Likness Studies of Oxadizole Derivatives as Potential COX-2 Selective Inhibitor. 2nd National Symposium in Organic Synthesis (NaSOS-II). Malaysia, Kuala Lumpur. (*Oral presentation*)

Formation of 1,3,4-oxadiazolines and 1,3,4-oxadiazepines through acetylation of salicylic hydrazones

CrossMark

Abeer A. Alhadi [a,d], Rozana Othman [b,d], Wageeh A. Yehye [c], Noorsaadah Abd Rahman [a,d,*]

[a] Department of Chemistry, University of Malaya, 50603 Kuala Lumpur, Malaysia
[b] Department of Pharmacy, University of Malaya, 50603 Kuala Lumpur, Malaysia
[c] Nanotechnology & Catalysis Research Centre, NANOCEN, University of Malaya, 50603 Kuala Lumpur, Malaysia
[d] Drug Design and Development Group, University of Malaya, 50603 Kuala Lumpur, Malaysia

ARTICLE INFO

ABSTRACT

A new series of 1,3,4-oxadiazolines and 1,3,4-oxadiazepines are prepared in a one-step reaction through cyclization of various N-benzylidene-2-hydroxybenzohydrazides. Cyclization in acetic anhydride yielded 1,3,4-oxadiazolines, while the reaction carried out in acetic anhydride–acetic acid gave 1,3,4-oxadiazepines, in some cases.

© 2014 Elsevier Ltd. All rights reserved.

Oxadiazolines and oxadiazepines are important compounds for both chemical and biological purposes.[1,2] They have been used extensively as synthons in various organic syntheses such as for the preparation of spiro-fused β-lactam oxadiazolines[3] and of fused oxadiazepines used as gamma secretase modulators for the treatment of Alzheimer's disease.[4] In addition, oxadiazolines and oxadiazepines have been reported to exhibit diverse pharmacological properties,[5] which include antimicrobial,[6] cytotoxic,[7] antifungal, and anticancer activities.[8] Various aldehyde and ketone acyl hydrazones have been cyclized to give 3-acyl-1,3,4-oxadiazolines under acylating conditions.[9,10] However, there are only three reports on acylhydrazones with a hydroxyl group at the *ortho* position of the benzene ring being cyclized to give 3-acyl-1,3,4-oxadiazolines.[11] In the case of oxadiazepines, several methods have been reported for their synthesis, all of which are multi-step in nature.[6,12–14] For example, El Badry and Taha[2] reported that the diazotization of ethyl 1-aminotetrazole-5-carboxylate in the presence of water resulted in the formation of ethyl 1-hydroxytetrazole-5-carboxylate. (Scheme 1).

Condensation of ethyl 1-hydroxytetrazole-5-carboxylate with bromoacetone and/or phenacyl bromide in absolute ethanol in the presence of anhydrous potassium carbonate provided acetyloxy and 2-oxyacetophenone compounds, which were then reacted

a, R = CH₃; R' = H
b, R = CH₃; R' = 4-CH₃
c, R = CH₃; R' = 4-OCH₃
d, R = CH₃; R' = 4-NH₂
e, R = CH₃; R' = 4-Cl
f, R = CH₃; R' = 4-NO₂
g, R = Ph; R' = H
h, R = Ph; R' = 4-CH₃
i, R = Ph; R' = 4-OCH₃
j, R = Ph; R' = 4-NH₂
k, R = Ph; R' = 4-Cl
l, R = Ph; R' = 4-NO₂
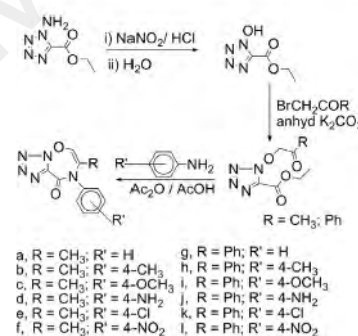
Scheme 1. El Badry and Taha's work.[2]

with various 4-substituted anilines in the presence of acetic anhydride/acetic acid to give 7-methyl(phenyl)-8-aryltetrazolo[1,5-*b*]-1,2,5-oxadiazepin-9-ones in three steps.[6] Herein, we report a novel, one-step intramolecular oxidative cyclization of a variety of substituted benzaldehyde acylhydrazones **1**[15] with a free hydroxyl group at the *ortho* position to give the oxadiazolines **2**, which

* Corresponding author. Tel.: +60 3 79674643; fax: +60 3 79674193.
 E-mail address: noorsaadah@um.edu.my (N.A. Rahman).
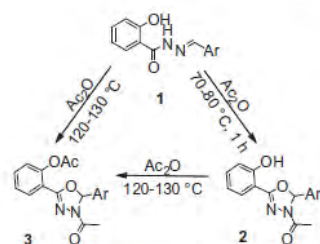
Scheme 2. Synthesis of 1,3,4-oxadiazoline derivatives **3**.

were isolated and characterized. Acetylation of the oxadiazoline **2** led to the formation of 1,3,4-oxadiazoline derivatives **3**[16–18] as shown in Scheme 2. Thus, reactions of substituted benzaldehyde acylhydrazones **1** in acetic anhydride at 120–130 °C resulted in the cyclized products **3** (Scheme 2). The reactions proceeded smoothly with no side products being observed under these conditions.[15,19]

Under these acylation conditions, compounds **1a–i**, possessing either electron-donating or electron-withdrawing substituents on the aryl ring cyclized to give 1,3,4-oxadiazolines **3a–i**[16–18,20] in 58–85% yields[18] (Table 1). The presence of an electron-withdrawing substituent on the phenyl ring tended to give better yields with the best yield being obtained with a nitro substituent, and the lowest with a *tert*-butyl substituent.[17,18] This is to be expected since a strong electron-withdrawing group such as NO_2 on the aryl ring would enhance the electrophilicity of the iminium carbon, while an electron-donating group would decrease the electrophilicity.[18]

In some cases, when the cyclization reactions of **1** were carried out at 50–60 °C in acetic anhydride/acetic acid solution, 1,3,4-oxadiazepines **4** were obtained instead of 1,3,4-oxadiazolines **3** (Scheme 3).[18,20,21]

Table 2 summarizes the products of the cyclization reactions of compound **1** using the Ac_2O–AcOH conditions. Presumably, the acidic conditions influenced the reaction to form the seven-membered oxadiazepines.[18,20,21]

We have proposed two pathways leading to the formation of oxadiazolines **3** (Scheme 4). One pathway involves acetylation of the free hydroxyl group on the benzene ring to form **5**, which then undergoes intramolecular oxidative cyclization to form **3** (Pathway A). An alternative pathway involves intramolecular oxidative cyclization of **1** to first produce **2a** and **2b**, followed by acylation of the phenol to form **3** (Pathway B).

However, since we isolated only the oxadiazolines **2a** and **2b** with a free *ortho* phenolic group and no product **5** from this reaction, we concluded that the cyclization occurred through pathway B. Compounds **2a** and **2b** (Scheme 4), then underwent acetylation to produce **3a** and **3b**.

It has been well established that compound **1** can undergo keto–enol tautomerisation as shown in Scheme 5.

We propose that the mechanism for the oxidative cyclization reactions leading to **2a** and **2b** involves attack of the enolic oxygen of the enol tautomer on the azomethine imine moiety as shown in Scheme 6.

In the case of the seven-membered oxadiazepines, we propose that the reaction occurs via nucleophilic attack of the phenolic oxygen on the iminium carbon as shown in Scheme 7. Here, the iminium carbon acts as a carbonyl analogue and participates in an intramolecular nucleophilic addition reaction[19,22] with the *ortho* phenolic group. Subsequently, the oxadiazepine underwent acetylation to give only the diacetylated product **4** (Scheme 7).

Table 1
Structures and yields of synthesized compounds **3a–i**

Entry	Ar	Product[a]	Yield[c] (%)
1	Cl–	**3a**	78
2	MeO–	**3b**	70
3	F_3CO–	**3c**[b]	70
4	MeS–	**3d**	65
5	Et–	**3e**	60
6	tBu–	**3f**	58
7	O_2N–	**3g**	85
8	AcO–	**3h**[b]	70
9	Ph–	**3i**[d]	75

[b] Structure was confirmed by X-ray crystallography.
[d] This compound was previously reported in Ref. 11 along with a crystal structure, but without any data.
[a] All products were identified by ATIR, NMR, and EI-HRMS analyses.
[c] Isolated yield after recrystallization.

126
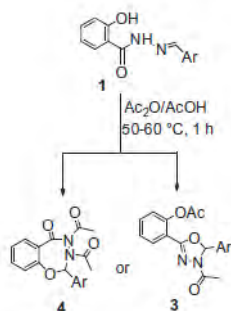
Scheme 3. Synthesis of 1,3,4-oxadiazepines 4 and 1,3,4-oxadiazolines 3.

Table 2
Structures and yields of compounds **4a,d,e,f** and **3b,c,g,h, i**
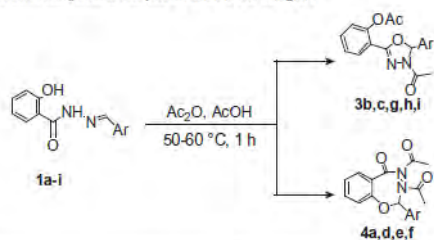
Entry	Ar	Product[a]	Yield[c] (%)
1	4-Cl-phenyl	**4a**[b]	63
2	4-S-phenyl	**4d**[b]	75
3	4-ethyl-phenyl	**4e**[b]	66
4	4-tBu-phenyl	**4f**	55

Table 2 (continued)

Entry	Ar	Product[a]	Yield[c] (%)
5	4-NO₂-phenyl	**3g**	70
6	4-OCF₃-phenyl	**3c**	65
7	4-OCH₃-phenyl	**3b**	65
8	4-OAc-phenyl	**3h**	63
9	biphenyl	**3i**	70

[b] Structure was confirmed by X-ray crystallography.
[a] All products were identified by ATIR, NMR, and EI-HRMS analyses.
[c] Isolated yield after recrystallization.
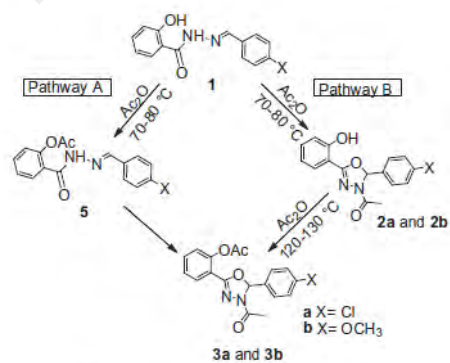
Scheme 4. Proposed pathways for the cyclization of **1**.

a X= Cl
b X= OCH₃
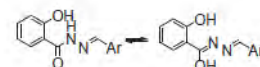
Scheme 5. Tautomerisation of compound **1**.
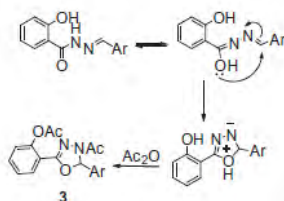
Scheme 6. A plausible mechanism for the formation of compounds **3a–i**.
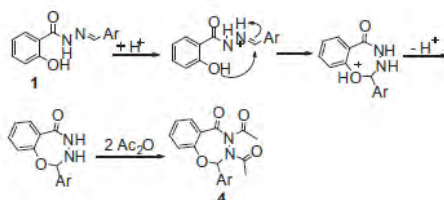
Scheme 7. A plausible mechanism for the formation of compounds **4**.

In summary, 1,3,4-oxadiazolines containing an acetoxy group at the *ortho* position of the benzene ring were prepared in one-step, via intramolecular oxidative cyclization of acylhydrazones in acetic anhydride, which serves both as a reactant and the solvent. However, 1,3,4-oxadiazolines or 1,3,4-oxadiazepines were obtained in some cases, when the reactions were carried out under acid-catalyzed conditions.

Acknowledgments

Supplementary data

Supplementary data associated with this article can be found, in the online version, at http://dx.doi.org/10.1016/j.tetlet.2014.12.037.

References and notes

1. Yang, J.-F.; Cao, H.; Liu, H.; Li, B.-Q.; Ma, Y.-M. *J. Chin. Chem. Soc.* **2011**, *58*, 369–375.
2. El Badry, S. M.; Taha, M. A. *J. Korean Chem. Soc.* **2011**, *55*, 974–977.
3. Zoghbi, M.; Warkentin, J. *Can. J. Chem.* **1993**, *71*, 912–918.
4. Li, H.; Qin, J.; Dhondi, P.; Zhou, W.; Vicarel, M.; Bara, T.; Cole, D.; Josien, H.; Pissarnitski, D.; Zhu, Z.; Palani, A.; Aslanian, R.; Clader, J.; Czarniecki, M.; Greenlee, W.; Cohen-Williams, M.; Hyde, L.; Song, L.; Zhang, L.; Chu, I.; Huang, X. *Bioorg. Med. Chem. Lett.* **2013**, *23*, 466–471.
5. Ke, S.; Liu, F.; Wang, N.; Yang, Q.; Qian, X. *Bioorg. Med. Chem. Lett.* **2009**, *19*, 332–335.
6. Fuloria, N. K.; Singh, V.; Shaharyar, M.; Ali, M. *Molecules* **2009**, *14*, 1898–1903.
7. Manojkumar, P.; Ravi, T. K.; Subbuchettiar, G. *Acta Pharm.* **2009**, *59*, 159–170.
8. (a) Daeniker, H. U.; Druey, J. *Helv. Chim. Acta* **1957**, *40*, 918–932; (b) Autio, K.; Pyysalo, H. *J. Agric. Food Chem.* **1983**, *31*, 568–571; (c) Ishiwata, S.; Shiokawa, Y. *Chem. Pharm. Bull.* **1970**, *18*, 1245–1248.
9. Somogyi, L. *J. Heterocycl. Chem.* **2007**, *44*, 1235–1246.
10. Arora, P.; Mittal, A.; Kaur, G.; Chauhan, A. *Int. J. Pharm. Sci. Res.* **2013**, *4*, 419–424.
11. Yehye, W. A.; Ariffin, A.; Rahman, N. A.; Ng, S. W. *Acta Crystallogr., Sect. E.* **2010**, *66*, o878.
12. Oe, K.; Tashiro, M.; Tsuge, O. *J. Org. Chem.* **1977**, *42*, 1496–1499.
13. Oe, K.; Tashiro, M.; Tsuge, O. *Bull. Chem. Soc. Jpn.* **1977**, *50*, 3281–3287.
14. Souldozi, A.; Ramazani, A.; Bouslimani, N.; Welter, R. *Tetrahedron Lett.* **2007**, *48*, 2617–2620.
15. General procedure for the synthesis of hydrazones **1a–i**: 2-Hydroxybenzohydrazide (0.30 g, 2 mmol) and different *para*-substituted benzaldehyde derivatives (0.2 g, 2 mmol) were refluxed in EtOH (20 ml) for 5 h. The solvent was removed by evaporation and the resulting products were obtained as white solids (**1a,c–i**) or as a yellow solid (**1b**).
16. General procedure for synthesis of oxadiazoline analogs (Table 1): A mixture of hydrazone **1a–i** (1.58 mmol) in Ac₂O (6 ml) was refluxed for 2 h under vigorous stirring. The solution was cooled and then poured onto crushed ice and stirred vigorously. A precipitate formed which was washed with distilled H₂O to remove the Ac₂O. The obtained solid was further purified by crystallization from an appropriate solvent.
17. Most products were found to be homogeneous by TLC and 400 MHz NMR analyses, but when necessary, heterogeneous products were readily purified by silica gel column chromatography using hexane/CHCl₃ as the eluent.
18. See Supplementary data for complete experimental details.
19. Jiang, L.; Chen, Y.-C. *Catal. Sci. Tech.* **2011**, *1*, 354–365.
20. Crystallographic data for compounds **3c**, **3h**, **4a**, **4d** and **4e** have been deposited at the Cambridge Crystallographic Data Centre, with the deposition numbers 963045, 963044, 963041, 963043 and 963042, respectively.
21. General procedure for the synthesis of oxadiazepine derivatives (Table 2): Compounds **4a,f,e,d** were obtained from the reaction of Ac₂O (6 ml) with hydrazones **1a,f,e,d** (2 mmol) in the presence of AcOH (6 ml), and the resulting solution was stirred vigorously for 1 h at 50–60 °C. A precipitate formed which was washed with distilled H₂O to remove the Ac₂O. The obtained solid was further purified by crystallization from an appropriate solvent.
22. Dewick, P. M. *Essentials of Organic Chemistry: For Students of Pharmacy, Medicinal Chemistry and Biological Chemistry*; Wiley: Chichester, 2006; pp 369–370.

Original article

PASS-assisted design, synthesis and antioxidant evaluation of new butylated hydroxytoluene derivatives

Azhar Ariffin [a], Noorsaadah Abdul Rahman [a], Wageeh A. Yehye [b, *], Abeer A. Alhadi [a], Farkaad A. Kadir [c]

[a] Department of Chemistry, Faculty of Science, University of Malaya, Kuala Lumpur 50603, Malaysia
[b] Nanotechnology & Catalysis Research Centre (NANOCAT), University of Malaya, Block 3A, Institute of Postgraduate Studies Building, Kuala Lumpur 50603, Malaysia
[c] Division of Basic Medical Sciences (Anatomy), Faculty of Medicine, Cyberjaya University College of Medical Sciences, Cyberjaya 63000, Selangor Darul Ehsan, Malaysia

ABSTRACT

New multipotent antioxidants (MPAOs), namely 1,3,4-thiadiazoles and 1,2,4-triazoles bearing the well-known free radical scavenger butylated hydroxytoluene (BHT), were designed and synthesized using an acid-(base-) catalyzed intramolecular dehydrative cyclization reaction of the corresponding 1-acylthiosemicarbazides. The structure–activity relationship (SAR) of the designed antioxidants was performed along with the prediction of activity spectra for substances (PASS) training set. Experimental studies based on antioxidant activity using DPPH and lipid peroxidation assays verified the predictions obtained by the PASS-assisted design strategy. Compounds 4a–b, 5a–b and 6a–b showed an inhibition of stable DPPH free radicals at a 10^{-4} M more than the well-known standard antioxidant BHT. Compounds with p-methoxy substituents (4b, 5b and 6b) were more active than o-methoxy substituents (4a, 5a and 6a). With an IC$_{50}$ of 2.85 ± 1.09 μM, compound 6b exhibited the most promising in vitro inhibition of lipid peroxidation, inhibiting Fe(2+)-induced lipid peroxidation of essential oils derived from the egg yolk-based lipid-rich medium by 86.4%. The parameters for the drug-likeness of these BHT derivatives were also evaluated according to Lipinski's 'rule-of-five'. All of the BHT derivatives were found to violate one of Lipinski's parameters (Log $P \geq 5$) even though they have been found to be soluble in protic solvents. The predictive TPSA and %ABS data allow for the conclusion that these compounds could have a good capacity for penetrating cell membranes. Therefore, these novel MPAOs containing lipophilic and hydrophilic groups can be proposed as potential antioxidants for tackling oxidative stress and lipid peroxidation processes.

© 2014 Elsevier Masson SAS. All rights reserved.

1. Introduction

The presence of free radicals in biological materials was discovered approximately 50 years ago [1]. Reactive oxygen species (ROS) are considered to be responsible for many undesired processes such as aging [2], inflammation [3] and many others [4–8]. It is becoming increasingly certain that certain types of inflammatory tissue injury are mediated by reactive oxygen metabolites. These reactive radicals and oxidants may injure cells and tissue directly via oxidative degradation of essential cellular components as well as injure cells indirectly by altering the protease/antiprotease balance that normally exists within the tissue interstitium [9]. Natural and synthetic antioxidants may protect against oxidant-mediated inflammation and tissue damage by virtue of their ability to scavenge free radicals.

BHT is a well-known antioxidant utilized in a wide variety of products. It was patented in 1947 [10] and has been approved for use in foods and food packaging in low concentrations by the U.S. FDA since 1954 [11]. Currently, BHT is one of the most commonly used antioxidants in foods containing fats [12], petroleum products and rubber [13]. Due to these widespread applications, BHT and its derivatives have become attractive antioxidants or even co-antioxidant groups [14]. It is therefore no surprise that BHT has been modified to prepare a series of new antioxidants with new properties for both the polymer and pharmaceutical industries [15–17]. For instance, Parke-Davis has disclosed a new class of

* Corresponding author.
E-mail addresses: wdabdoub@um.edu.my, wdabdoub@yahoo.com (W.A. Yehye).

129

potent, selective and orally active COX-2 inhibitors composed of 2,6-di-tert-butyl phenol [18,19]. This encouraged researchers to prepare new BHT derivatives as potential dual inhibitors of COX-2 and 5-lipoxygenase [20]. Most recently, we have reported that four different series of BHT derivatives improved the survival of *Staphylococcus aureus*-infected nematodes due to their antioxidant activities [21].

Thiosemicarbazides have been reported to show anti-inflammatory [22], antibacterial [23], antimicrobial [24,25] and anti-toxoplasmagondii [25] activities. Derivatives of thiosemicarbazide bearing BHT moieties are rarely synthesized. Compounds containing a 1,3,4-thiadiazole nucleus have been reported to have a variety of biological activities, such as anti-inflammatory [26], antimicrobial [27], antitubercular [28], anticancer [29,30] and urease inhibition activities [31]. 1,2,4-Triazoles are an important class of five-membered heterocyclic compounds. 3-Substituted-1,2,4-triazole-5-thiones are known for their anti-inflammatory [26], selective COX-2 inhibition [32], antimycotic [33] and urease inhibition [31] activities.

In the present study, SAR and rational design strategies were used to combine multiple functions that include a radical-scavenging ability and diversified pharmacological activities in designing hybrid compounds with markedly enhanced radical-scavenging ability and anti-lipid peroxidation. These strategies were performed together and tested based on the SAR analysis of the PASS training subsets, drugs and non-drugs. Antioxidant activities predicted by the PASS program were experimentally verified by DPPH and TBARS (thiobarbituric acid reactive substance) assays. Furthermore, a computational study for prediction of absorption and distribution (ADMET) properties of the molecules under study was performed by determination of polar surface area (PSA), absorption (ABS) and Lipinski parameters. The acid-(base-) catalyzed intramolecular dehydrative cyclization reactions of acylthiosemicarbazide **4a–b** to the corresponding 1,3,4-thiadiazole **5a–b** and 1,2,4-triazole **6a–b** are described. The synthesized compounds have been characterized by IR, NMR and mass spectral analysis. The X-ray structures of **4a** and **6a** will be further discussed in this paper.

2. Results and discussion

2.1. Rational MPAO design

Rational antioxidant design has two strategies. The first strategy is to modify the existing antioxidants to improve their activity according to specific demand, which does not need the aid of theoretical computation. The other is to find novel structures by computer-aided methodologies. In recent years, a great deal of effort has been devoted to finding MPAOs in an attempt to combine radical-scavenging (and/or radical-generation-preventing) activity and enzyme-inhibiting potential into a single structure [34–36].

2.1.1. SAR and rational design of MPAO

First, our design strategy involved assembling the beneficial features of two or more antioxidants into one structure. These designed structures were then evaluated for their potential antioxidant activities through SAR using the PASS training set, which involved two subsets of drug and non-drug databases. This strategy was applied to improve the antioxidant activities and other physical properties of the well-known antioxidant (BHT) to create MPAOs with specific functional groups that are very important in the design and introduction of promising new antioxidant candidates.

2.1.1.1. Phenolic ring. It has been reported that electron-donating substituents, such as methyl and *tert*-butyl at the 2,4,6-positions, increase the primary antioxidant activity of phenols [37]. This is due to the lowering of the bond dissociation enthalpy (BDE) of the phenol O—H group [38] and the stabilization of the phenoxyl radical by inductive and hyperconjugative effects. Two di-*tert*-butyl groups at the *ortho* position provide enough steric hindrance to minimize undesirable reactions, such as pro-oxidation [39–42] (Fig. 1). It has been observed that two *tert*-butyl groups flanking the OH group are required to retain *in vivo* anti-inflammatory potency [15].

2.1.1.2. Thioether groups. Thioethers are classified as secondary antioxidants that can be used in combination with primary antioxidants during processing to improve the performance of the primary antioxidant [40]. Thioethers do not act as radical scavengers but instead undergo redox reactions with hydroperoxidants to form non-radical stable products [43,44]. Phenols containing *p*-thioether groups —CH_2—S—R act as strong free radical scavengers [45]. Thioether bridges between phenol and heterocyclic rings could provide synergistic effects between different combinations of primary and secondary antioxidants in a given hyperstructure.

2.1.1.3. Amides and thioamides. The degree of conjugation in thioamides is considerably higher than that in amides. Both the amide and the thioamide functional groups withdraw electron density from the conjugated system, but the thioamide is a stronger π-electron attractor [46,47]; hence, thioamides are better antioxidants than amides [48].

2.1.1.4. Secondary aromatic amine group. Aromatic amines and their derivatives can easily transfer their amine hydrogen to aminyl radicals [49]. Phenolic or amine antioxidants are able to suppress two oxidative chains [50]. Interestingly, in 2002, Riccardo et al. [51] studied a mixture of α-TOH and a secondary aromatic amine and found that the aromatic amine can act as a co-antioxidant by reversibly recycling α-TOH.

2.1.1.5. Effect of the methoxy substituent position. Alkoxy groups linked at the *ortho* and/or *para* positions of phenols develop phenolic antioxidant activity for both naturally occurring compounds [52–56] and synthetic antioxidants [56]. Regarding the effect of the *m*-substituents, Tetsuto et al. [57] evaluated the antioxidant activities of different donating substituents on the *m*-substituted phenol and found that an *m*-substituent does not influence the antioxidant activity of a phenol. This is probably because an m-substituent does not make a significant contribution to the stability of free radical comparing observations of *ortho* and/or *para* positions [44]. Considering these results, the target compounds were designed to be have *ortho* and *para* methoxy substituents on the phenyl ring.

The analysis described above led to a proposed model of action of MPAOs based solely on SAR. Compounds **4a–b** (Fig. 1) were

Butylated hydroxytoluene (BHT)   BHT radical-ends chain reaction
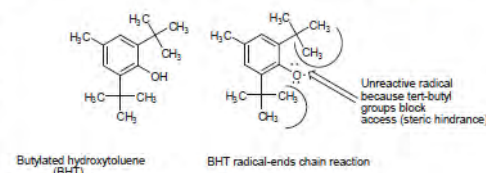
Fig. 1. Steric hindrance effects on stabilization of phenolic antioxidants.

130

designed to form an MPAO in a single structure by linking the well-known antioxidant BHT at the 4-position via a thioether bridge, which provides a linkage between an amide, thiourea (which is classified as a free radical scavenger [58] and secondary antioxidant [59]) and a secondary amine. Compounds **5a**–**b** (Fig. 1) were designed to contain secondary aromatic amines, which act as inhibitors of the radical-chain oxidation. Compounds **6a**–**b** (Fig. 1), which have N*H* ionizable protons and a thiourea system in the triazole ring, may have enhanced antioxidant activity as well as solubility and biological properties.

2.2. PASS — predication and assistant design

PASS prediction tools are constructed using 20,000 principal compounds and approximately 4000 types of biological activities at the molecular level, that providing an estimated profile of compound's action in biological space, including pharmacological effects, mechanisms of action, toxic and adverse effects, interaction with metabolic enzymes and transporters, influence on gene expression, etc. Such profiles can be used to recognize the most probable targets, interaction with which might be a reason of compound's toxicity [60]. PASS mean accuracy exceeds 90% in leave-one-out cross-validation [61–64].

Based on the prediction results, PASS is successfully applied in the pharmacological field, where a dozen of predictions were afterwards confirmed by the experiment [60]. For example, PASS is successfully applied in the pharmacological field, new anti-leishmanial agents were found among the benzothiazoles and their corresponding anthranilic acid derivatives [65], 7-substituted 9-chloro and 9-amino-2-methoxyacridines [66] and beta-carboline alkaloids [67]. PASS could be used for successfully prediction of adverse and toxic effects [60]. Thus, the present PASS approach can be very useful in designing drug molecules according to their properties. It would save unnecessary waste of chemicals as well as time [68]. The prediction results are presented as a list of activities with an appropriate Pa and Pi ratio. Pa and Pi are the estimates of probability for the compound to be active and inactive, respectively. Pa and Pi values are independent, and their values vary from 0 to 1. PASS result of prediction is valuable at planning of the experiment, but one should take into account some additional factors: Particular interest to some kinds of activity, desirable novelty of a substance, available facilities for experimental testing. Actually, each choice is always the compromise between the desirable novelty of studied substance and risk to obtain the negative result in testing. The more is Pa value, the less is the probability of false positives in the set of compounds selected for biological testing. For example, if one selects for testing only compounds for which a particular activity is predicted with Pa ≥ 0.9, the expected probability to find inactive compounds in the selected set is very low, but about 90% of active compounds are missed. If only compounds with Pa ≥ 0.8 are chosen, the probability to find inactive compounds is also low, but about 80% of active compounds are missed etc. By default, in PASS Pa = Pi value is chosen as a threshold, therefore, all compounds

with Pa > Pi are suggested to be active. Another criterion for selection is the compounds' novelty. If Pa value is high, sometimes one may find close analogs of known biologically active substances among the tested compounds. For example, if Pa > 0.7 the chance to find the activity in experiment is high, but in some cases the compound may occur to be the close analog of known pharmaceutical agents. If 0.5 < Pa < 0.7 the chance to find the activity in experiment is less, but the compound is not so similar to known pharmaceutical agents. If Pa < 0.5 the chance to find the activity in experiment is even more less, but if it will be confirmed, more than 50% chances that this structure has not been reported with this activity and might a valuable lead compound.

Obviously, the PASS approach has some important limitations. PASS is not able to predict the activity spectrum for essentially new compounds that have no identifier in the training set. The accuracy of the PASS predictions is significantly higher than random speculations. It can be applied to the activities for which the training set will include no less than 5 active compounds per activity. PASS predicts both drugs and nondrugs actions simultaneously. Thus, only experiments can clarify the intrinsic activity of a compound, but it probably has an affinity to an appropriate receptor (enzyme).

In this study, to accelerate the search for potent new MPAOs, computer-aided drug discovery program PASS was used to predict the cognition-enhancing action for BHT derivatives from chemical series. The potential biological effects of the designed compounds were predicted based on SAR analysis of the PASS training set. Therefore, before we started the synthesis planning process, we used the PASS program to validate whether using the SAR strategy to design the compounds resulted in designs that agreed with the SAR values of the PASS database training set. It is also to evaluate the level of similarity of the designed compound to the known pharmaceutical agents. PASS training set is compiled from many sources, including publications, patents, databases, private communications, etc. Therefore, PASS predicted different synonyms of antioxidants such as lipid peroxidase inhibition, antioxidant and free radical scavenging. A portion of the predicted biological activity spectra for the synthesized compounds and BHT are given in Table 1. Probable activities generated by PASS were validated by experimental bioassay. Only compounds that were predicted by PASS to have predicted antioxidant, free radical scavenging and lipid peroxidase activities were experimentally verified by DPPH and TBARS assays.

2.3. Chemistry

The preparation of the target compounds is outlined in the following Schemes 1–3. 2-(3,5-di-*tert*-butyl-4-hydroxybenzylthio) acetic acid **1** was prepared by the reaction between 3,5-di-tert-butyl-4-hydroxybenzyl alcohol with thioglycolic acid in the presence of PTSA. This new method gave compound **1** in very good yield (85%), while the established solvent-free procedure [69] gave low yield (35%) through the reaction between 2,6-di-*tert*-butyl-phenol with formaldehyde and thioglycolic acid in the presence of di-*n*-

Table 1
Part of the predicted biological activity spectra of the synthesized compounds **1**, **4**–**6** and BHT on the basis of PASS prediction software.

Mode of biological activity	1		4a		4b		5a		5b		6a		6b		BHT	
	Pa	Pi	Pa	Pi	Pa	Pi	Pa	Pi	Pa	Pi	Pa	Pi	Pa	Pi	Pa	Pi
Lipid peroxidase inhibitor	0.652	0.006	0.489	0.018	0.487	0.018	0.510	0.015	0.535	0.013	0.651	0.006	0.673	0.005	0.843	0.003
Antioxidant	0.712	0.004	0.437	0.025	0.466	0.022	0.471	0.021	0.512	0.017	0.573	0.011	0.589	0.010	0.845	0.003
Free radical scavenger	0.807	0.004	0.617	0.020	0.640	0.016	0.606	0.022	–	–	0.552	0.031	0.590	0.025	0.797	0.004
Prostaglandin E2 antagonist	–	–	0.351	0.010	0.357	0.008	–	–	–	–	0.229	0.104	0.380	0.039	–	–
Lipoxygenase inhibitor	–	–	0.296	0.027	0.309	0.025	0.377	0.014	–	–	0.308	0.025	0.345	0.019	–	–

Pa—probability 'to be active'; *Pi*—probability 'to be inactive'.
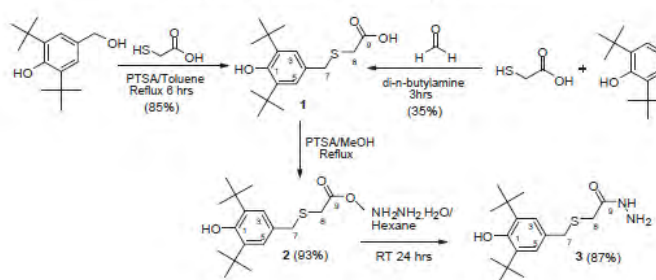
Scheme 1. Synthesis of acid hydrazide **3**.
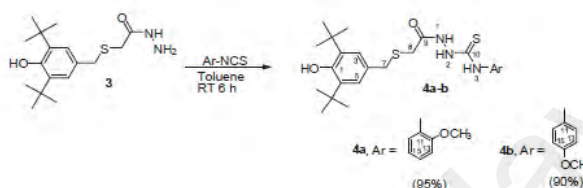
Scheme 2. Synthesis of acylthiosemicarbazides **4a–b**.

butylamine (Scheme 1). This carboxylic acid was then esterified to give the corresponding methyl ester **2** in very good yield (93%). This ester was then converted almost quantitatively to the acid hydrazide **3** after treatment with hydrazine hydrate in the presence of hexane as a solvent at room temperature (Scheme 1).

Hydrazide **3** was treated with arylisothiocyanates to give the corresponding acylthiosemicarbazides **4a–b** in very good yield (Scheme 2).

Compounds **4a–b** under acidic or basic conditions gave thiadiazoles **5a–b** or triazoles **6a–b**, respectively (Scheme 3).

The structures of the synthesized compounds were confirmed on the basis of their physical and spectral data. The structures of compounds **4a** and **6a** were further confirmed by X-ray crystallography.

The IR spectra of all synthesized compounds showed strong absorption at 3615-3655 cm^{-1}, attributed to free ν (Ar–O–H). Acylthiosemicarbazides **4a–b** showed NH stretching bands between 3211 and 3293 cm^{-1}, a C=O stretching band at 1655-1713 cm^{-1}, and did not show a ν(S–H) band at 2570, while the

presence of a C=S stretching band at 1247-1251 cm^{-1} indicated that **4a–b** exist in the thione form in the solid-state [70,71]. Compounds **6a–b** showed NH stretching bands at 3019-3088 cm^{-1} and ν(C=S) at 1253-1258 cm^{-1} due to the thione form. This result is in agreement with X-ray analysis showing that compounds **4a** and **6a** exist in the thione form in the solid-state.

Interestingly, the ^{1}H NMR spectrum of compound **6a**, recorded in CDCl$_3$, showed that each CH$_2$ of the thioether system clearly resonated as an AX system, with two separate doublets at 3.18–3.49 and 3.56–3.63 ppm (Fig. 2) due to $-$C**H**$_2$-triazole and BHT-C**H**$_2$- with coupling constants of 16 and 12 Hz, respectively. In contrast, each CH$_2$ of **6b** clearly resonated as an A$_2$ system, showing two singlets at 3.34 and 3.64 ppm (Fig. 3) that can be attributed to $-$C**H**$_2$-triazole and BHT-C**H**$_2$, respectively. This indicates a germinal coupling, suggesting that the protons of each CH$_2$ of **6a** are magnetically non-equivalent due to restricted rotation about the C–N (Fig. 4, I, II). The ^{2}J germinal coupling constant of the methylene group neighboring the triazole ring is larger than that of the
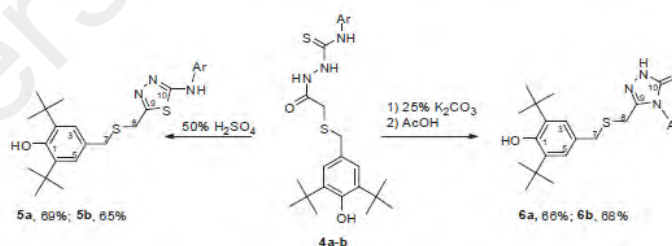
Scheme 3. Synthesis of thiadiazoles **5a–b** and triazoles **6a–b**.

Ar= o-, p-OMe to incese antioxidant activity

4a–b

5a–b

6a–b
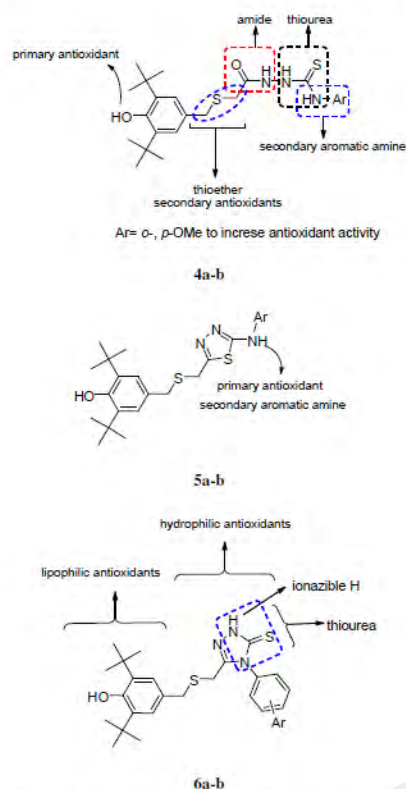
Fig. 2. SAR analysis of 1-acylthiosemicarbazide (**4a–b**), 1,3,4-thiadiazoles (**5a–b**) and 1,2,4-triazoles (**6a–b**) ionazible.

other methylene due to the HCH angle. In general, ^{2}J germinal coupling constants increase as the H–C–H angle α decreases [72].

Compounds **4a–b** showed a singlet peak at 7.2–8.3 ppm due to the N*H*-3 attached to the phenyl group, while the other two singlets at 7.9–8.3 ppm and 8.3–9.7 ppm were attributed to the N*H*'s of the hydrazido group. Both appeared as broad bands, which supports the formation of intramolecular hydrogen bonding [70,73].
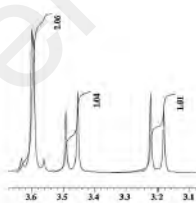
Fig. 3. Geminal H–H coupling (^{2}J$_{HH}$) of each CH$_2$ group of **6a**.
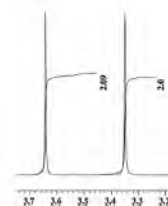
Fig. 4. Uncoupled protons with normal integrate of each CH$_2$ group of **6b**.

2.4. Single crystal X-ray crystallography of compounds **4a** and **6a**

The crystal structure of molecule **4a** is depicted in Fig. 5 and the selected bond lengths and angles are given in Table 2. In the crystal, the molecule exists in its thione form. The two methylene carbon atoms, C15 and C16, subtend an angle of 100.14 (7)° at the S1 atom. Pairs of the molecule are connected via N1–H1 … O2 hydrogen bonding in a bifurcated system to form centro-symmetric dimers. The hydroxyl group is shielded by the two di-*tert*-butyl residues and is therefore not involved in any hydrogen bonding.

Fig. 6 is an ORTEP diagram showing the structure of compound **6a**. The two methylene C atoms subtend an angle of 99.34(9)° at the S1 atom (C16 S1C15). The o-methoxy substituent is approximately coplanar with the aromatic ring as is usual in the absence of steric crowding with dehydral angle C25 O2 C24C23 0.2(3)°. The 1,2,4-triazole and o-anisol rings are, of course, nearly perpendicular to each other, making a dihedral angle of C18 N1 C19C24−90.9(7)° (Table 3). Similar to what was observed in the structure of **4a**, the hydroxyl group is not involved in any hydrogen bonding, as it is shielded by the two sterically hindered *tert*-butyl groups.

2.5. Molecular properties and drug-likeness

2.5.1. Lipophilicity

α-TOH is a fat-soluble antioxidant [74], and the distribution of α-TOH within the membrane has been shown to alter its antioxidant potency [75]. Generally, lipophilic antioxidants demonstrated more potent scavenging properties than hydrophilic antioxidants. The Partition Coefficient is a measure of how well a substance partitions between a lipid and water. It is therefore important to determine the physiochemical properties associated with a compound's antioxidant activity. The log *P* measurement is a useful parameter for understanding the behavior of antioxidant molecules. Log *P* was calculated using the computed log *P* values (where *P* is the partition coefficient of the molecule in the water−octanol system) by using ADMET predictive software, as shown in Table 4. Compounds having log *P* ≥ 5 were considered to have a higher lipophilicity and higher permeation across biological membranes but lower aqueous solubility [76]. The log *P* values of the designed compounds showed moderate lipophilic properties with log *P* values between 6.217 and 6.72, while the natural lipophilic antioxidant α-TOH had a log *P* value of 10.44 and the hydrophilic antioxidant ascorbic acid (AA) had a log *P* value of −1.7.

2.5.2. Calculation of drug-likeness properties

Drug-likeness can be deduced as a delicate balance of various structural features that determine whether a particular molecule is similar to known drugs, generally meaning "molecules which contain functional groups and/or have physical properties consistent with most of the known drugs". These properties are as follows: absorption, distribution, metabolism, and excretion from the

133
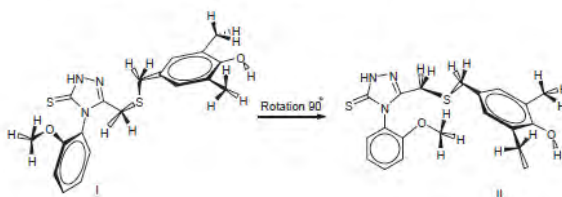
Fig. 5. Restricted internal rotation about aryl C–N bonds in an aryl substituted triazole.

Table 2
Selected bond lengths (Å), bond and torsion angles (deg) for **4a**.

S2–C18 (C=S)	1.6769(14)	C16 S1C15	100.14(7)	C15–O3–C24–C23	0.6(2)
O2–C17 (C=O)	1.3824(16)	N1–N2–C18	120.32(12)	C18N3C19C20	14.7(2)
C1–O1	1.3824(16)	C18–N3–C19	128.22(13)		
S1–C15	1.8211(14)				
S1–C16	1.8051(14)				
N1–C18	1.3557(18)				
N3–C18	1.3513(18)				
N3–C19	1.4173(18)				

Table 3
Selected bond lengths (Å), bond and torsion angles (deg) for **6a**.

C16–S1	1.820(2)	C16 S1C15	99.34(9)	C25–O2–C24–C23	0.2(3)
C16–S1	1820(2)	C24O2C25	116.26(18)	C18N1C19C24	90.9(7)
S1–C15	1.825(2)			C17N1C19C24	85.3(2)
O1–C1	1.378(2)				
N1–C19	1.429(2)				

in human body like a drug. Lipinski [77] used these molecular properties in formulating his Rule of Five. The rule states that most molecules with good membrane permeability have log $P \leq 5$, molecular weight ≤ 500, number of hydrogen bond acceptors ≤ 10 and number of hydrogen bond donors ≤ 5.

2.5.3. Violations of Lipinski's rule of five

It is important to note that there are many violations of this rule among existing drugs and vice versa. Therefore, qualifying according to the "rule of five" does not guarantee that a molecule is "drug-like" [78]. Polar surface area (PSA) is recognized as a good indicator of drug absorbance in the intestines, penetration of Caco-2 monolayers and the ability to cross the blood brain barrier [78]. The mentioned parameters were calculated for the BHT derivatives obtained in this analysis, and the results are depicted in Table 4. From the data obtained, one can notice that the synthesized

compounds possess an adequate number of proton acceptor and proton donor groups to ensure efficient interaction with the hydrogen bonding groups of the receptors. Hydrogen-bonding capacity has also been identified as an important parameter for describing drug permeability [79]. All of the BHT derivatives were found to violate one of the Lipinski's parameters (log P (cLog P) > 5), though they were found to be soluble in protic solvents. The magnitude of absorption is expressed by the percentage of absorption, which was calculated using the following equation: % ABS = $109 - 0.345 \times$ PSA [80]. According to their predictive low topological polar surface area (TPSA) (PSA values are considerably less than 90 A^2) and high %ABS data, it seems that these types of antioxidants could have a good capacity for penetrating cell membranes [81].

2.6. In vitro antioxidant activities

In the present study, the antioxidant activities of seven BHT derivatives were carried out by DPPH and TBARS, two well-known *in vitro* antioxidant assays. The effects of antioxidants in the DPPH-
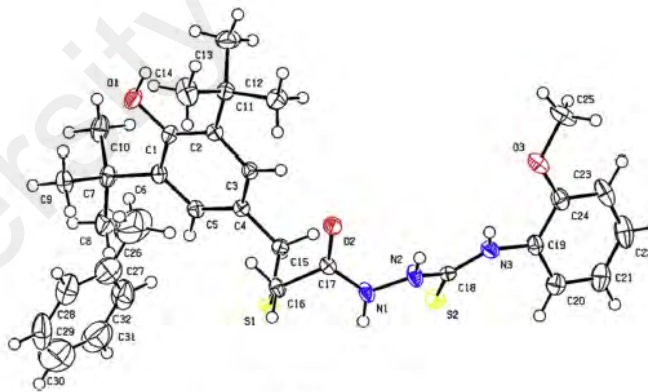
Fig. 6. ORTEP drawing of **4a**.

Table 4
Lipinski's rule of five main parameters.

Compound	Violation of rule of	HBA	HBD	Log P	MW	NROTB	%ABS	PSA A²
4a	1	5	4	6.217	489.694	11	79.51	85.476
4b	1	5	4	6.217	489.694	11	79.51	85.476
5a	1	6	2	6.721	471.678	9	86.30	65.077
5b	1	6	2	6.721	471.678	9	86.30	65.077
6a	1	5	2	6.621	471.678	8	89.12	57.615
6b	1	5	2	6.621	471.678	8	89.12	57.615
BHT	0	1	1	4.875	220.35	2	100	20.815
α–TOH[a]	–	–	–	6.217	430.71	–	98.73	29.745
AA[a]	–	–	–	−1.70	176.12	–	71.23	109.492

[a] α-TOH and AA are outside the 'rule of 5' [77]; Violation of Rule of 5 (≤ 1); HBA–hydrogen bond acceptor (≤ 10); HBD–hydrogen bond donor (≤ 5), Log P (≤ 5); MW (≤ 500), NROTB (≤ 10); %ABS PSA–polar surface area A2 ≤ 90.

radical-scavenging test reflect the hydrogen-donating capacity of a compound. In its radical form, DPPH• absorbs at 570 nm. The radical form of DPPH• is scavenged by an antioxidant through the donation of a hydrogen to form a stable DPPH molecule, resulting in a color change from purple to yellow and a decrease in absorbance [82,83]. The thiobarbituric acid reactive substances (TBARS) assay was chosen for screening and monitoring lipid peroxidation. The basis of the TBARS assay is the spectrophotometric absorbance of a pink color complex at 532−535 nm, which is formed by the interaction of thiobarbituric acid and the oxidation products of unsaturated lipids [84,85].

2.6.1. In vitro DPPH radical scavenging activity

Most compounds tested significantly inhibited DPPH radical levels compared to the standard antioxidants (AA and BHT) used in the study (Table 5). As observed in this table, thiosemicarbazide derivatives **4a−b** exhibited strong scavenging effects on the DPPH stable radical, with respective IC_{50} values of 52.03 ± 1.27 and 50.93 ± 1.47 μM. These values were lower than the positive controls in the study, BHT and AA, indicating that **4a−b** have good radical scavenging activities.

Recently, we noted a few papers in which thiosemicarbazides and related compounds have been evaluated for their ability to scavenge free radicals and found no evidence for their antioxidant activities or mechanisms [86−89]. Canan and coworkers [90] have reported that 1-acylthiosemicarbazides are more effective as free radical scavengers than triazoles and thiadiazoles. Consequently, the higher antioxidant activity of acylthiosemicarbazides **4a−b** could be attributed to two factors: First, the aryl radicals generated by thermal decomposition have been reported to react with compounds containing the S=C-NHR group to give S-substituted

Table 5
IC_{50} values and maximum inhibition of activity at 100 μM of the DPPH radical scavenging and lipid peroxidation inhibition assays.

Compounds	IC_{50}[a] values (μM) ± S.E.M[b] and max. Inhibition % ± S.E.M	
	DPPH radical scavenging	Lipid peroxidation inhibition
1	96.73 ± 1.87 (51.25±0.82)	38.84 ± 1.54 (73.99 ± 1.30)
4a	52.03 ± 1.27 (75.42 ± 0.47)	60.53 ± 1.8 (94.75 ± 1.27)
4b	50.93 ± 1.47 (76.76 ± 0.74)	30.10 ± 4.07 (96.58 ± 1.45)
5a	90.77 ± 0.98 (54.69 ± 0.58)	13.17 ± 1.90 (89.18 ± 0.51)
5b	76.80 ± 0.62 (59.29 ± 0.10)	7.98 ± 1.51(89.84 ± 1.50)
6a	>100 (27.83 ± 10)	38.87 ± 2.12 (76.47 ± 0.95)
6b	92.69 ± 1.86 (52.94 ± 0.90)	2.85 ± 1.09 (86.43 ± 1.23)
BHT	>100[c] (25.23 ± 0.17)	36.67 ± 1.78 (79.45 ± 1.27)
AA	67.77 ± 0.17 (71.39 ± 1.61)	–
α−TOH	–	5.63 ± 1.09 (84.69 ± 1.23)

[a] IC_{50}: 50% effective concentration.
[b] S.E.M: standard error of the mean.
[c] Did not reach 50% inhibition.

isothiosemicarbazides (Scheme 4); and second, when R = Ar, better yield was obtained due to hydrogen abstraction by the aryl radical from the substituted thioamide group [90,91].

Thus, the scavenging potential of the DPPH free radical reaction could occur as proposed in Scheme 5 (A).

Further evidence for the proposed mechanism came from a report that described the antioxidant activities of aromatic amine derivatives [49,92] and five-membered heterocyclic amines [93]. Similar to phenolic derivatives, aromatic amines form an important class of antioxidants [94]. They are also excellent H-donors [49,95] and can easily transfer their amine hydrogen to peroxyl radicals [50]. Thus, the reactions of aromatic amines of thiosemicarbazides (**4a−b**) with free radicals led to hydrogen abstraction from the N−H bond, neutralizing DPPH• by delocalizing the nitrogen electron pair over the aromatic system and the thione group to form a stable aminyl radical.

When the N−H BDE value is low, depending on the nature of the substituent [38], the scavenging of DPPH• by aryl thiourea is proposed to go through pathway B (Scheme 5) in which hydrogen radicals are extracted from the N−H of thiosemicarbazides. This pathway (B) showed that aryl thiourea in thiosemicarbazides is able to suppress two DPPH• radicals. Thus, DPPH was inhibited by 75% (**4a**), 76% (**4b**), 71% (AA) and 25% (BHT) (Table 5).

Further support for our proposed mechanism (Scheme 5, A and B) was obtained from the following results: phenethyl-5-bromopyridyl thiourea have thiol and thione forms, and the thiol has been shown to have antioxidative activity. Moreover, thiols and thiones found in S-alkylated derivatives (Fig. 7) have been found and evaluated, and all phenethyl-5-bromopyridyl thiourea compounds exhibited antioxidant activity (Fig. 7, I). Meanwhile, S-alkylation virtually eliminated the antioxidant activity (Fig. 7, I), indicating that an unalkylated thiourea group is critical for antioxidant activity. This result suggests that the thiol group (I) is responsible for the antioxidant activity due to it is favorable electron-donating characteristics [96]. Similar to thiol group, the reaction of aromatic amine of thiourea with free radicals led to hydrogen abstraction from the N−H bond to form a stable aminyl radical by delocalizing the nitrogen electron pair over the aromatic system.

Compounds 4 and 5 have secondary aromatic amines. Similarly, compounds 4 and 6 have thione groups that play a significant role in reducing DPPH. Thus, the antioxidant activities of thiadiazoles 5 and traiazoles 6 could be attributed to the same effects mentioned above (compounds **4a−b**).

2.6.1.1. Substituent effects on radical scavenging ability.
Table 5 shows the p-methoxy substituents to be more active than o-methoxy substituents. This result is in agreement with the literature in which phenol (or aniline) has been described to have radical scavenging activity that decreases with substitution on the o-position due to hydrogen bonding that can form between OH and NH
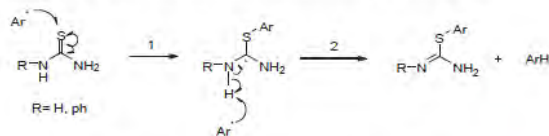
Scheme 4. Proposed mechanism of S-arylisothiouronium base formation [91].
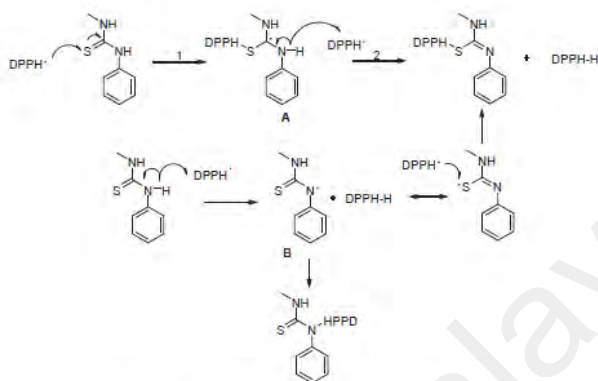
Scheme 5. Proposed scavenging of DPPH• by aryl thiourea.

(Fig. 8) [37]. The increase in this activity depends on the position of the substituent (para > ortho > meta) [97].

The antioxidant activity of methoxy substituents is known to increase the antioxidant activity of a mono-phenol [98]. However, the antioxidant activity of phenols reflects the differences not only in the degree of hydroxylation but also in the position of the hydroxyl groups and neighboring substituents such as methoxy groups [82]. Thus, the order of the antioxidant properties of phenol and o-, p- and m-methoxyphenols using a DPPH reagent is p–OMe > o-OMe > m-OMe > phenol [52,99].

Amorati et al. [14] found that an H-bond stabilizes phenols such that the energy needed to abstract the hydrogen atom from the hydroxyl group is larger than in non-H-bonded phenols. Similarly, the NH group of compounds **4a** and **5a** exhibited hydrogen bonding
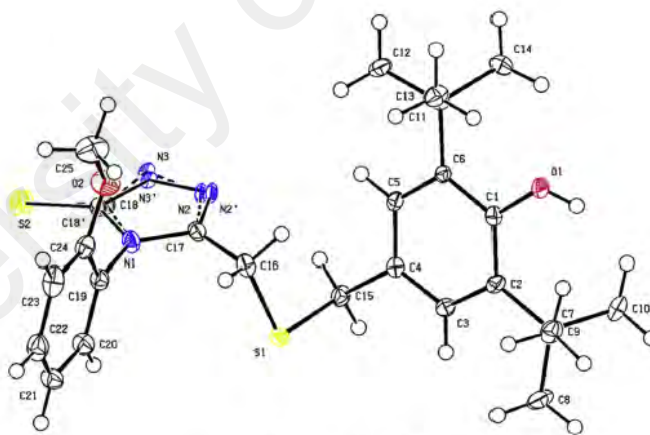
Fig. 7. ORTEP drawing of **6a**.
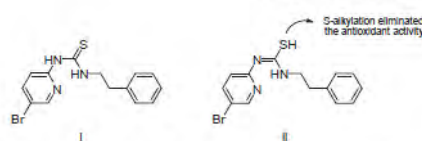
Fig. 8. Thiol-thione tautomerism and S-alkylation in phenethyl-5-bromo-pyridyl thiourea.

Fig. 9. Intramolecular hydrogen bond formation in compounds **4b** and **5b**.

with the oxygen of the o-methoxy group (Fig. 8). This is due to the formation of a bridge between the N−H and the oxygen atom of o-methoxy (N−H−O), which could increase the BDE by stabilizing the amine form and sterically hindering the approach of free radicals to the N−H group. This was contrary to p-methoxy, found in compounds **4b** and **5b**.

There is clear evidence that the stereoelectronic effects of p-methoxy stabilize the aryloxyl or arylaminyl radicals through the p-type lone-pair orbital on the para heteroatom with respect to the aromatic plane [100,101]. This observation was corroborated by the X-ray structure of compounds **4a** and **6a**, where there is clear evidence that the o-methoxy groups lie in the same plane as the benzene ring. Thus, the effect of the direct link between o-, p-, and m-methoxy substituents and phenols or aromatic amines has been evaluated, while those that are indirectly linked have not been evaluated. We attempted to further understand why compound **6b** was more active than **6a**. We anticipated that the stereoelectronic effects of the methoxyl group played an important role in determining the effectiveness of a phenolic antioxidant. Compound **6a** has been characterized by X-ray diffraction in the solid state and by ^{1}H NMR in CDCl$_3$. In the crystal structure of **6a**, the methoxy group was co-planar to the benzene ring such that the molecule was at its lowest energy level (Fig. 6). It is known that a p-methoxy group attached to a benzene ring prefers a planar conformation [102]. The maximum electron-donating effect occurred when the O−C bond of the methoxy group, which is co-planar with the benzene ring, overlaps the lone pair of the π-symmetry [103,104]. It is clear that the ^{1}H NMR spectrum of compound **6a** (o-methoxy) exhibited restricted internal rotation about the aryl C−N bond in the aryl-substituted triazole ring. The steric barriers to aryl group rotation in compound **6a** are expected to be high as there would be severe crowding between the o-methoxy phenyl and the triazole ring, particularly at the 3- and 5-positions of the triazole ring.

In contrast to compound **6a**, compound **6b** did not exhibit restricted internal rotation due to the p-methoxy group. The steric crowding in **6a** forced a large dihedral angle between the methoxy group and the ring, twisting the methoxy group out of the plane (Fig. 4). Thus, the electronic density effect was reduced. The absence of crowding in **6b** led to a lower dihedral angle and lowering of the electron density effect. Thus, restricted rotation could be a reason behind the changes in the position of the methoxy group. As a result the oxygen p-type lone-pair orbital overlapped less with the SOMO of the radical when $θ > 0°$. The maximum stabilization of the radical occurred when $θ = 0°$ and was at a minimum when $θ = 90°$, as shown in Fig. 9 [100,101,104].

2.6.2. In vitro lipid peroxidation

Peroxidation of lipids has been shown to be a cumulative effect of ROS, which disturbs the assembly of the membrane. This disturbance causes changes in fluidity and permeability as well as alterations in ion transport and inhibition of metabolic processes [105]. α-TOH has been demonstrated to be a potent inhibitor of lipid peroxidation in cellular membranes, preventing a one-electron oxidation from forming a tocopheryl radical that promotes the propagation of a lipid peroxidation chain reaction [106]. α-TOH is located in membranes, while AA is located in aqueous phases due to it is low lipid solubility [11,107]. However, it is worth noting that hydrophilic scavengers of oxygen radicals located in the aqueous region cannot scavenge radicals within the lipid region of membranes. Therefore, α-TOH could be a suitable control in lipid peroxidation assays (Fig. 10).
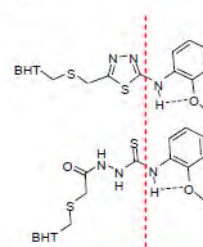
The TBARS assay was used to measure the formation of essential oils from lipid peroxide in the lipid-rich media provided by egg yolk homogenate. A review of antioxidant assays showed the most important parameters for increasing or decreasing the inhibition of free radicals to be the following: a multiphase medium (such as an emulsion) [108], steric inaccessibility [109], and a BDE of free radicals such as BDE(ROO−H) ≈ 88 [110]. With these parameters, we expected to observe different inhibition activities between DPPH and lipid peroxidation assays.

Contrary to the DPPH results, compound **4a** exhibited the lowest lipid peroxidation activity, yielding the highest IC$_{50}$ value of 60.53 ± 1.80 μM. Compound **4b** was observed to have a higher lipid peroxidation activity than BHT but had a low IC$_{50}$ value of 30.10 ± 4.07 μM.

Thiadiazoles **5a** and **5b** exhibited the strongest free radical scavenging activity, reducing power and anti-lipid peroxidative activity compared with two commercial antioxidants, namely α-TOH and BHT (Table 5). This seems to suggest that thiadiazoles bearing the BHT moiety can easily donate electrons and hydrogens.

The triazole compound **6a** demonstrated moderate lipid peroxidation activity due to intramolecular hydrogen bonding at the ortho position (Fig. 8). Table 5 shows that p-methoxy substituents were more active than o-methoxy substituents. This result is similar to our findings with the DPPH assay, which can be attributed to the stereoelectronic effect [100], intramolecular hydrogen bonding [37] and presumably intramolecular lipophilicity effects [11]. In support of our result, an antioxidant has to be highly active at a low concentration on the surface of the fat or oil phase. α-TOH and BHT are known to be strongly lipophilic antioxidants due to
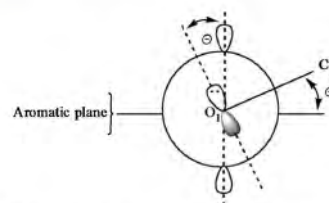
Fig. 10. Interpreting the stereoelectronic effect of the dihedral angle.

their long hydrocarbon chains and di-*tert*-butyl groups that are similar to fatty acid tails and therefore able to reach a higher level of bioavailability [111]. Presumably, the significantly greater value of lipid peroxidation could be attributed to the balance between the hydrophilicity of the polar moieties and the lipophilicity of the hydrocarbon moieties. Thus, the stronger inhibitory activity of compound **6b** (IC_{50} 2.85 ± 1.09 μM; inhibition = 86.43%) could be attributed to both hydrophilic and lipophilic effects on emulsified oils [112,113]. In the emulsified medium used in the TBARS assay, the non-polar free radical scavengers accumulated in the lipid phase and at the oil-water interface, where interactions between hydroperoxides at the droplet surface and pro-oxidants in the aqueous phase occur. Thus, the log*P* measurement (where *P* is the partition coefficient of the molecule in the water–octanol system) shown in Table 4 is a useful parameter for understanding the behavior of antioxidant molecules. In calculating log *P*, we used computed log *P* values predicted with ADMET software. Calculations for **5b** and **6b** showed **6b** (log *P* = 6.62) to be slight more polar than **5b** (log *P* = 6.72) due to the thiol–thione tautomerism effect. This suggested that compound **6b** may have hydrophilic and lipophilic groups that may act as amphiphilic antioxidants in one molecule rather than requiring the separate use of two antioxidants. Thus, the inhibition of lipid peroxidation by **6b** suggested that this compound could be a possible candidate with promising antioxidant activity.

3. Conclusion

The PASS-assisted design strategy for improving the antioxidant activity of BHT has been successfully applied. The results of PASS indicated that the most probable activities are lipid peroxidation inhibition, antioxidant, scavenging of free radicals and anti-inflammatory effects. This strategy prevents the unnecessary waste of chemicals and saves time, thus allowing the present approach to be very useful in designing drug molecules according to their required properties without undesirable side effects. This makes the use of PASS-assisted design generally important. Using PASS, we improved the free radical scavenging capacity of BHT inhibition (25%) by more than two-fold in most compounds. The DPPH and lipid peroxidation assays of the tested compounds showed that *para* substituents possessed higher antioxidant activities than *ortho* substituents. The ^{1}H NMR spectrum helped us to understand the relationship between restricted rotation of *o*-methoxy substituents and the effect of the electronic density, which could increase or decrease antioxidant activities. The synthesized compounds **4**, **5** and **6** satisfied Lipinski's RO5 and ADMET properties. RO5 and ADMET predictions can be important initial steps toward the development of novel pharmaceuticals in the fight against free radicals. Compounds **5** and **6** have the exact same molecular weight with different polarity and antioxidant activity, and therefore this wide range of properties could help us to solve problems in the pharmacological sciences. Compounds **5b** and **6b** may be possible candidates for PASS-ADMET-assisted design strategies. These interesting findings encouraged us to consider the BHT moiety as a building block for new synthetic antioxidant projects.

4. Experimental section

4.1. General

All materials and solvents were obtained from Sigma–Aldrich. Melting points were determined on a MEL-TEMP II melting point instrument. IR spectra were recorded on a Perkin–Elmer RX1 FT-IR spectrometer. The ^{1}H and ^{13}C NMR spectra were recorded on a

400 MHz FT-NMR using $CDCl_3$ or DMSO-d_6 as a solvent and tetramethylsilane as an internal standard. The abbreviations s = singlet, d = doublet, t = triplet, q = quadruplet, m = multiplet and bs = broad signal were used throughout. HR-mass spectra (ESI) were obtained with a MAT 95 xl-T mass spectrometer at 70 ev. UV–visible spectra were recorded on a UV-1650PC model UV–visible spectrophotometer.

The Supplementary Data section reports the synthesis and physicochemical characterization of S-(3,5-di-tert-butyl-4-hydroxybenzyl)thioglycolic acid (**1**), methyl-S-(3,5-di-tert-butyl-4-hydroxybenzyl)thioglycolate (**2**), and S-(3,5-di-tert-butyl-4-hydroxybenzyl)thioglycolic acid hydrazide (**3**) and the synthesis of 2-(2-(3, 5-di-tert-butyl-4-hydroxybenzylthio)acetyl)-N-(substituted phenyl) hydrazinecarbothioamide (**4a**–**b**), 2,6-di-tert-butyl-4-(((5-(substituted phenylamino)-1,3,4-thiadiazol-2-yl) methylthio)methyl)phenol (**5a**–**b**) and 3-((3,5-Di-tert-butyl-4-hydroxybenzylthio)methyl)-4-(substitutedphenyl)-1H-1,2,4-triazole-5(4H)-thione (**6a**–**b**). The general synthetic procedures and one example of a compound are given below.

4.2. General procedure for the synthesis of 2-(2-(3, 5-di-tert-butyl-4-hydroxybenzylthio)acetyl)-N-(substituted phenyl) hydrazinecarbothioamide (4)

To a solution of S-(3,5-di-*tert*-butyl-4-hydroxybenzyl)thioglycolic acid hydrazide (**3**; 0.45 g, 1.39 mmol), dry toluene or benzene (5 ml) was added isothiocyanate (1.39 mmol), and the reaction mixture was stirred under nitrogen gas for 2 h at rt. The precipitate was collected by filtration, washed with boiled hexane, dried at rt, and recrystallized using the appropriate solvent.

4.2.1. 2-(2-(3,5-Di-tert-butyl-4-hydroxybenzylthio)acetyl)-N-(2-methoxyphenyl)hydrazine carbothioamide (4a)

2-(2-(3,5-Di-tert-butyl-4-hydroxybenzylthio)acetyl)-N-(2-methoxyphenyl)hydrazine carbothioamide (**4a**) was recrystallized from toluene to give 0.64 g of a colorless crystal (95%). Mp 119–121 °C. IR (KBr pellet), cm^{-1}: v = 3615 (free OH), 3211–3293 (NH), 2880–2952 (C–H of t-Bu and –OCH$_3$), 1655 (C=O). ^{1}H NMR (CDCl$_3$, 400 MHz), δ, ppm: 1.40 (s, 18H, 2 × t-Bu), 3.22 (s, 2H, H-8), 3.80 (s, 3H, –OCH$_3$), 3.82 (s, 2H, H-7), 5.19 (s, 1H, OH), 6.91 (d, 1H, H-16, ^{3}J = 8 Hz), 6.98 (t, 1H, H-15, ^{3}J = 8, ^{3}J = 8 Hz), 7.10 (s, 2H, H-3, H-5), 7.16 (dt, 1H, H-14, ^{3}J = 8.8, ^{3}J = 8, ^{4}J = 2.4 Hz), 7.92 (d, 1H, H-13, ^{3}J = 6.4 Hz), 8.32 (s, 1H, NH-3), 9.26 (b, 1H, NH-2), 9.84 (b, 1H, NH-1). ^{13}C NMR (CDCl$_3$, 100 MHz), δ, ppm: 30.31 (6C, 2 × –C(CH$_3$)$_3$), 33.76 (1C, C-8), 34.42 (2C, 2 × –C(CH$_3$)$_3$), 37.71 (1C, C-7), 55.90 (1C, –OCH$_3$), 111.42 (1C, C-16), 120.96 (1C, C-15), 124.07 (1C, C-13), 125.39 (1C, C-4), 125.99 (2C,C-3, C-5), 126.11 (1C, C-11), 129.13 (1C, C-14), 136.40 (2C, C-2, C-6), 151.26 (1C, C-12), 153.34 (1C, C-1), 165.22 (1C, C-9), 177.21 (1C, 10). HREIMS m/z 489.2108 [M]$^+$ (calcd for C$_{25}$H$_{35}$O$_3$N$_3$ S$_2$ 489.2120).

4.3. General procedure for the synthesis of 2,6-di-tert-butyl-4-(((5-(substituted phenylamino)-1,3,4-thiadiazol- 2-yl)methylthio) methyl)phenol (5)

Thiosemicarbazide (**4a**–**b**) (0.50 mmol) was added gradually under stirring to cold sulfuric acid (50%, 5 ml) in 10 min. The reaction mixture was heated for 20 min at 100 °C. It was then poured over crushed ice under stirring. After 1 h, the precipitate was filtered, washed with distilled water, dried at rt, and recrystallized using the appropriate solvent.

4.3.1. 2,6-Di-tert-butyl-4-(((5-(2-methoxyphenylamino)-1,3,4-thiadiazol-2-yl) methylthio)methyl)phenol (5a)

2,6-Di-tert-butyl-4-(((5-(2-methoxyphenylamino)-1,3,4-thiadiazol-2-yl) methylthio)methyl)phenol (5a) was recrystallized from MeOH 4:1H$_2$O to give 0.17 g of a white solid (72%). Mp 113–115 °C. IR (KBr pellet), cm^{-1}: ν = 3614 (free OH), 3210–3293 (NH), 2881–2953 (C–H of t-Bu and –OCH$_3$), 1655, 1604 (2C=N). ^{1}H NMR (CDCl$_3$, 400 MHz), δ, ppm: 1.42 (s, 18H, 2 × t-Bu), 3.69 (s, 2H, H-7), 3.89 (s, 2H, H-8), 3.90 (s, 3H, –OCH$_3$), 5.14 (s, 1H, OH), 6.89–6.91 (dd, 1H, H-16, ^3J = 7.2, ^4J = 1.2 Hz), 6.97–7.05 (m, 2H, H-14, H-15) 7.07 (s, 2H, H-3, H-5), 7.11–7.17 (b, 1H, NH), 7.78–7.80 (dd, 1H, H-13, ^3J = 8.8, ^4J = 1.6 Hz). ^{13}C NMR (CDCl$_3$, 100 MHz), δ, ppm: 30.08 (1C, C-8), 30.36 (6C, 2 × –C(CH$_3$)$_3$), 34.42 (2C, 2 × –C(CH$_3$)$_3$), 36.58 (1C, C-7), 55.87 (1C, –OCH$_3$), 110.43 (1C, C-16), 116.60 (1C, C-13), 121.25 (1C, C-15), 123.02 (1C, C-14), 125.99 (2C, C-3, C-5), 127.61 (1C, C-4), 129.53 (1C, C-11), 136.14 (2C, C-2, C-6), 147.89 (1C, C-12), 153.14 (1C, C-1), 160.13 (1C, C-9), 165.92 (1C, C-10). HREIMS m/z 471.2034 [M]$^+$ (calcd for C$_{25}$H$_{33}$O$_2$N$_3$S$_2$ 471.2014).

4.4. General procedure for the synthesis of 3-((3,5-di-tert-butyl-4-hydroxybenzylthio)methyl)-4-(substituted phenyl)-1H-1,2,4-triazole-5(4H)-thione (6)

A mixture of thiosemicarbazide (4a–b; 0.50 mmol) and potassium carbonate (25%, 5 ml) was stirred for 18 h. Then, 250 ml water was added with stirring for 1 h. The solution was adjusted to pH (5–6) with diluted hydrochloric acid and was kept aside for 1 h. A white precipitate was filtered, washed with water, dried and recrystallized using the appropriate solvent.

4.4.1. 2,6-Di-tert-butyl-4-(((5-mercapto-4-(2-methoxyphenyl)-4H-1,2,4-triazol-3-yl)methylthio)methyl)phenol (6a)

2,6-Di-tert-butyl-4-(((5-mercapto-4-(2-methoxyphenyl)-4H-1,2,4-triazol-3-yl)methylthio)methyl)phenol (6a) was recrystallized from toluene 3:1 hexane to give 0.15 g of a colorless crystal (66%). Mp 150–152 °C. IR (KBr pellet), cm^{-1}: ν = 3589 (free OH), 3039, 3101 (NH), 2870–2957 (C–H of t-Bu), 1603 (C=N), 1256 (C=S). ^{1}H NMR (CDCl$_3$, 400 MHz), δ, ppm: 1.41 (s, 18H, 2 × t-Bu), 3.18, 3.22 (d, 1H$_a$, H-8, $^2J_{HaHb\text{-geminal}}$ = 16 Hz), 3.45, 3.49 (d, 1H$_b$, H-8, $^2J_{HbHa\text{-geminal}}$ = 16 Hz), 3.56, 3.59 (d, 1H$_a$, H-7, $^2J_{HaHb\text{-geminal}}$ = 12 Hz), 3.60, 3.63 (d, 1H$_b$, H-7, $^2J_{HbHa\text{-geminal}}$ = 12 Hz), 3.79 (s, 3H, –OCH$_3$), 5.16 (s, 1H, OH), 7.06–7.07 (m, 3H, H-3, H-5 and 1H of H-16), 7.11 (t, 1H, H-15, ^3J = 8, ^3J = 8 Hz), 7.36 (d, 1H, H-14, ^3J = 8 Hz), 7.49 (m, 1H, H-13), 11.93 (s, 1H, NH). ^{13}C NMR (CDCl$_3$, 100 MHz): δ, ppm: 24.92 (1C, C-8), 30.37 (6C, 2 × –C(CH$_3$)$_3$), 34.41 (2C, 2 × –C(CH$_3$)$_3$), 36.31 (1C, C-7), 56.06 (1C, –OCH$_3$), 112.60 (1C, C-16), 121.29 (1C, C-15), 121.55 (1C, C-4), 126.04 (2C, C-3, C-5), 127.29 (1C, C-11), 130.57 (1C, C-14), 131.95 (1C, C-13), 136.06 (2C, C-2, C-6), 151.07 (1C, C-9), 153.12 (1C, C-1), 154.69 (1C, C-12), 169.21 (1C, C-10). HREIMS m/z 471.2011 [M]$^+$ (calcd for C$_{25}$H$_{33}$O$_2$N$_3$S$_2$ 471.2014).

4.5. X-ray crystallography

Diffraction data were measured using a Bruker SMART Apex II CCD area-detector diffractometer (graphite-monochromated Mo K radiation, = 0.71073 Å). The orientation matrix, unit cell refinement and data reduction were all handled by the Apex2 software (SAINT integration, SADABS absorption correction) [114]. The structures were solved using direct methods in the program SHELXS-97 [115] and were refined by the full matrix least-squares method on F2 with SHELXL-97. Drawings of the molecules were produced with XSEED [116].

4.6. Antioxidant assay

4.6.1. Materials and methods

4.6.1.1. DPPH free radical scavenging assay. The DPPH radical scavenging assay was carried out according to the literature [117] with some modifications. Briefly, 1.0 ml of DPPH solution (200 μM in DMSO) was added to a range of various sample concentrations (100, 10, 1, 0.1 and 0.01 μM). Then, 22.03–47.76 mg (1×10^{-4} M) of the test compound was dissolved in 1.0 ml DMSO (100%) as a stock solution. This stock solution was then diluted to a range of final extraction concentrations of 100, 10, 1, 0.1 and 0.01 μM. As a negative control, the same DPPH concentration in DMSO without sample was used. Each assay was carried out in triplicate. The mixture was then incubated in the dark for 60 min at room temperature. Absorbance at 570 nm for each sample was then measured. AA was used as a positive control. The free radical scavenging activity of the compounds was calculated as a percentage of radical inhibition using the following formula:

$$\text{Percentage of Inhibition}(\%) = [(A_c - A_s)/A_c] \times 100.$$

where A_s = Absorbance of the compounds/positive control and A_c = Absorbance of control (DPPH solution and DMSO). To determine the concentration required to achieve 50% inhibition (IC50) of the DPPH radical, the percentage of DPPH inhibition for each compound was plotted against the extract concentration.

4.6.1.2. Lipid peroxidation inhibition assay. The lipid peroxidation inhibition assay was carried out according to the reported method with some modifications [118]. Fowl egg yolk composed mainly of phospholipids, proteins and triacylglycerol, was used as an alternative to rat liver microsomes and linoleic acid. The reactive mixture for the induction of lipid peroxidation included 1.0 ml egg yolk emulsified with phosphate buffer saline (0.1 M, pH 7.4) to a final concentration of 12.5 g/l and 200 μl of 3000 μM FeSO$_4$. Next, 22.03–47.76 mg (1×10^{-4} M) of test compound was dissolved in 1.0 ml DMSO (100%) as a stock solution. This stock solution was then diluted to a range of final extraction concentrations of 100, 10, 1, 0.1, 0.01 and 0.001 μM. Each assay was carried out in triplicate. The mixture was incubated at 37 °C for 1 h and was then treated with 0.5 ml freshly prepared TCA (15%) and 1.0 ml of TBA (1%). The reaction mixtures were incubated in boiling water for 10 min. Upon cooling, the mixtures were centrifuged at 3500 rpm for 10 min. The formation of TBARS was measured by removing 100 μl of supernatant and measuring the absorbance at 532 nm, using α-TOH as a positive control. The percentage of inhibition was calculated from the following equation:

$$\% \text{ inhibition} = [A_s/A_c] \times 100.$$

where A_s = Absorbance with compound and A_c = Absorbance of control. To determine the concentration required to achieve 50% inhibition (IC$_{50}$) of phospholipid oxidation in egg yolk, the percentage of lipid peroxidation inhibition was plotted against the extract concentration.

139

Appendix A. Supplementary data

Supplementary data related to this article can be found at http://dx.doi.org/10.1016/j.ejmech.2014.10.001.

References

[1] W. Dröge, Free radicals in the physiological control of cell function, Physiol. Rev. 82 (2002) 47–95.
[2] C. Schöneich, Reactive oxygen species and biological aging: a mechanistic approach, Exp. Gerontol. 34 (1999) 19–34.
[3] T. Sahinoglu, C.R. Stevens, B. Bhatt, D.R. Blake, The role of reactive oxygen species in inflammatory disease: evaluation of methodology, Methods 9 (1996) 628–634.
[4] C. Schöneich, Methionine oxidation by reactive oxygen species: reaction mechanisms and relevance to Alzheimer's disease, Biochim. Biophys. Acta Proteins Proteomics 1703 (2005) 111–119.
[5] M. Oka, M. Tachibana, K. Noda, N. Inoue, M. Tanaka, K. Kuwabara, Relevance of anti-reactive oxygen species activity to anti-inflammatory activity of components of eviprostat, a phytotherapeutic agent for benign prostatic hyperplasia, Phytomedicine 14 (2007) 465–472.
[6] M.B. Kirkinezos, C.T. Moraes, Reactive oxygen species and mitochondrial diseases, Semin. Cell Dev. Biol. 12 (2001) 449–457.
[7] N. De Maria, A. Colantoni, S. Fagiuoli, G.-J. Liu, B.K. Rogers, F. Farinati, D.H. Van Thiel, R.A. Floyd, Association between reactive oxygen species and disease activity in chronic hepatitis C, Free Radic. Biol. Med. 21 (1996) 291–295.
[8] C. Smith, Y. Zhang, C. Koboldt, J. Muhammad, B. Zweifel, A. Shaffer, J. Talley, J. Masferrer, K. Seibert, P. Isakson, Pharmacological analysis of cyclooxygenase-1 in inflammation, Proc. Natl. Acad. Sci. U. S. A. 95 (1998) 13313.
[9] E.M. Conner, M.B. Grisham, Inflammation, free radicals, and antioxidants, Nutrition 12 (1996) 274–277.
[10] P. Stecher, Butylated hydroxytoluene, in: M.J. O'Neil (Ed.), The Merck Index, Merck Research Laboratories, Rahway, New Jersey, USA, 1968, p. 179.
[11] J. Hilton, Antioxidants: function, types and necessity of inclusion in pet foods, Can. Veterinary J. 30 (1989) 682–684.
[12] B. Stuckey, Antioxidants as Food Stabilizers, in: Handbook of Food Additives, 1972, pp. 185–221.
[13] J. Dacre, The metabolism of 3: 5-di-tert.-butyl-4-hydroxytoluene and 3: 5-di-tert.-butyl-4-hydroxybenzoic acid in the rabbit, Biochem. J. 78 (1961) 758.
[14] R. Amorati, M. Lucarini, V. Mugnaini, G. Pedulli, Antioxidant activity of o-bisphenols: the role of intramolecular hydrogen bonding, J. Org. Chem. 68 (2003) 5198–5204.
[15] E.S. Lazer, H.C. Wong, G.J. Possanza, A.G. Graham, P.R. Farina, Antiinflammatory 2,6-di-tert-butyl-4-(2-arylethenyl)phenols, J. Med. Chem. 32 (1989) 100–104.
[16] G. Moore, K. Swingle, 2, 6-di-tert-butyl-4-(2 -thenoyl) phenol (R-830): a novel nonsteroidal anti-inflammatory agent with antioxidant properties, Inflamm. Res. 12 (1982) 674–683.
[17] P. Grosso, O. Vogl, Functional polymers, Polym. Bull. 14 (1985) 245–250.
[18] Y. Song, D. Connor, A. Sercel, R. Sorenson, R. Doubleday, P. Unangst, B. Roth, V. Beylin, R. Gilbertsen, K. Chan, Synthesis, structure- activity relationships, and in vivo evaluations of substituted di-tert-butylphenols as a novel class of potent, selective, and orally active cyclooxygenase-2 inhibitors. 2. 1, 3, 4-and 1, 2, 4-thiadiazole series 1, J. Med. Chem. 42 (1999) 1161–1169.
[19] L.J. Marnett, A.S. Kalgutkar, Design of selective inhibitors of cyclooxygenase-2 as nonulcerogenic anti-inflammatory agents, Curr. Opin. Chem. Biol. 2 (1998) 482–490.
[20] M. Inagaki, T. Tsuri, H. Jyoyama, T. Ono, K. Yamada, M. Kobayashi, Y. Hori, A. Arimura, K. Yasui, K. Ohno, Novel antiarthritic agents with 1, 2-isothiazolidine-1, 1-dioxide ([gamma]-sultam) skeleton: cytokine suppressive dual inhibitors of cyclooxygenase-2 and 5-lipoxygenase, J. Med. Chem. 43 (2000) 2040–2048.
[21] C. Kong, W.A. Yehye, N.A. Rahman, M.-W. Tan, S. Nathan, Discovery of potential anti-infectives against Staphylococcus aureus using a caenorhabditis elegans infection model, BMC Complem. Altern. Med. 14 (2014) 4.
[22] S. Kaur, B. Ali, Effect of anti-inflammatory thiosemicarbazone indoles on hyaluronidase, acid phosphatase and trypsin, Pharmacology 24 (1982) 162–168.
[23] A. Dobek, D. Klayman, E. Dickson Jr., J. Scovill, C. Oster, Thiosemicarbazones of 2-acetylpyridine, 2-acetylquinoline, 2-acetylisoquinoline and related compounds as inhibitors of clinically significant bacteria in vitro, Arzneim. 33 (1983) 1583–1591.
[24] A.I. Eid, F.A. Ragab, S.L. El-Ansary, S.M. El-Gazayerly, F.E. Mourad, Synthesis of new 7-substituted 4-methylcoumarin derivatives of antimicrobial activity, Arch. Pharm. 327 (1994) 211–213.
[25] A.P. Liesen, T.M. de Aquino, C.S. Carvalho, V.T. Lima, J.M. de Araújo, J.G. de Lima, A.R. de Faria, E.J.T. de Melo, A.J. Alves, E.W. Alves, A.Q. Alves, A.J.S. Góes, Synthesis and evaluation of anti-toxoplasma gondii and antimicrobial activities of thiosemicarbazides, 4-thiazolidinones and 1,3,4-thiadiazoles, Eur. J. Med. Chem. 45 (2010) 3685–3691.

[26] E. Palaska, G. Sahin, P. Kelicen, N.T. Durlu, G. Altinok, Synthesis and anti-inflammatory activity of 1-acylthiosemicarbazides, 1, 3, 4-oxadiazoles, 1, 3, 4-thiadiazoles and 1, 2, 4-triazole-3-thiones, Il Farm. 57 (2002) 101–107.
[27] S. Hussain, J. Sharma, M. Amir, Synthesis and antimicrobial activities of 1,2,4-triazole and 1,3,4-thiadiazole derivatives of 5-amino-2-hydroxybenzoic acid, E. J. Chem. 5 (2008) 963–968.
[28] S.L. Vasoya, D.J. Paghdar, P.T. Chovatia, H.S. Joshi, Synthesis of some new thiosemicarbazide and 1,3,4-thiadiazole heterocycles bearing benzo[b]Thiophene nucleus as a potent antitubercular and antimicrobial agents, J. Sci. Islam.Repub. Iran 16 (2005) 33–36.
[29] W. Rzeski, J. Matysiak, M. Kandefer-Szerszen, Anticancer, neuroprotective activities and computational studies of 2-amino-1,3,4-thiadiazole based compound, Bioorg. Med. Chem. 15 (2007) 3201–3207.
[30] T.M. Abdel-Rahman, Synthesis, reactions, and anticancer activity of some 1,3,4-thiadiazole/thiadiazine derivatives of carbazole, Phosphorus Sulfur Silicon Relat. Elem. 181 (2006) 1737–1754.
[31] I. Khan, S. Ali, S. Hameed, N. Rama, M. Hussain, A. Wadood, R. Uddin, Z. Ul-Haq, A. Khan, Synthesis, antioxidant activities and urease inhibition of some new 1, 2, 4-triazole and 1, 3, 4-thiadiazole derivatives, Eur. J. Med. Chem. 45 (2010) 5200–5207.
[32] L. Navidpour, H. Shafaroodi, K. Abdi, M. Amini, M.H. Ghahremani, A.R. Dehpour, A. Shafiee, Design, synthesis, and biological evaluation of substituted 3-alkylthio-4,5-diaryl-4H-1,2,4-triazoles as selective COX-2 inhibitors, Bioorg. Med. Chem. 14 (2006) 2507–2517.
[33] M. Wujec, M. Pitucha, M. Dobosz, U. Kosikowska, A. Malm, Synthesis and potential antimycotic activity of 4-substituted-3-(thiophene-2-yl-methyl)-delta2-1,2,4-triazoline-5-thiones, Acta Pharm. Short. Commun. 54 (2004) 251–260.
[34] J. Wright, E. Johnson, G. DiLabio, Predicting the activity of phenolic antioxidants: theoretical method, analysis of substituent effects, and application to major families of antioxidants, J. Am. Chem. Soc. 123 (2001) 1173–1183.
[35] H. Zhang, Structure-activity relationships and rational design strategies for radical-scavenging antioxidants, Curr. Comp. Aided Drug Des. 1 (2005) 257–273.
[36] H.-Y. Zhang, D.-P. Yang, G.-Y. Tang, Multipotent antioxidants: from screening to design, Drug Discov. Today 11 (2006) 749–754.
[37] T. Kajiyama, Y. Ohkatsu, Effect of para-substituents of phenolic antioxidants, Polym. Degrad. Stab. 71 (2001) 445–452.
[38] M. Lucarini, G.F. Pedulli, M. Cipollone, Bond dissociation enthalpy of.alpha.-tocopherol and other phenolic antioxidants, J. Org. Chem. 59 (1994) 5063–5070.
[39] L.R.C. Barclay, M.R. Vinqvist, Phenols as Antioxidants, John Wiley and Sons, Ltd, 2003.
[40] E. Klein, V. Lukeš, Z. Cibulková, On the energetics of phenol antioxidants activity, Pet. Coal 47 (2005).
[41] L.R. Fukumoto, G. Mazza, Assessing antioxidant and prooxidant activities of phenolic compounds, J. Agric. food Chem. 48 (2000) 3597–3604.
[42] V. Bondet, W. Brand-Williams, C. Berset, Kinetics and mechanisms of antioxidant activity using the DPPH. Free radical method, Lebensm. und Technologie 30 (1997) 609–615.
[43] A. Pizzi, K.L. Mittal, in: A. Pizz, K.L. Mittal (Eds.), Handbook of Adhesive Technology, Marcel Dekker, 2003.
[44] G. Scott, Antioxidants, Bull. Chem. Soc. Jpn. 61 (1988).
[45] J. Pospíšil, S. Nespurek, Chain-breaking stabilizers in polymers: the current status, Polym. Degrad. Stab. 49 (1995) 99–110.
[46] Z. Velkov, E. Balabanova, A. Tadjer, Radical scavenging activity prediction of o-coumaric acid thioamide, J. Mol. Struct. Theochem 821 (2007) 133–138.
[47] K.B. Wiberg, Y. Wang, A comparison of some properties of C=O and C=S bonds, Arkivoc 5 (2011) 45–56.
[48] Z. Velkov, Y. Velkov, E. Balabanova, A. Tadjer, First principle study of the structure of conjugated amides and thioamides, Int. J. Quantum Chem. 107 (2007) 1765–1771.
[49] M. Lucarini, P. Pedrielli, G.F. Pedulli, L. Valgimigli, D. Gigmes, P. Tordo, Bond dissociation energies of the N–H bond and rate constants for the reaction with alkyl, alkoxyl, and peroxyl radicals of phenothiazines and related compounds, J. Am. Chem. Soc. 121 (1999) 11546–11553.
[50] F. Minisci, Free Radicals in Biology and Environment, Springer, Netherlands, 1997.
[51] R. Amorati, F. Ferroni, G.F. Pedulli, L. Valgimigli, Modeling the co-antioxidant behavior of monofunctional phenols. Applications to some relevant compounds, J. Org. Chem. 68 (2003) 9654–9658.
[52] M.I. de Heer, H.G. Korth, P. Mulder, Poly methoxy phenols in solution: O–H bond dissociation enthalpies, structures, and hydrogen bonding, J. Org. Chem. 64 (1999) 6969–6975.
[53] B. Dimitrios, Sources of natural phenolic antioxidants, Trends Food Sci. Technol. 17 (2006) 505–512.
[54] M.I. de Heer, P. Mulder, H.-G. Korth, K.U. Ingold, J. Lusztyk, Hydrogen atom abstraction kinetics from intramolecularly hydrogen bonded ubiquinol-0 and other (poly)methoxy phenols, J. Am. Chem. Soc. 122 (2000) 2355–2360.
[55] C. Araujo, L. Leon, Biological activities of curcuma longa L, Memórias do Inst. Oswaldo Cruz 96 (2001) 723–728.
[56] M. Roudsari, Subcritical water extraction of antioxidant compounds from canola meal, Department of Food and Bioproduct Sciences, University of Saskatchewan, Canada, 2007.

[57] T. Kajiyama, Y. Ohkatsu, Effect of meta-substituents of phenolic anti-oxidants –proposal of secondary substituent effect, Polym. Degrad. Stab. 75 (2002) 535–542.

[58] O. Akkus, R.M. Belaney, P. Das, Free radical scavenging alleviates the biomechanical impairment of gamma radiation sterilized bone tissue, J. Orthop. Res. 23 (2005) 838–845.

[59] M. Sorimachi, Y. Nakamura, H. Kimura, S. Matsuyama, Radiation-proof Sheath Material and Radiation-proof Cable, HITACHI CABLE, LTD, 2009.

[60] V. Poroikov, D. Filimonov, A. Lagunin, T. Gloriozova, A. Zakharov, PASS: identification of probable targets and mechanisms of toxicity, SAR QSAR Environ. Res. 18 (2007) 101–110.

[61] F.A. Kadir, N.M. Kassim, M.A. Abdulla, W.A. Yehye, PASS-predicted vitex negundo activity: antioxidant and antiproliferative properties on human hepatoma cells-an in vitro study, BMC Complem. Altern. Med. 13 (2013) 343.

[62] A.V. Stepanchikova, A.A. Lagunin, D.A. Filimonov, V.V. Poroikov, Prediction of biological activity spectra for substances: evaluation on the diverse sets of drug-like structures, Curr. Med. Chem. 10 (2003) 225–233.

[63] S. Anzali, G. Barnickel, B. Cezanne, M. Krug, D. Filimonov, V. Poroikov, Discriminating between drugs and nondrugs by prediction of activity spectra for substances (PASS), J. Med. Chem. 44 (2001) 2432–2437.

[64] F. Kadir, N.B.M. Kassim, M.A. Abdulla, B. Kamalidehghan, F. Ahmadipour, W. Yehye, PASS-predicted hepatoprotective activity of Caesalpinia sappan in thioacetamide-induced liver fibrosis in rats, Sci. World J. (2014) 1–12.

[65] F. Delmas, C. Di Giorgio, M. Robin, N. Azas, M. Gasquet, C. Detang, M. Costa, P. Timon-David, J.-P. Galy, In vitro activities of position 2 substitution-bearing 6-nitro-and 6-amino-benzothiazoles and their corresponding anthranilic acid derivatives against leishmania infantum and trichomonas vaginalis, Antimicrob. Agents Chemother. 46 (2002) 2588–2594.

[66] C. Di Giorgio, F. Delmas, N. Filloux, M. Robin, L. Seferian, N. Azas, M. Gasquet, M. Costa, P. Timon-David, J.-P. Galy, In vitro activities of 7-substituted 9-chloro and 9-amino-2-methoxyacridines and their bis-and tetra-acridine complexes against leishmania infantum, Antimicrob. Agents Chemother. 47 (2003) 174–180.

[67] C. Di Giorgio, F. Delmas, E. Ollivier, R. Elias, G. Balansard, P. Timon-David, In vitro activity of the β-carboline alkaloids harmane, harmine, and harmaline toward parasites of the species leishmania infantum, Exp. Parasitol. 106 (2004) 67–74.

[68] P.K. Baroliya, P. Joshi, R. Chauhan, A. Goswami, Synthesis, characterization and activity prediction of some new class of hydroxytriazenes, Int. J. Chem. Sci. Technol. 1 (2011) 1–4.

[69] E. Phillips, R.C. Wasson, in: Phenols as corrosion inhibitors and antioxidants, Aug, 30, 1989, p. 23. Ciba-Geigy A.-G., Switz.

[70] N.T. Akinchan, D.X. West, Y. Yang, M.M. Salberg, T.L. Klein, Magnetic and spectroscopic properties of copper(II) complexes with 1-salicoyl-4-phenylthiosemicarbazide, Transit. Metal. Chem. 20 (1995) 481–484.

[71] M.V. Angelusiu, G.L. Almajan, T. Rosu, M. Negoiu, E.-R. Almajan, J. Roy, Copper(II) and uranyl(II) complexes with acylthiosemicarbazide: synthesis, characterization, antibacterial activity and effects on the growth of pro-myelocytic leukemia cells HL-60, Eur. J. Med. Chem. 44 (2009) 3323–3329.

[72] D.L. Pavia, G.M. Lampman, G.S. Kriz, Introduction to spectroscopy, in: Thomson Learning, 2001. USA.

[73] J. Jampilek, M. Doležal, J. Kuneš, I. Raich, F. Liška, 4-Substituted aryl bromides coupling with 4-methoxybenzene-1-thiol by means of copper catalysts, Chem. Pap. 59 (2005) 178–181.

[74] S. Tafazoli, J.S. Wright, P.J. O'Brien, Prooxidant and antioxidant activity of vitamin e analogues and troglitazone, Chem. Res. Toxicol. 18 (2005) 1567–1574.

[75] H. Massaeli, S. Sobrattee, G.N. Pierce, The importance of lipid solubility in antioxidants and free radical generating systems for determining lipoprotein peroxidation, Free Radic. Biol. Med. 26 (1999) 1524–1530.

[76] M.A. Bakht, M.S. Yar, S.G. Abdel-Hamid, S.I. Al Qasoumi, A. Samad, Molecular properties prediction, synthesis and antimicrobial activity of some newer oxadiazole derivatives, Eur. J. Med. Chem. 45 (2010) 5862–5869.

[77] C.A. Lipinski, F. Lombardo, B.W. Dominy, P.J. Feeney, Experimental and computational approaches to estimate solubility and permeability in drug discovery and development settings, Adv. Drug Deliv. Rev. 23 (1997) 3–25.

[78] H. Mishra, N. Singh, T. Lahiri, K. Misra, A comparative study on the molecular descriptors for predicting drug-likeness of small molecules, Bioinformation 3 (2009) 384–388.

[79] H.H.F. Refsgaard, B.F. Jensen, P.B. Brockhoff, M. Guldbrandt, M.S. Christensen, In silico prediction of membrane permeability from calculated molecular parameters, J. Med. Chem. 48 (2005) 805–811.

[80] R. Wang, Y. Fu, L. Lai, A new atom-additive method for calculating partition coefficients, J. Chem. Inf. Comput. Sci. 37 (1997) 615–621.

[81] D.E. Clark, Rapid calculation of polar molecular surface area and its application to the prediction of transport phenomena. 2. Prediction of blood-brain barrier penetration, J. Pharm. Sci. 88 (1999) 815–821.

[82] P.C. Eklund, O.K. Langvik, J.P. Warna, T.O. Salmi, S.M. Willfor, R.E. Sjoholm, Chemical studies on antioxidant mechanisms and free radical scavenging properties of lignans, Org. Biomol. Chem. 3 (2005) 3336–3347.

[83] O.P. Sharma, T.K. Bhat, DPPH antioxidant assay revisited, Food Chem. 113 (2009) 1202–1205.

[84] E. Frankel, Lipid oxidation, Oily Press Lipid Library Bridgewater, England, 2005, pp. 1–470.

[85] W. Nawar, Chapter 5. Lipids, Food Chemistry, third ed., Marcel Dekker, Inc, Fennema, OR New York, 1996, pp. 254–299.

[86] M.H. Shih, F.Y. Ke, Syntheses and evaluation of antioxidant activity of syd-nonyl substituted thiazolidinone and thiazoline derivatives, Bioorg. Med. Chem. 12 (2004) 4633–4643.

[87] F. Karatas, M. Koca, H. Kara, S. Servi, Synthesis and oxidant properties of novel (5-bromobenzofuran-2-yl)(3-methyl-3-mesitylcyclobutyl)ketonethio-semicarbazone, Eur. J. Med. Chem. 41 (2006) 664–669.

[88] S. Ghosh, A.K. Misra, G. Bhatia, M.M. Khan, A.K. Khanna, Syntheses and evaluation of glucosyl aryl thiosemicarbazide and glucosyl thio-semicarbazone derivatives as antioxidant and anti-dyslipidemic agents, Bioorg. Med. Chem. Lett. 19 (2009) 386–389.

[89] M. Poyraz, M. Sari, F. Demirci, M. Kosar, S. Demirayak, O. Büyükgüngör, Synthesis, crystal structure and biological activity of 1-(1H-benzoimidazol-2-yl)-ethanone thiosemicarbazone and its cobalt complex, Polyhedron 27 (2008) 2091–2096.

[90] C. Kus, G. Ayhan-Kilcigil, S. Özbey, F. Kaynak, M. Kaya, T. Çoban, B. Can-Eke, Synthesis and antioxidant properties of novel N-methyl-1, 3, 4-thiadiazol-2-amine and 4-methyl-2H-1, 2, 4-triazole-3 (4H)-thione derivatives of benz-imidazole class, Bioorg. Med. Chem. 16 (2008) 4294–4303.

[91] B.V. Kopylova, R.G. Gasanov, R.K. Freidlina, Radical arylation of thio-semicarbazide and acetone thiosemicarbazone by aryldiazonium boro-fluorides, Russ. Chem. Bull. 30 (1981) 1059–1062.

[92] H. Zweifel, R. Maier, M. Schiller, Plastics Additives Handbook, sixth ed., Hanser Verlag, 2009.

[93] S.F. Barbuceanu, D.C. Ilies, G. Saramet, V. Uivarosi, C. Draghici, V. Radulescu, Synthesis and antioxidant activity evaluation of new compounds from hydrazinecarbothioamide and 1,2,4-triazole class containing diarylsulfone and 2,4-difluorophenyl moieties, Int. J. Mol. Sci. 15 (2014) 10908–10925.

[94] T. Nishiyama, T. Yamaguchi, T. Fukui, K. Tomii, Chain-breaking fused het-erocyclic antioxidants: antioxidant activities of phenothiazines compared to related compounds, Polym. Degrad. Stab. 64 (1999) 33–38.

[95] M. Lucarini, P. Pedrielli, G. Pedulli, S. Cabiddu, C. Fattuoni, Bond dissociation energies of O- H bonds in substituted phenols from equilibration studies, J. Org. Chem. 61 (1996) 9259–9263.

[96] Y. Dong, T. Venkatachalam, R. Narla, V. Trieu, E. Sudbeck, F. Uckun, Antiox-idant function of phenethyl-5-bromo-pyridyl thiourea compounds with potent anti-HIV activity, Bioorg. Med. Chem. Lett. 10 (2000) 87–90.

[97] S.N. Lawandy, A.B. Shehata, A.F. Younan, Acrylamides as phenolic antioxi-dants for acrylonitrile-butadiene rubber compounds, Polym. Plast. Technol. Eng. 35 (1996) 813–825.

[98] H.B. Niemeyer, M. Metzler, Differences in the antioxidant activity of plant and mammalian lignans, J. Food Eng. 56 (2003) 255–256.

[99] C.F. Mario, D. Carmelo, D.M. Iain, A.D. Gino, K.U. Ingold, Reaction of phenols with the 2,2-diphenyl-1-picrylhydrazyl radical. Kinetics and DFT calculations applied to determine ArO-h bond dissociation enthalpies and reaction mechanism, J. Org. Chem. 73 (2008) 9270–9282.

[100] G. Burton, T. Doba, E. Gabe, L. Hughes, F. Lee, L. Prasad, K. Ingold, Autoxi-dation of biological molecules. 4. Maximizing the antioxidant activity of phenols, J. Am. Chem. Soc. 107 (1985) 7053–7065.

[101] G. Burton, K. Ingold, Autoxidation of biological molecules. 1. Antioxidant activity of vitamin E and related chain-breaking phenolic antioxidants in vitro, J. Am. Chem. Soc. 103 (1981) 6472–6477.

[102] S. Tsuzuki, H. Houjou, Y. Nagawa, K. Hiratani, The second stable conforma-tion of the methoxy groups of o-dimethoxybenzene: stabilization of perpendicular conformation by CH-O interaction, J. Chem. Soc. Perkin Trans. 2 (2002) 1271–1273.

[103] J.S. Wright, E.R. Johnson, G.A. DiLabio, Predicting the activity of phenolic antioxidants; theoretical method, analysis of substituent effects, and appli-cation to major families of antioxidants, J. Am. Chem. Soc. 123 (2001) 1173–1183.

[104] K. Ingold, G. Burton, Vitamin E; or why we don't go rancid1, J. Chin. Chem. Soc. 39 (1992) 199–204.

[105] R. Muralikrishna Adibhatla, J. Hatcher, Phospholipase A2, reactive oxygen species, and lipid peroxidation in cerebral ischemia, Free Radic. Biol. Med. 40 (2006) 376–387.

[106] V. Preedy, R. Watson, The Encyclopedia of Vitamin E, CABI Publishing, 2006.

[107] P.-C. Hsu, M.-Y. Liu, C.-C. Hsu, L.-Y. Chen, Y. Leon Guo, Effects of vitamin E and/or C on reactive oxygen species-related lead toxicity in the rat sperm, Toxicology 128 (1998) 169–179.

[108] R. Apak, K. Guclu, B. Demirata, M. Ozyurek, S. Çelik, B. Bektasoglu, K. Berker, D. Ozyurt, Comparative evaluation of various total antioxidant capacity as-says applied to phenolic compounds with the CUPRAC assay, Molecules 12 (2007) 1496–1547.

[109] R.L. Prior, X. Wu, K. Schaich, Standardized methods for the determination of antioxidant capacity and phenolics in foods and dietary supplements, J. Agric. Food Chem. 53 (2005) 4290–4302.

[110] M.C. Foti, R. Amorati, G.F. Pedulli, C. Daquino, D.A. Pratt, K.U. Ingold, Influ-ence of "remote" intramolecular hydrogen bonds on the stabilities of phe-noxyl radicals and benzyl cations, J. Org. Chem. 75 (2010) 4434–4440.

[111] D. Huang, B. Ou, M. Hampsch-Woodill, J. Flanagan, E. Deemer, Development and validation of oxygen radical absorbance capacity assay for lipophilic antioxidants using randomly methylated -cyclodextrin as the solubility enhancer, J. Agric. Food Chem. 50 (2002) 1815–1821.

141

[112] D. McClements, E. Decker, Lipid oxidation in oil in water emulsions: impact of molecular environment on chemical reactions in heterogeneous food systems, J. Food Sci. 65 (2000) 1270–1282.
[113] J. Alamed, Impact of Chemical and Physical Properties on the Ability of Antioxidants to Inhibit Lipid Oxidation in Foods, University of Massachusetts Amherst, 2008.
[114] M. Bruker, APEX2 and SAINT, Bruker AXS Inc, Wisconsin, USA, 2007.
[115] G. Sheldrick, A short history of SHELX, Acta Crystallogr. Sect. A 64 (2008) 112–122.

[116] L.J. Barbour, X-Seed—a software tool for supramolecular crystallography, J. Supramol. Chem. 1 (2001) 189–191.
[117] M.S. Blois, Antioxidant determination by the use of a stable free radical, Nature 181 (1958) 1199–1200.
[118] M. Daker, N. Abdullah, S. Vikineswary, P.C. Goh, U.R. Kuppusamy, Antioxidant from maize and maize fermented by marasmiellus sp. as stabiliser of lipid-rich foods, Food Chem. 107 (2008) 1092–1098.

DOCKING OUTPUT FILES

SC-558 A Docking output file (extracted from *.dlg file

An example of clustering histogram from docking result of SC-558 docked towards 1CX2 by AutoDock 4.2 software. The lowest binding energy -7.95 kcal/mol indicates the conformation that fulfilled the selection requirement and was chosen for further analysis.

```
Number of distinct conformational clusters found = 12,  out of 100 runs,
Using an rmsd-tolerance of 1.5 A


        CLUSTERING HISTOGRAM
        _____


_____ _____ _____ _____ _____ _____
     |         |     |         |     |
Clus | Lowest  | Run | Mean    | Num | Histogram
-ter | Binding |     | Binding | in  |
Rank | Energy  |     | Energy  | Clus|   5    10   15   20   25   30   35
_____|_____|_____|_____|_____|____:____|____:____|____:____|____:___
   1 |   -7.95 | 14  |   -7.80 | 11  |###########
   2 |   -6.85 | 49  |   -6.85 |  1  |#
   3 |   -6.58 | 23  |   -6.53 | 47  |################################################
   4 |   -6.32 | 27  |   -6.28 |  2  |##
   5 |   -5.91 | 89  |   -5.91 |  1  |#
   6 |   -5.64 |  1  |   -5.47 | 15  |###############
   7 |   -5.31 | 30  |   -5.28 |  6  |######
   8 |   -5.15 | 41  |   -5.12 |  2  |##
   9 |   -4.79 | 11  |   -4.79 |  1  |#
  10 |   -4.67 | 64  |   -4.58 | 10  |##########
  11 |   -4.52 | 31  |   -4.52 |  3  |###
  12 |   -4.40 | 98  |   -4.40 |  1  |#
_____|_____|_____|_____|_____|_____
```

An example of the calculation of estimated free energy of binding from docking result (towards 1CX2) for the chosen SC-558 conformation. Its atomic coordinates are surround in blue line box.

```
MODEL        14
USER    Run = 14
USER    Cluster Rank = 1
USER    Number of conformations in this cluster = 11
USER
USER    RMSD from reference structure        = 50.245 A
USER
USER    Estimated Free Energy of Binding    =   -7.95 kcal/mol  [=(1)+(2)+(3)-(4)]
USER    Estimated Inhibition Constant, Ki   =    1.50 uM (micromolar)  [Temperature = 298.15 K]
USER
USER    (1) Final Intermolecular Energy     =   -9.14 kcal/mol
USER        vdW + Hbond + desolv Energy     =   -8.94 kcal/mol
USER        Electrostatic Energy            =   -0.20 kcal/mol
USER    (2) Final Total Internal Energy     =   -0.38 kcal/mol
USER    (3) Torsional Free Energy           =   +1.19 kcal/mol
USER    (4) Unbound System's Energy  [=(2)] =   -0.38 kcal/mol
USER
USER
USER
USER    DPF = sc558.dpf
USER    NEWDPF move   sc_58_ds.pdbqt
USER    NEWDPF about  70.086899 14.536000 40.849499
USER    NEWDPF tran0  25.021724 21.793514 16.475155
USER    NEWDPF axisangle0  0.073094 -0.637846 0.766688 179.364119
USER    NEWDPF quaternion0 0.073092 -0.637836 0.766676 0.005549
USER    NEWDPF dihe0 -72.16 132.36 -0.67 162.05
```

```
USER                            x       y       z    vdW   Elec      q     RMS
ATOM     1  C1  SUB dUNIT    27.874  22.361  16.577 -0.25 +0.04   +0.044 50.245
ATOM     2  C2  SUB dUNIT    26.620  22.184  16.140 -0.18 +0.06   +0.084 50.245
ATOM     3  C3  SUB dUNIT    27.990  21.715  17.896 -0.15 +0.16   +0.174 50.245
ATOM     4  N17 SUB dUNIT    25.922  21.480  17.079 -0.12 -0.19   -0.230 50.245
ATOM     5  N18 SUB dUNIT    26.840  21.184  18.179 -0.21 -0.16   -0.161 50.245
ATOM     6  C5  SUB dUNIT    24.515  21.274  17.153 -0.22 +0.07   +0.083 50.245
ATOM     7  C6  SUB dUNIT    23.685  22.289  16.665 -0.32 +0.01   +0.020 50.245
ATOM     8  C7  SUB dUNIT    22.317  22.119  16.652 -0.30 +0.01   +0.015 50.245
ATOM     9  C8  SUB dUNIT    21.755  20.934  17.132 -0.23 +0.10   +0.107 50.245
ATOM    10  C9  SUB dUNIT    22.583  19.902  17.633 -0.25 +0.02   +0.015 50.245
ATOM    11  C10 SUB dUNIT    23.965  20.074  17.646 -0.20 +0.02   +0.020 50.245
ATOM    12  S26 SUB dUNIT    19.929  20.789  17.154 -0.33 +0.35   +0.302 50.245
ATOM    13  N19 SUB dUNIT    19.296  22.031  16.105 -0.55 -0.03   -0.043 50.245
ATOM    14  O20 SUB dUNIT    19.495  20.991  18.489 -0.86 -0.26   -0.197 50.245
ATOM    15  O21 SUB dUNIT    19.537  19.494  16.666 -0.97 -0.35   -0.197 50.245
ATOM    16  C11 SUB dUNIT    26.130  22.645  14.822 -0.28 +0.01   +0.018 50.245
ATOM    17  C12 SUB dUNIT    26.372  23.963  14.431 -0.32 +0.00   +0.002 50.245
ATOM    18  C13 SUB dUNIT    26.068  24.362  13.122 -0.42 +0.00   +0.007 50.245
ATOM    19  C14 SUB dUNIT    25.513  23.458  12.225 -0.47 +0.02   +0.035 50.245
ATOM    20  C15 SUB dUNIT    25.239  22.156  12.603 -0.50 +0.00   +0.007 50.245
ATOM    21  Br22 SUB dUNIT   25.195  23.978  10.507 -1.12 -0.03   -0.049 50.245
ATOM    22  C16 SUB dUNIT    25.550  21.737  13.915 -0.37 +0.00   +0.002 50.245
ATOM    23  C4  SUB dUNIT    29.183  21.742  18.776 -0.07 +0.40   +0.437 50.245
ATOM    24  F23 SUB dUNIT    29.964  20.695  18.530 -0.10 -0.18   -0.164 50.245
ATOM    25  F24 SUB dUNIT    28.760  21.666  20.018 -0.10 -0.15   -0.164 50.245
ATOM    26  F25 SUB dUNIT    29.864  22.868  18.577 -0.05 -0.13   -0.164 50.245
TER
ENDMDL
```

Flurbiprofen A Docking output file (extracted from *.dlg file

An example of clustering histogram from docking result of Flurbiprofen docked towards 1CX2 by AutoDock 4.2 software. The lowest binding energy -7.26 kcal/mol indicates the conformation that fulfilled the selection requirement and was chosen for further analysis.

144

```
Number of distinct conformational clusters found = 7,  out of 100 runs,
Using an rmsd-tolerance of 1.5 A


        CLUSTERING HISTOGRAM
        _____


____|_____|_____|_____|_____|_____
    |          |      |          |     |
Clus| Lowest   | Run  | Mean     | Num | Histogram
-ter| Binding  |      | Binding  | in  |
Rank| Energy   |      | Energy   | Clus|   5    10    15    20    25    30    35
____|_____|_____|_____|_____|____:____|____:____|____:____|____:____|____:
   1|    -7.26 |  73  |    -7.21 |  42 |##########################################
   2|    -6.68 |  33  |    -6.60 |   6 |######
   3|    -6.58 |  28  |    -6.58 |   3 |###
   4|    -6.52 |  21  |    -6.46 |  32 |################################
   5|    -6.26 |  61  |    -6.26 |   1 |#
   6|    -5.76 |  72  |    -5.70 |  12 |############
   7|    -5.43 |  50  |    -5.43 |   4 |####

____|_____|_____|_____|_____|_____
```

An example of the calculation of estimated free energy of binding from docking result
(towards 1CX2) for the chosen Flurbiprofen conformation. Its atomic coordinates are
surround in blue line box.

```
MODEL        73
USER    Run = 73
USER    Cluster Rank = 1
USER    Number of conformations in this cluster = 42
USER
USER    RMSD from reference structure       = 184.050 A
USER
USER    Estimated Free Energy of Binding    =   -7.26 kcal/mol  [=(1)+(2)+(3)-(4)]
USER    Estimated Inhibition Constant, Ki   =    4.74 uM (micromolar)  [Temperature = 298.15 K]
USER
USER    (1) Final Intermolecular Energy     =   -8.16 kcal/mol
USER        vdW + Hbond + desolv Energy     =   -6.12 kcal/mol
USER        Electrostatic Energy            =   -2.03 kcal/mol
USER    (2) Final Total Internal Energy     =   -0.33 kcal/mol
USER    (3) Torsional Free Energy           =   +0.89 kcal/mol
USER    (4) Unbound System's Energy  [=(2)] =   -0.33 kcal/mol
USER
USER
USER
USER    DPF = florbiprofen.dpf
USER    NEWDPF move   Ligand_cox1.pdbqt
USER    NEWDPF about  68.441299 22.862700 196.768494
USER    NEWDPF tran0  26.938807 22.316792 15.480219
USER    NEWDPF axisangle0  0.145680 -0.542210 0.827518 174.595204
USER    NEWDPF quaternion0 0.145518 -0.541607 0.826597 0.047148
USER    NEWDPF dihe0  -150.50 -15.92 4.94
USER
```

```
USER                               x       y       z     vdW   Elec      q      RMS
ATOM    1   C7       0       26.608  22.826  14.719 -0.28 +0.02   +0.028 184.050
ATOM    2   C8       0       27.978  23.090  15.004 -0.33 +0.00   +0.002 184.050
ATOM    3   C9       0       28.530  22.713  16.260 -0.35 -0.00   -0.004 184.050
ATOM    4   C10      0       27.757  22.109  17.225 -0.25 -0.01   -0.010 184.050
ATOM    5   C11      0       26.447  21.857  16.988 -0.22 +0.02   +0.026 184.050
ATOM    6   C12      0       25.857  22.204  15.765 -0.16 +0.10   +0.140 184.050
ATOM    7   F18      0       24.573  21.917  15.653 -0.03 -0.14   -0.204 184.050
ATOM    8   C3       0       26.067  23.176  13.476 -0.39 +0.00   +0.002 184.050
ATOM    9   C2       0       26.364  24.406  12.905 -0.45 +0.00   +0.000 184.050
ATOM   10   C1       0       25.867  24.743  11.616 -0.53 +0.00   +0.000 184.050
ATOM   11   C6       0       25.073  23.817  10.944 -0.59 +0.00   +0.000 184.050
ATOM   12   C5       0       24.791  22.584  11.562 -0.61 +0.00   +0.000 184.050
ATOM   13   C4       0       25.267  22.285  12.784 -0.49 +0.00   +0.000 184.050
ATOM   14   C13      0       28.273  21.720  18.613 -0.24 +0.10   +0.110 184.050
ATOM   15   C14      0       29.663  22.324  18.954 -0.30 +0.01   +0.016 184.050
ATOM   16   C15      0       28.230  20.241  18.815 -0.23 +0.28   +0.189 184.050
ATOM   17   O16      0       29.284  19.606  18.720 -0.47 -1.25   -0.647 184.050
ATOM   18   O17      0       27.139  19.719  19.179 -0.21 -1.17   -0.647 184.050
TER
ENDMDL
MODEL      33
```

3f A Docking output file (extracted from *.dlg file

An example of clustering histogram from docking result of **3f** docked towards 1CX2 by AutoDock 4.2 software. The lowest binding energy -7.64 kcal/mol indicates the conformation that fulfilled the selection requirement and was chosen for further analysis.

```
Number of distinct conformational clusters found = 23,  out of 100 runs,
Using an rmsd-tolerance of 1.5 A


         CLUSTERING HISTOGRAM
         _____

_____
Clus | Lowest  | Run | Mean    | Num | Histogram
-ter | Binding |     | Binding | in  |
Rank | Energy  |     | Energy  | Clus|   5    10   15   20   25   30   35
_____|_____|_____|_____|_____|____:____|____:____|____:____|____:___
   1 |   -7.64 | 41  |   -7.45 |   5 |#####
   2 |   -6.34 | 60  |   -6.32 |   5 |#####
   3 |   -6.16 | 92  |   -6.10 |  11 |###########
   4 |   -6.11 | 25  |   -6.07 |  13 |#############
   5 |   -5.94 | 78  |   -5.83 |   2 |##
   6 |   -5.83 | 62  |   -5.77 |   4 |####
   7 |   -5.69 | 37  |   -5.61 |   6 |######
   8 |   -5.68 |  1  |   -5.68 |   3 |###
   9 |   -5.65 | 34  |   -5.50 |   3 |###
  10 |   -5.62 | 12  |   -5.59 |   8 |########
  11 |   -5.53 | 46  |   -5.52 |   3 |###
  12 |   -5.52 | 64  |   -5.40 |  15 |###############
  13 |   -5.47 | 28  |   -5.44 |   2 |##
  14 |   -5.40 | 95  |   -5.40 |   2 |##
  15 |   -5.39 |  9  |   -5.39 |   1 |#
  16 |   -5.33 | 45  |   -5.25 |   9 |#########
  17 |   -5.23 |  5  |   -5.20 |   2 |##
  18 |   -5.22 | 19  |   -5.22 |   1 |#
  19 |   -5.14 | 81  |   -5.14 |   1 |#
  20 |   -5.08 |  4  |   -5.08 |   1 |#
  21 |   -4.94 | 97  |   -4.94 |   1 |#
  22 |   -4.65 | 15  |   -4.65 |   1 |#
  23 |   -3.79 | 73  |   -3.79 |   1 |#
_____
```

An example of the calculation of estimated free energy of binding from docking result (towards 1CX2) for the chosen **3f** conformation. Its atomic coordinates are surround in blue line box.

```
MODEL       41
USER     Run = 41
USER     Cluster Rank = 1
USER     Number of conformations in this cluster = 5
USER
USER     RMSD from reference structure       = 38.440 A
USER
USER     Estimated Free Energy of Binding    =    -7.64 kcal/mol  [=(1)+(2)+(3)-(4)]
USER     Estimated Inhibition Constant, Ki   =     2.51 uM (micromolar)  [Temperature = 298.15 K]
USER
USER     (1) Final Intermolecular Energy     =    -9.13 kcal/mol
USER         vdW + Hbond + desolv Energy     =    -9.22 kcal/mol
USER         Electrostatic Energy            =    +0.09 kcal/mol
USER     (2) Final Total Internal Energy     =    -1.14 kcal/mol
USER     (3) Torsional Free Energy           =    +1.49 kcal/mol
USER     (4) Unbound System's Energy  [=(2)] =    -1.14 kcal/mol
USER
USER
USER
USER     DPF = 27S.dpf
USER     NEWDPF move   27S.pdbqt
USER     NEWDPF about -2.420100 -0.130700 -0.506500
USER     NEWDPF tran0 26.581588 22.055612 15.399309
USER     NEWDPF axisangle0 -0.027941 -0.683022 -0.729863 100.524622
USER     NEWDPF quaternion0 -0.021486 -0.525230 -0.561250 0.639274
USER     NEWDPF dihe0 88.48 -136.32 -11.68 -13.20 -63.25
USER
```

```
USER                            x       y       z     vdW   Elec      q    RMS
ATOM     1  N1_ <1> _         24.058  21.680  15.687 -0.18 -0.14   -0.201 38.440
ATOM     2  C2_ <1> _         25.281  20.815  15.485 +0.05 +0.20   +0.292 38.440
ATOM     3  O3_ <1> _         25.767  21.264  14.209 -0.23 -0.16   -0.300 38.440
ATOM     4  C4_ <1> _         25.035  22.370  13.809 -0.33 +0.12   +0.199 38.440
ATOM     5  N5_ <1> _         24.076  22.653  14.657 -0.26 -0.09   -0.140 38.440
ATOM     6  C9_ <1> _         23.590  22.073  17.015 -0.21 +0.17   +0.238 38.440
ATOM     7  O24 <1> _         23.373  23.240  17.259 -0.20 -0.15   -0.272 38.440
ATOM     8  C25 <1> _         23.326  20.939  17.970 -0.29 +0.11   +0.119 38.440
ATOM     9  C8_ <1> _         26.348  20.919  16.546 -0.20 -0.01   -0.008 38.440
ATOM    10  C19 <1> _         26.381  19.956  17.557 -0.27 +0.01   +0.012 38.440
ATOM    11  C20 <1> _         27.334  20.029  18.563 -0.23 +0.01   +0.008 38.440
ATOM    12  C21 <1> _         28.276  21.061  18.580 -0.31 -0.06   -0.051 38.440
ATOM    13  C22 <1> _         28.259  22.001  17.547 -0.26 +0.01   +0.008 38.440
ATOM    14  C23 <1> _         27.308  21.931  16.537 -0.24 +0.01   +0.012 38.440
ATOM    15  C26 <1> _         29.335  21.126  19.663 -0.47 -0.02   -0.024 38.440
ATOM    16  C27 <1> _         28.636  20.896  21.005 -0.37 +0.02   +0.019 38.440
ATOM    17  C28 <1> _         30.028  22.490  19.678 -0.45 +0.02   +0.019 38.440
ATOM    18  C29 <1> _         30.400  20.049  19.454 -0.44 +0.02   +0.019 38.440
ATOM    19  C6_ <1> _         25.339  23.074  12.563 -0.45 +0.03   +0.052 38.440
ATOM    20  C10 <1> _         24.510  22.823  11.460 -0.61 +0.01   +0.019 38.440
ATOM    21  C11 <1> _         24.725  23.461  10.246 -0.57 +0.00   +0.001 38.440
ATOM    22  C12 <1> _         25.775  24.363  10.103 -0.53 +0.00   +0.003 38.440
ATOM    23  C13 <1> _         26.612  24.630  11.177 -0.41 +0.02   +0.038 38.440
ATOM    24  C14 <1> _         26.398  23.990  12.407 -0.38 +0.06   +0.093 38.440
ATOM    25  O15 <1> _         27.350  24.209  13.395 -0.27 -0.17   -0.278 38.440
ATOM    26  C16 <1> _         27.277  25.368  14.132 -0.25 +0.16   +0.260 38.440
ATOM    27  O17 <1> _         27.784  26.257  13.485 -0.52 -0.18   -0.265 38.440
ATOM    28  C18 <1> _         26.689  25.439  15.508 -0.35 +0.08   +0.126 38.440
TER
ENDMDL
```

3c A Docking output file (extracted from *.dlg file

An example of clustering histogram from docking result of **3c** docked towards 1CX2 by AutoDock 4.2 software. The lowest binding energy -6.89 kcal/mol indicates the conformation that fulfilled the selection requirement and was chosen for further analysis.

```
Number of distinct conformational clusters found = 30,  out of 100 runs,
Using an rmsd-tolerance of 1.5 A


        CLUSTERING HISTOGRAM
        _____

    |        |     |        |    |
Clus | Lowest | Run | Mean   | Num| Histogram
-ter | Binding|     | Binding| in |
Rank | Energy |     | Energy | Clus|   5    10   15   20   25   30   35
____|_____|_____|_____|____|____:____|____:____|____:____|____:___
  1 |  -6.89 | 78 |  -6.77 | 15 |###############
  2 |  -6.00 | 45 |  -5.90 | 23 |#######################
  3 |  -5.96 | 30 |  -5.96 |  1 |#
  4 |  -5.84 | 26 |  -5.59 |  2 |##
  5 |  -5.66 | 20 |  -5.66 |  1 |#
  6 |  -5.11 | 97 |  -5.10 |  3 |###
  7 |  -5.10 | 85 |  -5.02 | 15 |###############
  8 |  -5.06 | 25 |  -4.94 |  5 |#####
  9 |  -4.68 | 93 |  -4.50 |  2 |##
 10 |  -4.65 | 43 |  -4.53 |  2 |##
 11 |  -4.63 | 22 |  -4.63 |  1 |#
 12 |  -4.60 | 55 |  -4.60 |  1 |#
 13 |  -4.54 |  9 |  -4.54 |  1 |#
 14 |  -4.54 | 58 |  -4.54 |  1 |#
 15 |  -4.53 | 74 |  -4.48 |  2 |##
 16 |  -4.48 | 70 |  -4.46 |  2 |##
 17 |  -4.41 | 21 |  -4.41 |  1 |#
 18 |  -4.36 |  5 |  -4.33 |  3 |###
 19 |  -4.33 | 48 |  -4.33 |  2 |##
 20 |  -4.32 | 71 |  -4.32 |  1 |#
 21 |  -4.29 | 37 |  -4.29 |  1 |#
 22 |  -4.28 |  1 |  -4.28 |  1 |#
 23 |  -4.26 |  6 |  -4.18 |  2 |##
 24 |  -4.25 | 56 |  -4.25 |  1 |#
 25 |  -4.15 | 52 |  -4.15 |  1 |#
 26 |  -4.14 | 92 |  -4.14 |  1 |#
 27 |  -4.10 | 69 |  -4.10 |  1 |#
 28 |  -4.05 | 95 |  -3.98 |  5 |#####
 29 |  -4.02 | 67 |  -3.99 |  2 |##
 30 |  -3.72 | 51 |  -3.72 |  1 |#
    |        |     |        |    |
```

An example of the calculation of estimated free energy of binding from docking result (towards 1CX2) for the chosen **3c** conformation. Its atomic coordinates are surround in blue line box.

```
MODEL        78
USER     Run = 78
USER     Cluster Rank = 1
USER     Number of conformations in this cluster = 15
USER
USER     RMSD from reference structure       = 37.570 A
USER
USER     Estimated Free Energy of Binding    =   -6.89 kcal/mol  [=(1)+(2)+(3)-(4)]
USER     Estimated Inhibition Constant, Ki   =    8.86 uM (micromolar)  [Temperature = 298.15 K]
USER
USER     (1) Final Intermolecular Energy     =   -8.68 kcal/mol
USER         vdW + Hbond + desolv Energy     =   -8.77 kcal/mol
USER         Electrostatic Energy            =   +0.09 kcal/mol
USER     (2) Final Total Internal Energy     =   -0.86 kcal/mol
USER     (3) Torsional Free Energy           =   +1.79 kcal/mol
USER     (4) Unbound System's Energy  [=(2)] =   -0.86 kcal/mol
USER
USER
USER
USER     DPF = 8bs.dpf
USER     NEWDPF move   8bs.pdbqt
USER     NEWDPF about  -1.407200 0.034100 0.435700
USER     NEWDPF tran0  26.416801 21.897656 15.464633
USER     NEWDPF axisangle0  -0.066325 -0.709095 -0.701987 102.806533
USER     NEWDPF quaternion0 -0.051837 -0.554197 -0.548642 0.623835
USER     NEWDPF dihe0  97.70 107.24 149.07 32.51 -91.87 111.43
USER
```

USER				x	y	z	vdW	Elec	q	RMS
ATOM	1	N1_ <1>	_	24.250	22.020	16.100	-0.19	-0.14	-0.201	37.570
ATOM	2	C2_ <1>	_	25.382	21.056	15.844	-0.02	+0.21	+0.292	37.570
ATOM	3	O3_ <1>	_	25.799	21.402	14.513	-0.23	-0.18	-0.300	37.570
ATOM	4	C4_ <1>	_	24.995	22.424	14.040	-0.25	+0.12	+0.199	37.570
ATOM	5	N5_ <1>	_	24.073	22.769	14.906	-0.20	-0.09	-0.140	37.570
ATOM	6	C9_ <1>	_	23.087	21.609	16.870	-0.20	+0.18	+0.238	37.570
ATOM	7	O24 <1>	_	22.012	22.120	16.639	-0.31	-0.14	-0.272	37.570
ATOM	8	C25 <1>	_	23.331	20.614	17.976	-0.29	+0.11	+0.119	37.570
ATOM	9	C8_ <1>	_	26.539	21.196	16.803	-0.23	-0.01	-0.007	37.570
ATOM	10	C19 <1>	_	27.619	21.996	16.416	-0.24	+0.01	+0.014	37.570
ATOM	11	C20 <1>	_	28.709	22.169	17.257	-0.29	+0.03	+0.038	37.570
ATOM	12	C21 <1>	_	28.710	21.527	18.504	-0.28	+0.08	+0.078	37.570
ATOM	13	C22 <1>	_	27.637	20.734	18.909	-0.32	+0.05	+0.038	37.570
ATOM	14	C23 <1>	_	26.551	20.578	18.051	-0.29	+0.02	+0.014	37.570
ATOM	15	O26 <1>	_	29.848	21.799	19.256	-0.28	-0.23	-0.255	37.570
ATOM	16	C27 <1>	_	30.493	20.786	19.950	-0.06	+0.51	+0.530	37.570
ATOM	17	F28 <1>	_	29.750	20.661	21.053	-0.16	-0.14	-0.144	37.570
ATOM	18	F29 <1>	_	30.495	19.619	19.295	-0.18	-0.18	-0.144	37.570
ATOM	19	F30 <1>	_	31.751	21.088	20.298	-0.18	-0.12	-0.144	37.570
ATOM	20	C6_ <1>	_	25.231	22.995	12.714	-0.44	+0.03	+0.052	37.570
ATOM	21	C10 <1>	_	24.310	22.702	11.697	-0.60	+0.01	+0.019	37.570
ATOM	22	C11 <1>	_	24.472	23.226	10.421	-0.62	+0.00	+0.001	37.570
ATOM	23	C12 <1>	_	25.543	24.065	10.133	-0.56	+0.00	+0.003	37.570
ATOM	24	C13 <1>	_	26.471	24.368	11.120	-0.50	+0.02	+0.038	37.570
ATOM	25	C14 <1>	_	26.325	23.824	12.403	-0.37	+0.06	+0.093	37.570
ATOM	26	O15 <1>	_	27.217	24.220	13.393	-0.26	-0.17	-0.278	37.570
ATOM	27	C16 <1>	_	27.133	25.506	13.872	-0.27	+0.16	+0.260	37.570
ATOM	28	O17 <1>	_	27.780	26.222	13.139	-0.57	-0.20	-0.265	37.570
ATOM	29	C18 <1>	_	26.349	25.888	15.090	-0.38	+0.08	+0.126	37.570
TER										
ENDMDL										

3b A Docking output file (extracted from *.dlg file

An example of clustering histogram from docking result of **3b** docked towards 1CX2 by AutoDock 4.2 software. The lowest binding energy -7.43 kcal/mol indicates the conformation that fulfilled the selection requirement and was chosen for further analysis.

```
Number of distinct conformational clusters found = 22,  out of 100 runs,
Using an rmsd-tolerance of 1.5 A


          CLUSTERING HISTOGRAM
          _____


_____|_____|_____|_____|_____|_____
Clus  | Lowest    | Run | Mean      | Num | Histogram
-ter  | Binding   |     | Binding   | in  |
Rank  | Energy    |     | Energy    | Clus|    5    10   15   20   25   30   35
_____|_____|_____|_____|_____|____:____|____:____|____:____|____:___
   1  |     -7.43 | 48  |     -7.14 | 19  |###################
   2  |     -7.05 | 91  |     -6.84 |  4  |####
   3  |     -7.03 | 17  |     -7.03 |  1  |#
   4  |     -6.71 | 20  |     -6.71 |  1  |#
   5  |     -6.65 | 23  |     -6.65 |  1  |#
   6  |     -6.29 | 43  |     -6.20 | 20  |####################
   7  |     -5.94 | 83  |     -5.94 |  1  |#
   8  |     -5.79 | 85  |     -5.79 |  1  |#
   9  |     -5.62 | 58  |     -5.62 |  1  |#
  10  |     -5.61 | 93  |     -5.39 |  4  |####
  11  |     -5.61 | 14  |     -5.43 |  8  |########
  12  |     -5.59 | 28  |     -5.47 | 13  |#############
  13  |     -5.59 | 32  |     -5.42 |  2  |##
  14  |     -5.52 | 82  |     -5.52 |  1  |#
  15  |     -5.41 | 18  |     -5.31 |  3  |###
  16  |     -5.39 |  9  |     -5.34 |  9  |#########
  17  |     -5.36 | 64  |     -5.36 |  2  |##
  18  |     -5.28 | 66  |     -5.28 |  1  |#
  19  |     -5.24 | 78  |     -5.18 |  4  |####
  20  |     -5.04 | 44  |     -5.04 |  1  |#
  21  |     -4.86 | 55  |     -4.86 |  1  |#
  22  |     -4.72 | 63  |     -4.72 |  2  |##
_____|_____|_____|_____|_____|_____
```

An example of the calculation of estimated free energy of binding from docking result (towards 1CX2) for the chosen **3b** conformation. Its atomic coordinates are surround in blue line box.

```
MODEL        17
USER    Run = 17
USER    Cluster Rank = 3
USER    Number of conformations in this cluster = 1
USER
USER    RMSD from reference structure      = 36.091 A
USER
USER    Estimated Free Energy of Binding    =    -7.03 kcal/mol  [=(1)+(2)+(3)-(4)]
USER    Estimated Inhibition Constant, Ki   =     6.98 uM (micromolar)  [Temperature = 298.15 K]
USER
USER    (1) Final Intermolecular Energy     =    -8.53 kcal/mol
USER        vdW + Hbond + desolv Energy     =    -8.42 kcal/mol
USER        Electrostatic Energy            =    -0.10 kcal/mol
USER    (2) Final Total Internal Energy     =    -1.05 kcal/mol
USER    (3) Torsional Free Energy           =    +1.49 kcal/mol
USER    (4) Unbound System's Energy  [=(2)] =    -1.05 kcal/mol
USER
USER
USER
USER    DPF = ome.dpf
USER    NEWDPF move   p-ome.pdbqt
USER    NEWDPF about -2.032900 -0.106500 -0.055500
USER    NEWDPF tran0 26.219124 21.859561 16.360172
USER    NEWDPF axisangle0 -0.731306 0.254828 -0.632657 140.068526
USER    NEWDPF quaternion0 -0.687352 0.239512 -0.594632 0.341458
USER    NEWDPF dihe0 -14.86 26.63 168.06 -164.57 8.92
USER
USER                                    x       y       z     vdW   Elec       q      RMS
ATOM     1  O1_ <1> _              25.292  23.252  15.991 -0.15 -0.20    -0.300 36.091
ATOM     2  C2_ <1> _              24.925  22.781  17.300 -0.19 +0.21    +0.292 36.091
ATOM     3  N3_ <1> _              23.716  21.939  16.994 -0.23 -0.15    -0.201 36.091
ATOM     4  N4_ <1> _              23.647  21.800  15.581 -0.25 -0.10    -0.140 36.091
ATOM     5  C5_ <1> _              24.539  22.594  15.037 -0.20 +0.13    +0.199 36.091
ATOM     6  C8_ <1> _              23.165  20.919  17.846 -0.20 +0.22    +0.238 36.091
ATOM     7  C9_ <1> _              22.222  19.908  17.257 -0.03 +0.15    +0.119 36.091
ATOM     8  O10 <1> _              23.451  20.992  19.028 -0.06 -0.27    -0.272 36.091
ATOM     9  C7_ <1> _              26.081  22.071  17.964 -0.27 -0.01    -0.008 36.091
ATOM    10  C21 <1> _              26.963  21.346  17.161 -0.24 +0.01    +0.013 36.091
ATOM    11  C22 <1> _              28.044  20.686  17.731 -0.31 +0.03    +0.024 36.091
ATOM    12  C23 <1> _              28.266  20.731  19.109 -0.33 +0.07    +0.058 36.091
ATOM    13  C24 <1> _              27.371  21.447  19.906 -0.32 +0.02    +0.024 36.091
ATOM    14  C25 <1> _              26.287  22.111  19.343 -0.12 +0.01    +0.013 36.091
ATOM    15  S26 <1> _              29.664  19.880  19.829 -0.49 +0.23    +0.171 36.091
ATOM    16  O27 <1> _              30.397  19.161  18.780 -0.66 -0.33    -0.223 36.091
ATOM    17  O28 <1> _              29.229  19.119  21.005 -0.18 -0.31    -0.223 36.091
ATOM    18  C29 <1> _              30.631  21.293  20.361 -0.40 +0.15    +0.167 36.091
ATOM    19  C11 <1> _              24.751  22.842  13.611 -0.40 +0.03    +0.052 36.091
ATOM    20  C12 <1> _              26.000  23.159  13.044 -0.34 +0.06    +0.093 36.091
ATOM    21  C13 <1> _              26.131  23.367  11.666 -0.35 +0.03    +0.038 36.091
ATOM    22  C14 <1> _              25.014  23.272  10.846 -0.61 +0.00    +0.003 36.091
ATOM    23  C15 <1> _              23.772  22.966  11.394 -0.60 +0.00    +0.001 36.091
ATOM    24  C16 <1> _              23.641  22.752  12.760 -0.42 +0.01    +0.019 36.091
ATOM    25  O17 <1> _              27.112  23.403  13.845 -0.25 -0.18    -0.278 36.091
ATOM    26  C18 <1> _              27.386  24.696  14.231 -0.23 +0.16    +0.260 36.091
ATOM    27  C19 <1> _              28.354  24.752  15.377 -0.30 +0.08    +0.126 36.091
ATOM    28  O20 <1> _              26.865  25.615  13.638 -0.31 -0.17    -0.265 36.091
TER
ENDMDL
```

3a A Docking out put file (extracted from *.dlg file

An example of clustering histogram from docking result of **3a** docked towards 1CX2 by AutoDock 4.2 software. The lowest binding energy -6.50 kcal/mol indicates the conformation that fulfilled the selection requirement and was chosen for further analysis.

```
Number of distinct conformational clusters found = 22,  out of 100 runs,
Using an rmsd-tolerance of 1.5 A


        CLUSTERING HISTOGRAM
        _____


____ | _____ | ____ | _____ | _____ | _____
     |           |      |           |       |
Clus | Lowest    | Run  | Mean      | Num   | Histogram
-ter | Binding   |      | Binding   | in    |
Rank | Energy    |      | Energy    | Clus  |    5    10   15   20   25   30   35
____ | _____ | ____ | _____ | _____ | ___:____|____:____|____:____|____:___
   1 |     -6.50 | 29   |     -6.43 |    5  |#####
   2 |     -6.12 | 41   |     -6.10 |   13  |#############
   3 |     -6.08 | 59   |     -6.03 |    2  |##
   4 |     -6.07 | 66   |     -5.99 |   12  |############
   5 |     -5.99 | 76   |     -5.88 |   18  |##################
   6 |     -5.95 | 81   |     -5.95 |    1  |#
   7 |     -5.89 |  2   |     -5.88 |    4  |####
   8 |     -5.83 | 35   |     -5.81 |    5  |#####
   9 |     -5.79 |  7   |     -5.79 |    1  |#
  10 |     -5.71 | 49   |     -5.68 |    7  |#######
  11 |     -5.48 | 87   |     -5.40 |    8  |########
  12 |     -5.41 |  4   |     -5.36 |    9  |#########
  13 |     -5.24 |  5   |     -5.24 |    1  |#
  14 |     -5.21 | 20   |     -5.15 |    4  |####
  15 |     -5.04 | 34   |     -5.04 |    1  |#
  16 |     -4.86 |  1   |     -4.86 |    1  |#
  17 |     -4.86 | 56   |     -4.85 |    2  |##
  18 |     -4.81 | 30   |     -4.81 |    1  |#
  19 |     -4.81 | 95   |     -4.81 |    1  |#
  20 |     -4.75 | 92   |     -4.75 |    1  |#
  21 |     -4.71 | 65   |     -4.71 |    1  |#
  22 |     -4.70 | 54   |     -4.70 |    2  |##
____ | _____ | ____ | _____ | _____ | _____
```

An example of the calculation of estimated free energy of binding from docking result (towards 1CX2) for the chosen **3a** conformation. Its atomic coordinates are surround in blue line box.

```
MODEL        29
USER     Run = 29
USER     Cluster Rank = 1
USER     Number of conformations in this cluster = 5
USER
USER     RMSD from reference structure      = 37.045 A
USER
USER     Estimated Free Energy of Binding    =   -6.50 kcal/mol  [=(1)+(2)+(3)-(4)]
USER     Estimated Inhibition Constant, Ki   =   17.07 uM (micromolar)  [Temperature = 298.15 K]
USER
USER     (1) Final Intermolecular Energy     =   -7.70 kcal/mol
USER         vdW + Hbond + desolv Energy     =   -7.52 kcal/mol
USER         Electrostatic Energy            =   -0.18 kcal/mol
USER     (2) Final Total Internal Energy     =   -1.07 kcal/mol
USER     (3) Torsional Free Energy           =   +1.19 kcal/mol
USER     (4) Unbound System's Energy  [=(2)] =   -1.07 kcal/mol
USER
USER
USER
USER     DPF = cl.dpf
USER     NEWDPF move   P_CL_R.pdbqt
USER     NEWDPF about -2.622800 -0.038700 0.039400
USER     NEWDPF tran0 26.511799 22.148137 15.988581
USER     NEWDPF axisangle0 -0.722699 0.068834 -0.687726 -174.263741
USER     NEWDPF quaternion0 -0.721794 0.068748 -0.686865 -0.050037
USER     NEWDPF dihe0 -154.96 67.65 -1.45 60.42
USER
```

USER			x	y	z	vdW	Elec	q	RMS
ATOM	1	O1_ <1> _	25.573	22.289	16.256	-0.13	-0.22	-0.300	37.045
ATOM	2	C2_ <1> _	25.689	21.254	17.249	-0.11	+0.25	+0.292	37.045
ATOM	3	N3_ <1> _	25.471	20.018	16.422	-0.13	-0.17	-0.201	37.045
ATOM	4	N4_ <1> _	25.535	20.407	15.057	-0.07	-0.08	-0.140	37.045
ATOM	5	C5_ <1> _	25.561	21.720	14.997	-0.22	+0.13	+0.199	37.045
ATOM	6	C8_ <1> _	25.815	18.676	16.807	-0.13	+0.24	+0.238	37.045
ATOM	7	C9_ <1> _	25.935	17.618	15.747	-0.16	+0.06	+0.119	37.045
ATOM	8	O10 <1> _	25.909	18.469	18.004	-0.06	-0.43	-0.272	37.045
ATOM	9	C11 <1> _	25.555	22.549	13.792	-0.36	+0.03	+0.052	37.045
ATOM	10	C12 <1> _	26.641	23.349	13.373	-0.30	+0.06	+0.093	37.045
ATOM	11	C13 <1> _	26.551	24.120	12.209	-0.45	+0.02	+0.038	37.045
ATOM	12	C14 <1> _	25.390	24.094	11.450	-0.54	+0.00	+0.003	37.045
ATOM	13	C15 <1> _	24.314	23.308	11.846	-0.61	+0.00	+0.001	37.045
ATOM	14	C16 <1> _	24.395	22.545	13.005	-0.50	+0.01	+0.019	37.045
ATOM	15	O17 <1> _	27.766	23.292	14.175	-0.28	-0.18	-0.278	37.045
ATOM	16	C18 <1> _	28.156	24.315	15.006	-0.22	+0.17	+0.260	37.045
ATOM	17	C19 <1> _	26.994	25.211	15.334	-0.34	+0.08	+0.126	37.045
ATOM	18	O20 <1> _	29.302	24.419	15.389	-0.32	-0.18	-0.265	37.045
ATOM	19	C7_ <1> _	27.007	21.349	17.978	-0.28	-0.01	-0.008	37.045
ATOM	20	C21 <1> _	26.999	21.296	19.374	-0.33	+0.01	+0.013	37.045
ATOM	21	C22 <1> _	28.189	21.381	20.087	-0.36	+0.02	+0.024	37.045
ATOM	22	C23 <1> _	29.389	21.527	19.398	-0.37	+0.03	+0.034	37.045
ATOM	23	C24 <1> _	29.411	21.587	18.006	-0.29	+0.02	+0.024	37.045
ATOM	24	Cl26 <1> _	30.835	21.634	20.256	-0.66	-0.07	-0.084	37.045
ATOM	25	C25 <1> _	28.218	21.498	17.300	-0.31	+0.01	+0.013	37.045
TER									
ENDMDL									

3d A Docking out put file (extracted from *.dlg file

An example of clustering histogram from docking result of **3d** docked towards 1CX2 by AutoDock 4.2 software. The lowest binding energy -7.38 kcal/mol indicates the conformation that fulfilled the selection requirement and was chosen for further analysis.

```
Number of distinct conformational clusters found = 31,   out of 100 runs,
Using an rmsd-tolerance of 1.5 A


         CLUSTERING HISTOGRAM
         _____


 _____|_____|_____|_____|_____|_____
 Clus | Lowest   | Run | Mean     | Num | Histogram
 -ter | Binding  |     | Binding  | in  |
 Rank | Energy   |     | Energy   | Clus|   5    10   15   20   25   30   35
 _____|_____|_____|_____|_____|____:____|____:____|____:____|____:___
    1 |   -7.38  | 53  |   -7.24  |  13 |#############
    2 |   -6.77  | 34  |   -6.72  |   3 |###
    3 |   -6.44  | 29  |   -6.37  |   3 |###
    4 |   -6.42  | 62  |   -6.34  |  23 |#######################
    5 |   -6.40  | 18  |   -6.40  |   1 |#
    6 |   -6.36  | 25  |   -6.36  |   1 |#
    7 |   -6.36  | 72  |   -6.08  |   2 |##
    8 |   -6.23  | 97  |   -6.23  |   1 |#
    9 |   -6.04  | 76  |   -6.00  |   2 |##
   10 |   -5.73  | 80  |   -5.73  |   1 |#
   11 |   -5.62  | 15  |   -5.56  |   2 |##
   12 |   -5.59  | 83  |   -5.59  |   1 |#
   13 |   -5.51  | 88  |   -5.48  |  11 |###########
   14 |   -5.41  | 65  |   -5.41  |   1 |#
   15 |   -5.31  |  8  |   -5.28  |   8 |########
   16 |   -5.21  | 44  |   -5.21  |   1 |#
   17 |   -5.21  | 84  |   -5.21  |   1 |#
   18 |   -5.19  | 27  |   -5.19  |   1 |#
   19 |   -5.11  | 51  |   -5.11  |   1 |#
   20 |   -4.97  | 11  |   -4.97  |   1 |#
   21 |   -4.95  | 54  |   -4.93  |   2 |##
   22 |   -4.92  | 82  |   -4.92  |   1 |#
   23 |   -4.92  | 17  |   -4.76  |   4 |####
   24 |   -4.91  | 81  |   -4.87  |   2 |##
   25 |   -4.87  |100  |   -4.87  |   1 |#
   26 |   -4.80  | 20  |   -4.80  |   1 |#
   27 |   -4.79  |  4  |   -4.77  |   2 |##
   28 |   -4.70  | 67  |   -4.68  |   5 |#####
   29 |   -4.62  | 85  |   -4.62  |   2 |##
   30 |   -4.62  |  1  |   -4.62  |   1 |#
   31 |   -4.51  | 14  |   -4.51  |   1 |#
 _____|_____|_____|_____|_____|_____
```

An example of the calculation of estimated free energy of binding from docking result (towards 1CX2) for the chosen **3d** conformation. Its atomic coordinates are surround in blue line box.

```
MODEL        53
USER     Run = 53
USER     Cluster Rank = 1
USER     Number of conformations in this cluster = 13
USER
USER     RMSD from reference structure        = 38.883 A
USER
USER     Estimated Free Energy of Binding    =   -7.38 kcal/mol  [=(1)+(2)+(3)-(4)]
USER     Estimated Inhibition Constant, Ki   =    3.87 uM (micromolar)  [Temperature = 298.15 K]
USER
USER     (1) Final Intermolecular Energy     =   -8.88 kcal/mol
USER         vdW + Hbond + desolv Energy     =   -8.94 kcal/mol
USER         Electrostatic Energy            =   +0.07 kcal/mol
USER     (2) Final Total Internal Energy     =   -0.87 kcal/mol
USER     (3) Torsional Free Energy           =   +1.49 kcal/mol
USER     (4) Unbound System's Energy  [=(2)] =   -0.87 kcal/mol
USER
USER
USER
USER     DPF = 17.dpf
USER     NEWDPF move   17.pdbqt
USER     NEWDPF about -3.484100 -0.144800 -0.130000
USER     NEWDPF tran0 25.964142 21.773831 14.899447
USER     NEWDPF axisangle0 -0.103128 -0.744340 -0.659790 102.952082
USER     NEWDPF quaternion0 -0.080682 -0.582333 -0.516185 0.622842
USER     NEWDPF dihe0 45.51 96.23 146.27 -52.33 -108.21
USER
```

```
USER                              x       y       z    vdW   Elec      q     RMS
ATOM     1  N1_ <1> _        24.435  22.022  16.186 -0.19 -0.14   -0.201 38.883
ATOM     2  C2_ <1> _        25.529  21.028  15.873 -0.03 +0.22   +0.292 38.883
ATOM     3  O3_ <1> _        25.905  21.385  14.530 -0.23 -0.18   -0.300 38.883
ATOM     4  C4_ <1> _        25.081  22.403  14.090 -0.24 +0.12   +0.199 38.883
ATOM     5  N5_ <1> _        24.210  22.770  14.998 -0.21 -0.09   -0.140 38.883
ATOM     6  C9_ <1> _        23.301  21.662  17.017 -0.20 +0.18   +0.238 38.883
ATOM     7  O24 <1> _        22.248  22.248  16.866 -0.27 -0.13   -0.272 38.883
ATOM     8  C25 <1> _        23.538  20.624  18.083 -0.28 +0.11   +0.119 38.883
ATOM     9  C6_ <1> _        25.244  22.962  12.746 -0.44 +0.03   +0.052 38.883
ATOM    10  C10 <1> _        24.310  21.766  11.766 -0.59 +0.01   +0.019 38.883
ATOM    11  C11 <1> _        24.415  23.103  10.473 -0.63 +0.00   +0.001 38.883
ATOM    12  C12 <1> _        25.446  23.972  10.134 -0.55 +0.00   +0.003 38.883
ATOM    13  C13 <1> _        26.389  24.337  11.088 -0.50 +0.02   +0.038 38.883
ATOM    14  C14 <1> _        26.297  23.823  12.388 -0.37 +0.06   +0.093 38.883
ATOM    15  O15 <1> _        27.206  24.264  13.344 -0.26 -0.17   -0.278 38.883
ATOM    16  C16 <1> _        27.134  25.578  13.747 -0.28 +0.16   +0.260 38.883
ATOM    17  O17 <1> _        27.785  26.243  12.971 -0.59 -0.22   -0.265 38.883
ATOM    18  C18 <1> _        26.359  26.036  14.943 -0.41 +0.08   +0.126 38.883
ATOM    19  C8_ <1> _        26.725  21.122  16.788 -0.21 -0.01   -0.008 38.883
ATOM    20  C19 <1> _        26.832  20.198  17.832 -0.28 +0.02   +0.013 38.883
ATOM    21  C20 <1> _        27.910  20.246  18.705 -0.30 +0.03   +0.019 38.883
ATOM    22  C21 <1> _        28.904  21.218  18.547 -0.36 -0.00   -0.000 38.883
ATOM    23  C22 <1> _        28.806  22.122  17.490 -0.29 +0.02   +0.019 38.883
ATOM    24  C23 <1> _        27.727  22.077  16.615 -0.26 +0.01   +0.013 38.883
ATOM    25  S26 <1> _        30.220  21.194  19.714 -0.53 -0.13   -0.134 38.883
ATOM    26  C27 <1> _        30.406  22.909  20.242 -0.45 +0.07   +0.095 38.883
TER
ENDMDL
```

3h A Docking out put file (extracted from *.dlg file

An example of clustering histogram from docking result of **3h** docked towards 1CX2 by AutoDock 4.2 software. The lowest binding energy -7.46 kcal/mol indicates the conformation that fulfilled the selection requirement and was chosen for further analysis.

```
Number of distinct conformational clusters found = 34,  out of 100 runs,
Using an rmsd-tolerance of 1.5 A

        CLUSTERING HISTOGRAM
        _____


_____
     |           |     |           |     |
Clus | Lowest    | Run | Mean      | Num | Histogram
-ter | Binding   |     | Binding   | in  |
Rank | Energy    |     | Energy    | Clus|    5    10   15   20   25   30   35
_____|_____|_____|_____|_____|____:____|____:____|____:____|____:___
   1 |    -7.46  | 98  |    -7.12  | 13  |#############
   2 |    -6.95  | 37  |    -6.65  |  7  |#######
   3 |    -6.95  | 57  |    -6.94  |  2  |##
   4 |    -6.95  | 47  |    -6.95  |  1  |#
   5 |    -6.79  |  5  |    -6.48  |  4  |####
   6 |    -6.39  | 36  |    -6.39  |  1  |#
   7 |    -6.38  | 11  |    -6.31  |  2  |##
   8 |    -6.16  |  2  |    -6.04  |  3  |###
   9 |    -6.09  | 18  |    -6.09  |  1  |#
  10 |    -5.77  | 29  |    -5.68  |  2  |##
  11 |    -5.64  | 40  |    -5.64  |  1  |#
  12 |    -5.63  | 79  |    -5.62  |  2  |##
  13 |    -5.63  | 75  |    -5.63  |  1  |#
  14 |    -5.55  | 17  |    -5.25  | 17  |#################
  15 |    -5.48  | 25  |    -5.48  |  1  |#
  16 |    -5.41  | 77  |    -5.26  |  6  |######
  17 |    -5.26  | 88  |    -5.26  |  2  |##
  18 |    -5.26  | 50  |    -4.97  |  3  |###
  19 |    -5.21  |  6  |    -5.08  |  3  |###
  20 |    -5.20  | 82  |    -5.08  |  7  |#######
  21 |    -5.01  | 43  |    -5.01  |  1  |#
  22 |    -4.97  | 21  |    -4.74  |  4  |####
  23 |    -4.95  | 42  |    -4.95  |  1  |#
  24 |    -4.94  | 91  |    -4.93  |  3  |###
  25 |    -4.87  | 22  |    -4.87  |  1  |#
  26 |    -4.87  | 20  |    -4.87  |  1  |#
  27 |    -4.78  | 60  |    -4.78  |  1  |#
  28 |    -4.74  | 34  |    -4.63  |  3  |###
  29 |    -4.68  | 10  |    -4.68  |  1  |#
  30 |    -4.54  | 13  |    -4.54  |  1  |#
  31 |    -4.52  | 51  |    -4.52  |  1  |#
  32 |    -4.51  | 12  |    -4.51  |  1  |#
  33 |    -4.50  | 78  |    -4.50  |  1  |#
  34 |    -4.47  | 48  |    -4.47  |  1  |#
_____|_____|_____|_____|_____|_____
```

An example of the calculation of estimated free energy of binding from docking result (towards 1CX2) for the chosen **3h** conformation. Its atomic coordinates are surround in blue line box.

```
MODEL        98
USER     Run = 98
USER     Cluster Rank = 1
USER     Number of conformations in this cluster = 13
USER
USER     RMSD from reference structure        = 37.696 A
USER
USER     Estimated Free Energy of Binding     =   -7.46 kcal/mol  [=(1)+(2)+(3)-(4)]
USER     Estimated Inhibition Constant, Ki    =    3.41 uM (micromolar)  [Temperature = 298.15 K]
USER
USER     (1) Final Intermolecular Energy      =   -9.25 kcal/mol
USER         vdW + Hbond + desolv Energy      =   -9.24 kcal/mol
USER         Electrostatic Energy             =   -0.01 kcal/mol
USER     (2) Final Total Internal Energy      =   -0.90 kcal/mol
USER     (3) Torsional Free Energy            =   +1.79 kcal/mol
USER     (4) Unbound System's Energy  [=(2)] =   -0.90 kcal/mol
USER
USER
USER
USER     DPF = 2.dpf
USER     NEWDPF move   2_S.pdbqt
USER     NEWDPF about -2.190900 -0.125600 0.157900
USER     NEWDPF tran0 25.735634 21.711626 15.274061
USER     NEWDPF axisangle0 0.047895 0.715976 0.696480 -97.315208
USER     NEWDPF quaternion0 0.035958 0.537537 0.522900 -0.660557
USER     NEWDPF dihe0 159.27 100.43 15.86 150.87 91.66 -96.99
USER
```

USER				x	y	z	vdW	Elec	q	RMS
ATOM	1	N1_	<1> _	23.741	22.099	15.886	-0.23	-0.14	-0.201	37.696
ATOM	2	C2_	<1> _	24.855	21.097	15.729	+0.08	+0.21	+0.292	37.696
ATOM	3	O3_	<1> _	25.411	21.436	14.446	-0.26	-0.18	-0.300	37.696
ATOM	4	C4_	<1> _	24.697	22.492	13.912	-0.26	+0.12	+0.199	37.696
ATOM	5	N5_	<1> _	23.708	22.866	14.688	-0.15	-0.09	-0.140	37.696
ATOM	6	C9_	<1> _	22.488	21.713	16.518	-0.19	+0.16	+0.238	37.696
ATOM	7	O24	<1> _	21.452	22.228	16.154	-0.31	-0.13	-0.272	37.696
ATOM	8	C25	<1> _	22.591	20.737	17.662	-0.32	+0.12	+0.119	37.696
ATOM	9	C8_	<1> _	25.933	21.174	16.784	-0.23	-0.01	-0.007	37.696
ATOM	10	C19	<1> _	27.123	21.819	16.432	-0.22	+0.01	+0.014	37.696
ATOM	11	C20	<1> _	28.154	21.949	17.353	-0.26	+0.03	+0.038	37.696
ATOM	12	C21	<1> _	27.987	21.421	18.637	-0.26	+0.08	+0.079	37.696
ATOM	13	C22	<1> _	26.802	20.775	19.001	-0.28	+0.04	+0.038	37.696
ATOM	14	C23	<1> _	25.776	20.658	18.069	-0.27	+0.01	+0.014	37.696
ATOM	15	O26	<1> _	28.973	21.667	19.588	-0.24	-0.26	-0.279	37.696
ATOM	16	C27	<1> _	30.049	20.813	19.644	-0.30	+0.27	+0.260	37.696
ATOM	17	O28	<1> _	29.723	19.766	19.130	-0.76	-0.40	-0.265	37.696
ATOM	18	C29	<1> _	31.365	21.182	20.257	-0.34	+0.11	+0.126	37.696
ATOM	19	C6_	<1> _	25.085	23.074	12.626	-0.46	+0.03	+0.052	37.696
ATOM	20	C10	<1> _	24.217	22.901	11.539	-0.62	+0.01	+0.019	37.696
ATOM	21	C11	<1> _	24.525	23.432	10.294	-0.59	+0.00	+0.001	37.696
ATOM	22	C12	<1> _	25.703	24.151	10.109	-0.53	+0.00	+0.003	37.696
ATOM	23	C13	<1> _	26.581	24.333	11.168	-0.50	+0.02	+0.038	37.696
ATOM	24	C14	<1> _	26.278	23.791	12.423	-0.37	+0.06	+0.093	37.696
ATOM	25	O15	<1> _	27.117	24.079	13.494	-0.25	-0.17	-0.278	37.696
ATOM	26	C16	<1> _	27.091	25.348	14.028	-0.26	+0.16	+0.260	37.696
ATOM	27	O17	<1> _	27.776	26.058	13.328	-0.50	-0.18	-0.265	37.696
ATOM	28	C18	<1> _	26.320	25.716	15.259	-0.36	+0.08	+0.126	37.696
TER										
ENDMDL										

3e A Docking out put file (extracted from *.dlg file

An example of clustering histogram from docking result of **3e** docked towards 1CX2 by AutoDock 4.2 software. The lowest binding energy -6.33 kcal/mol indicates the conformation that fulfilled the selection requirement and was chosen for further analysis.

```
Number of distinct conformational clusters found = 28,  out of 100 runs,
Using an rmsd-tolerance of 1.5 A


        CLUSTERING HISTOGRAM
        _____

_____
     |           |     |          |      |
Clus | Lowest    | Run | Mean     | Num  | Histogram
-ter | Binding   |     | Binding  | in   |
Rank | Energy    |     | Energy   | Clus |   5    10   15   20   25   30   35
_____|_____|_____|_____|_____|___:____|____:____|____:____|____:___
   1 |     -6.33 | 67  |    -6.32 |   3  |###
   2 |     -6.16 | 50  |    -5.78 |   2  |##
   3 |     -6.08 |  8  |    -6.08 |   1  |#
   4 |     -5.98 | 30  |    -5.97 |   4  |####
   5 |     -5.97 | 15  |    -5.97 |   2  |##
   6 |     -5.79 | 29  |    -5.76 |   4  |####
   7 |     -5.74 | 75  |    -5.74 |   1  |#
   8 |     -5.70 | 55  |    -5.37 |  15  |###############
   9 |     -5.68 | 35  |    -5.68 |   1  |#
  10 |     -5.67 | 84  |    -5.67 |   1  |#
  11 |     -5.52 | 52  |    -5.52 |   1  |#
  12 |     -5.42 | 85  |    -5.15 |  10  |##########
  13 |     -5.41 | 19  |    -5.28 |   4  |####
  14 |     -5.39 | 88  |    -5.24 |  18  |##################
  15 |     -5.35 | 91  |    -5.35 |   1  |#
  16 |     -5.27 | 16  |    -5.23 |   9  |#########
  17 |     -5.09 | 95  |    -5.09 |   1  |#
  18 |     -5.08 | 98  |    -4.95 |   3  |###
  19 |     -4.75 | 17  |    -4.75 |   1  |#
  20 |     -4.73 |  6  |    -4.71 |   3  |###
  21 |     -4.70 | 97  |    -4.68 |   4  |####
  22 |     -4.67 | 62  |    -4.67 |   1  |#
  23 |     -4.64 | 80  |    -4.64 |   1  |#
  24 |     -4.60 | 24  |    -4.52 |   2  |##
  25 |     -4.50 |  5  |    -4.41 |   3  |###
  26 |     -4.49 | 65  |    -4.49 |   1  |#
  27 |     -4.37 | 51  |    -4.37 |   1  |#
  28 |     -4.26 | 74  |    -4.26 |   2  |##
_____|_____|_____|_____|_____|_____
```

An example of the calculation of estimated free energy of binding from docking result (towards 1CX2) for the chosen **3e** conformation. Its atomic coordinates are surround in blue line box.

```
MODEL        67
USER    Run = 67
USER    Cluster Rank = 1
USER    Number of conformations in this cluster = 3
USER
USER    RMSD from reference structure        = 34.570 A
USER
USER    Estimated Free Energy of Binding     =   -6.33 kcal/mol  [=(1)+(2)+(3)-(4)]
USER    Estimated Inhibition Constant, Ki    =   22.75 uM (micromolar)  [Temperature = 298.15 K]
USER
USER    (1) Final Intermolecular Energy      =   -7.83 kcal/mol
USER        vdW + Hbond + desolv Energy      =   -7.66 kcal/mol
USER        Electrostatic Energy             =   -0.17 kcal/mol
USER    (2) Final Total Internal Energy      =   -1.27 kcal/mol
USER    (3) Torsional Free Energy            =   +1.49 kcal/mol
USER    (4) Unbound System's Energy  [=(2)] =   -1.27 kcal/mol
USER
USER
USER
USER    DPF = 30.dpf
USER    NEWDPF move   30.pdbqt
USER    NEWDPF about 0.732900 -0.007800 -0.393000
USER    NEWDPF tran0 26.650443 21.971298 16.286371
USER    NEWDPF axisangle0 0.708318 -0.078104 0.701559 169.183335
USER    NEWDPF quaternion0 0.705165 -0.077756 0.698436 0.094253
USER    NEWDPF dihe0 -4.48 4.64 166.64 147.40 83.69
USER
```

USER				x	y	z	vdW	Elec	q	RMS
ATOM	1	O1_	<1> _	25.417	22.172	16.376	-0.13	-0.22	-0.300	34.570
ATOM	2	C2_	<1> _	25.596	21.086	17.304	-0.12	+0.26	+0.292	34.570
ATOM	3	N3_	<1> _	25.456	19.897	16.392	-0.13	-0.17	-0.201	34.570
ATOM	4	N4_	<1> _	25.542	20.376	15.059	-0.01	-0.08	-0.140	34.570
ATOM	5	C5_	<1> _	25.491	21.689	15.082	-0.21	+0.13	+0.199	34.570
ATOM	6	C8_	<1> _	25.818	18.541	16.699	-0.15	+0.24	+0.238	34.570
ATOM	7	C9_	<1> _	26.068	17.575	15.575	-0.03	+0.05	+0.119	34.570
ATOM	8	O10	<1> _	25.822	18.241	17.882	-0.06	-0.41	-0.272	34.570
ATOM	9	C11	<1> _	25.503	22.591	13.931	-0.35	+0.03	+0.052	34.570
ATOM	10	C12	<1> _	26.638	23.294	13.484	-0.29	+0.06	+0.093	34.570
ATOM	11	C13	<1> _	26.569	24.133	12.365	-0.44	+0.02	+0.038	34.570
ATOM	12	C14	<1> _	25.368	24.278	11.685	-0.53	+0.00	+0.003	34.570
ATOM	13	C15	<1> _	24.238	23.592	12.117	-0.57	+0.00	+0.001	34.570
ATOM	14	C16	<1> _	24.302	22.760	13.226	-0.48	+0.01	+0.019	34.570
ATOM	15	O17	<1> _	27.818	23.277	14.223	-0.27	-0.19	-0.278	34.570
ATOM	16	C18	<1> _	28.002	24.220	15.210	-0.22	+0.17	+0.260	34.570
ATOM	17	C19	<1> _	29.366	24.129	15.830	-0.36	+0.09	+0.126	34.570
ATOM	18	O20	<1> _	27.104	24.989	15.475	-0.24	-0.17	-0.265	34.570
ATOM	19	C7_	<1> _	26.906	21.207	18.044	-0.29	-0.01	-0.008	34.570
ATOM	20	C21	<1> _	28.095	21.063	17.328	-0.30	+0.01	+0.012	34.570
ATOM	21	C22	<1> _	29.321	21.147	17.979	-0.34	+0.01	+0.008	34.570
ATOM	22	C23	<1> _	29.373	21.361	19.356	-0.35	-0.06	-0.059	34.570
ATOM	23	C24	<1> _	28.183	21.499	20.071	-0.36	+0.01	+0.008	34.570
ATOM	24	C25	<1> _	26.958	21.430	19.421	-0.32	+0.01	+0.012	34.570
ATOM	25	C26	<1> _	30.688	21.429	20.064	-0.51	+0.03	+0.034	34.570
ATOM	26	C27	<1> _	31.046	22.848	20.453	-0.59	+0.01	+0.010	34.570
TER										
ENDMDL										

3c A Docking output file (extracted from *.dlg file

An example of clustering histogram from docking result of **3c** docked towards 1CQE by AutoDock 4.2 software. The lowest binding energy -8.92 kcal/mol indicates the conformation that fulfilled the selection requirement and was chosen for further analysis.

```
Number of distinct conformational clusters found = 49,   out of 100 runs,
Using an rmsd-tolerance of 1.5 A

|
        CLUSTERING HISTOGRAM
        _____


Clus | Lowest    | Run | Mean      | Num | Histogram
-ter | Binding   |     | Binding   | in  |
Rank | Energy    |     | Energy    | Clus|    5    10   15   20   25   30   35
_____|_____|_____|_____|_____|____:____|____:____|____:____|____:____
   1 |    -10.22 | 38  |    -10.02 |   3 |###
   2 |     -9.69 | 21  |     -9.69 |   1 |#
   3 |     -9.54 | 30  |     -9.49 |   2 |##
   4 |     -8.92 | 90  |     -8.92 |   1 |#
   5 |     -8.86 | 51  |     -8.74 |   3 |###
   6 |     -8.79 | 36  |     -8.78 |   2 |##
   7 |     -8.75 | 95  |     -8.75 |   1 |#
   8 |     -8.66 | 53  |     -8.65 |   2 |##
   9 |     -8.50 | 57  |     -8.50 |   1 |#
  10 |     -8.49 | 72  |     -8.40 |   9 |#########
  11 |     -8.47 | 37  |     -8.47 |   1 |#
  12 |     -8.47 | 33  |     -8.47 |   1 |#
  13 |     -8.43 | 66  |     -8.30 |   2 |##
  14 |     -8.43 | 34  |     -8.43 |   1 |#
  15 |     -8.30 | 91  |     -8.30 |   1 |#|
  16 |     -8.24 | 68  |     -8.19 |   2 |##
  17 |     -8.18 | 10  |     -8.02 |   6 |######
  18 |     -8.10 | 60  |     -8.02 |   3 |###
  19 |     -8.03 | 20  |     -8.00 |   2 |##
  20 |     -8.02 | 52  |     -8.02 |   1 |#
  21 |     -7.92 | 56  |     -7.90 |   2 |##
  22 |     -7.87 |  5  |     -7.87 |   1 |#
  23 |     -7.79 | 76  |     -7.79 |   1 |#
  24 |     -7.53 | 12  |     -7.53 |   1 |#
  25 |     -7.50 | 16  |     -7.45 |   4 |####
  26 |     -7.49 | 41  |     -7.49 |   1 |#
  27 |     -7.34 | 78  |     -7.12 |   7 |#######
  28 |     -7.34 | 87  |     -7.34 |   1 |#
  29 |     -7.32 | 31  |     -7.26 |   4 |####
  30 |     -7.29 | 32  |     -7.25 |   4 |####
  31 |     -7.14 | 70  |     -7.14 |   1 |#
  32 |     -7.07 | 11  |     -7.07 |   1 |#
  33 |     -7.04 |  7  |     -7.04 |   1 |#
  34 |     -6.95 | 27  |     -6.95 |   1 |#
  35 |     -6.91 | 74  |     -6.81 |   3 |###
  36 |     -6.87 | 69  |     -6.83 |   2 |##
  37 |     -6.84 | 92  |     -6.72 |   2 |##
  38 |     -6.84 | 45  |     -6.84 |   1 |#
  39 |     -6.82 | 55  |     -6.69 |   3 |###
  40 |     -6.74 |  8  |     -6.48 |   3 |###
  41 |     -6.72 | 22  |     -6.71 |   2 |##
  42 |     -6.70 | 82  |     -6.70 |   1 |#
  43 |     -6.63 | 40  |     -6.60 |   2 |##
  44 |     -6.58 | 58  |     -6.58 |   1 |#
  45 |     -6.55 |  6  |     -6.55 |   1 |#
  46 |     -6.53 | 19  |     -6.53 |   1 |#
  47 |     -6.48 | 67  |     -6.48 |   1 |#
  48 |     -6.41 | 80  |     -6.41 |   1 |#
  49 |     -6.19 |  2  |     -6.19 |   1 |#
_____|_____|_____|_____|_____|_____
```

An example of the calculation of estimated free energy of binding from docking result (towards 1CQE) for the chosen **3c** conformation. Its atomic coordinates are surround in blue line box.

```
MODEL        90
USER     Run = 90
USER     Cluster Rank = 4
USER     Number of conformations in this cluster = 1
USER
USER     RMSD from reference structure      = 209.832 A
USER
USER     Estimated Free Energy of Binding   =   -8.92 kcal/mol  [=(1)+(2)+(3)-(4)]
USER     Estimated Inhibition Constant, Ki  =  289.46 nM (nanomolar)  [Temperature = 298.15 K]
USER
USER     (1) Final Intermolecular Energy    =  -10.71 kcal/mol
USER         vdW + Hbond + desolv Energy    =  -10.71 kcal/mol
USER         Electrostatic Energy           =   -0.00 kcal/mol
USER     (2) Final Total Internal Energy    =   -1.04 kcal/mol
USER     (3) Torsional Free Energy          =   +1.79 kcal/mol
USER     (4) Unbound System's Energy  [=(2)] =  -1.04 kcal/mol
USER
USER
USER
USER     DPF = 8bs.dpf
USER     NEWDPF move   8bs.pdbqt
USER     NEWDPF about  -1.407200 0.034100 0.435700
USER     NEWDPF tran0  26.485305 33.727320 208.201086
USER     NEWDPF axisangle0  -0.148758 -0.775109 -0.614066 99.124643
USER     NEWDPF quaternion0 -0.113222 -0.589945 -0.467373 0.648621
USER     NEWDPF dihe0 -21.20 180.00 168.87 4.20 -85.24 -27.31
USER
```

```
USER                              x        y        z      vdW    Elec      q      RMS
ATOM      1  N1_ <1> _        24.453  34.297 209.013  -0.36  -0.00   -0.201 209.832
ATOM      2  C2_ <1> _        25.352  33.121 208.722  -0.20  +0.03   +0.292 209.832
ATOM      3  O3_ <1> _        25.695  33.318 207.340  -0.35  -0.02   -0.300 209.832
ATOM      4  C4_ <1> _        25.057  34.454 206.875  -0.39  -0.01   +0.199 209.832
ATOM      5  N5_ <1> _        24.306  35.011 207.794  -0.37  +0.01   -0.140 209.832
ATOM      6  C9_ <1> _        23.314  34.156 209.906  -0.35  -0.00   +0.238 209.832
ATOM      7  O24 <1> _        22.338  34.855 209.738  -0.47  +0.04   -0.272 209.832
ATOM      8  C25 <1> _        23.473  33.184 211.048  -0.33  -0.00   +0.119 209.832
ATOM      9  C8_ <1> _        26.603  33.077 209.566  -0.40  -0.00   -0.007 209.832
ATOM     10  C19 <1> _        26.873  31.905 210.280  -0.44  +0.00   +0.014 209.832
ATOM     11  C20 <1> _        28.010  31.802 211.067  -0.44  +0.01   +0.038 209.832
ATOM     12  C21 <1> _        28.888  32.894 211.135  -0.39  +0.02   +0.078 209.832
ATOM     13  C22 <1> _        28.639  34.066 210.420  -0.27  +0.01   +0.038 209.832
ATOM     14  C23 <1> _        27.494  34.146 209.633  -0.35  +0.00   +0.014 209.832
ATOM     15  O26 <1> _        29.996  32.653 211.939  -0.27  -0.05   -0.255 209.832
ATOM     16  C27 <1> _        30.802  33.700 212.361  -0.10  +0.07   +0.530 209.832
ATOM     17  F28 <1> _        30.322  34.742 211.676  -0.19  -0.01   -0.144 209.832
ATOM     18  F29 <1> _        30.690  33.954 213.670  -0.06  -0.01   -0.144 209.832
ATOM     19  F30 <1> _        32.098  33.537 212.062  -0.12  -0.02   -0.144 209.832
ATOM     20  C6_ <1> _        25.265  34.906 205.499  -0.56  -0.01   +0.052 209.832
ATOM     21  C10 <1> _        24.169  34.884 204.625  -0.66  -0.00   +0.019 209.832
ATOM     22  C11 <1> _        24.302  35.314 203.311  -0.60  -0.00   +0.001 209.832
ATOM     23  C12 <1> _        25.521  35.791 202.843  -0.65  -0.00   +0.003 209.832
ATOM     24  C13 <1> _        26.623  35.821 203.688  -0.62  -0.01   +0.038 209.832
ATOM     25  C14 <1> _        26.501  35.368 205.007  -0.45  -0.02   +0.093 209.832
ATOM     26  O15 <1> _        27.596  35.497 205.853  -0.26  +0.05   -0.278 209.832
ATOM     27  C16 <1> _        27.721  36.652 206.590  -0.27  -0.04   +0.260 209.832
ATOM     28  O17 <1> _        28.395  36.403 207.565  -0.27  +0.00   -0.265 209.832
ATOM     29  C18 <1> _        27.110  37.960 206.189  -0.50  -0.03   +0.126 209.832
TER
ENDMDL
```
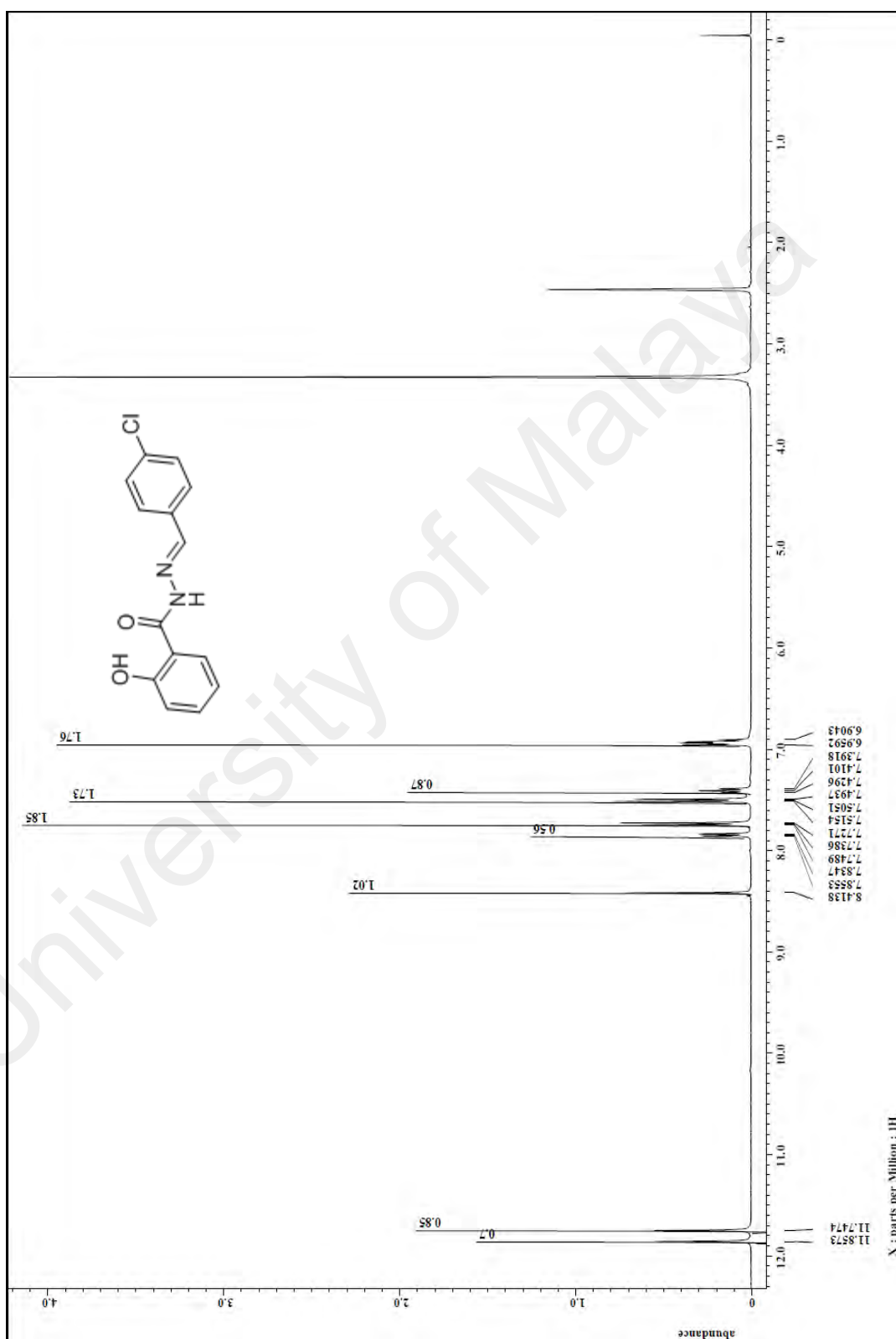
¹H & ¹³C NMR SPECTRA OF SYNTHESIZED MOLECULES

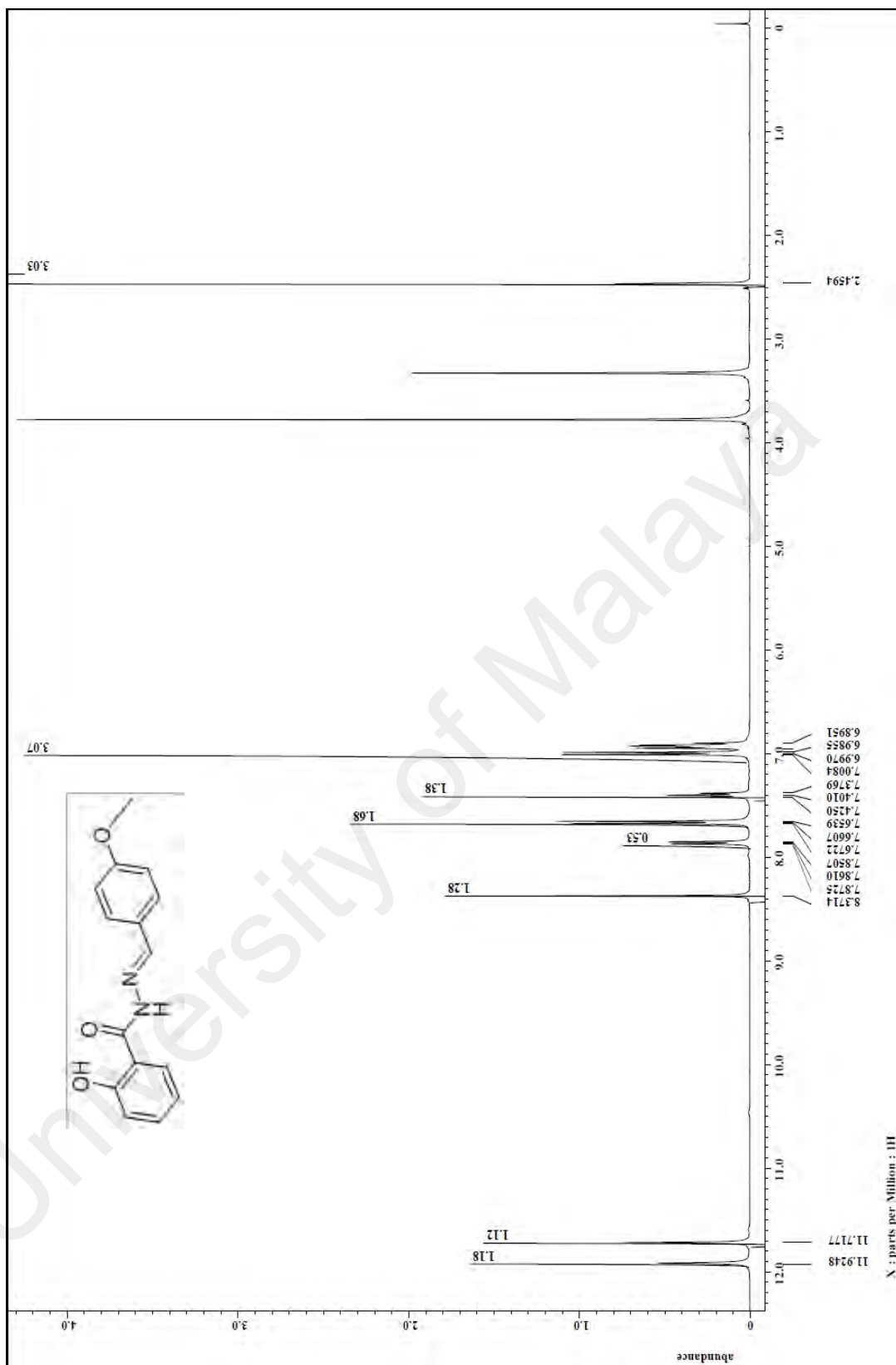Figure B. 1: ¹H spectrum (CDCl₃, 400MHz) of **1a**
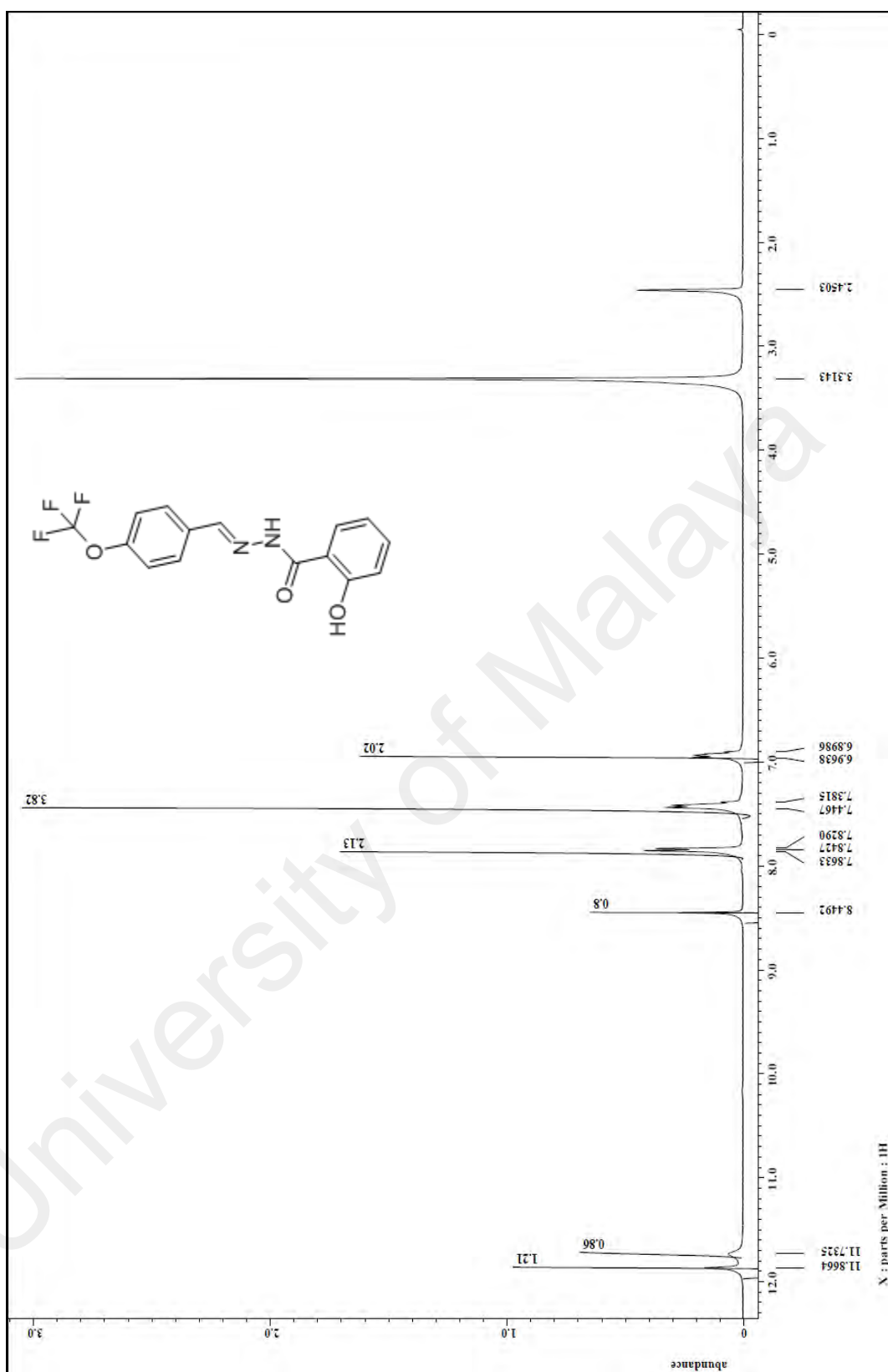
Figure B. 2: ^{1}H spectrum (CDCl$_3$, 400MHz) of **1b**
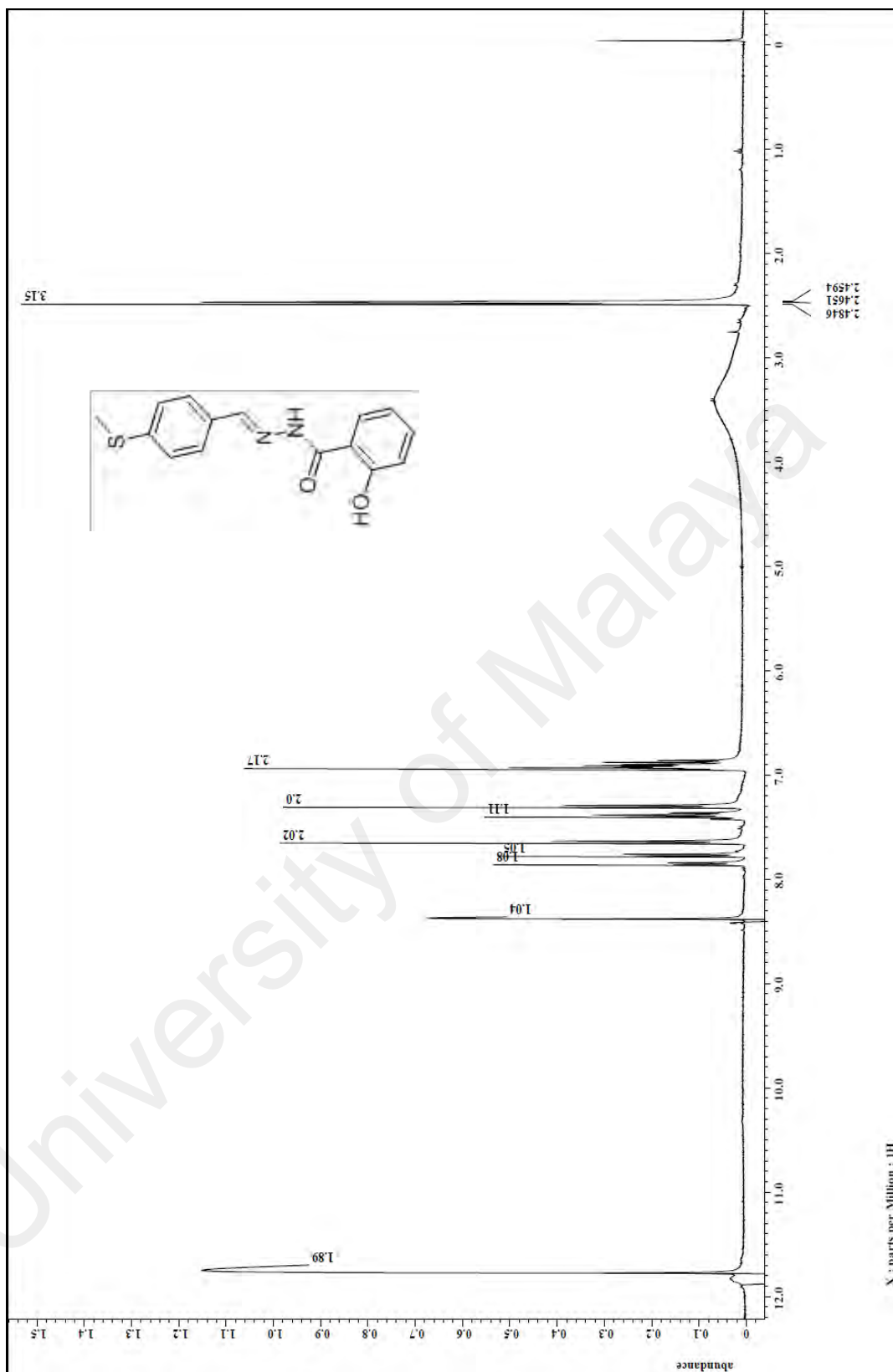
Figure B. 3: ¹H spectrum (CDCl₃, 400MHz) of **1c**

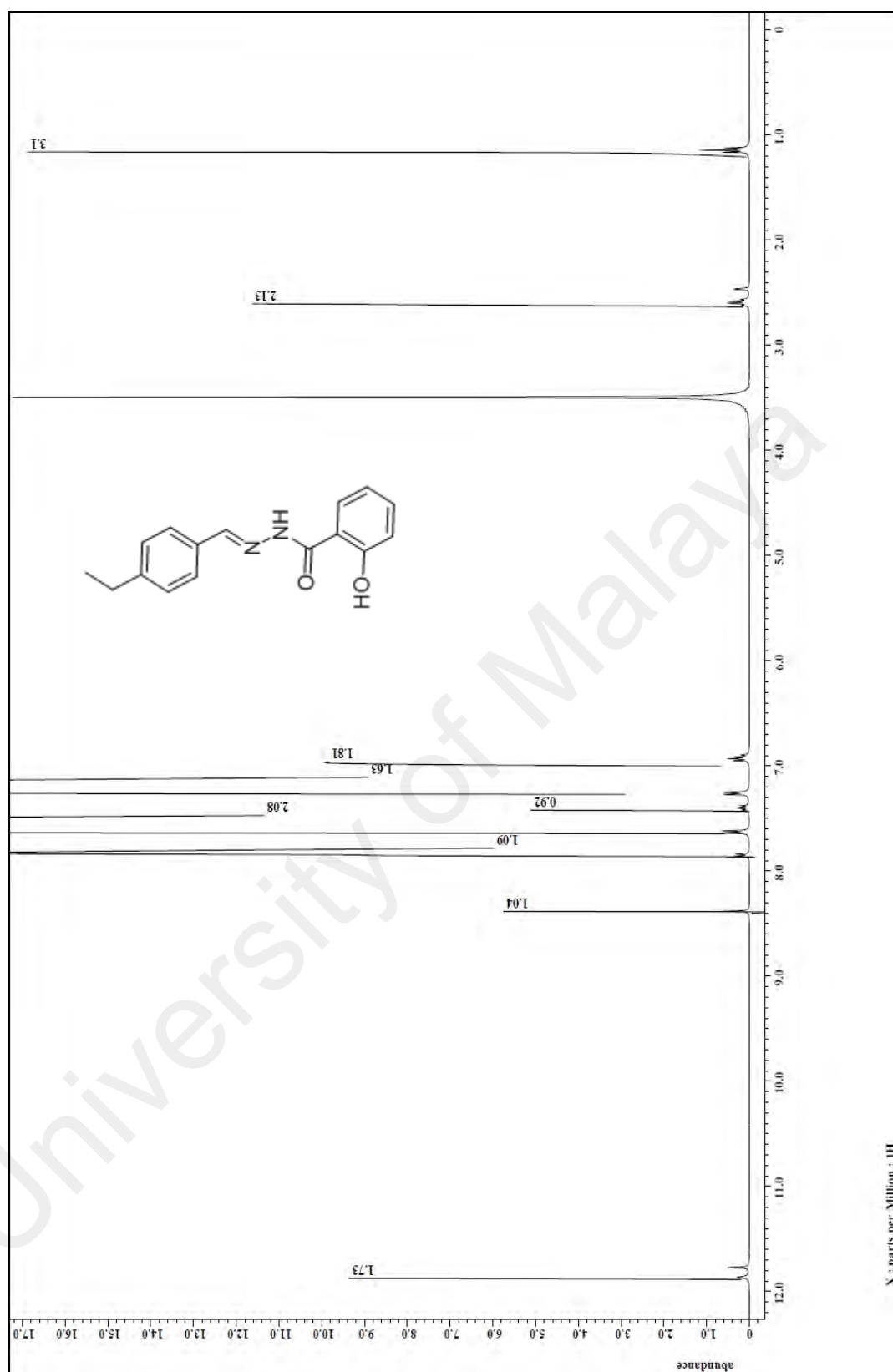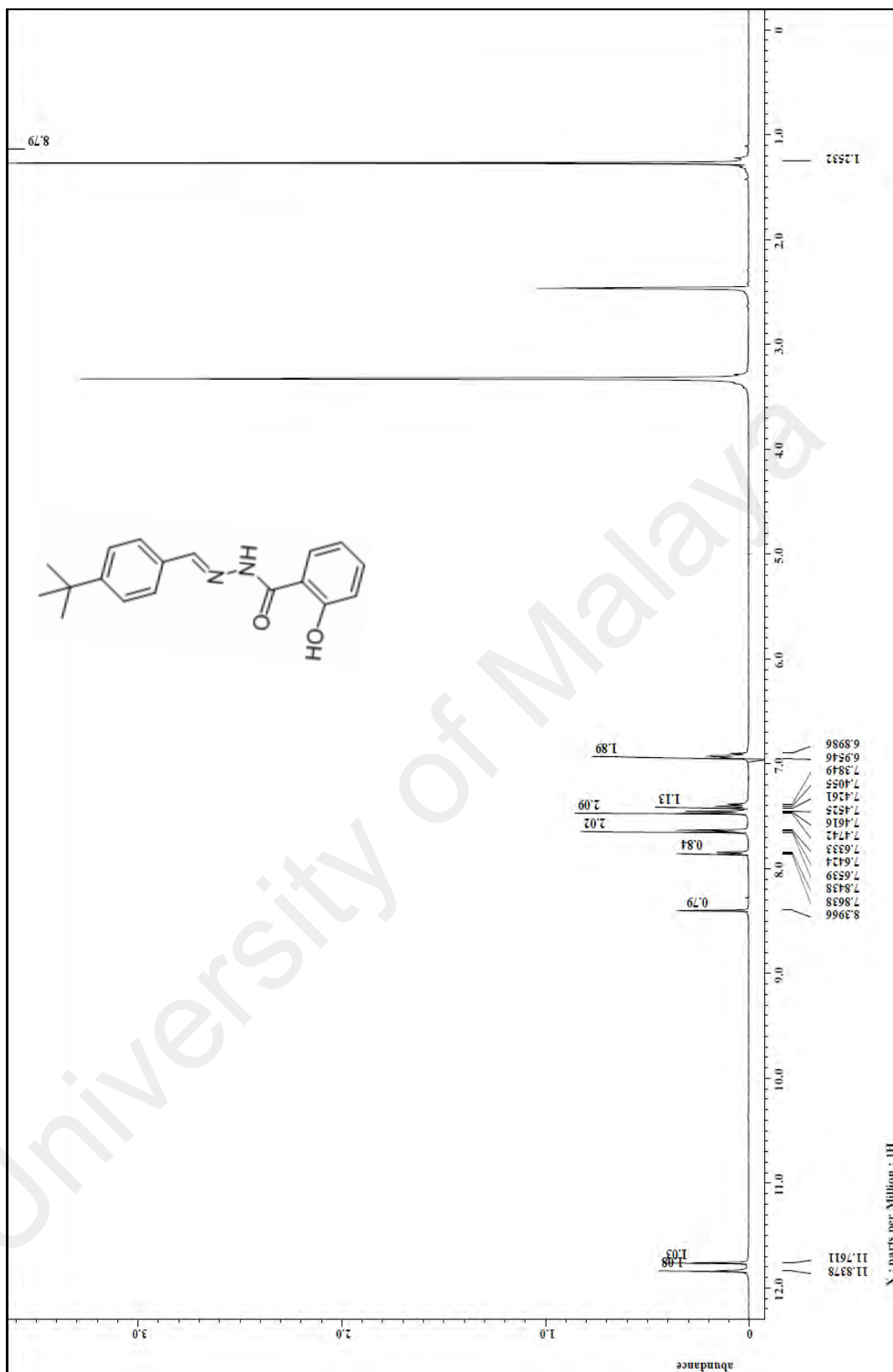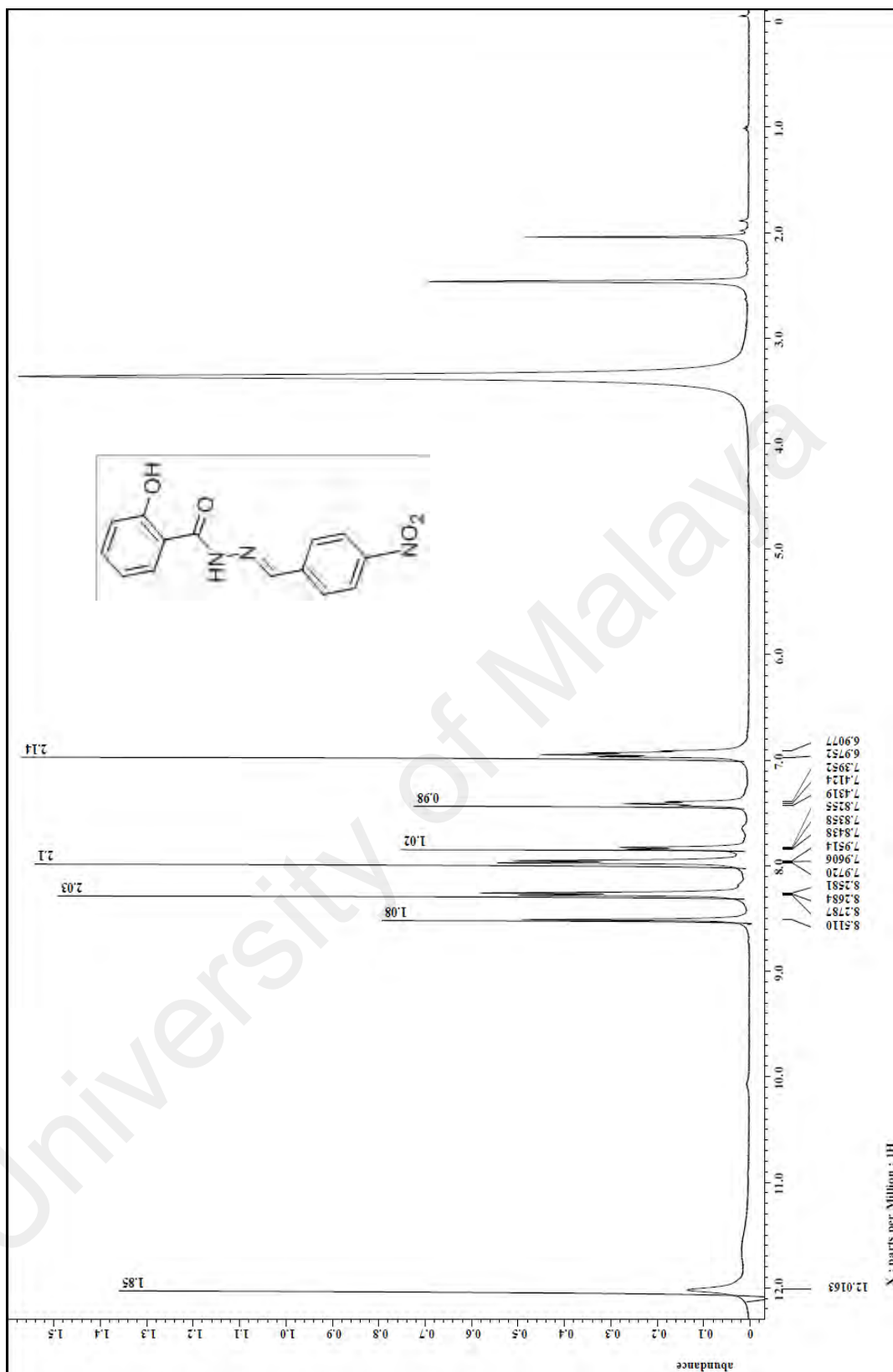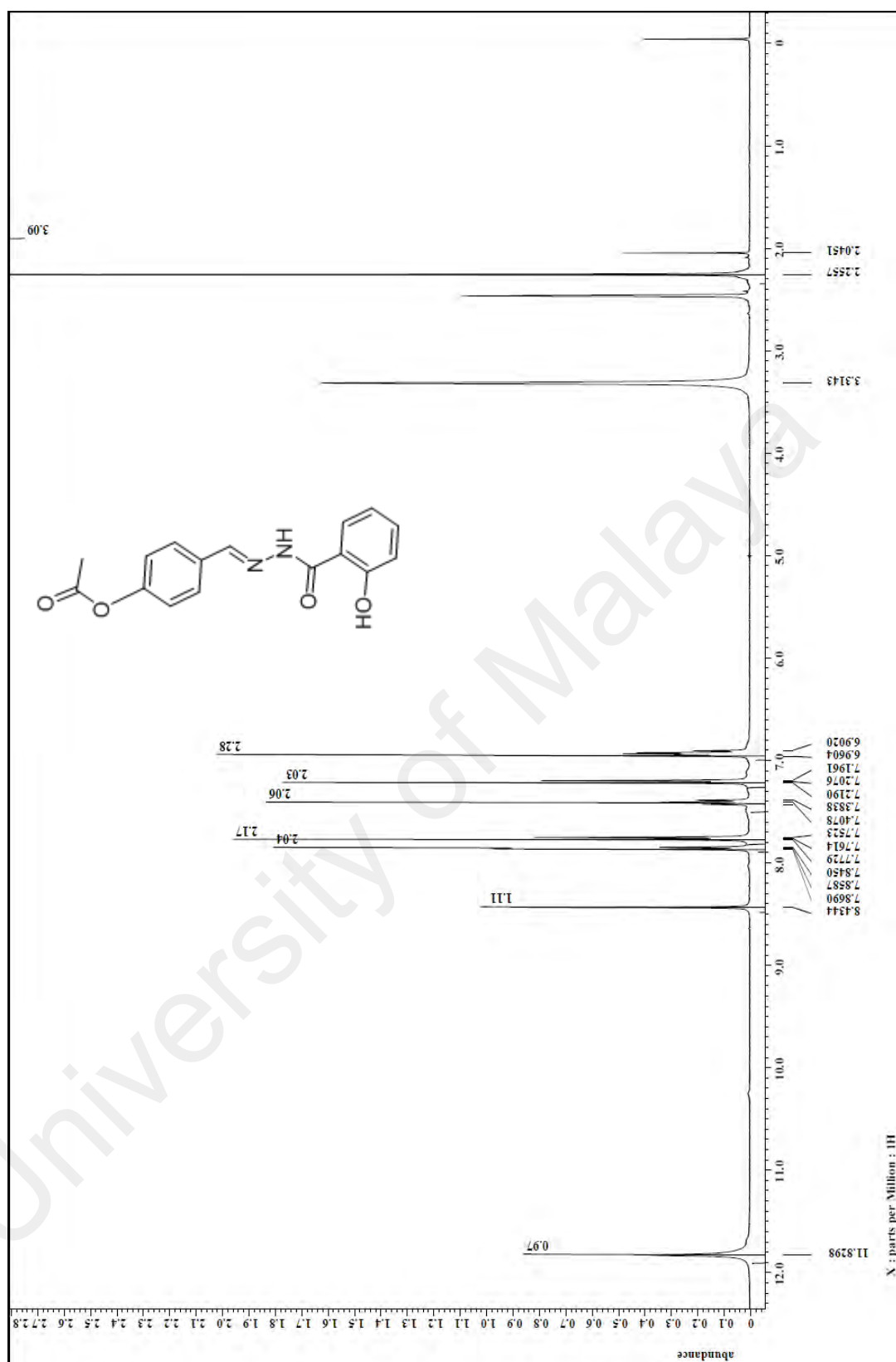Figure B. 4: ^{1}H spectrum (CDCl$_3$, 400MHz) of **1d**

Figure B. 5: ^{1}H spectrum (CDCl$_3$, 400MHz) of **1e**

Figure B. 6: ^{1}H spectrum (CDCl$_3$, 400MHz) of **1f**

Figure B. 7: ^{1}H spectrum (CDCl$_3$, 400MHz) of **1g**

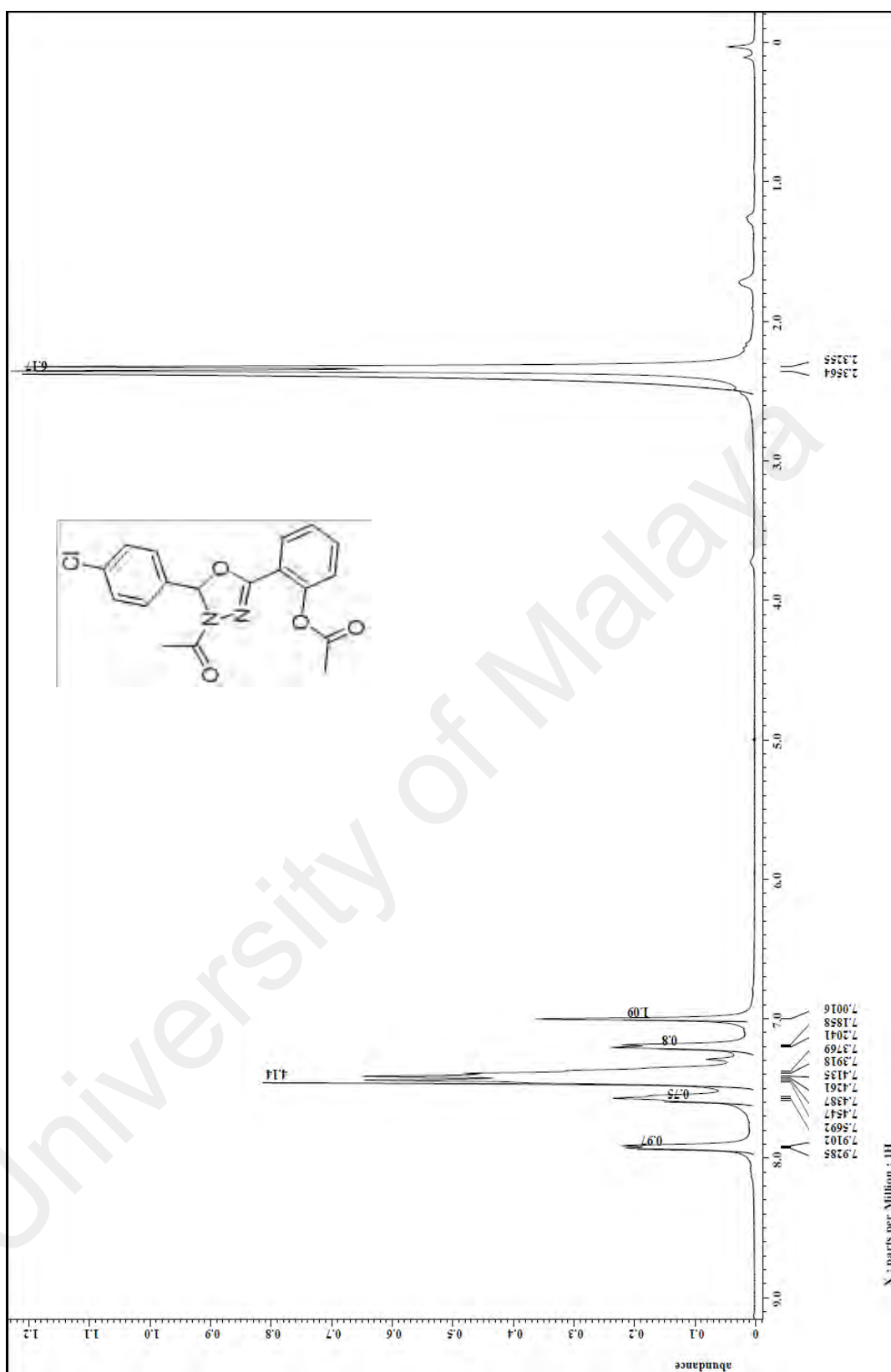Figure B. 8: ^{1}H spectrum (CDCl$_3$, 400MHz) of **1h**

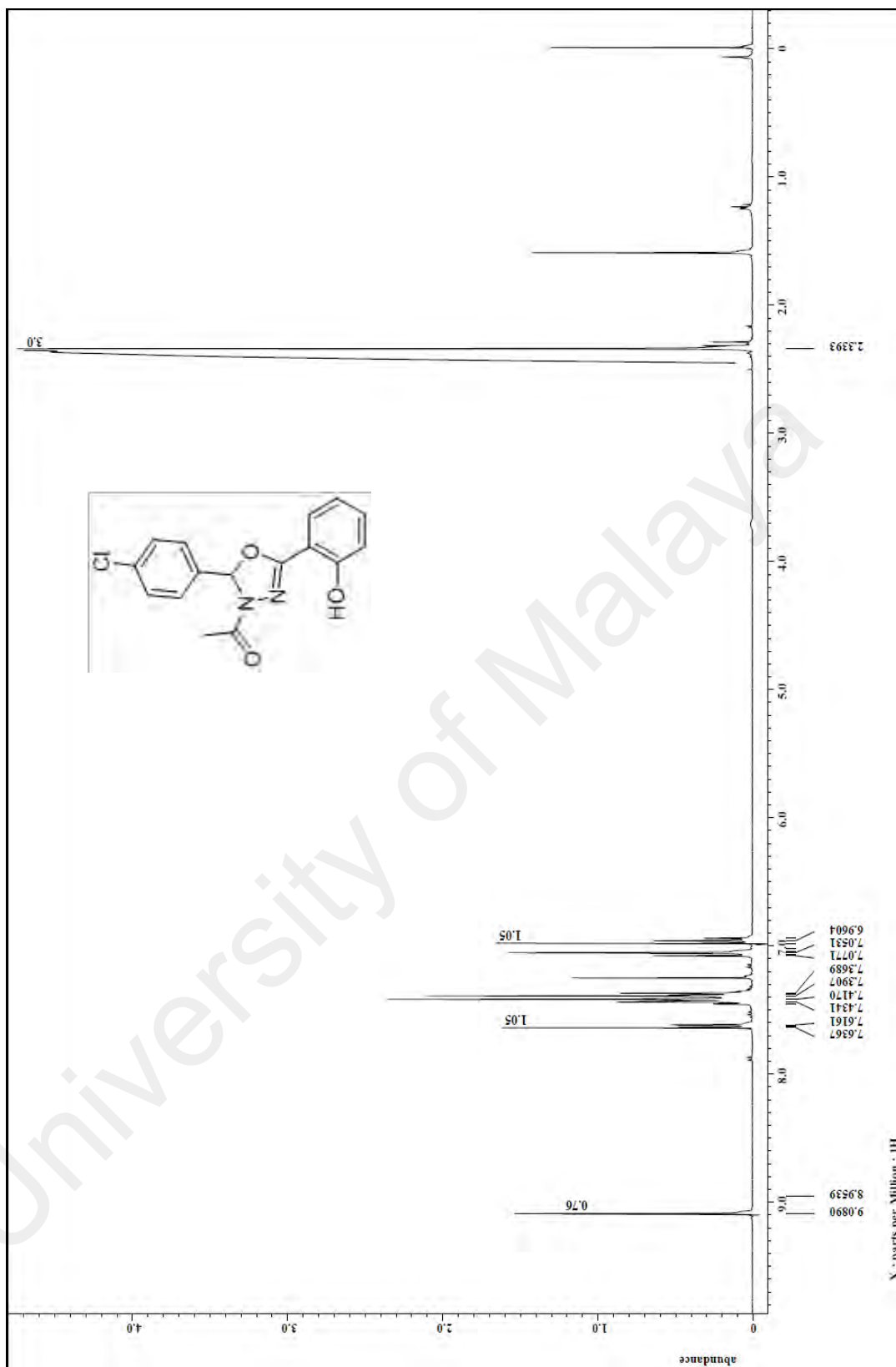Figure B. 9: ^{1}H spectrum (CDCl$_3$, 400MHz) of **3a**

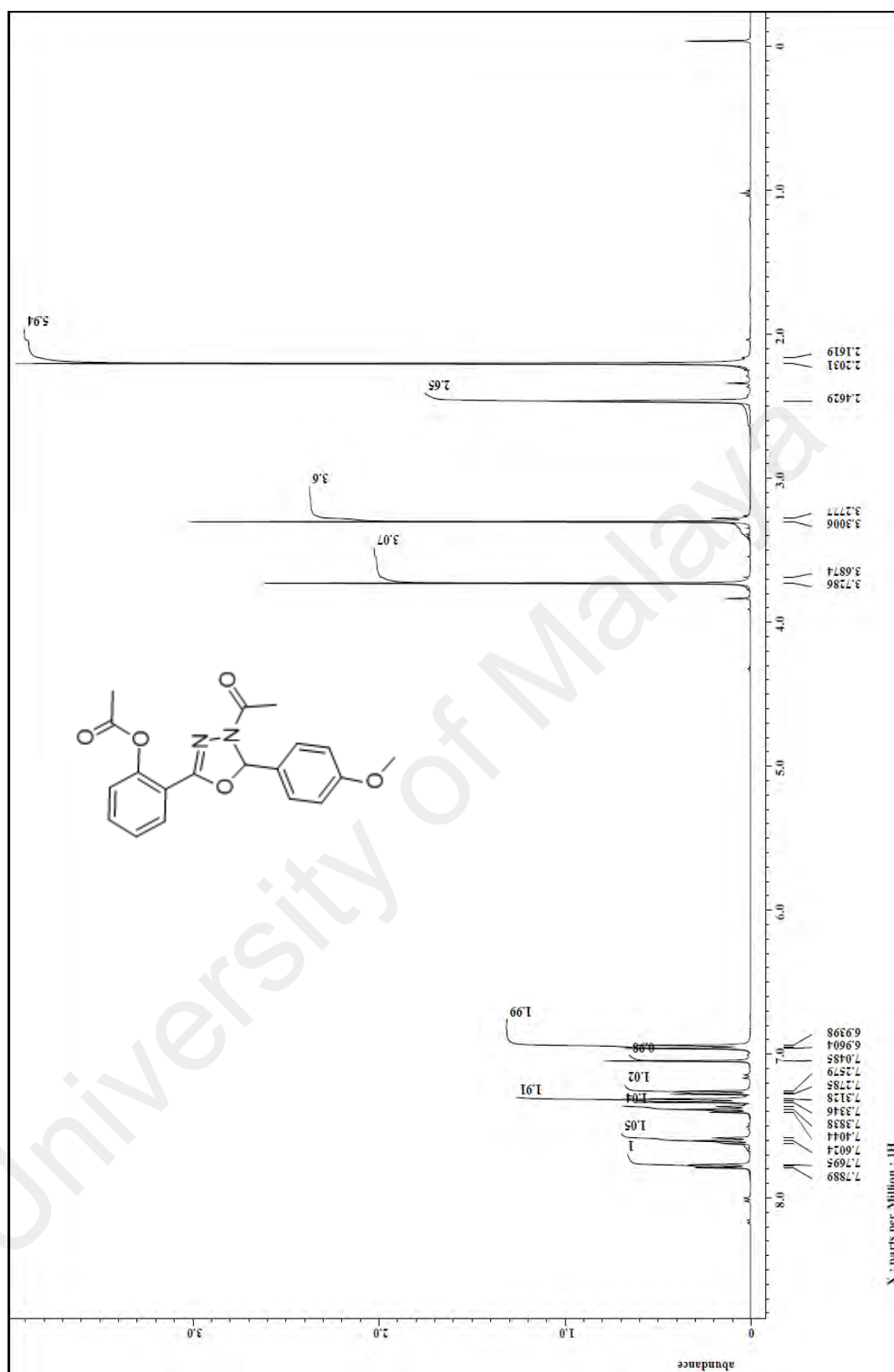Figure B. 10: ^{1}H spectrum (CDCl$_3$, 400MHz) of **2a**

Figure B. 11: ^{1}H spectrum (CDCl$_3$, 400MHz) of **3b**

Figure B. 12: ^{1}H spectrum (CDCl$_3$, 400MHz) of **2b**
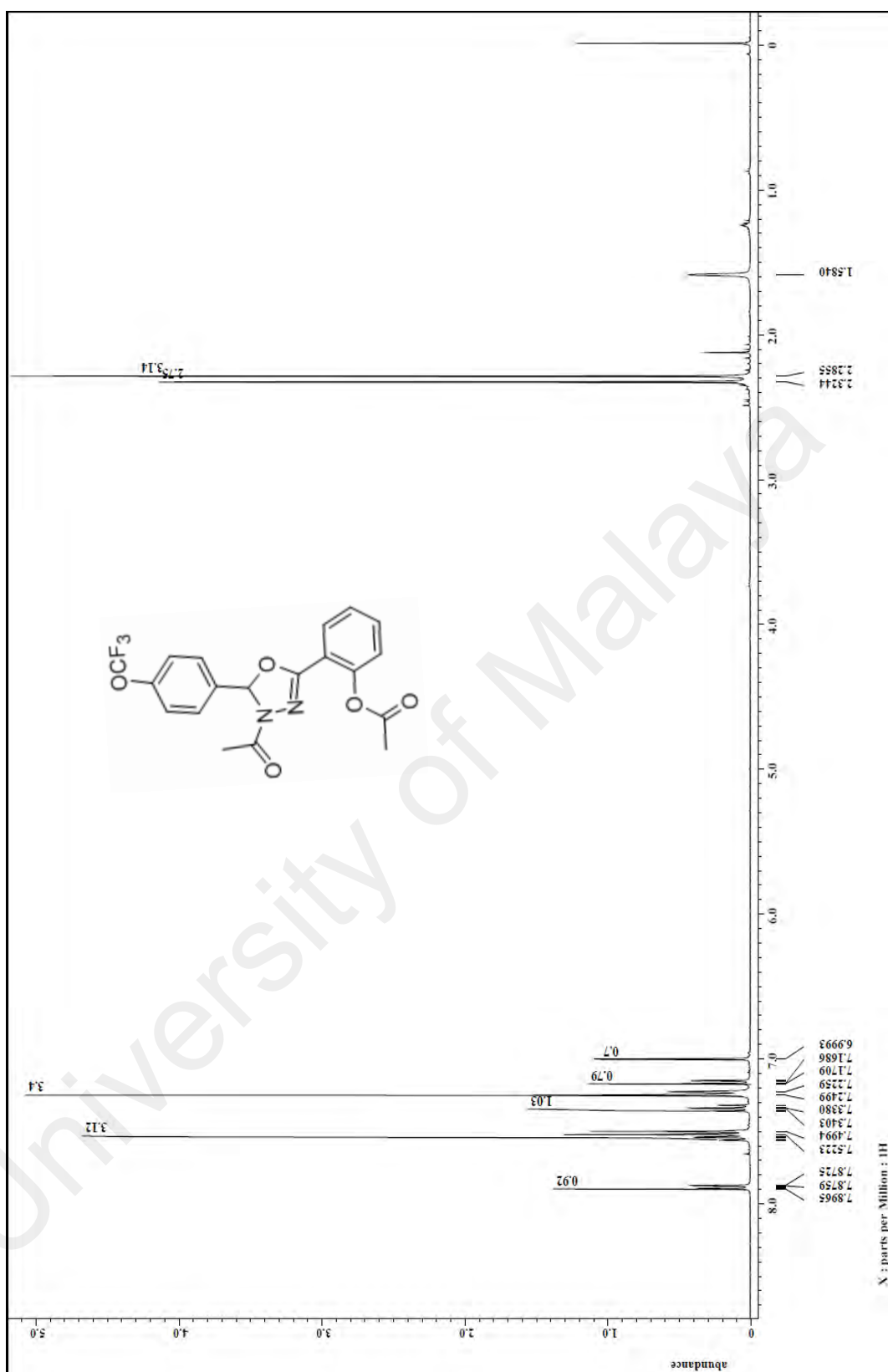
Figure B. 13: ^{1}H spectrum (CDCl$_3$, 400MHz) of **3c**
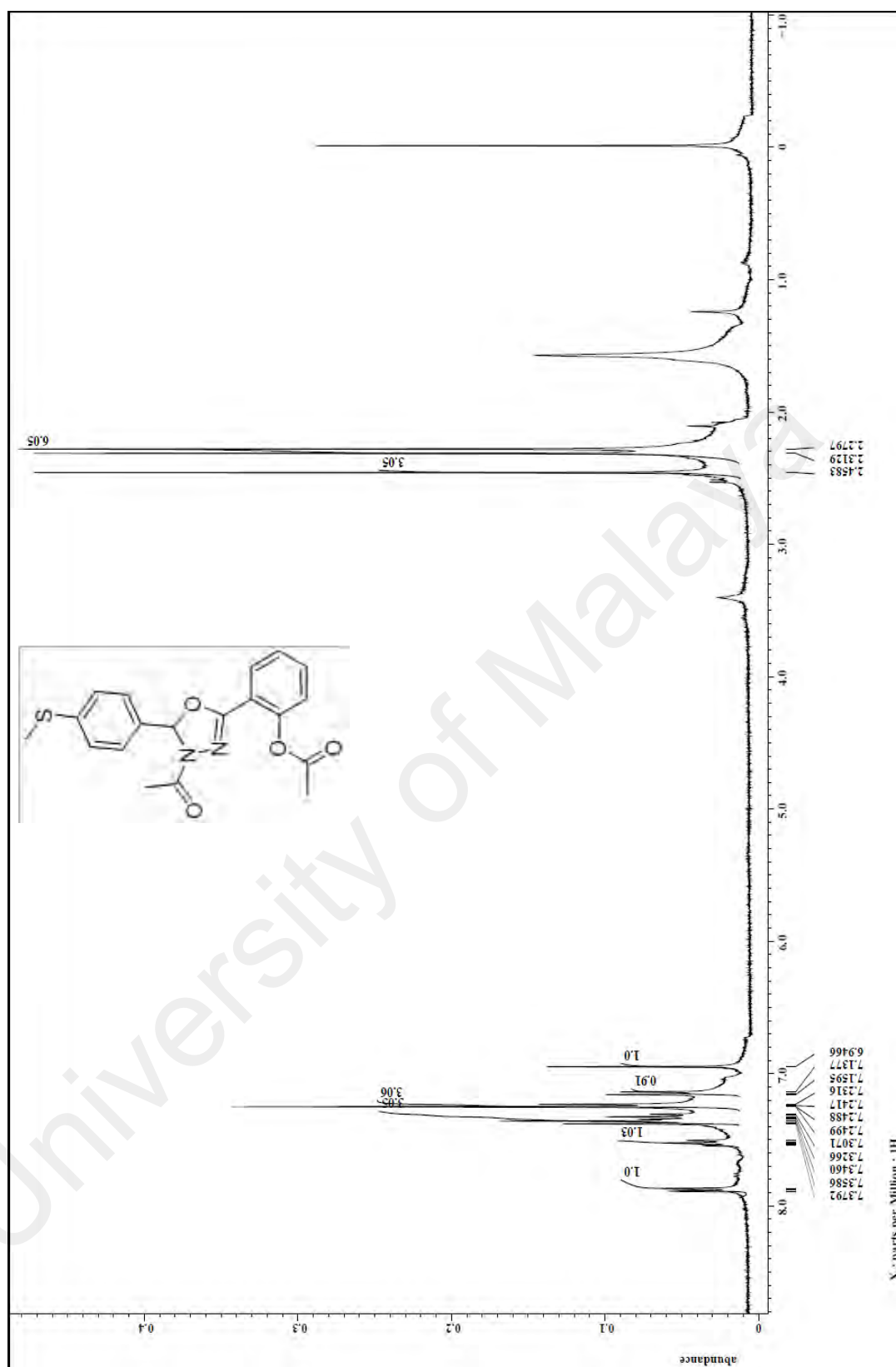
Figure B. 14: ^{1}H spectrum (CDCl$_3$, 400MHz) of **3d**
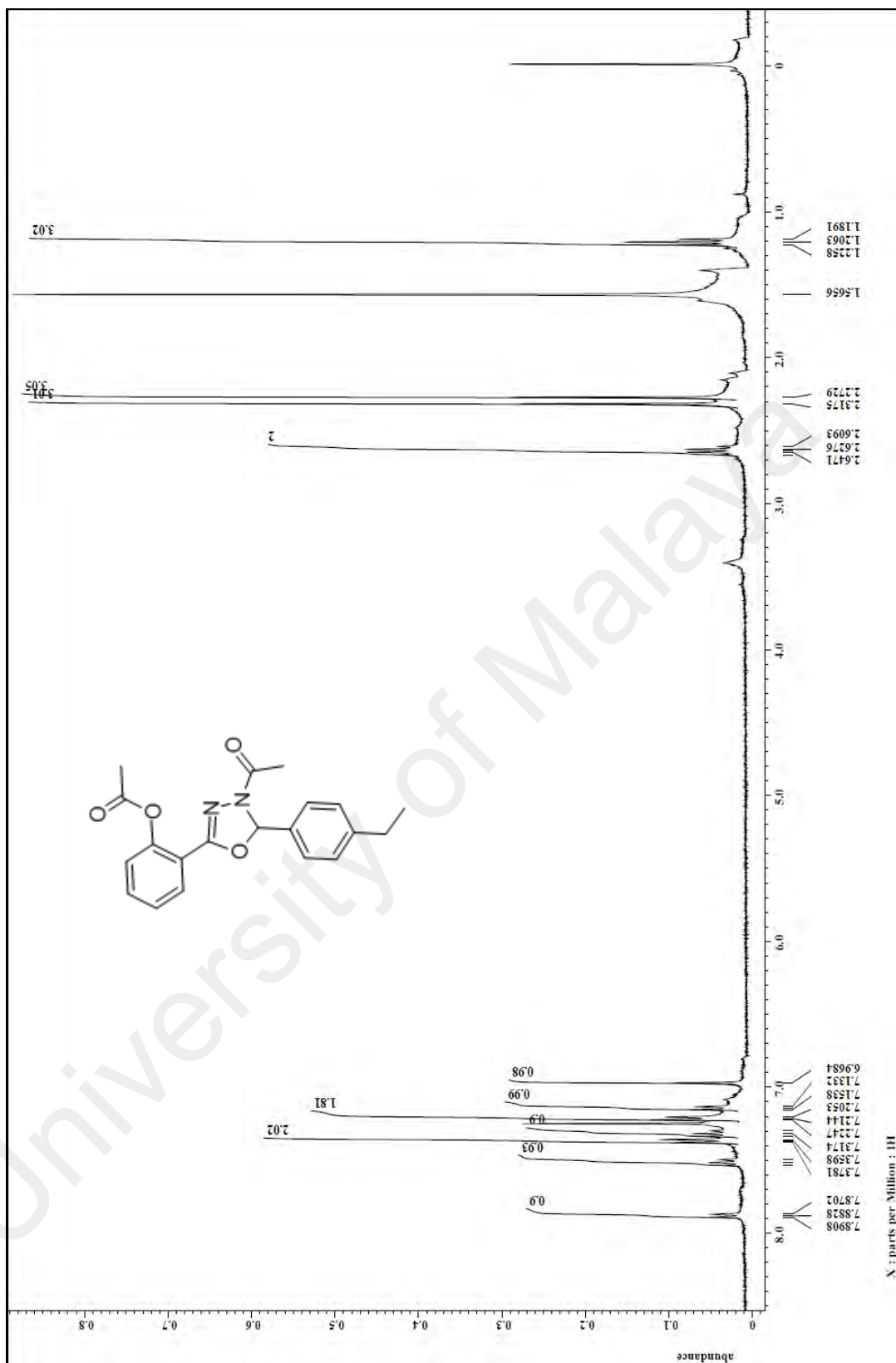
Figure B. 15: ^{1}H spectrum (CDCl$_3$, 400MHz) of **3e**

Figure B. 16: ^{1}H spectrum (CDCl$_3$, 400MHz) of **3f**

Figure B. 17: ^{1}H spectrum (CDCl$_3$, 400MHz) of **3g**

Figure B. 18: ^{1}H spectrum (CDCl$_3$, 400MHz) of **4a**
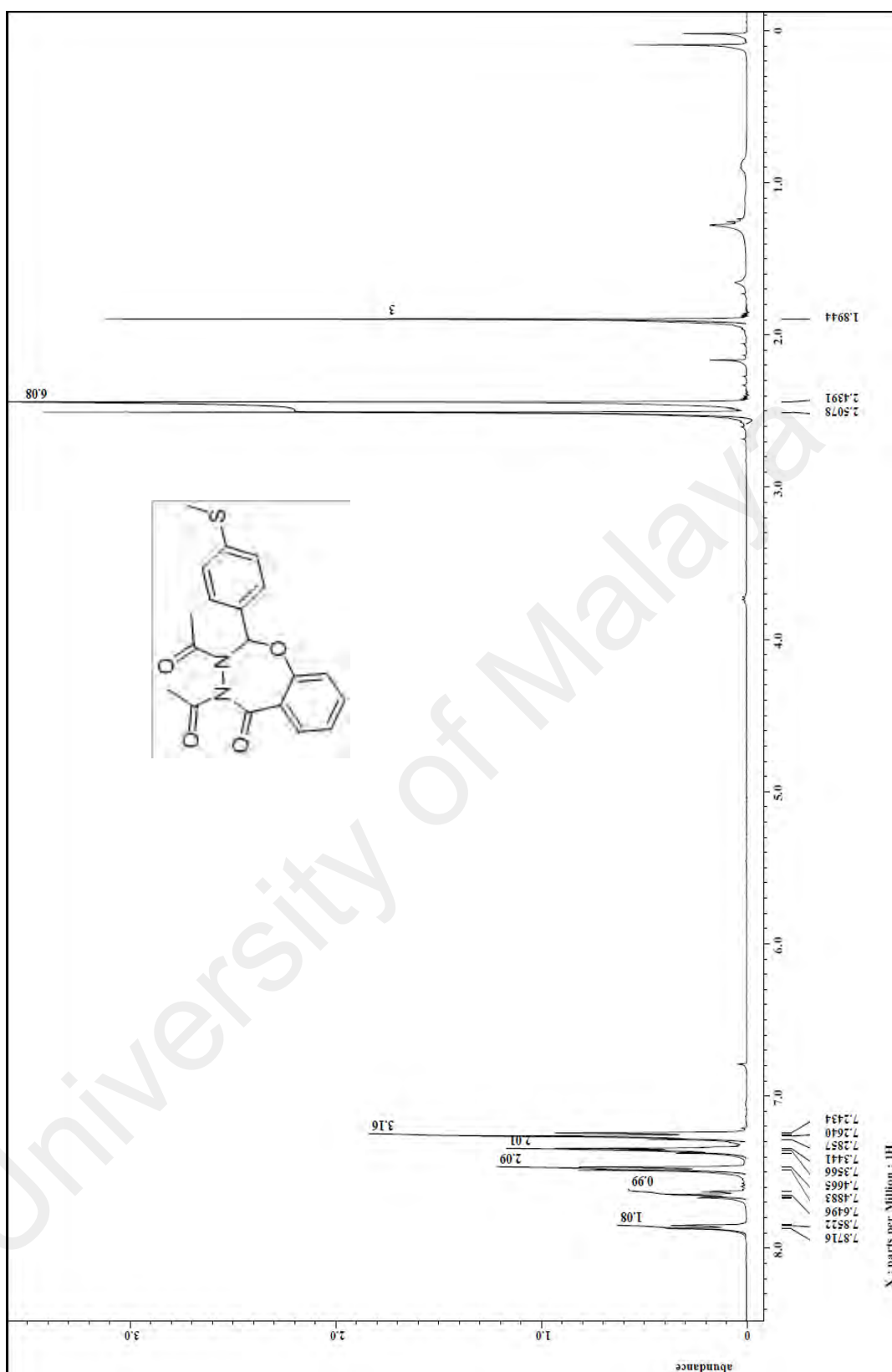
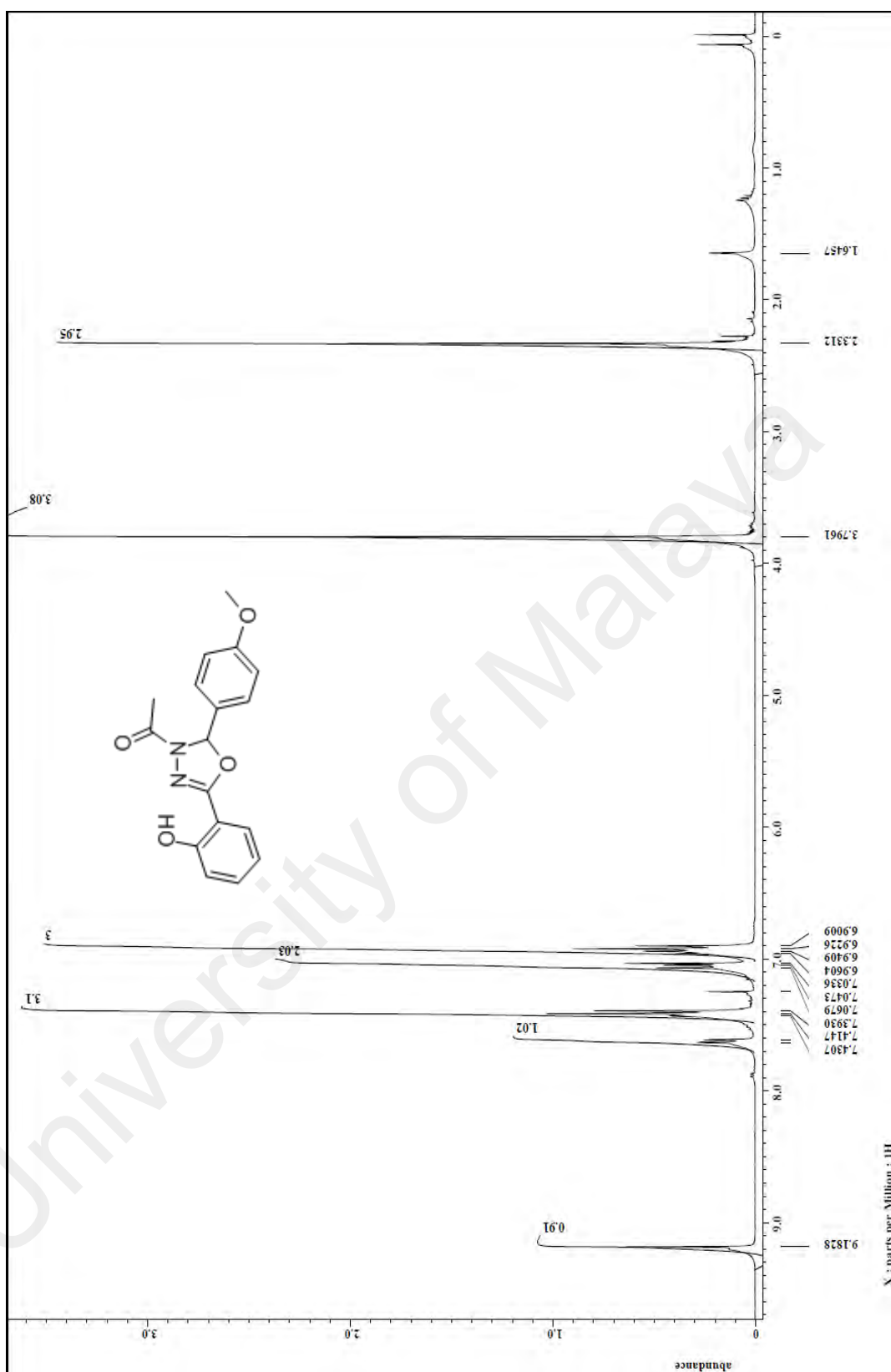Figure B. 19: ^{1}H spectrum (CDCl$_3$, 400MHz) of **4d**

181
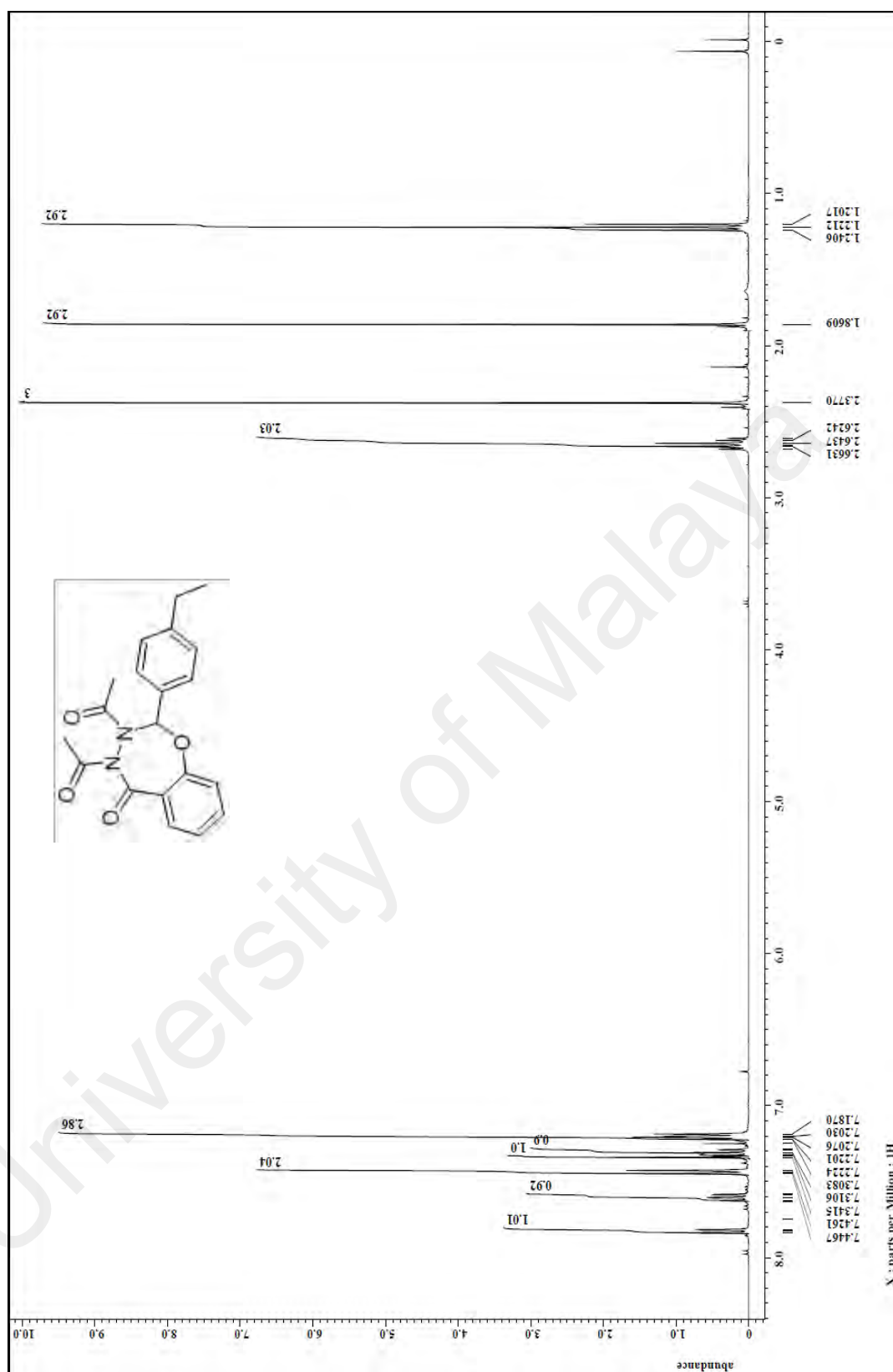
Figure B. 20: ^{1}H spectrum (CDCl$_3$, 400MHz) of **4e**
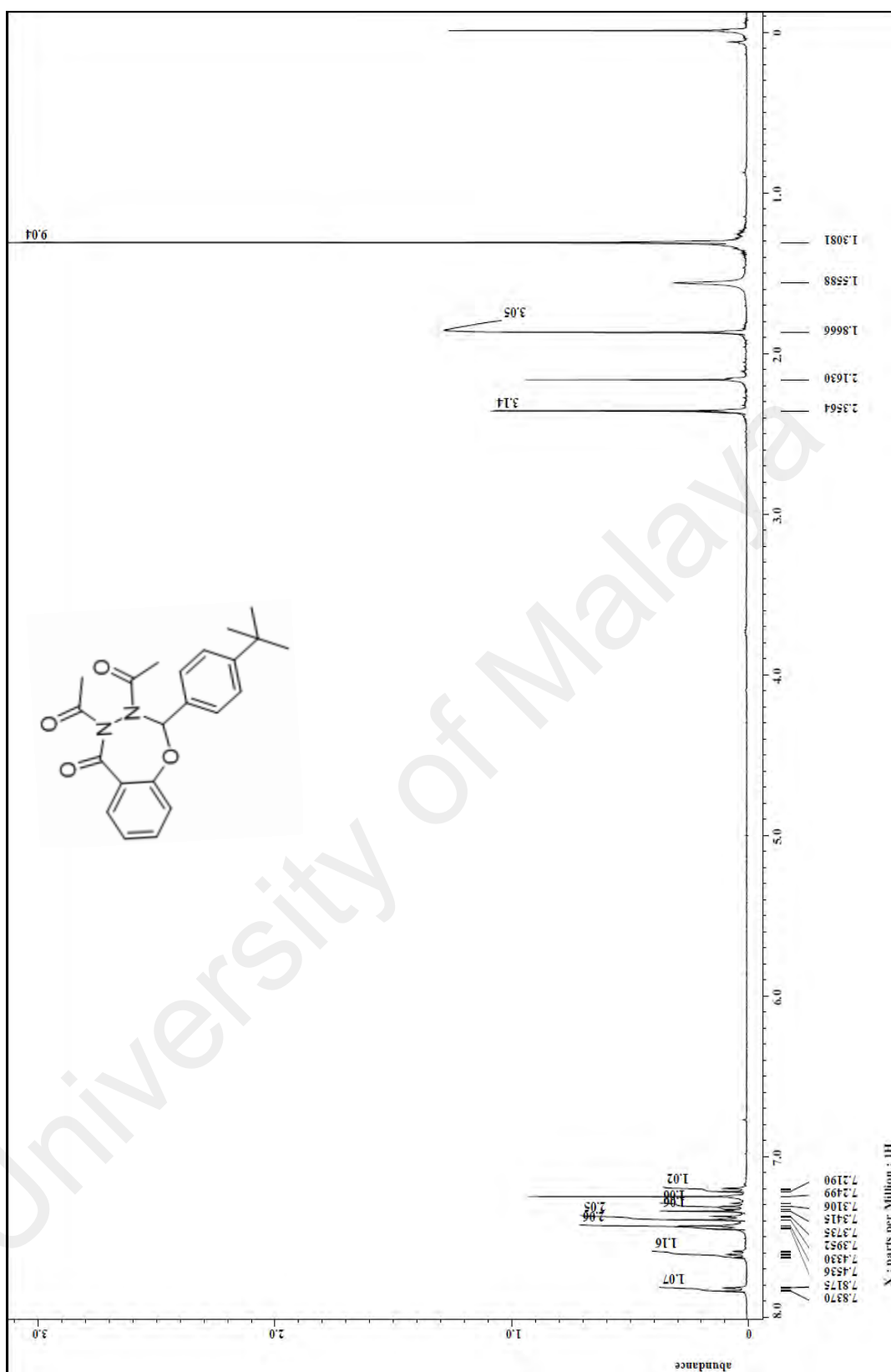
Figure B. 21: ^{1}H spectrum (CDCl$_3$, 400MHz) of **4f**
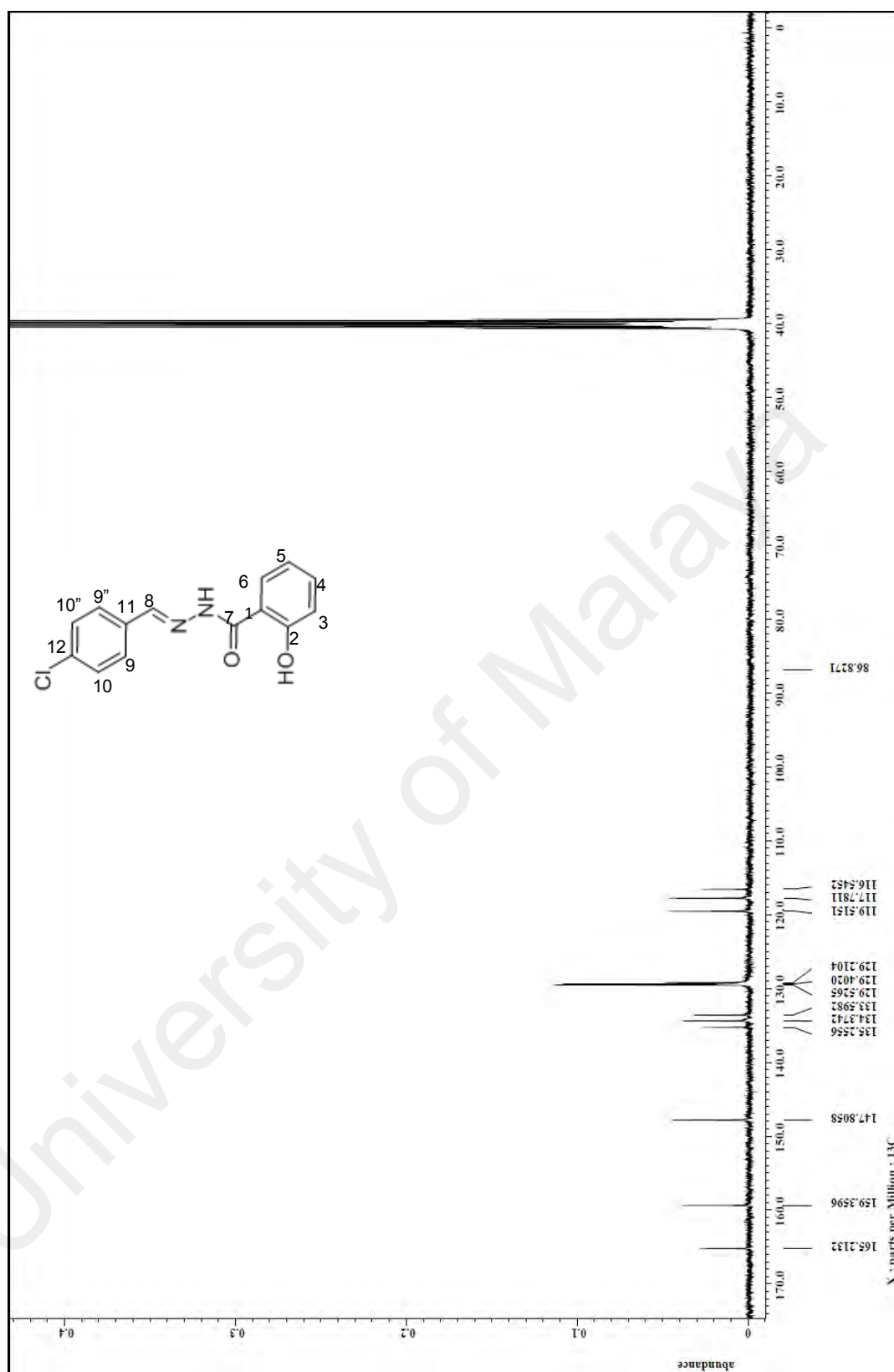
Figure B. 22: ^{13}C spectrum (CDCl$_3$, 400MHz) of **1a**
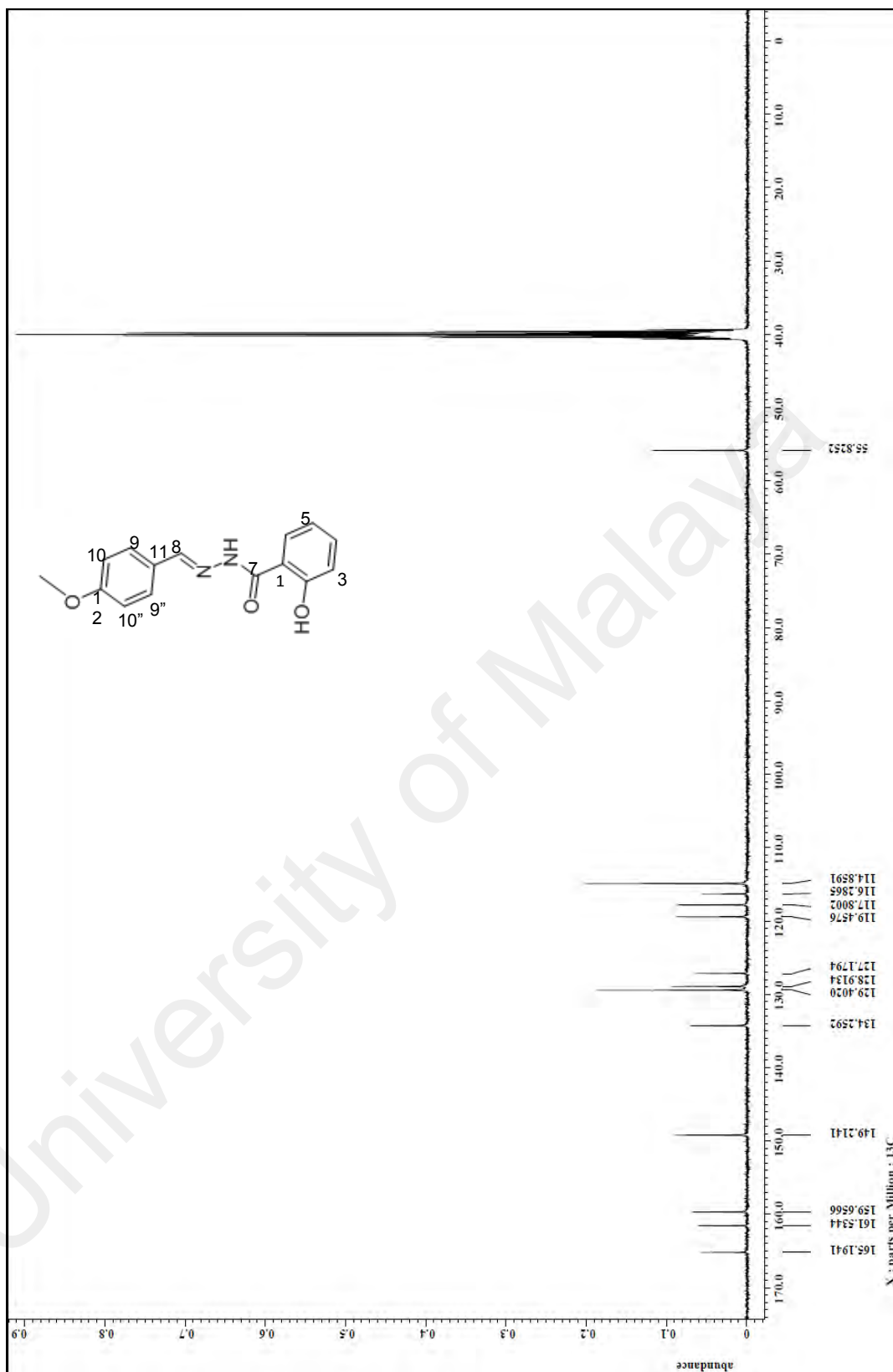
Figure B. 23: ^{13}C spectrum (CDCl$_3$, 400MHz) of **1b**
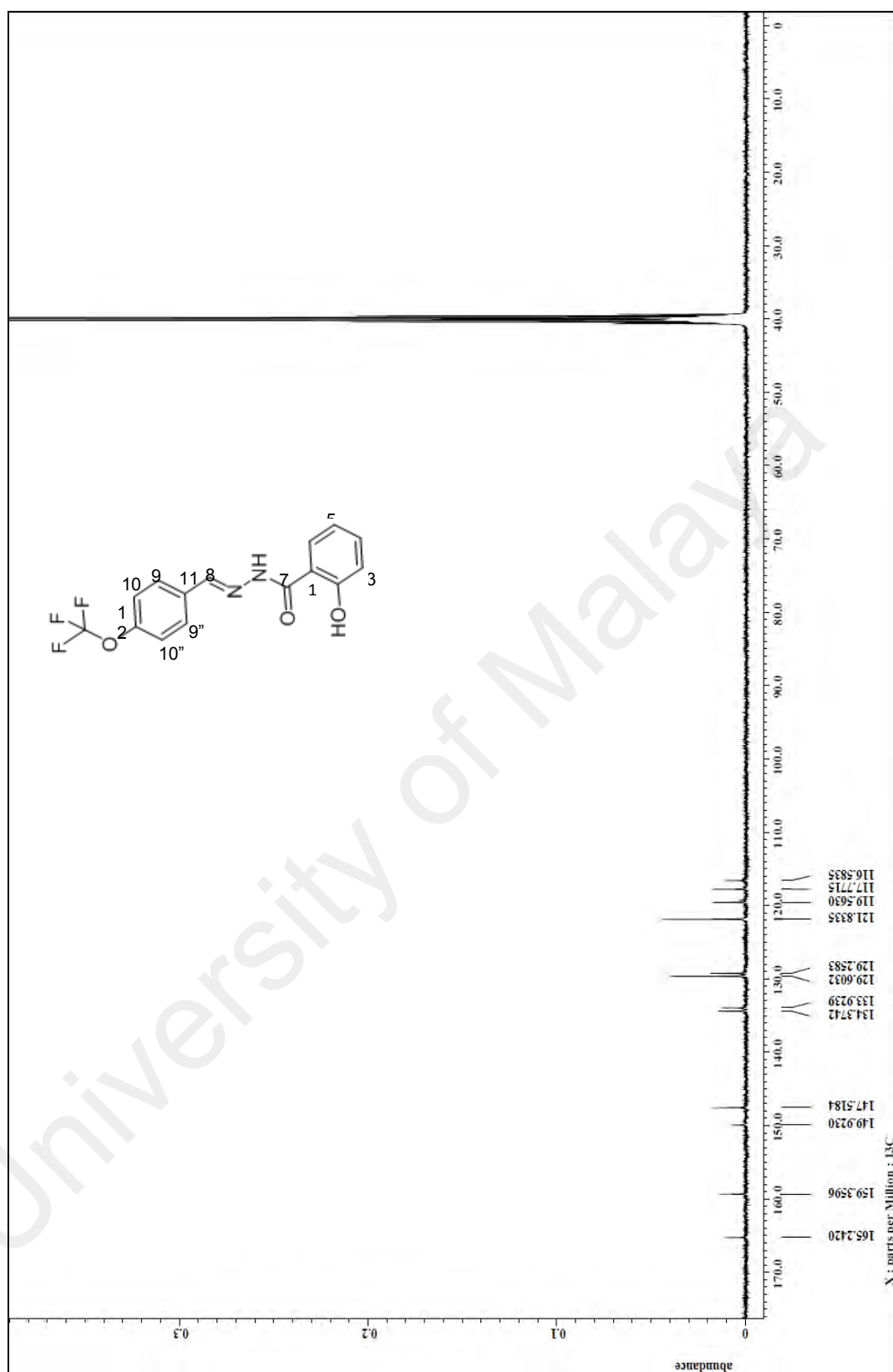
Figure B. 24: ^{13}C spectrum (CDCl$_3$, 400MHz) of **1c**
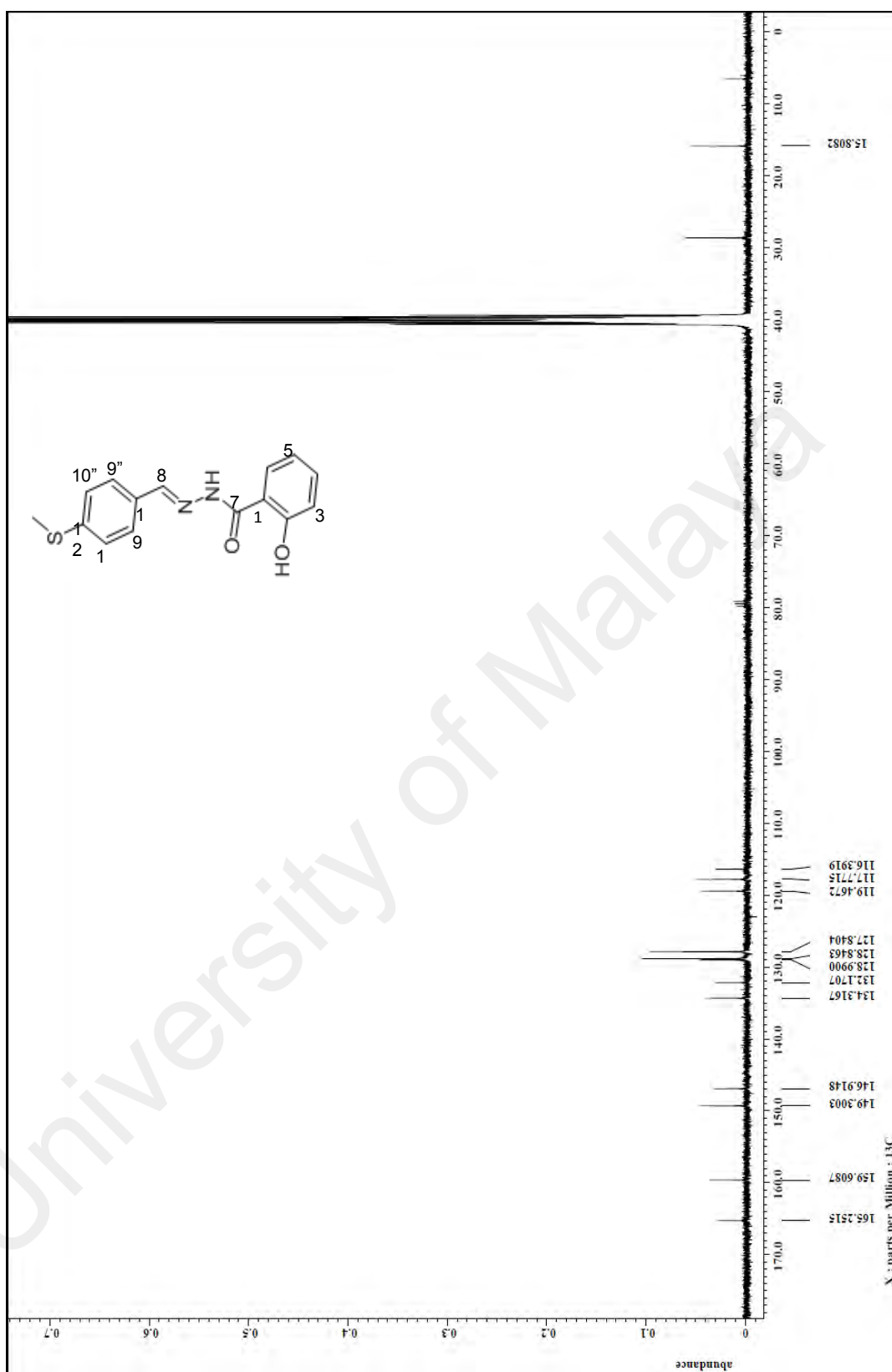
Figure B. 25: ^{13}C spectrum (CDCl$_3$, 400MHz) of **1d**
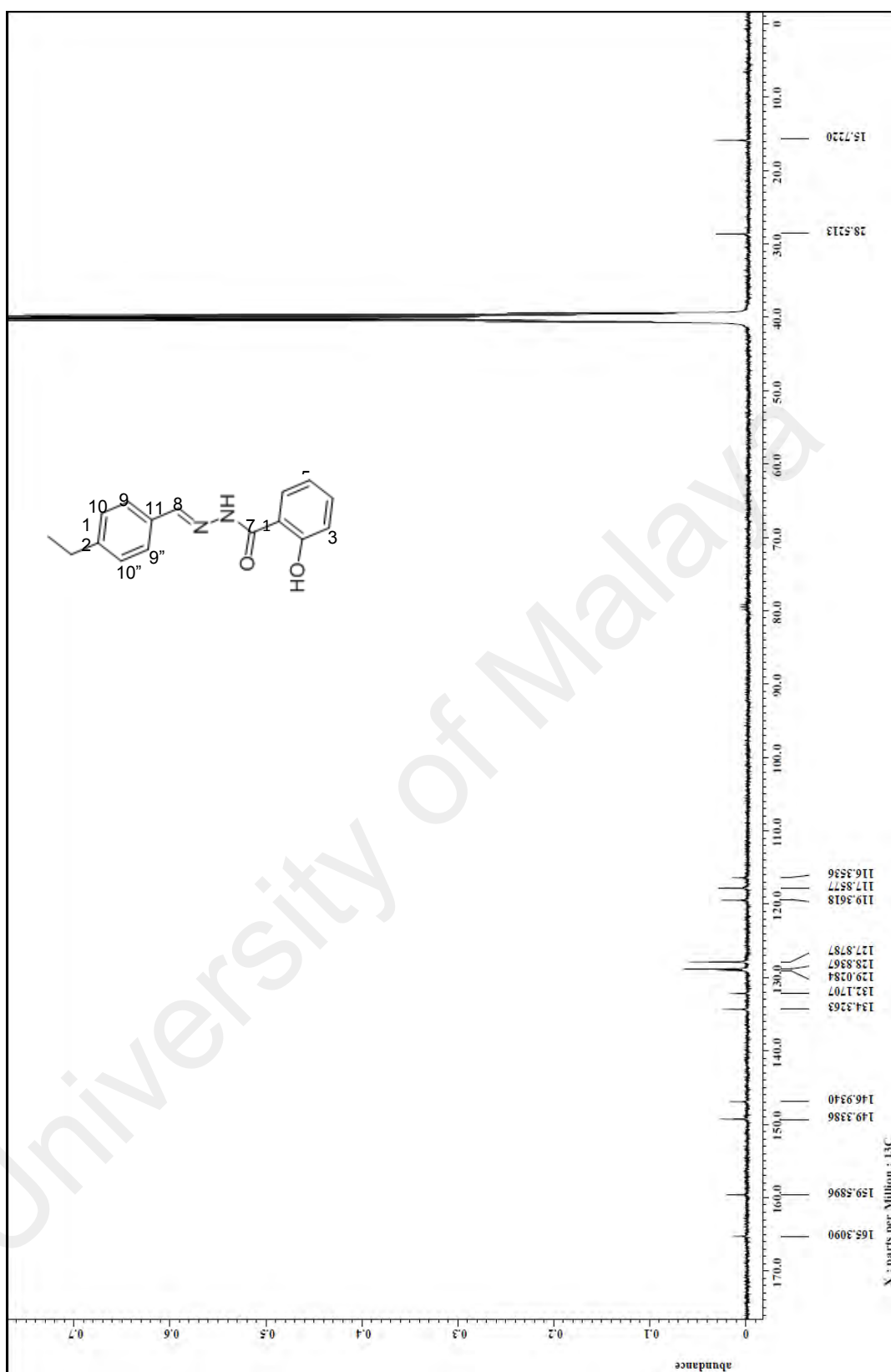
Figure B. 26: ^{13}C spectrum (CDCl$_3$, 400MHz) of **1e**
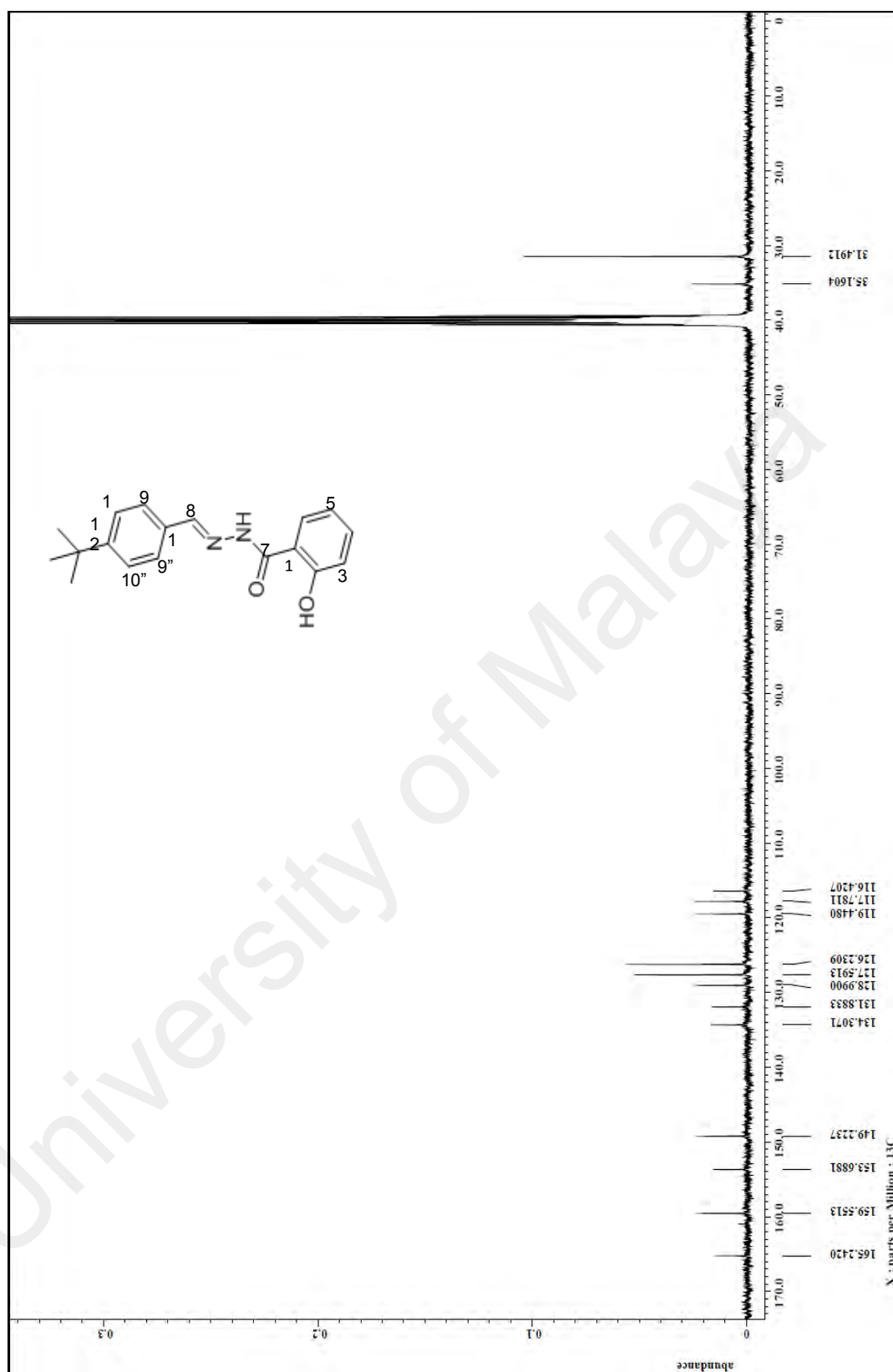
Figure B. 27: ^{13}C spectrum (CDCl$_3$, 400MHz) of **1f**
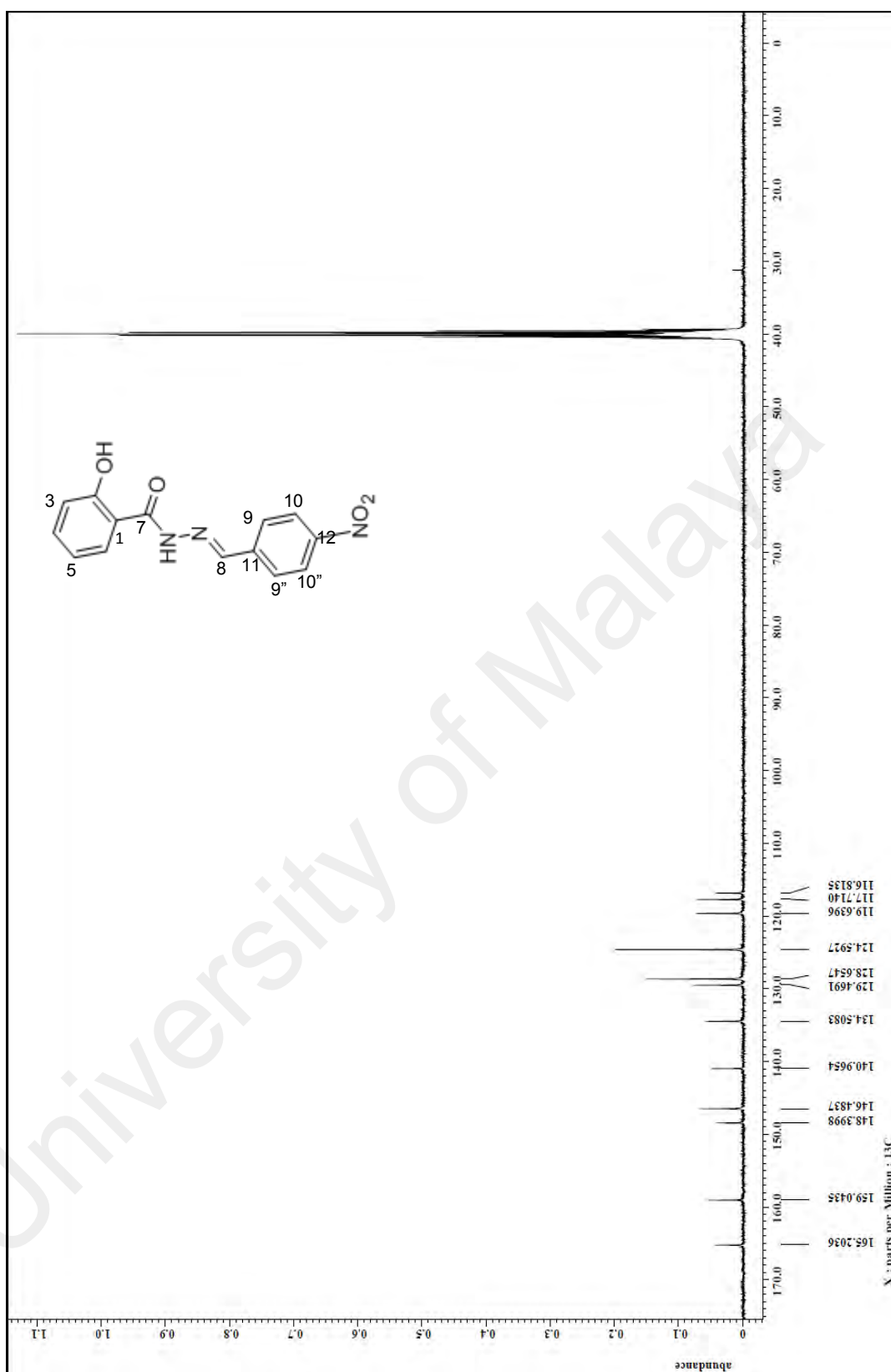
Figure B. 28: ^{13}C spectrum (CDCl$_3$, 400MHz) of **1g**
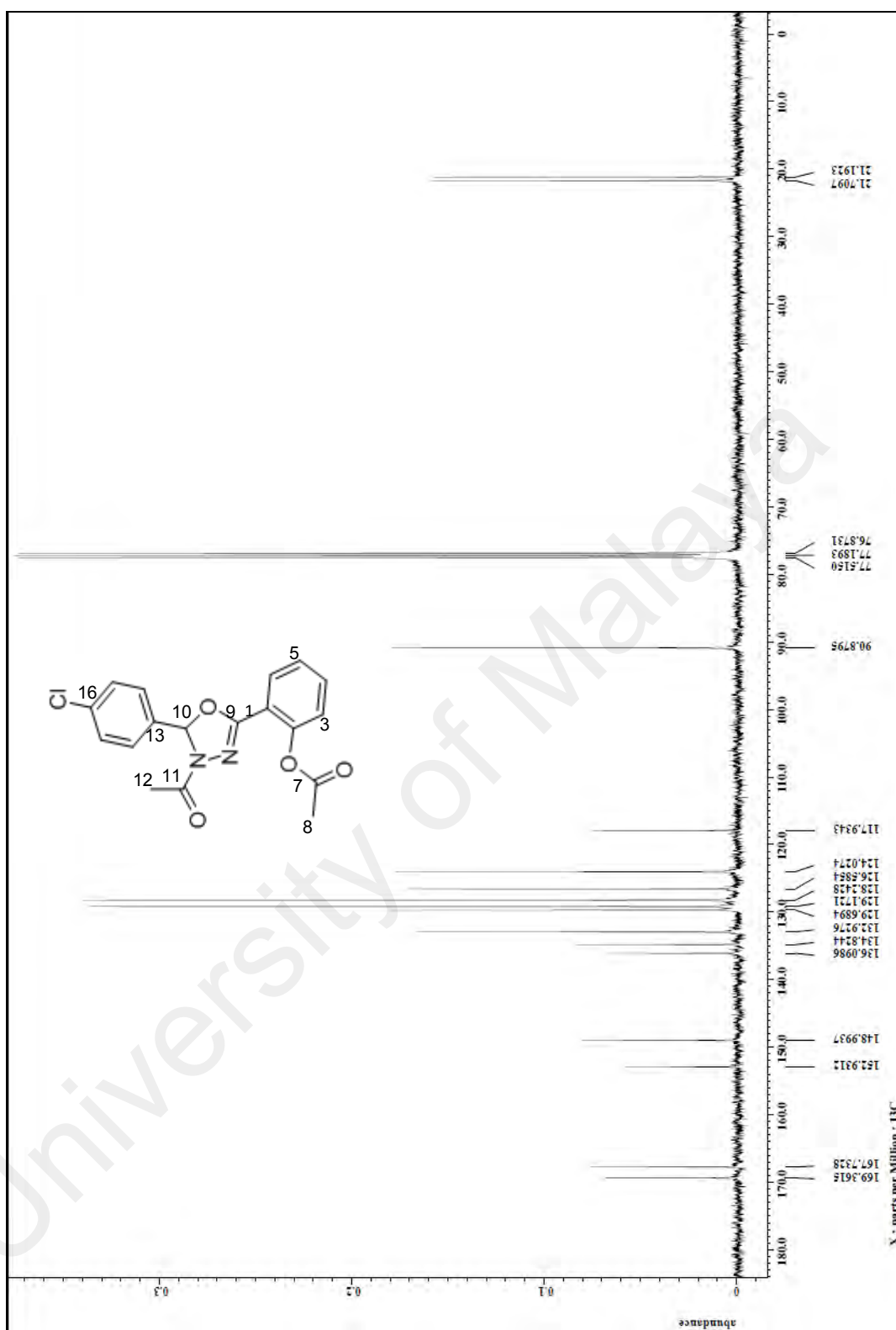
Figure B. 29: ^{13}C spectrum (CDCl$_3$, 400MHz) of **3a**
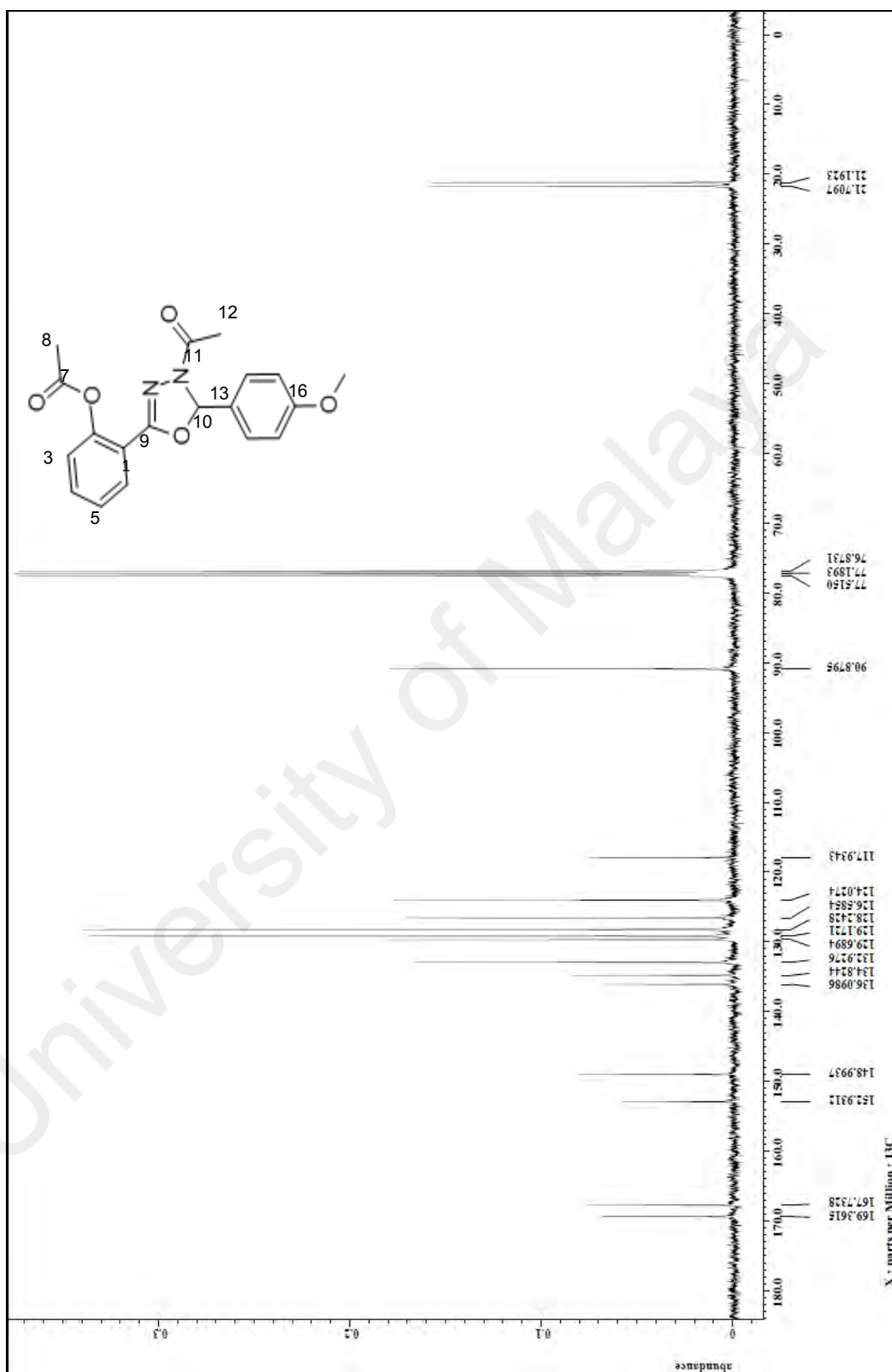
Figure B. 29: ^{13}C spectrum (CDCl$_3$, 400MHz) of **3b**
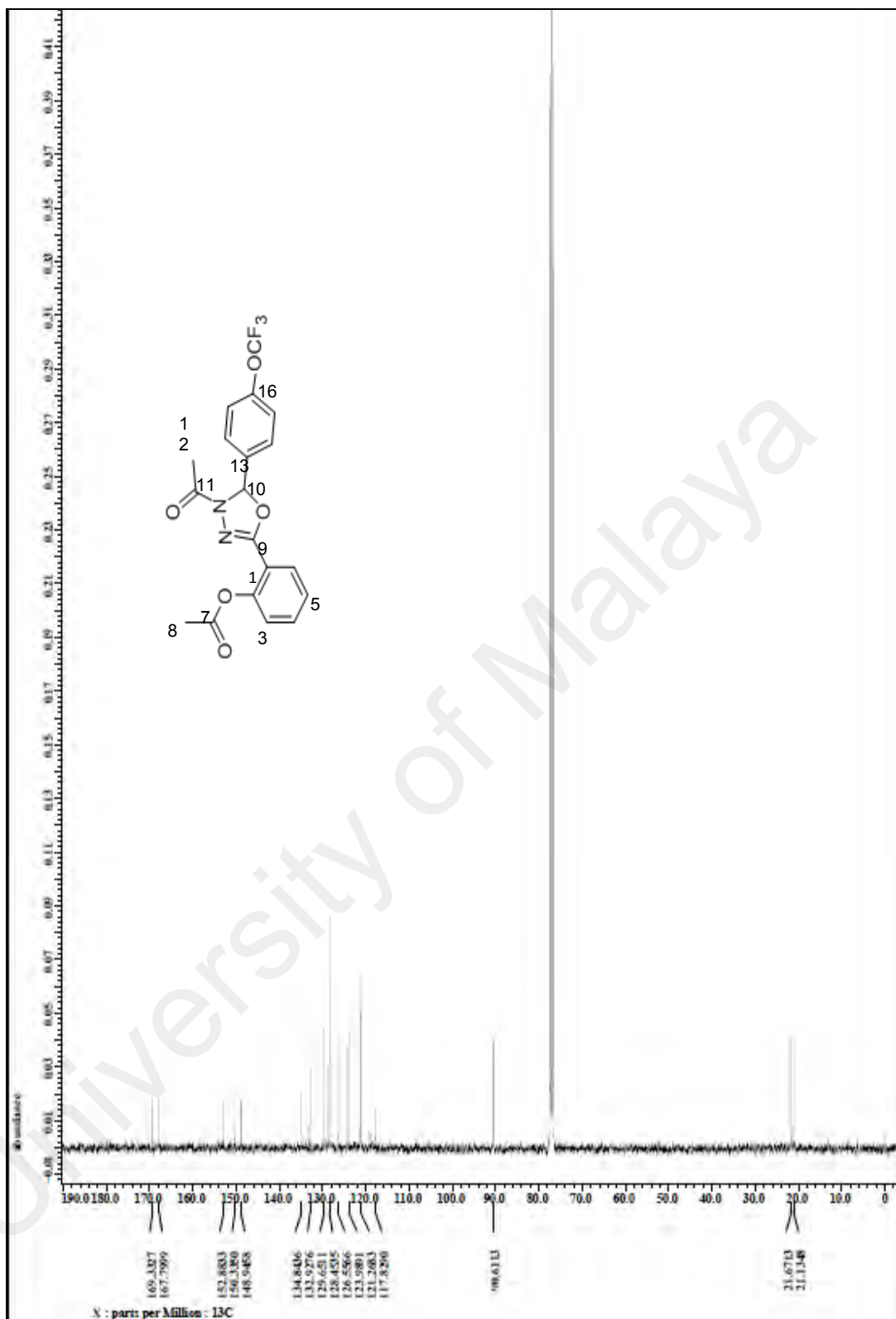
Figure B. 30: ^{13}C spectrum (CDCl$_3$, 400MHz) of **3c**
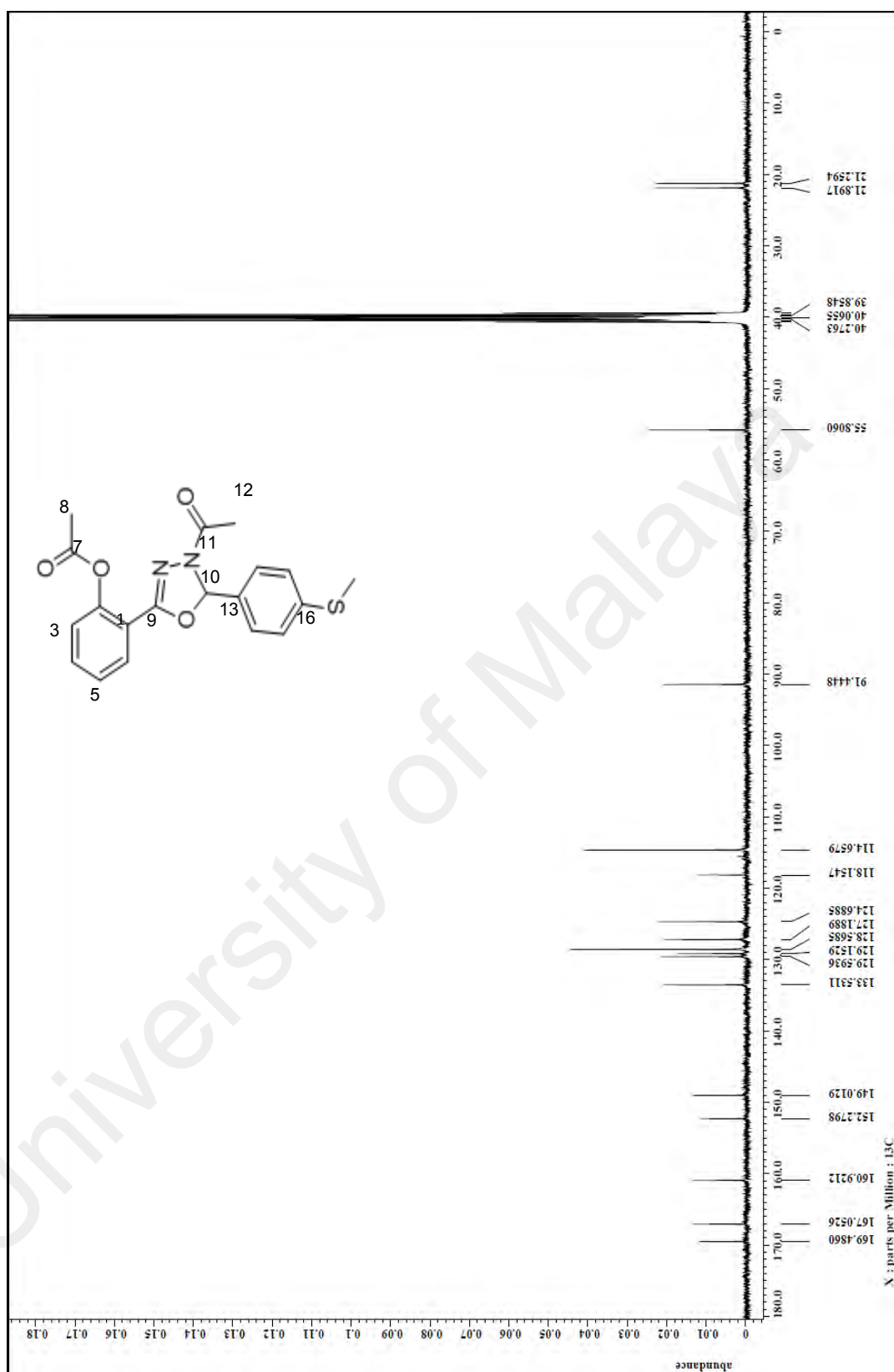
Figure B. 31: ^{13}C spectrum (CDCl$_3$, 400MHz) of **3d**
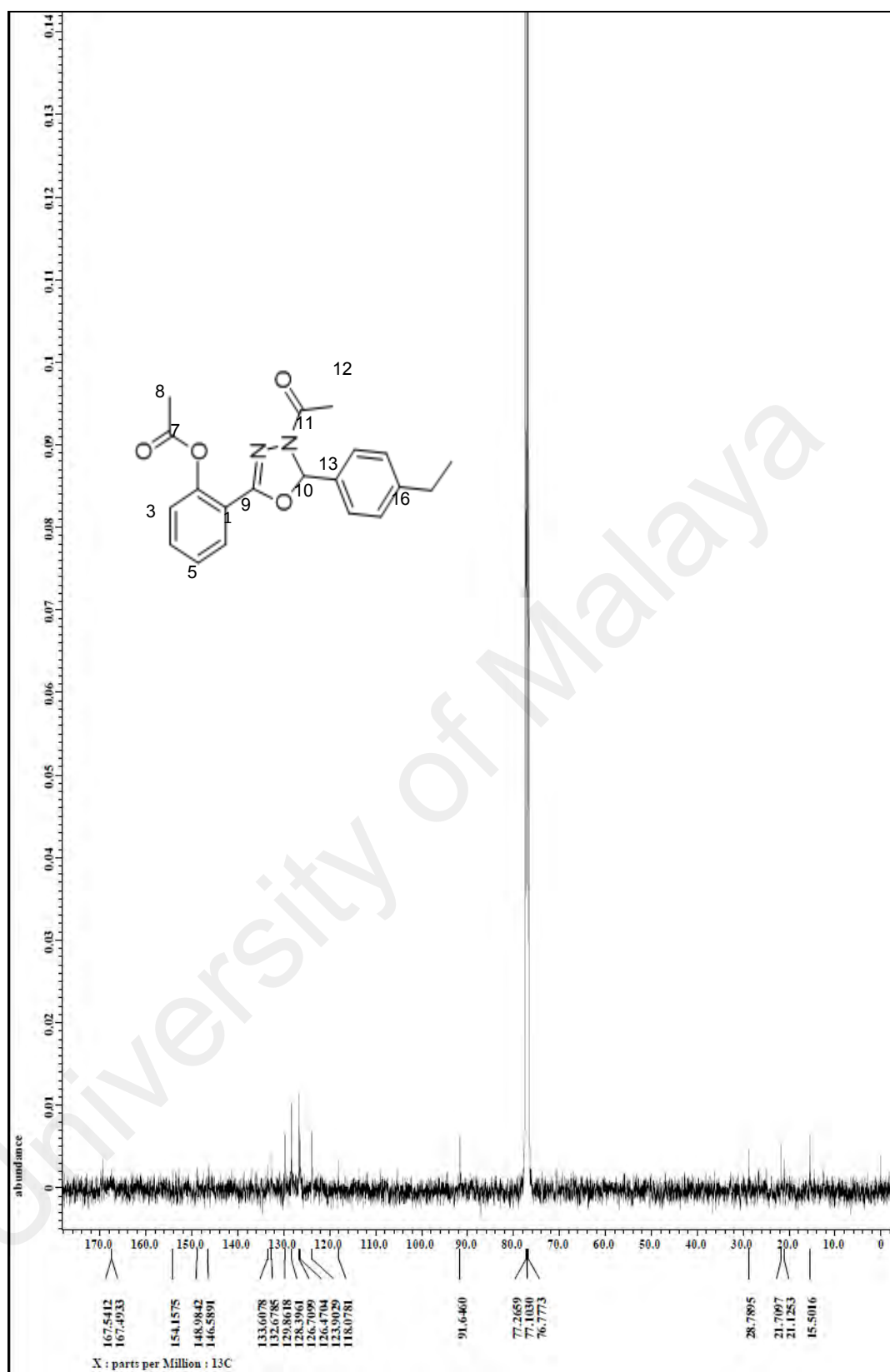
Figure B. 32: ^{13}C spectrum (CDCl$_3$, 400MHz) of **3e**
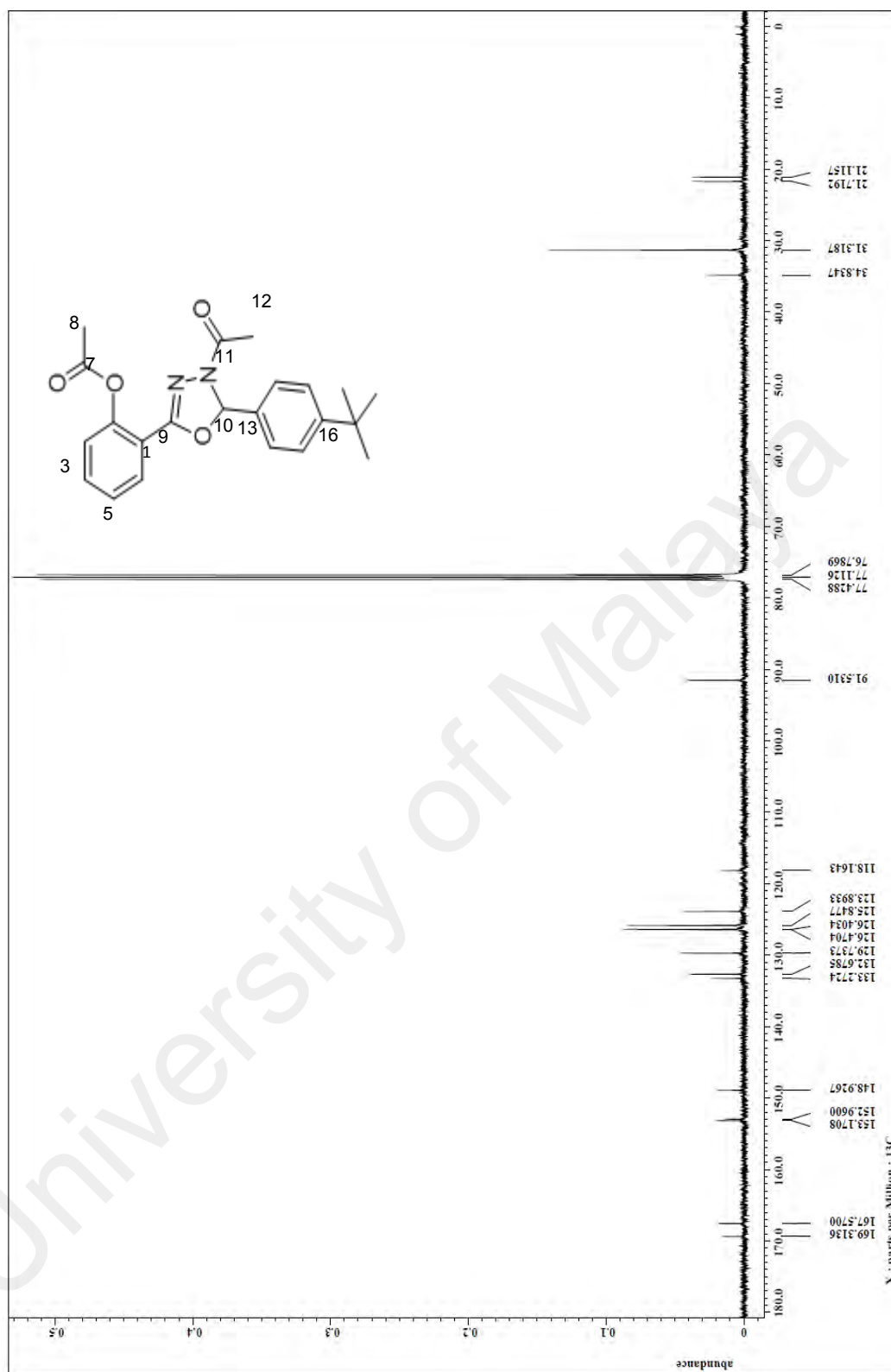
Figure B. 33: ^{13}C spectrum (CDCl$_3$, 400MHz) of **3f**
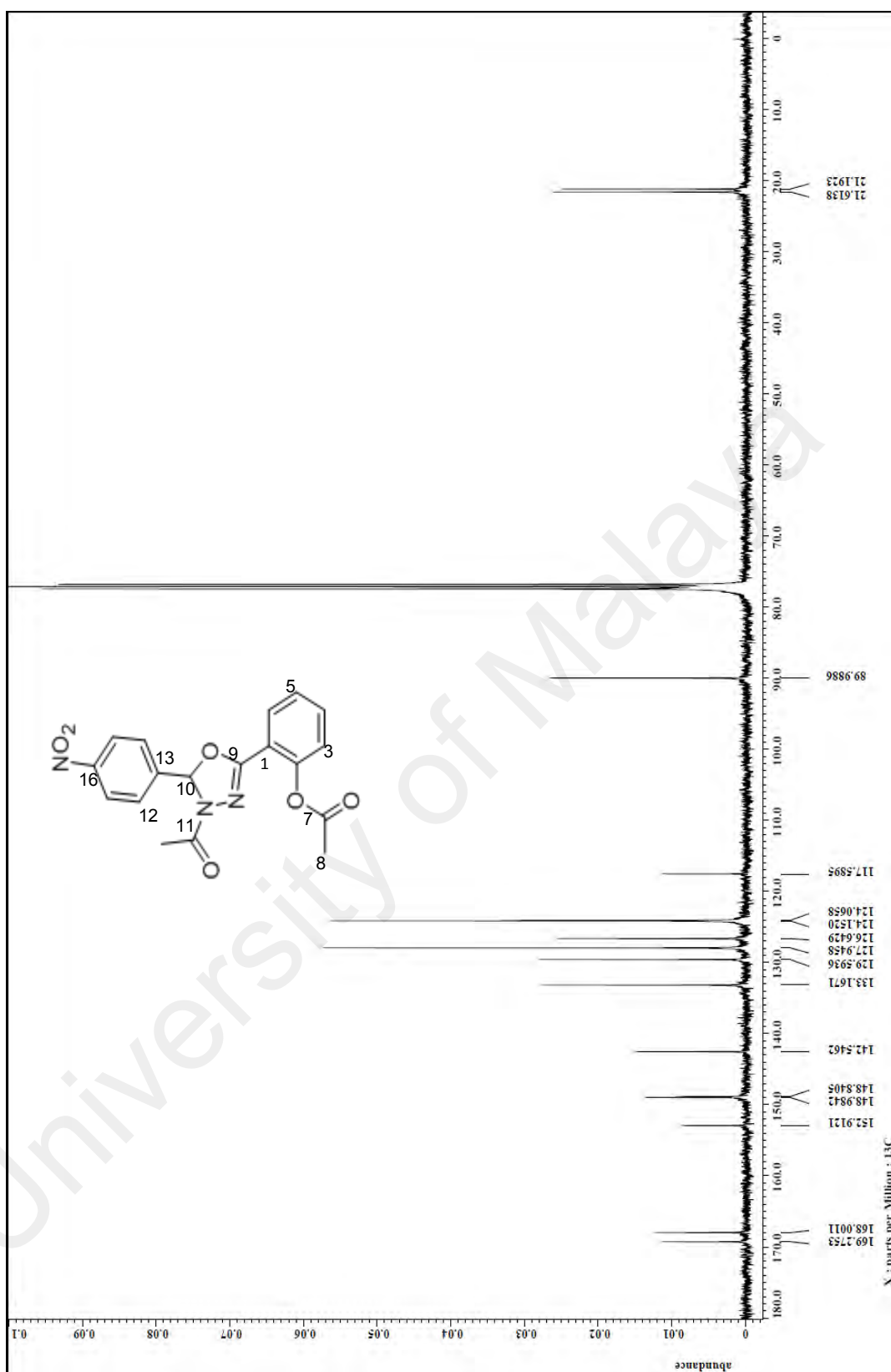
Figure B. 34: ¹³C spectrum (CDCl_{3,} 400MHz) of **3g**
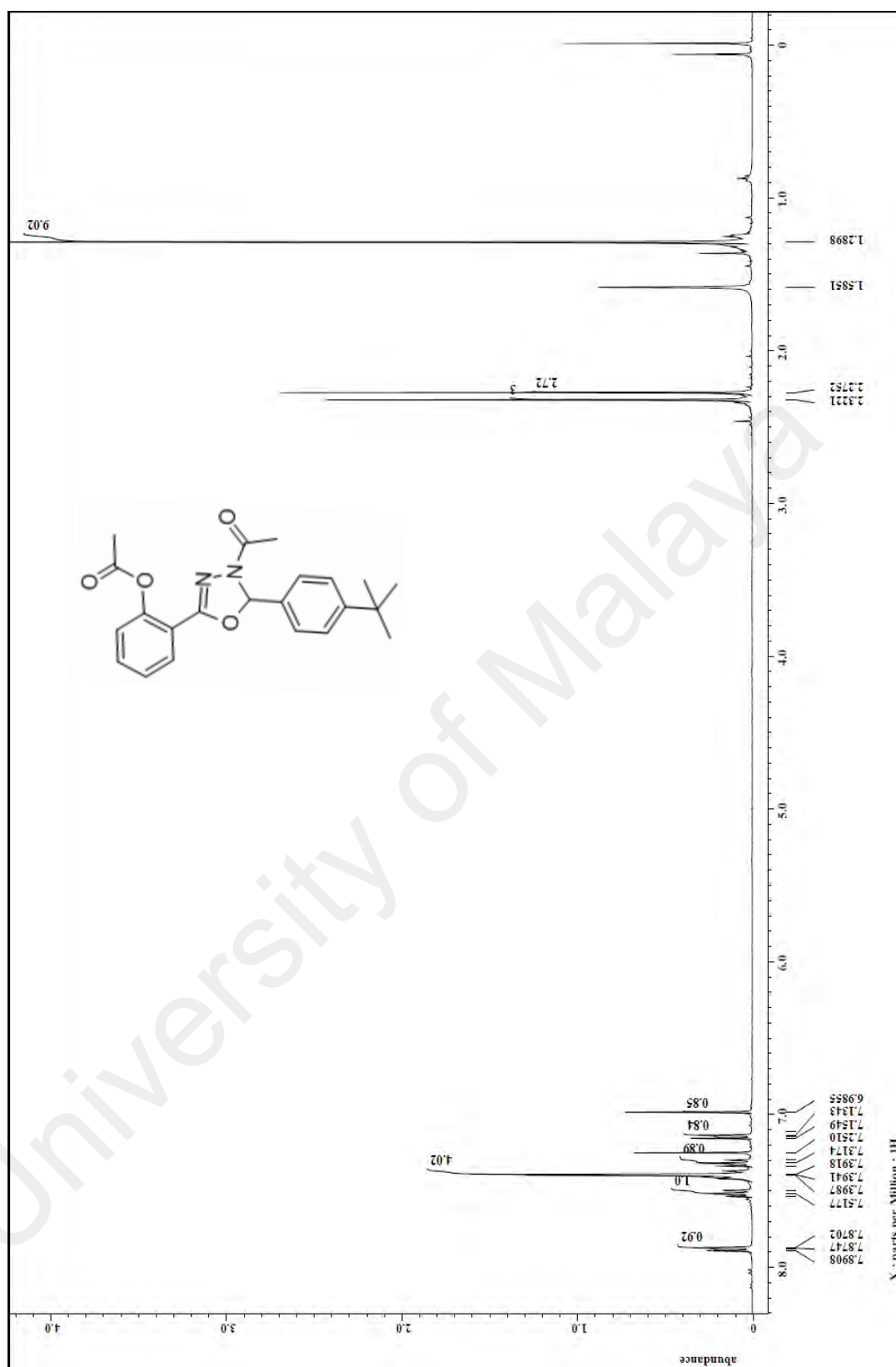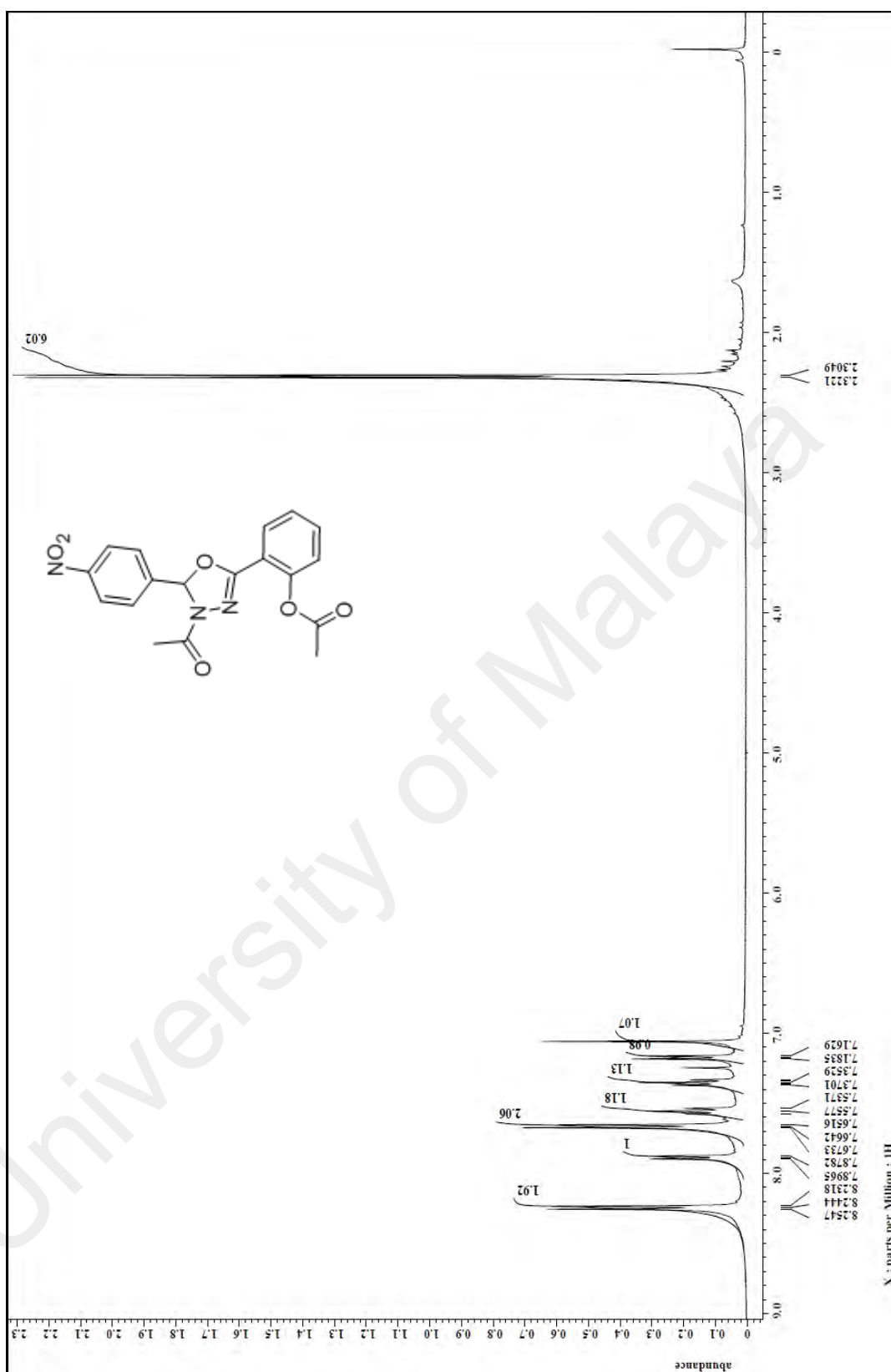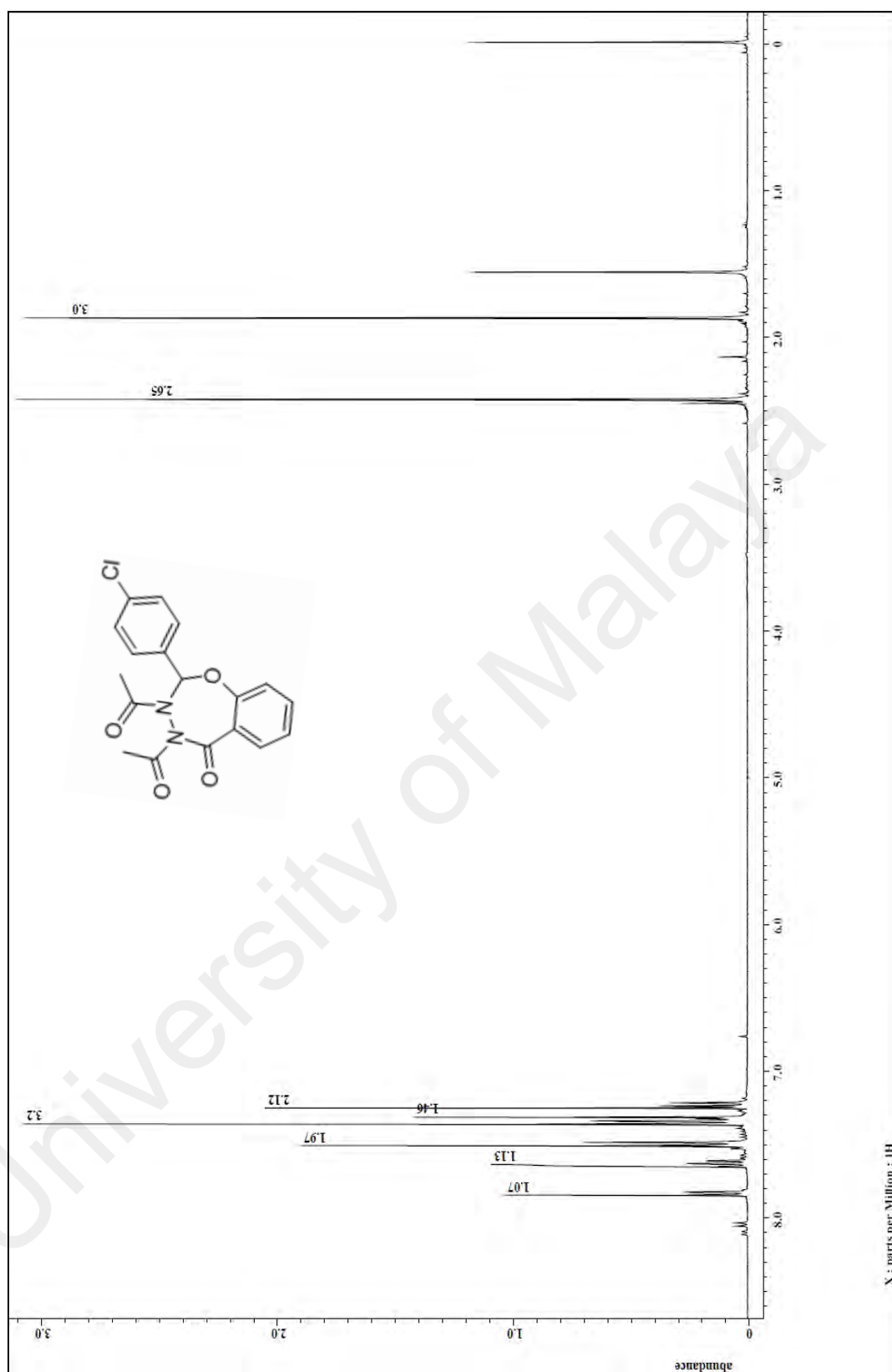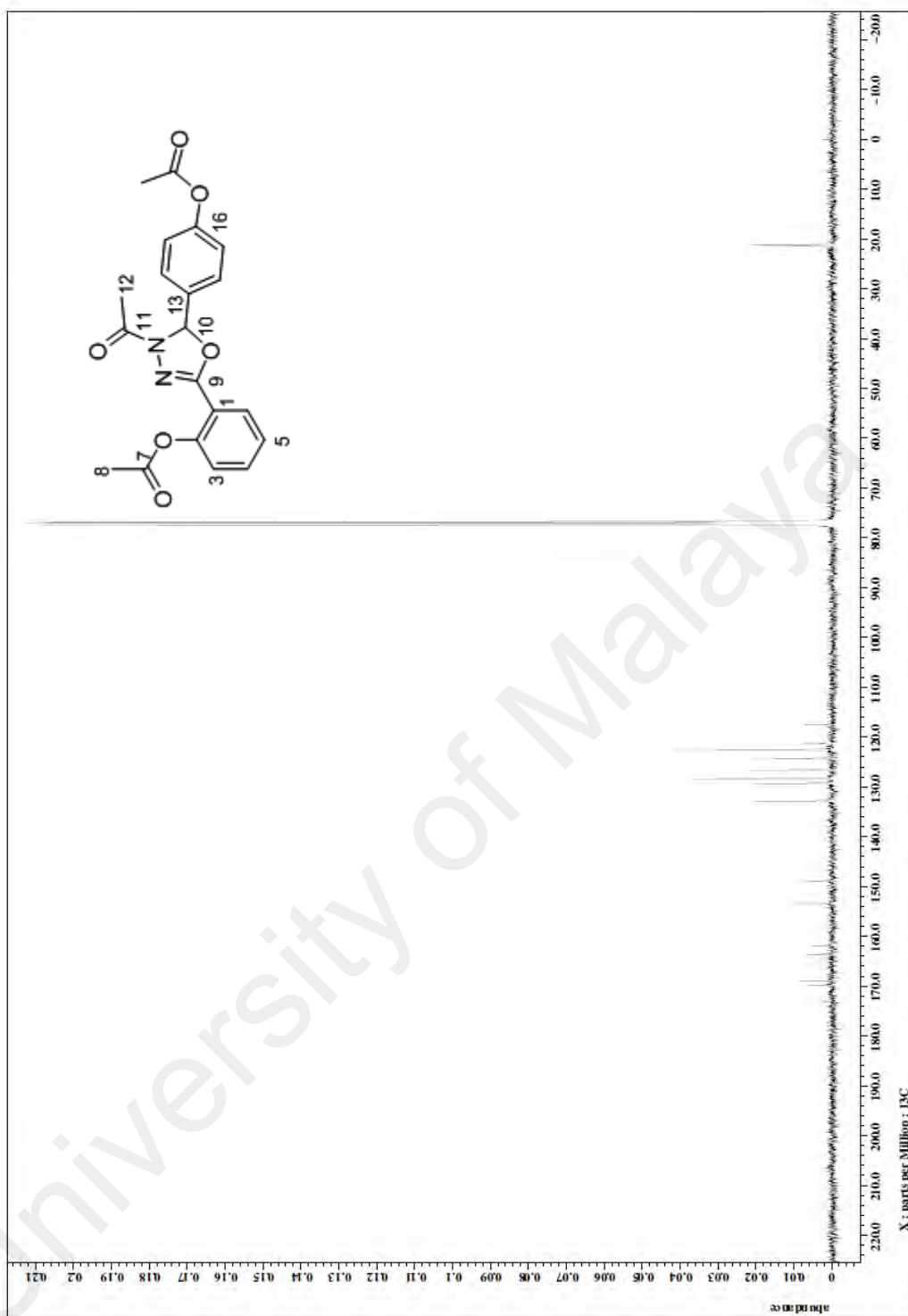
Figure B. 35: ^{13}C spectrum (CDCl$_3$, 400MHz) of **3h**

Figure B. 36 : ^{13}C spectrum (CDCl$_3$, 400MHz) of **4a**
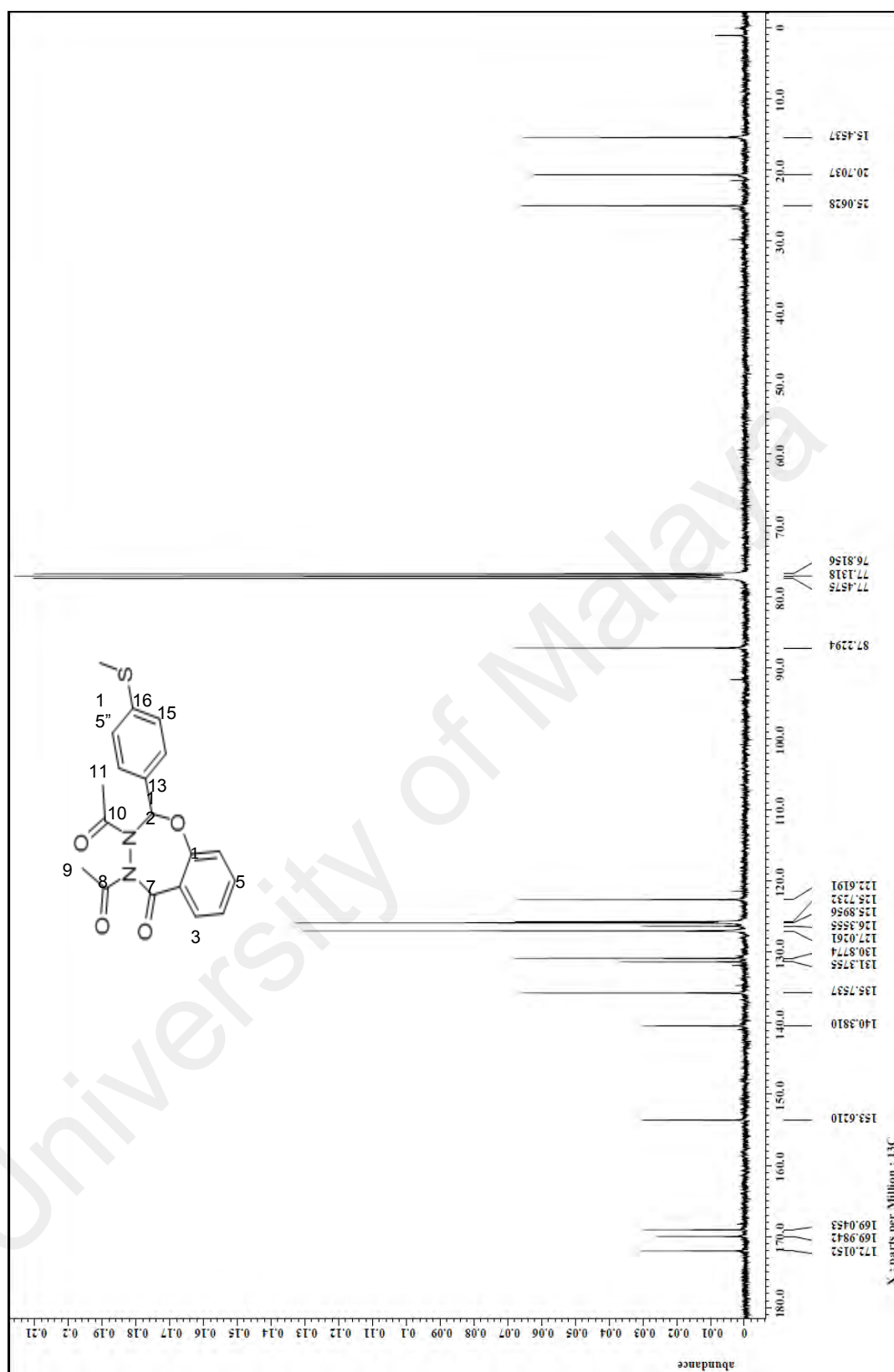
Figure B. 37 : ^{13}C spectrum (CDCl$_3$, 400MHz) of **4d**
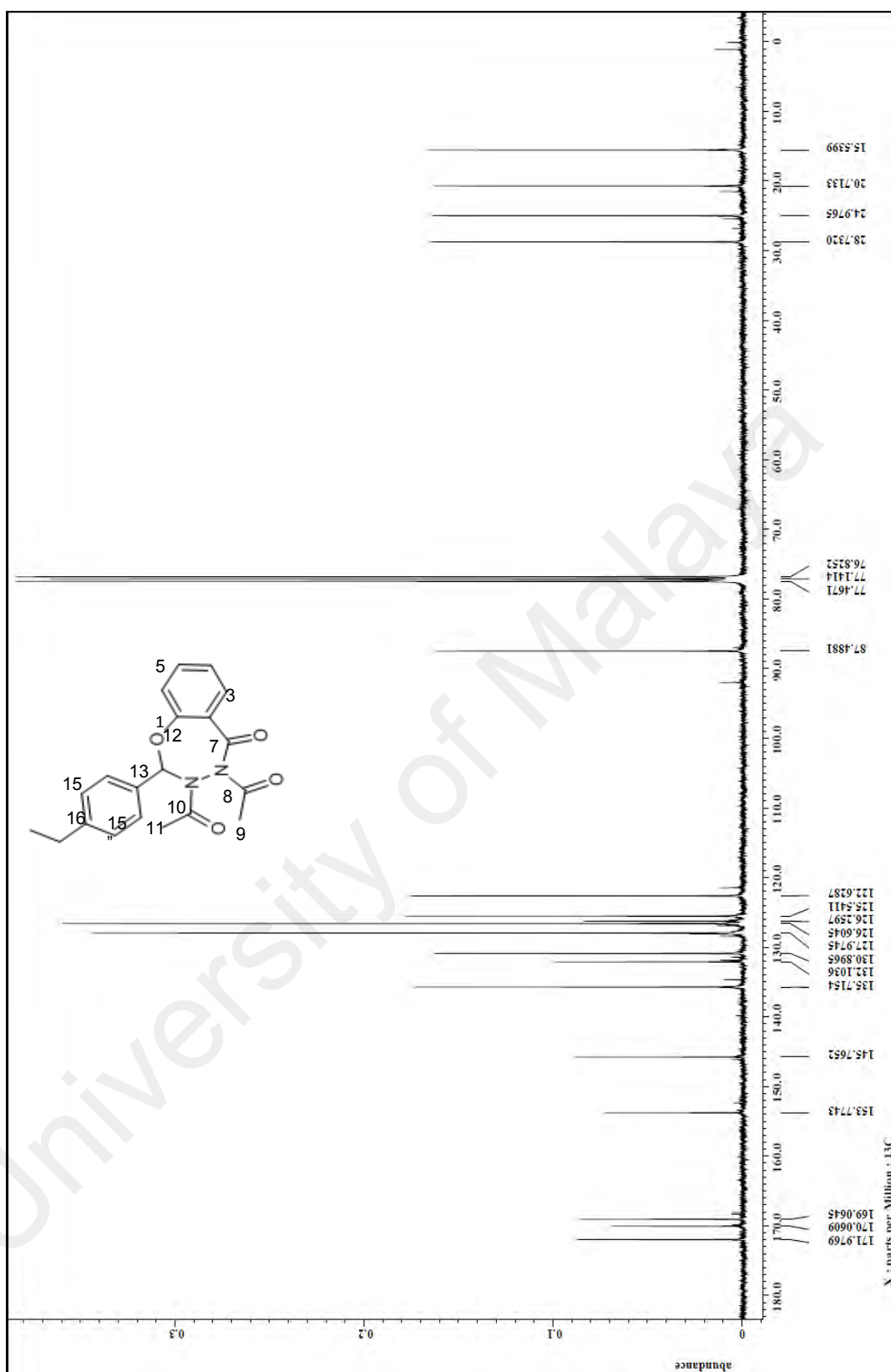
Figure B. 39 : ^{13}C spectrum (CDCl$_3$, 400MHz) of **4e**
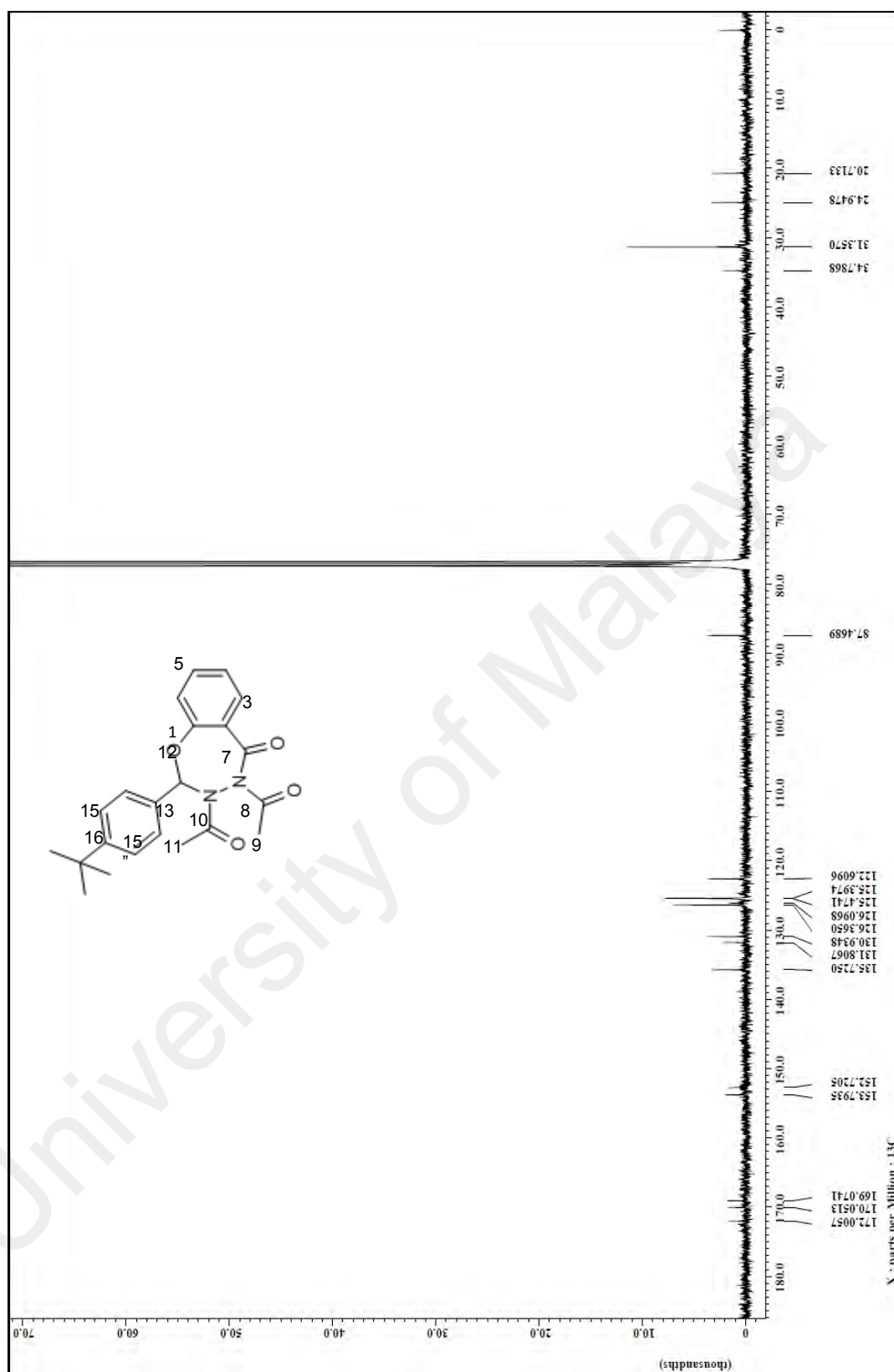
Figure B. 38 : ^{13}C spectrum (CDCl$_3$, 400MHz) of **4f**

X-RAY CRYSTALLOGRAPHIC DATA

Appendix C .1: X-ray Crystallographic Data of **3c**

Table 1: Crystal data and structure refinement for (**3c**)

Identification code	3C
Empirical formula	$C_{19}H_{15}F_3N_2O_5$
Formula weight	408.33
Temperature/K	100(2)
Crystal system	monoclinic
Space group	$P2_1/c$
a/Å	16.991(2)
b/Å	5.2923(7)
c/Å	40.845(5)
α/°	90
β/°	101.217(7)
γ/°	90
Volume/Å^3	3602.7(8)
Z	8
ρ_{calc}mg/mm^3	1.506
m/mm^{-1}	0.130
F(000)	1680.0
2Θ range for data collection	2.444 to 50.494°
Index ranges	$-20 \leq h \leq 19$, $-6 \leq k \leq 6$, $-9 \leq l \leq 49$
Reflections collected	18793
Independent reflections	6515[R(int) = 0.0759]
Data/restraints/parameters	6515/0/527
Goodness-of-fit on F^2	1.002
Final R indexes [I>=2σ (I)]	$R_1 = 0.0506$, $wR_2 = 0.0925$
Final R indexes [all data]	$R_1 = 0.1036$, $wR_2 = 0.1089$
Largest diff. peak/hole / e Å^{-3}	0.45/-0.35

Table 2 Fractional Atomic Coordinates ($\times 10^4$) and Equivalent Isotropic Displacement Parameters ($\text{Å}^2 \times 10^3$) for (**3C**). U_{eq} is defined as 1/3 of of the trace of the orthogonalised U_{IJ} tensor.

Atom	*x*	*y*	*z*	U(eq)
F1	4731.9(16)	-2937(4)	369.0(5)	76.8(8)
F2	3724.1(13)	-1341(5)	532.3(6)	68.3(7)
F3	3977.3(11)	-347(4)	54.3(5)	46.1(5)
O1	8418.0(12)	6481(4)	2774.0(5)	26.6(5)
O2	8243.9(11)	9105(3)	2331.0(5)	18.7(5)
O3	7576.8(10)	2459(3)	1745.1(4)	17.2(4)
O4	5522.8(11)	1185(4)	2100.6(5)	22.0(5)
O5	4744.7(13)	1118(4)	492.5(5)	35.5(6)
N1	7167.1(13)	5210(4)	2098.2(6)	17.3(5)
N2	6532.5(12)	3508(4)	1982.8(5)	15.0(5)
C1	7507.1(17)	9987(6)	2746.9(7)	23.0(7)
C2	8099.7(16)	8295(5)	2631.2(7)	18.3(7)
C3	8783.4(16)	7722(5)	2180.3(7)	17.9(7)
C4	9547.2(16)	8707(5)	2201.0(7)	19.4(7)
C5	10084.8(17)	7529(6)	2034.7(7)	21.3(7)
C6	9860.1(17)	5357(5)	1850.8(7)	20.8(7)
C7	9098.3(16)	4385(5)	1830.0(7)	17.7(6)
C8	8542.2(16)	5544(5)	1993.9(7)	15.8(6)
C9	7738.5(16)	4485(5)	1956.6(7)	14.4(6)
C10	5945.2(16)	3075(6)	2163.5(7)	18.1(7)
C11	5855.1(16)	5015(5)	2419.9(7)	20.4(7)
C12	6786.2(15)	1561(5)	1766.4(7)	15.9(6)
C13	6256.3(16)	1384(5)	1424.9(7)	16.8(6)
C14	5709.5(16)	-559(5)	1357.1(7)	20.2(7)
C15	5189.2(17)	-733(6)	1052.3(8)	25.0(7)
C16	5239.7(17)	1051(6)	812.6(7)	24.0(7)
C17	5792.9(17)	2990(6)	871.6(8)	25.3(7)
C18	6292.3(17)	3157(5)	1180.4(7)	22.1(7)
C19	4313(2)	-869(7)	367.3(9)	39.1(9)
F4	2231.7(10)	1975(3)	-1342.1(4)	29.1(4)
F5	1693.6(12)	4482(3)	-1035.6(4)	41.1(5)
F6	1258.0(11)	720(4)	-1116.6(5)	46.0(6)
O6	1448.7(11)	6880(4)	1539.0(5)	23.0(5)
O7	2184.7(11)	9542(3)	1287.6(5)	18.4(5)
O8	2479.8(10)	2916(3)	721.5(4)	18.0(5)
O9	146.2(11)	2419(4)	256.4(5)	24.2(5)
O10	2481.0(11)	1332(4)	-811.5(5)	22.9(5)

N3	1603.3(13)	5980(4)	789.7(6)	16.1(5)
N4	1242.0(13)	4416(4)	522.5(6)	16.8(5)
C20	844.2(17)	10695(5)	1280.5(8)	25.5(7)
C21	1492.3(17)	8798(6)	1387.4(7)	19.1(7)
C22	2847.2(16)	7908(5)	1365.9(7)	17.7(7)
C23	3437.7(17)	8561(5)	1634.7(7)	20.5(7)
C24	4116.0(17)	7079(6)	1717.1(7)	24.6(7)
C25	4203.9(17)	4952(6)	1529.8(7)	24.0(7)
C26	3617.0(16)	4325(6)	1257.8(7)	20.0(7)
C27	2919.0(16)	5788(5)	1172.0(7)	16.3(6)
C28	2299.3(16)	4995(5)	889.8(7)	15.8(6)
C29	419.6(16)	4220(5)	430.0(7)	18.0(6)
C30	-72.5(16)	6245(5)	545.1(8)	22.9(7)
C31	1767.1(16)	2271(5)	482.9(7)	18.2(7)
C32	1960.7(15)	2024(5)	140.3(7)	16.0(6)
C33	1644.4(16)	11(5)	-61.8(7)	18.4(7)
C34	1809.9(16)	-230(5)	-380.1(7)	20.2(7)
C35	2280.9(16)	1569(5)	-489.6(7)	18.7(7)
C36	2600.5(16)	3583(6)	-294.9(7)	21.5(7)
C37	2437.2(16)	3800(6)	22.8(7)	20.5(7)
C38	1920.5(18)	2104(6)	-1069.4(8)	24.6(7)

Table 3 Anisotropic Displacement Parameters ($Å^2 \times 10^3$) for (**3C**). The Anisotropic displacement factor exponent takes the form: $-2\pi^2[h^2a^{*2}U_{11}+...+2hka \times b \times U_{12}]$

Atom	U_{11}	U_{22}	U_{33}	U_{23}	U_{13}	U_{12}
F1	114(2)	48.7(15)	46.4(15)	-21.3(12)	-37.0(13)	44.0(14)
F2	43.4(13)	101(2)	52.5(15)	12.1(14)	-11.1(11)	-27.4(13)
F3	50.5(12)	49.5(13)	27.8(11)	-6.1(10)	-18.8(9)	12.7(10)
O1	29.6(12)	26.7(13)	22.6(12)	4.2(10)	3.1(10)	11.1(10)
O2	20.4(11)	15.8(11)	19.4(11)	-2.6(9)	2.7(9)	2.6(8)
O3	13.4(10)	17.3(10)	21.5(11)	-6.0(9)	5.1(8)	-2.5(8)
O4	17.1(11)	22.3(12)	27.1(12)	1.7(9)	5.7(9)	-4.8(9)
O5	39.1(14)	33.3(14)	26.3(13)	0.9(11)	-13.3(11)	-6.9(11)
N1	15.3(12)	16.4(13)	19.7(13)	-1.4(11)	2.4(10)	-1.3(10)
N2	12.0(12)	17.5(13)	16.1(13)	-5.8(10)	3.8(10)	-4(1)
C1	23.2(16)	23.2(17)	21.0(17)	-3.8(14)	-0.1(13)	5.0(14)
C2	18.0(15)	20.4(17)	15.1(16)	-2.2(14)	-0.5(13)	-2.5(14)
C3	20.2(16)	17.1(16)	16.0(16)	2.0(13)	2.3(12)	2.4(13)
C4	23.9(16)	17.0(16)	14.9(16)	-0.1(13)	-2.2(13)	-4.4(13)
C5	15.7(15)	25.8(17)	21.3(17)	5.3(14)	1.2(13)	-4.2(13)
C6	20.7(16)	22.2(17)	20.9(17)	3.2(14)	7.7(13)	2.2(13)

205

C7	18.4(15)	19.6(16)	15.6(16)	1.1(13)	4.8(12)	1.8(13)
C8	16.3(15)	13.9(15)	16.0(15)	3.5(13)	0.6(12)	-1.2(12)
C9	17.0(15)	11.0(15)	14.5(15)	-0.7(12)	1.2(12)	4.0(12)
C10	13.4(15)	24.4(18)	15.4(16)	5.9(14)	0.1(12)	6.2(14)
C11	17.5(15)	23.3(17)	22.4(17)	-0.6(14)	8.9(13)	3.0(13)
C12	13.6(14)	16.5(16)	18.2(16)	-2.0(13)	4.5(12)	-1.8(12)
C13	16.0(15)	15.0(15)	20.2(17)	-1.0(13)	5.2(13)	0.3(12)
C14	23.1(16)	20.6(17)	17.1(16)	2.8(13)	4.9(13)	-2.5(14)
C15	22.8(17)	23.0(18)	27.4(19)	-1.3(15)	0.5(14)	-7.1(14)
C16	22.5(17)	27.0(18)	19.9(17)	-0.8(15)	-2.7(13)	2.4(14)
C17	27.0(17)	21.9(18)	26.4(19)	8.2(14)	3.9(14)	-0.2(14)
C18	19.0(16)	20.5(17)	25.9(18)	-3.2(14)	1.9(14)	-3.1(13)
C19	44(2)	39(2)	30(2)	-3.5(18)	-6.1(18)	10.7(19)
F4	37.8(11)	33.2(11)	18.2(10)	-0.7(8)	10.1(8)	6.2(8)
F5	61.5(13)	36.2(12)	25.4(11)	3.1(9)	7.8(9)	26.9(10)
F6	34.8(11)	70.1(15)	29.7(12)	4.7(10)	-1.8(9)	-21.2(11)
O6	23.9(11)	23.0(12)	23.5(12)	4.3(10)	8.2(9)	-3.0(9)
O7	18.1(10)	16.8(11)	20.9(11)	0.7(9)	5.1(9)	-3.4(9)
O8	16.5(10)	20.6(11)	15.2(11)	-2.3(9)	-1.0(8)	2.7(9)
O9	19.4(11)	22.0(12)	28.7(13)	-2.3(10)	-1.1(9)	-4.6(9)
O10	22.5(11)	32.4(12)	13.8(11)	0.7(9)	3.6(9)	8.6(9)
N3	17.2(13)	14.5(13)	15.1(13)	-0.2(10)	-0.3(10)	-2.4(10)
N4	13.4(12)	16.4(13)	19.9(14)	-3.5(11)	1.9(10)	-1(1)
C20	25.2(17)	21.7(17)	31.3(19)	-0.9(15)	9.7(14)	3.8(14)
C21	21.5(16)	21.2(17)	15.6(16)	-6.6(14)	6.2(13)	-1.3(13)
C22	17.3(15)	20.4(16)	16.9(16)	2.5(13)	6.7(13)	-1.6(13)
C23	23.8(17)	21.9(17)	15.9(16)	-2.6(13)	4.4(13)	-9.2(14)
C24	19.5(16)	34.0(19)	18.2(17)	0.1(15)	-1.8(13)	-12.0(15)
C25	18.0(16)	28.5(18)	23.4(18)	3.8(15)	-0.9(13)	-0.5(14)
C26	18.6(15)	22.3(17)	19.5(17)	4.2(14)	5.0(13)	-0.7(13)
C27	17.1(15)	17.2(16)	14.6(16)	3.3(13)	3.1(12)	-3.9(13)
C28	18.5(15)	14.4(15)	14.4(16)	1.4(13)	3.3(12)	-1.0(13)
C29	16.5(15)	18.5(16)	18.1(16)	5.3(14)	1.2(12)	-2.0(13)
C30	15.9(15)	22.6(17)	30.0(18)	-1.8(14)	4.0(13)	1.7(13)
C31	16.0(15)	15.8(16)	21.1(17)	-2.1(13)	-0.9(12)	0.4(12)
C32	13.0(14)	16.4(16)	17.7(16)	0.7(13)	0.6(12)	2.3(12)
C33	17.7(15)	17.6(16)	18.8(17)	1.0(13)	0.9(12)	-0.6(13)
C34	21.2(16)	17.9(16)	19.2(17)	-3.1(13)	-1.5(13)	-0.1(13)
C35	18.3(15)	23.7(17)	14.7(16)	0.5(13)	5.0(12)	7.8(13)
C36	18.7(16)	23.6(17)	22.8(17)	4.6(14)	5.1(13)	-3.9(13)
C37	20.4(16)	22.3(17)	17.8(17)	-0.7(13)	1.5(13)	-1.0(13)
C38	26.3(17)	27.1(19)	21.3(18)	-2.1(15)	7.1(14)	-0.3(15)

Table 4 Bond Lengths for **3c**

Atom	Atom	Length/Å	Atom	Atom	Length/Å
F1	C19	1.304(4)	F4	C38	1.325(3)
F2	C19	1.335(4)	F5	C38	1.331(3)
F3	C19	1.324(4)	F6	C38	1.325(3)
O1	C2	1.196(3)	O6	C21	1.199(3)
O2	C2	1.365(3)	O7	C21	1.376(3)
O2	C3	1.405(3)	O7	C22	1.406(3)
O3	C9	1.371(3)	O8	C28	1.364(3)
O3	C12	1.443(3)	O8	C31	1.440(3)
O4	C10	1.229(3)	O9	C29	1.224(3)
O5	C16	1.411(3)	O10	C35	1.427(3)
O5	C19	1.326(4)	O10	C38	1.339(3)
N1	N2	1.413(3)	N3	N4	1.411(3)
N1	C9	1.282(3)	N3	C28	1.284(3)
N2	C10	1.371(3)	N4	C29	1.379(3)
N2	C12	1.476(3)	N4	C31	1.472(3)
C1	C2	1.491(4)	C20	C21	1.491(4)
C3	C4	1.386(4)	C22	C23	1.379(4)
C3	C8	1.399(4)	C22	C27	1.392(4)
C4	C5	1.388(4)	C23	C24	1.381(4)
C5	C6	1.386(4)	C24	C25	1.385(4)
C6	C7	1.380(4)	C25	C26	1.381(4)
C7	C8	1.401(4)	C26	C27	1.403(4)
C8	C9	1.456(4)	C27	C28	1.463(4)
C10	C11	1.495(4)	C29	C30	1.491(4)
C12	C13	1.509(4)	C31	C32	1.504(4)
C13	C14	1.377(4)	C32	C33	1.390(4)
C13	C18	1.381(4)	C32	C37	1.386(4)
C14	C15	1.383(4)	C33	C34	1.389(4)
C15	C16	1.375(4)	C34	C35	1.373(4)
C16	C17	1.381(4)	C35	C36	1.377(4)
C17	C18	1.379(4)	C36	C37	1.383(4)

Table 5 Bond Angles for (**3c**).

Atom	Atom	Atom	Angle/°	Atom	Atom	Atom	Angle/°
C2	O2	C3	118.4(2)	C21	O7	C22	116.7(2)
C9	O3	C12	107.12(19)	C28	O8	C31	106.89(19)
C19	O5	C16	121.5(3)	C38	O10	C35	115.9(2)
C9	N1	N2	104.8(2)	C28	N3	N4	104.1(2)

N1	N2	C12	110.60(19)	N3	N4	C31	110.8(2)
C10	N2	N1	121.0(2)	C29	N4	N3	121.4(2)
C10	N2	C12	122.3(2)	C29	N4	C31	121.0(2)
O1	C2	O2	123.1(3)	O6	C21	O7	122.5(3)
O1	C2	C1	126.6(3)	O6	C21	C20	127.2(3)
O2	C2	C1	110.3(2)	O7	C21	C20	110.2(2)
C4	C3	O2	117.4(2)	C23	C22	O7	116.9(2)
C4	C3	C8	121.0(3)	C23	C22	C27	121.6(3)
C8	C3	O2	121.4(2)	C27	C22	O7	121.4(2)
C3	C4	C5	119.9(3)	C22	C23	C24	119.7(3)
C6	C5	C4	120.0(3)	C23	C24	C25	120.1(3)
C7	C6	C5	119.9(3)	C26	C25	C24	120.1(3)
C6	C7	C8	121.3(3)	C25	C26	C27	120.8(3)
C3	C8	C7	117.9(3)	C22	C27	C26	117.8(3)
C3	C8	C9	122.9(2)	C22	C27	C28	123.4(2)
C7	C8	C9	119.2(2)	C26	C27	C28	118.8(3)
O3	C9	C8	115.8(2)	O8	C28	C27	115.5(2)
N1	C9	O3	116.2(2)	N3	C28	O8	116.8(2)
N1	C9	C8	128.0(3)	N3	C28	C27	127.7(3)
O4	C10	N2	118.7(3)	O9	C29	N4	117.9(3)
O4	C10	C11	124.8(3)	O9	C29	C30	124.7(3)
N2	C10	C11	116.5(2)	N4	C29	C30	117.4(3)
O3	C12	N2	100.95(19)	O8	C31	N4	101.0(2)
O3	C12	C13	111.1(2)	O8	C31	C32	110.1(2)
N2	C12	C13	114.0(2)	N4	C31	C32	114.6(2)
C14	C13	C12	119.4(2)	C33	C32	C31	119.3(2)
C14	C13	C18	119.0(3)	C37	C32	C31	120.8(2)
C18	C13	C12	121.6(2)	C37	C32	C33	119.9(3)
C13	C14	C15	121.3(3)	C34	C33	C32	120.1(3)
C16	C15	C14	118.5(3)	C35	C34	C33	118.6(3)
C15	C16	O5	124.7(3)	C34	C35	O10	119.8(3)
C15	C16	C17	121.4(3)	C34	C35	C36	122.6(3)
C17	C16	O5	114.0(3)	C36	C35	O10	117.6(3)
C18	C17	C16	119.0(3)	C35	C36	C37	118.5(3)
C17	C18	C13	120.8(3)	C36	C37	C32	120.4(3)
F1	C19	F2	107.6(3)	F4	C38	F5	107.9(2)
F1	C19	F3	108.2(3)	F4	C38	F6	108.4(2)
F1	C19	O5	113.8(3)	F4	C38	O10	107.8(2)
F3	C19	F2	107.6(3)	F5	C38	O10	112.5(2)
F3	C19	O5	108.0(3)	F6	C38	F5	106.4(2)
O5	C19	F2	111.5(3)	F6	C38	O10	113.6(3)

Table 6 Torsion Angles for (**3c**).

A	B	C	D	Angle/°	A	B	C	D	Angle/°
O2	C3	C4	C5	-174.9(2)	O7	C22	C23	C24	-177.8(2)
O2	C3	C8	C7	175.1(2)	O7	C22	C27	C26	177.0(2)
O2	C3	C8	C9	-3.2(4)	O7	C22	C27	C28	-4.3(4)
O3	C12	C13	C14	143.8(2)	O8	C31	C32	C33	136.3(2)
O3	C12	C13	C18	-37.7(3)	O8	C31	C32	C37	-44.8(3)
O5	C16	C17	C18	178.0(3)	O10	C35	C36	C37	-177.8(2)
N1	N2	C10	O4	-162.7(2)	N3	N4	C29	O9	-162.5(2)
N1	N2	C10	C11	18.9(4)	N3	N4	C29	C30	18.3(4)
N1	N2	C12	O3	-5.3(3)	N3	N4	C31	O8	-6.3(3)
N1	N2	C12	C13	-124.5(2)	N3	N4	C31	C32	-124.5(2)
N2	N1	C9	O3	1.2(3)	N4	N3	C28	O8	0.7(3)
N2	N1	C9	C8	-178.4(3)	N4	N3	C28	C27	-177.1(3)
N2	C12	C13	C14	-102.9(3)	N4	C31	C32	C33	-110.7(3)
N2	C12	C13	C18	75.5(3)	N4	C31	C32	C37	68.2(3)
C2	O2	C3	C4	-102.8(3)	C21	O7	C22	C23	-101.9(3)
C2	O2	C3	C8	82.2(3)	C21	O7	C22	C27	80.9(3)
C3	O2	C2	O1	0.9(4)	C22	O7	C21	O6	1.3(4)
C3	O2	C2	C1	-179.4(2)	C22	O7	C21	C20	-178.9(2)
C3	C4	C5	C6	-0.6(4)	C22	C23	C24	C25	0.3(4)
C3	C8	C9	O3	175.1(2)	C22	C27	C28	O8	178.1(2)
C3	C8	C9	N1	-5.2(4)	C22	C27	C28	N3	-4.0(4)
C4	C3	C8	C7	0.3(4)	C23	C22	C27	C26	-0.2(4)
C4	C3	C8	C9	-178.1(3)	C23	C22	C27	C28	178.5(3)
C4	C5	C6	C7	0.8(4)	C23	C24	C25	C26	0.7(4)
C5	C6	C7	C8	-0.5(4)	C24	C25	C26	C27	-1.5(4)
C6	C7	C8	C3	-0.1(4)	C25	C26	C27	C22	1.2(4)
C6	C7	C8	C9	178.3(2)	C25	C26	C27	C28	-177.6(3)
C7	C8	C9	O3	-3.1(4)	C26	C27	C28	O8	-3.2(4)
C7	C8	C9	N1	176.5(3)	C26	C27	C28	N3	174.7(3)
C9	O3	C12	N2	5.7(3)	C28	O8	C31	N4	6.3(3)
C9	O3	C12	C13	126.9(2)	C28	O8	C31	C32	127.8(2)
C9	N1	N2	C10	155.9(2)	C28	N3	N4	C29	155.2(2)
C9	N1	N2	C12	2.8(3)	C28	N3	N4	C31	3.7(3)
C10	N2	C12	O3	-158.0(2)	C29	N4	C31	O8	-157.9(2)
C10	N2	C12	C13	82.9(3)	C29	N4	C31	C32	83.9(3)
C12	O3	C9	N1	-4.8(3)	C31	O8	C28	N3	-4.9(3)
C12	O3	C9	C8	174.9(2)	C31	O8	C28	C27	173.2(2)
C12	N2	C10	O4	-12.8(4)	C31	N4	C29	O9	-13.9(4)
C12	N2	C10	C11	168.8(2)	C31	N4	C29	C30	166.9(2)
C12	C13	C14	C15	177.3(3)	C31	C32	C33	C34	179.3(2)

Table 7 Hydrogen Atom Coordinates ($\text{Å}\times10^4$) and Isotropic Displacement Parameters ($\text{Å}^2\times10^3$) for (**3c**).

Atom	x	y	z	U(eq)
H1A	6978	9751	2604	35
H1B	7675	11750	2734	35
H1C	7479	9572	2978	35
H4	9703	10187	2329	23
H5	10607	8212	2047	26
H6	10230	4537	1739	25
H7	8948	2902	1702	21
H11A	5361	4690	2503	31
H11B	5829	6701	2319	31
H11C	6316	4924	2606	31
H12	6824	-122	1880	19
H14	5689	-1803	1523	24
H15	4805	-2057	1009	30
H17	5829	4190	702	30
H18	6666	4509	1225	27
H20A	681	10666	1037	38
H20B	1043	12383	1353	38
H20C	382	10283	1381	38
H23	3378	10024	1762	25
H24	4523	7518	1903	30
H25	4668	3924	1588	29
H26	3687	2886	1127	24
H30A	-643	5893	463	34
H30B	65	7880	458	34
H30C	37	6294	790	34
H31	1533	659	549	22
H33	1315	-1201	18	22
H34	1602	-1610	-519	24
H36	2926	4797	-377	26
H37	2653	5174	161	25

Appendix C .2: X-ray Crystallographic Data of **3h**

Table 1: Crystal data and structure refinement for (**3h**)

Identification code	3h
Empirical formula	$C_{20}H_{18}N_2O_6$
Fomula weight	382.36
Temperature/K	296(2)
Crystal system	orthorhombic
Space group	$P2_12_12_1$
a/Å	9.011(12)
b/Å	11.244(15)
c/Å	18.96(2)
α/°	90.00
β/°	90.00
γ/°	90.00
Volume/Å^3	1921(4)
Z	4
ρ_{calc} mg/mm^3	1.322
m/mm^{-1}	0.099
F(000)	800.0
Crystal size/mm^3	0.38 × 0.34 × 0.09
2Θ range for data collection	4.22 to 54°
Index ranges	-11 = h = 10, -14 = k = 14, -24 = l = 23
Reflections collected	9491
Independent reflections	4112[R(int) = 0.0395]
Data/restraints/parameters	4112/0/256
Goodness of-fit on F^2	0.946
Final R indexes [I>=2σ (I)]	R_1 = 0.0453, wR_2 = 0.0952
Final R indexes [all data]	R_1 = 0.1055, wR_2 = 0.1198
Largest diff. peak/hole / e Å^{-3}	0.12/-0.14

Table 2 Fractional Atomic Coordinates (×10^4) and Equivalent Isotropic Displacement Parameters (Å^2×10^3) for (**3h**). U_{eq} is defined as 1/3 of of the trace of the orthogonalised U_{IJ} tensor.

Atom	x	y	z	U(eq)
O1	10816(3)	5136(2)	2501.1(12)	93.0(8)
O2	10018(2)	6426.5(15)	1687.6(10)	64.5(5)
O3	5918(2)	4666.4(17)	2089.0(9)	66.5(6)
O4	4666(3)	6897.1(18)	3692.6(11)	79.1(7)
O5	4652(3)	1805.6(19)	4930.0(11)	79.8(7)
O6	5925(3)	393(2)	4390.1(17)	110.2(10)
N1	7398(3)	6157.8(19)	2433.6(12)	58.7(6)

N2	6162(3)	6129(2)	2882.9(12)	63.6(6)
C1	11089(5)	7226(3)	2713.7(19)	95.9(12)
C2	10651(3)	6145(3)	2315.4(17)	66.2(8)
C3	9506(3)	5481(2)	1267.7(14)	55.6(7)
C4	10363(4)	5148(3)	702.7(16)	70.0(9)
C5	9879(4)	4264(3)	256.0(17)	78.9(10)
C6	8534(4)	3729(3)	378.4(16)	72.4(9)
C7	7658(3)	4064(2)	945.5(14)	61.7(8)
C8	8128(3)	4962(2)	1400.5(13)	49.3(6)
C9	7189(3)	5310(2)	1995.3(14)	51.4(7)
C10	5163(3)	5142(3)	2701.3(14)	61.8(8)
C11	5845(4)	6968(2)	3376.2(16)	63.7(8)
C12	7019(4)	7890(3)	3498.0(17)	80.4(10)
C13	5035(3)	4232(2)	3278.8(15)	57.3(7)
C14	3681(3)	3782(3)	3478.6(15)	61.6(8)
C15	3573(4)	2946(3)	4013.1(15)	64.0(8)
C16	4825(4)	2575(2)	4345.3(15)	61.7(8)
C17	6204(4)	2999(3)	4157.5(17)	76.0(9)
C18	6300(4)	3827(3)	3616.2(16)	71.7(9)
C19	5281(4)	727(3)	4900(2)	77.5(10)
C20	5029(5)	32(3)	5558(2)	110.6(13)

Table 3 Anisotropic Displacement Parameters ($\text{Å}^2\times10^3$) for (**3h**). The Anisotropic displacement factor exponent takes the form: $-2\pi^2[h^2a^{*2}U_{11}+...+2hka\times b\times U_{12}]$

Atom	U_{11}	U_{22}	U_{33}	U_{23}	U_{13}	U_{12}
O1	113(2)	68.3(15)	97.6(17)	-0.8(13)	-43.6(16)	14.5(13)
O2	69.6(13)	56.8(12)	67.1(12)	2.7(9)	-2.5(12)	-7(1)
O3	65.4(14)	75.9(13)	58.1(12)	-11(1)	6.3(11)	-13.1(11)
O4	84.6(17)	78.6(15)	74.0(14)	3.7(11)	18.8(14)	21.0(12)
O5	92.0(17)	70.8(15)	76.8(14)	2.8(11)	19.2(14)	13.0(13)
O6	110(2)	80.6(17)	140(2)	-17.2(17)	33(2)	13.8(15)
N1	66.3(17)	49.7(13)	60.2(15)	-2.3(12)	3.6(14)	0.4(11)
N2	66.1(16)	56.5(14)	68.2(15)	-10.6(12)	17.1(15)	-3.1(12)
C1	98(3)	76(2)	113(3)	-26(2)	-26(3)	-14(2)
C2	61(2)	65(2)	73(2)	-1.7(16)	-13.9(18)	1.4(15)
C3	64(2)	50.9(16)	51.6(16)	2.4(13)	1.8(16)	1.0(14)
C4	63(2)	81(2)	65.6(19)	6.2(17)	8.8(18)	0.3(17)
C5	80(3)	94(3)	63(2)	-9.6(18)	11(2)	14(2)
C6	89(3)	74(2)	54.4(19)	-10.8(15)	-10(2)	8.9(19)
C7	68(2)	62.0(19)	55.3(18)	-1.2(14)	-7.9(17)	-0.2(15)
C8	54.9(17)	48.1(15)	45.0(14)	4.0(12)	-2.5(14)	2.9(13)
C9	54.2(19)	46.4(16)	53.6(16)	3.6(13)	-4.2(15)	-1.1(13)

Table 4 Bond Lengths for (**3h**).

Atom	Atom	Length/Å	Atom	Atom	Length/Å
O1	C2	1.198(4)	C3	C8	1.395(4)
O2	C2	1.357(4)	C4	C5	1.377(4)
O2	C3	1.406(3)	C5	C6	1.372(5)
O3	C9	1.367(4)	C6	C7	1.387(4)
O3	C10	1.448(3)	C7	C8	1.394(4)
O4	C11	1.223(4)	C8	C9	1.463(4)
O5	C16	1.415(4)	C10	C13	1.503(4)
O5	C19	1.340(4)	C11	C12	1.499(5)
O6	C19	1.188(4)	C13	C14	1.374(4)
N1	N2	1.403(3)	C13	C18	1.384(4)
N1	C9	1.279(3)	C14	C15	1.386(4)
N2	C10	1.470(4)	C15	C16	1.357(4)
N2	C11	1.359(4)	C16	C17	1.378(5)
C1	C2	1.484(4)	C17	C18	1.388(4)
C3	C4	1.373(4)	C19	C20	1.490(5)

Table 5 Bond Angles for (**3h**).

Atom	Atom	Atom	Angle/°	Atom	Atom	Atom	Angle/°
C2	O2	C3	117.3(2)	N1	C9	O3	115.7(2)
C9	O3	C10	107.6(2)	N1	C9	C8	128.0(3)
C19	O5	C16	118.2(3)	O3	C10	N2	100.3(2)
C9	N1	N2	105.1(2)	O3	C10	C13	111.7(2)
N1	N2	C10	111.2(2)	N2	C10	C13	113.0(2)
C11	N2	N1	124.7(3)	O4	C11	N2	118.4(3)
C11	N2	C10	123.8(3)	O4	C11	C12	125.6(3)
O1	C2	O2	122.1(3)	N2	C11	C12	116.0(3)
O1	C2	C1	126.4(3)	C14	C13	C10	121.3(3)
O2	C2	C1	111.6(3)	C14	C13	C18	118.8(3)
C4	C3	O2	117.6(3)	C18	C13	C10	119.8(3)
C4	C3	C8	121.8(3)	C13	C14	C15	120.9(3)
C8	C3	O2	120.4(2)	C16	C15	C14	119.3(3)
C3	C4	C5	119.9(3)	C15	C16	O5	117.4(3)
C6	C5	C4	119.5(3)	C15	C16	C17	121.6(3)
C5	C6	C7	121.0(3)	C17	C16	O5	120.9(3)
C6	C7	C8	120.2(3)	C16	C17	C18	118.6(3)
C3	C8	C9	122.8(2)	C13	C18	C17	120.7(3)
C7	C8	C3	117.5(3)	O5	C19	C20	112.0(3)
C7	C8	C9	119.7(3)	O6	C19	O5	121.9(3)
O3	C9	C8	116.3(2)	O6	C19	C20	126.2(3)

Table 6 Hydrogen Atom Coordinates ($Å×10^4$) and Isotropic Displacement Parameters ($Å^2×10^3$) for (**3h**).

Atom	x	y	z	U(eq)
H1A	11620	6998	3131	144
H1B	10217	7665	2844	144
H1C	11714	7715	2424	144
H4	11269	5519	622	84
H5	10459	4031	-125	95
H6	8206	3133	76	87
H7	6753	3689	1023	74
H10	4181	5444	2571	74
H12A	6620	8521	3781	121
H12B	7342	8204	3053	121
H12C	7846	7535	3738	121
H14	2826	4042	3252	74
H15	2653	2642	4143	77
H17	7053	2735	4388	91
H18	7224	4112	3479	86
H20A	4015	-229	5575	166
H20B	5234	525	5960	166
H20C	5675	-647	5563	166

Table 1: Crystal data and structure refinement for (**4a**)

Identification code	FileName()
Empirical formula	$C_{18}H_{15}ClN_2O_4$
Formula weight	358.77
Temperature/K	100(2)
Crystal system	triclinic
Space group	P-1
a/Å	7.7019(3)
b/Å	10.2692(4)
c/Å	11.0947(4)
$\alpha/°$	101.965(2)
$\beta/°$	98.272(2)
$\gamma/°$	105.260(2)
Volume/Å^3	809.66(5)
Z	2
ρ_{calc} mg/mm^3	1.472
m/mm^{-1}	0.263
F(000)	372.0
2Θ range for data collection	4.26 to 51°
Index ranges	-9 = h = 9, -12 = k = 12, -13 = l = 13
Reflections collected	5061
Independent reflections	2968[R(int) = 0.0157]
Data/restraints/parameters	2968/0/228
Goodness-of-fit on F^2	1.061
Final R indexes [I>=2σ (I)]	R$_1$ = 0.0318, wR$_2$ = 0.0796
Final R indexes [all data]	R$_1$ = 0.0352, wR$_2$ = 0.0821
Largest diff.peak/hole / e Å^3	0.24/-0.24

Table 2 Fractional Atomic Coordinates (×10^4) and Equivalent Isotropic Displacement Parameters (Å^2×10^3) for (**4a**). U$_{eq}$ is defined as 1/3 of of the trace of the orthogonalised U$_{IJ}$ tensor.

Atom	x	y	z	U(eq)
Cl1	14779.4(5)	7152.8(4)	8809.7(4)	25.63(13)
O1	10988.7(14)	280.9(10)	7664(1)	15.9(2)
O2	6827.7(16)	-389.3(12)	4794.4(10)	24.3(3)
O3	7698.9(16)	3247.3(11)	7347.4(10)	21.5(3)
O4	7560.2(14)	320.1(11)	9687.4(10)	19.7(2)
N1	7984.0(17)	1071.7(12)	6776.8(11)	14.1(3)
N2	8453.7(16)	1064.8(13)	8037.4(11)	13.6(3)

C1	9784(2)	-1054.0(15)	7233.9(13)	14.8(3)
C2	10285(2)	-2142.3(16)	7599.6(14)	17.2(3)
C3	9164(2)	-3505.7(16)	7074.6(15)	20.0(3)
C4	7565(2)	-3786.1(16)	6182.3(15)	21.0(3)
C5	7074(2)	-2704.4(16)	5809.6(14)	19.3(3)
C6	8162(2)	-1326.0(15)	6344.4(13)	15.2(3)
C7	7604(2)	-208.7(15)	5870.4(14)	16.4(3)
C8	7853(2)	2350.0(15)	6517.0(14)	16.3(3)
C9	8026(2)	2515.7(17)	5227.9(15)	22.6(3)
C10	7109(2)	556.1(14)	8679.1(13)	14.5(3)
C11	5161(2)	375.6(16)	8081.0(14)	18.5(3)
C12	10396(2)	1260.9(15)	8499.2(14)	14.6(3)
C13	11556.3(19)	2713.3(15)	8550.4(14)	14.7(3)
C14	11610(2)	3799.0(16)	9558.3(14)	19.4(3)
C15	12584(2)	5163.9(16)	9643.7(15)	20.8(3)
C16	13516(2)	5438.6(15)	8703.2(15)	18.3(3)
C17	13495(2)	4377.6(16)	7698.9(15)	21.5(3)
C18	12509(2)	3009.9(16)	7622.6(14)	18.5(3)

Table 3 Anisotropic Displacement Parameters ($\mathrm{\AA}^2 \times 10^3$) for (**4a**). The Anisotropic displacement factor exponent takes the form: $-2\pi^2[h^2a^{*2}U_{11}+...+2hka \times b \times U_{12}]$

Atom	U_{11}	U_{22}	U_{33}	U_{23}	U_{13}	U_{12}
Cl1	24.3(2)	13.5(2)	36.0(2)	5.58(16)	4.68(17)	2.08(15)
O1	14.6(5)	12.7(5)	20.2(5)	2.5(4)	5.5(4)	4.2(4)
O2	33.7(7)	23.7(6)	14.6(6)	1.6(5)	-0.9(5)	12.8(5)
O3	29.6(6)	17.5(6)	20.5(6)	4.9(5)	10.3(5)	9.8(5)
O4	18.5(6)	25.9(6)	15.6(5)	8.7(4)	4.4(4)	5.2(5)
N1	16.7(6)	15.3(6)	11.3(6)	3.9(5)	3.1(5)	6.3(5)
N2	12.8(6)	17.0(6)	11.3(6)	4.2(5)	2.7(5)	4.4(5)
C1	15.0(7)	14.6(7)	14.9(7)	2.9(6)	6.6(6)	3.7(6)
C2	18.5(7)	20.2(8)	15.6(7)	5.9(6)	5.6(6)	8.3(6)
C3	26.2(8)	16.9(8)	21.1(8)	6.9(6)	9.6(7)	9.6(6)
C4	21.9(8)	14.4(7)	24.1(8)	1.7(6)	7.1(7)	2.6(6)
C5	17.7(8)	19.4(8)	18.4(8)	0.4(6)	3.5(6)	5.3(6)
C6	16.9(7)	15.7(7)	14.5(7)	2.7(6)	6.4(6)	6.3(6)
C7	15.9(7)	17.9(8)	15.1(8)	2.8(6)	4.8(6)	5.1(6)
C8	14.5(7)	17.5(8)	18.5(8)	6.1(6)	4.1(6)	5.8(6)
C9	32.7(9)	21.4(8)	19.9(8)	9.3(6)	9.7(7)	13.3(7)
C10	17.5(7)	11.2(7)	14.3(7)	1.3(5)	4.9(6)	4.2(6)
C11	14.8(7)	22.1(8)	18.8(8)	6.3(6)	4.1(6)	5.0(6)
C12	14.1(7)	16.5(7)	13.5(7)	3.2(6)	3.3(6)	5.7(6)

C13	11.7(7)	15.7(7)	15.8(7)	3.5(6)	0.7(6)	4.1(6)
C14	19.1(8)	22.2(8)	16.5(8)	3.0(6)	6.3(6)	5.3(6)
C15	21.7(8)	17.5(8)	19.9(8)	-1.1(6)	2.6(6)	5.9(6)
C16	15.3(7)	13.4(7)	24.2(8)	3.9(6)	0.9(6)	3.3(6)
C17	22.8(8)	20.8(8)	21.8(8)	6.3(6)	9.5(7)	4.9(7)
C18	20.0(8)	17.0(8)	17.6(8)	1.7(6)	5.6(6)	5.5(6)

Table 4 Bond Lengths for (**4a**).

Atom	Atom	Length/Å	Atom	Atom	Length/Å
Cl1	C16	1.7431(15)	C3	C4	1.387(2)
O1	C1	1.3783(17)	C4	C5	1.383(2)
O1	C12	1.4343(17)	C5	C6	1.394(2)
O2	C7	1.2088(18)	C6	C7	1.491(2)
O3	C8	1.2038(18)	C8	C9	1.495(2)
O4	C10	1.2148(18)	C10	C11	1.497(2)
N1	N2	1.3953(16)	C12	C13	1.508(2)
N1	C7	1.4108(19)	C13	C14	1.393(2)
N1	C8	1.4264(19)	C13	C18	1.386(2)
N2	C10	1.3908(19)	C14	C15	1.381(2)
N2	C12	1.4555(18)	C15	C16	1.384(2)
C1	C2	1.390(2)	C16	C17	1.382(2)
C1	C6	1.400(2)	C17	C18	1.388(2)
C2	C3	1.388(2)			

Table 5 Bond Angles for (**4a**).

Atom	Atom	Atom	Angle/°	Atom	Atom	Atom	Angle/°
C1	O1	C12	115.85(11)	O3	C8	N1	119.07(13)
N2	N1	C7	116.80(11)	O3	C8	C9	123.94(14)
N2	N1	C8	117.53(11)	N1	C8	C9	116.90(13)
C7	N1	C8	125.62(12)	O4	C10	N2	119.53(13)
N1	N2	C12	114.89(11)	O4	C10	C11	123.86(13)
C10	N2	N1	120.90(11)	N2	C10	C11	116.58(12)
C10	N2	C12	122.25(12)	O1	C12	N2	109.27(11)
O1	C1	C2	119.12(13)	O1	C12	C13	108.16(11)
O1	C1	C6	120.12(13)	N2	C12	C13	111.18(12)
C2	C1	C6	120.46(14)	C14	C13	C12	117.86(13)
C3	C2	C1	119.47(14)	C18	C13	C12	122.82(13)
C4	C3	C2	120.45(14)	C18	C13	C14	119.28(14)
C5	C4	C3	120.10(14)	C15	C14	C13	121.19(14)
C4	C5	C6	120.31(14)	C14	C15	C16	118.61(14)
C1	C6	C7	122.79(13)	C15	C16	Cl1	119.14(12)

C5 C6 C1	119.18(14)	C17 C16 Cl1	119.58(12)
C5 C6 C7	117.89(13)	C17 C16 C15	121.26(14)
O2 C7 N1	121.75(14)	C16 C17 C18	119.59(14)
O2 C7 C6	122.80(13)	C13 C18 C17	120.06(14)
N1 C7 C6	115.41(12)		

Table 6 Hydrogen Atom Coordinates ($\text{Å}\times10^4$) and Isotropic Displacement Parameters ($\text{Å}^2\times10^3$) for (**4a**).

Atom	*x*	*y*	*z*	U(eq)
H2	11386	-1954	8204	21
H3	9494	-4252	7328	24
H4	6805	-4722	5827	25
H5	5991	-2902	5186	23
H9A	6822	2092	4651	34
H9B	8903	2053	4928	34
H9C	8468	3511	5260	34
H11A	4743	-424	7339	28
H11B	5093	1222	7825	28
H11C	4373	211	8687	28
H12	10576	1100	9361	18
H14	10966	3597	10199	23
H15	12613	5899	10334	25
H17	14151	4583	7065	26
H18	12488	2277	6934	22

Table 1: Crystal data and structure refinement for (**4d**)

Identification code	**4d**
Empirical formula	$C_{19}H_{18}N_2O_4S$
Formula weight	370.41
Temperature/K	296(2)
Crystal system	triclinic
Space group	P-1
a/Å	7.9736(6)
b/Å	10.3607(8)
c/Å	11.3712(9)
$\alpha/°$	92.451(2)
$\beta/°$	97.2450(10)
$\gamma/°$	103.7230(10)
Volume/Å³	902.72(12)
Z	2
ρ_{calc} mg/mm³	1.363
m/mm⁻¹	0.206
F(000)	388.0
Crystal size/mm³	0.46 × 0.27 × 0.22
2Θ range for data collection	4.06 to 50.48°
Index ranges	-9 = h = 9, -12 = k = 12, -13 = l = 13
Reflections collected	4704
Independent reflections	3184[R(int) = 0.0117]
Data/restraints/parameters	3184/0/238
Goodness-of-fit on F^2	1.018
Final R indexes [I>=2σ (I)]	$R_1 = 0.0373$, w$R_2 = 0.1040$
Final R indexes [all data]	$R_1 = 0.0419$, w$R_2 = 0.1094$
Largest diff. peak/hole / e Å⁻³	0.18/-0.28

Table 2 Fractional Atomic Coordinates (×10⁴) and Equivalent Isotropic Displacement Parameters (Å²×10³) for (**4d**). U_{eq} is defined as 1/3 of of the trace of the orthogonalised U_{IJ} tensor.

Atom	x	y	z	U(eq)
S1	755.1(7)	-1348.0(5)	6494.5(5)	66.19(18)
O1	8251(2)	5504.4(14)	10185.1(11)	71.2(4)
O2	4368.9(14)	5178.8(11)	7566.1(10)	48.7(3)
O3	7709.9(15)	4961.4(14)	5435.2(10)	59.0(3)
O4	7575.0(19)	2243.5(12)	7940.7(12)	63.4(4)
N1	7249.7(16)	4309.9(12)	8396.4(10)	38.3(3)
N2	6849.4(15)	4474.8(12)	7191.1(10)	37.3(3)
C1	7538(2)	5450.5(17)	9178.3(13)	45.8(4)

Atom				
C2	6959(2)	6599.7(16)	8667.6(14)	44.7(4)
C3	7926(3)	7881.7(18)	9053.5(18)	59.8(5)
C4	7399(3)	8972.2(19)	8619(2)	70.2(6)
C5	5899(3)	8795(2)	7830(2)	69.5(6)
C6	4907(3)	7528.6(19)	7455.3(17)	57.6(5)
C7	5440(2)	6437.9(16)	7871.0(14)	44.2(4)
C8	5010.8(19)	4361.7(16)	6776.6(13)	41.9(3)
C9	3924.0(19)	2956.8(16)	6722.9(13)	43.4(4)
C10	3007(2)	2453.8(18)	7624.7(15)	51.4(4)
C11	2087(2)	1135.0(19)	7532.8(16)	56.7(4)
C12	2050(2)	291.9(17)	6542.0(15)	49.1(4)
C13	2980(2)	799.8(19)	5644.5(16)	57.3(4)
C14	3895(2)	2114.9(19)	5740.1(15)	55.9(4)
C15	883(3)	-2057(2)	5064(2)	72.3(6)
C16	8126.4(19)	4824.0(15)	6477.6(12)	39.1(3)
C17	9976(2)	5013.2(18)	7037.4(15)	50.0(4)
C18	7397(2)	3008.1(16)	8701.6(14)	46.2(4)
C19	7217(3)	2680(2)	9948.3(17)	69.3(6)

Table 3 Anisotropic Displacement Parameters ($\text{Å}^2 \times 10^3$) for (**4d**).
The Anisotropic displacement factor exponent takes the form: -
$2\pi^2[h^2a^{*2}U_{11}+...+2hka \times b \times U_{12}]$

Atom	U_{11}	U_{22}	U_{33}	U_{23}	U_{13}	U_{12}
S1	64.5(3)	54.0(3)	75.8(4)	-1.4(2)	8.7(2)	7.8(2)
O1	104.0(11)	78.9(9)	37.5(7)	-6.7(6)	-9.2(7)	47.7(8)
O2	40.0(6)	54.3(7)	56.2(7)	2.5(5)	13.6(5)	17.1(5)
O3	49.1(7)	96.3(10)	35.2(6)	14.2(6)	10.1(5)	21.0(6)
O4	89.1(10)	45.4(7)	64.0(8)	4.9(6)	22.8(7)	26.5(6)
N1	45.5(7)	45.0(7)	29.5(6)	5.7(5)	7.4(5)	19.4(5)
N2	36.9(6)	48.3(7)	28.9(6)	4.7(5)	5.5(5)	14.2(5)
C1	53.2(9)	53.6(9)	36.3(8)	1.0(7)	7.4(7)	23.7(7)
C2	51.5(9)	47.6(9)	41.5(8)	2.3(7)	12.4(7)	21.9(7)
C3	60.6(11)	55.2(10)	65.4(11)	-8.2(8)	9.1(9)	20.1(8)
C4	79.0(14)	44.9(10)	93.0(15)	2.3(9)	27.6(12)	20.1(9)
C5	86.0(15)	53.5(11)	85.8(14)	22.8(10)	32.9(12)	36.3(11)
C6	60.2(11)	66.8(12)	59.7(10)	17.5(9)	17.5(8)	35.8(9)
C7	46.8(9)	47.6(9)	45.8(8)	7.7(7)	17.0(7)	20.2(7)
C8	37.8(8)	54.5(9)	35.8(7)	5.1(6)	5.7(6)	15.5(7)
C9	35.9(8)	55.5(9)	38.2(8)	1.5(7)	3.2(6)	11.5(7)
C10	51.6(9)	59.1(10)	41.4(9)	-4.0(7)	11.4(7)	8.2(8)
C11	58.0(11)	60.7(11)	49.6(10)	3.2(8)	17.3(8)	5.9(8)

Atom						
C12	41.9(8)	53.1(9)	52.3(9)	0.0(7)	1.5(7)	14.6(7)
C13	57(1)	63.5(11)	49.9(10)	-11.5(8)	9.3(8)	13.5(8)
C14	53.6(10)	68.6(11)	44.3(9)	-2.3(8)	15.3(8)	9.2(8)
C15	72.2(13)	57.7(11)	81.3(14)	-12.4(10)	-6.2(11)	16.9(10)
C16	41.9(8)	43.7(8)	33.5(7)	1.6(6)	8.2(6)	13.1(6)
C17	39.1(8)	65.2(10)	45.5(9)	4.9(7)	7.3(7)	11.3(7)
C18	48.1(9)	47.7(9)	47.8(9)	11.5(7)	11.5(7)	17.6(7)
C19	92.8(15)	71.3(13)	57.2(11)	29.5(10)	23(1)	35.4(11)

Table 4 Bond Lengths for (**4d**).

Atom	Atom	Length/Å	Atom	Atom	Length/Å
S1	C12	1.7610(18)	C2	C7	1.389(2)
S1	C15	1.781(2)	C3	C4	1.385(3)
O1	C1	1.205(2)	C4	C5	1.371(3)
O2	C7	1.3818(19)	C5	C6	1.379(3)
O2	C8	1.4287(18)	C6	C7	1.380(2)
O3	C16	1.2137(18)	C8	C9	1.501(2)
O4	C18	1.192(2)	C9	C10	1.383(2)
N1	N2	1.3946(16)	C9	C14	1.382(2)
N1	C1	1.403(2)	C10	C11	1.382(2)
N1	C18	1.4348(19)	C11	C12	1.389(2)
N2	C8	1.4576(19)	C12	C13	1.386(3)
N2	C16	1.3729(19)	C13	C14	1.377(3)
C1	C2	1.490(2)	C16	C17	1.495(2)
C2	C3	1.389(2)	C18	C19	1.489(2)

Table 5 Bond Angles for (**4d**).

Atom	Atom	Atom	Angle/°	Atom	Atom	Atom	Angle/°
C12	S1	C15	104.03(10)	C6	C7	C2	120.78(16)
C7	O2	C8	114.80(11)	O2	C8	N2	108.63(12)
N2	N1	C1	116.45(12)	O2	C8	C9	108.88(12)
N2	N1	C18	116.66(12)	N2	C8	C9	112.77(12)
C1	N1	C18	126.84(12)	C10	C9	C8	123.27(14)
N1	N2	C8	115.30(11)	C10	C9	C14	118.63(16)
C16	N2	N1	121.68(12)	C14	C9	C8	118.06(14)
C16	N2	C8	122.83(12)	C9	C10	C11	120.04(16)
O1	C1	N1	121.96(14)	C10	C11	C12	121.31(16)
O1	C1	C2	122.47(15)	C11	C12	S1	117.23(14)
N1	C1	C2	115.54(13)	C13	C12	S1	124.37(14)
C3	C2	C1	118.60(16)	C13	C12	C11	118.37(16)

C3 C2 C7	118.88(15)	C14 C13 C12	120.11(16)
C7 C2 C1	122.42(15)	C13 C14 C9	121.53(16)
C4 C3 C2	120.06(19)	O3 C16 N2	119.12(14)
C5 C4 C3	120.28(19)	O3 C16 C17	123.35(14)
C4 C5 C6	120.34(17)	N2 C16 C17	117.53(13)
C5 C6 C7	119.62(18)	O4 C18 N1	118.67(14)
O2 C7 C2	119.84(14)	O4 C18 C19	124.26(16)

Table 6 Hydrogen Atom Coordinates ($\text{Å}\times10^4$) and Isotropic Displacement Parameters ($\text{Å}^2\times10^3$) for (**4d**).

Atom	x	y	z	U(eq)
H3	8928	8008	9604	72
H4	8065	9829	8864	84
H5	5549	9532	7546	83
H6	3885	7411	6926	69
H8	4900	4687	5981	50
H10	3010	3004	8294	62
H11	1481	805	8147	68
H13	2986	252	4976	69
H14	4509	2444	5129	67
H15A	506	-1522	4464	108
H15B	147	-2944	4944	108
H15C	2066	-2086	5012	108
H17A	10720	5097	6429	75
H17B	10085	4258	7475	75
H17C	10312	5806	7567	75
H19A	6964	1731	9989	104
H19B	6284	3011	10204	104
H19C	8285	3087	10456	104

Table 1 Crystal data and structure refinement for (**4e**)

Identification code	**4e**
Empirical formula	$C_{20}H_{20}N_2O_4$
Formula weight	352.38
Temperature/K	296(2)
Crystal system	triclinic
Space group	P-1
a/Å	7.962(2)
b/Å	10.595(3)
c/Å	11.338(3)
$\alpha/°$	103.812(19)
$\beta/°$	98.84(2)
$\gamma/°$	101.12(2)
Volume/Å^3	891.1(5)
Z	2
ρ_{calc} mg/mm^3	1.313
m/mm^{-1}	0.092
F(000)	372.0
Crystal size/mm^3	$0.58 \times 0.48 \times 0.09$
2Θ range for data collection	3.78 to 54°
Index ranges	-10 = h = 9, -13 = k = 13, -14 = l = 14
Reflections collected	6908
Independent reflections	3795[R(int) = 0.0259]
Data/restraints/parameters	3795/0/238
Goodness-of-fit on F^2	1.060
Final R indexes [I>=2σ (I)]	$R_1 = 0.0513$, w$R_2 = 0.1606$
Final R indexes [all data]	$R_1 = 0.0702$, w$R_2 = 0.1756$
Largest diff. peak/hole / e Å^3	0.30/-0.25

Table 2 Fractional Atomic Coordinates (×10^4) and Equivalent Isotropic Displacement Parameters (Å^2×10^3) for (**4e**). U$_{eq}$ is defined as 1/3 of of the trace of the orthogonalised U$_{IJ}$ tensor.

Atom	x	y	z	U(eq)
O1	8294(2)	10579.0(15)	5216.6(11)	68.7(5)
O2	4262.6(16)	10002.1(13)	2430.6(11)	48.6(3)
O3	7500.0(18)	9531.2(17)	284.2(11)	64.0(4)
O4	7523(2)	7084.1(14)	2627.7(13)	67.8(4)
N1	7211.5(18)	9199.8(14)	3255.1(11)	39.3(4)
N2	6743.1(17)	9223.4(14)	2025.7(11)	38.9(3)
C1	7517(2)	10419.3(19)	4169.1(15)	45.1(4)
C2	6881(2)	11509.0(18)	3765.6(15)	45.3(4)
C3	7797(3)	12808(2)	4336(2)	63.9(6)
C4	7219(4)	13856(2)	4024(3)	81.1(7)

Atom				
C5	5707(4)	13599(2)	3151(2)	74.2(7)
C6	4747(3)	12319(2)	2591.8(19)	57.7(5)
C7	5322(2)	11266.7(18)	2896.0(15)	44.5(4)
C8	4879(2)	9068.9(18)	1571.3(14)	41.7(4)
C9	3823(2)	7693.2(19)	1427.7(15)	43.4(4)
C10	2923(3)	7366(2)	2297.1(17)	51.3(5)
C11	2039(3)	6055(2)	2124(2)	61.6(5)
C12	2021(3)	5044(2)	1097(2)	56.9(5)
C13	2926(3)	5387(2)	227(2)	64.5(6)
C14	3807(3)	6677(2)	385.3(18)	60.2(5)
C15	1018(3)	3603(2)	863(3)	78.4(7)
C16	173(5)	3294(3)	1859(4)	114.0(11)
C17	7977(2)	9475.9(18)	1334.7(14)	41.9(4)
C18	9846(2)	9649(2)	1918.9(18)	56.5(5)
C19	7360(2)	7943.7(19)	3458.2(16)	47.3(4)
C20	7204(4)	7785(2)	4714(2)	69.3(6)

Table 3 Anisotropic Displacement Parameters ($\text{Å}^2 \times 10^3$) for (**4e**). The Anisotropic displacement factor exponent takes the form: $-2\pi^2[h^2a^{*2}U_{11}+...+2hka \times b \times U_{12}]$

Atom	U_{11}	U_{22}	U_{33}	U_{23}	U_{13}	U_{12}
O1	96.2(12)	72.7(10)	34.7(6)	4.2(6)	-1.9(7)	40.0(9)
O2	39.3(7)	48.1(8)	59.1(7)	11.1(6)	13.9(5)	14.1(6)
O3	50.4(8)	106.0(12)	41.2(7)	30.0(7)	12.1(6)	17.8(8)
O4	90.7(12)	53.2(9)	62.8(9)	8.5(7)	19.9(8)	31.1(8)
N1	42.6(8)	48.2(9)	29.5(6)	9.9(6)	8.0(5)	16.8(7)
N2	35.8(8)	51.8(9)	28.3(6)	9.9(6)	4.8(5)	11.5(6)
C1	49.6(10)	52.9(11)	34.8(8)	9.4(7)	9.5(7)	20.2(9)
C2	48.9(11)	45.8(11)	41.0(8)	7.7(7)	10.5(7)	15.2(8)
C3	64.6(14)	51.1(13)	63.6(12)	1.1(10)	-0.5(10)	14(1)
C4	89.2(19)	46.3(13)	98.1(18)	10.7(12)	8.0(15)	14.1(13)
C5	93.3(18)	52.6(14)	85.8(15)	26.4(12)	16.6(14)	31.7(13)
C6	63.8(13)	58.4(13)	57.5(11)	20.0(9)	10.3(9)	26.8(11)
C7	46.5(11)	47.0(11)	43.9(8)	12.7(8)	13.8(7)	16.6(9)
C8	36.4(9)	53.4(11)	35.4(7)	11.5(7)	6.2(6)	13.1(8)
C9	34.8(9)	54.2(11)	38.2(8)	7.7(7)	5.1(6)	11.9(8)
C10	55.3(12)	51.9(11)	45.5(9)	9.3(8)	14.6(8)	12.6(9)
C11	65.3(14)	59.9(13)	62.8(11)	21(1)	20.8(10)	11.9(11)
C12	48.1(12)	49.9(12)	67.9(12)	10.4(10)	-0.1(9)	17.9(10)
C13	57.2(13)	59.4(14)	63.5(12)	-8.8(10)	10(1)	16.9(11)
C14	52.9(12)	69.0(15)	49.7(10)	-0.8(9)	17.2(9)	9.6(11)
C15	70.1(16)	52.8(14)	101.5(18)	16.2(13)	-7.8(13)	16.3(12)
C16	124(3)	73(2)	147(3)	50(2)	31(2)	1.6(18)

C17	39.3(9)	48(1)	36.5(8)	9.0(7)	8.9(7)	8.9(8)
C18	37.3(10)	78.6(14)	53.8(10)	20.3(10)	10.2(8)	11.7(10)
C19	47.5(11)	49.3(11)	47.3(9)	13.9(8)	9.1(8)	17.1(9)
C20	93.7(17)	67.6(15)	59.9(12)	32.9(11)	20.2(11)	28.1(13)

Table 4 Bond Lengths for (**4e**).

Atom	Atom	Length/Å	Atom	Atom	Length/Å
O1	C1	1.208(2)	C4	C5	1.372(4)
O2	C7	1.369(2)	C5	C6	1.366(3)
O2	C8	1.429(2)	C6	C7	1.380(3)
O3	C17	1.2121(19)	C8	C9	1.493(3)
O4	C19	1.186(2)	C9	C10	1.375(3)
N1	N2	1.3940(17)	C9	C14	1.392(3)
N1	C1	1.402(2)	C10	C11	1.384(3)
N1	C19	1.427(2)	C11	C12	1.378(3)
N2	C8	1.458(2)	C12	C13	1.383(3)
N2	C17	1.373(2)	C12	C15	1.520(3)
C1	C2	1.485(2)	C13	C14	1.367(3)
C2	C3	1.373(3)	C15	C16	1.470(4)
C2	C7	1.400(3)	C17	C18	1.491(2)
C3	C4	1.380(3)	C19	C20	1.493(3)

Table 5 Bond Angles for (**4e**).

Atom	Atom	Atom	Angle/°	Atom	Atom	Atom	Angle/°
C7	O2	C8	116.36(14)	O2	C8	N2	108.91(13)
N2	N1	C1	116.63(13)	O2	C8	C9	108.43(14)
N2	N1	C19	116.91(13)	N2	C8	C9	112.59(13)
C1	N1	C19	126.45(13)	C10	C9	C8	123.33(16)
N1	N2	C8	115.15(12)	C10	C9	C14	118.23(19)
C17	N2	N1	121.72(13)	C14	C9	C8	118.39(16)
C17	N2	C8	122.95(12)	C9	C10	C11	119.92(18)
O1	C1	N1	121.57(15)	C12	C11	C10	122.16(19)
O1	C1	C2	122.17(17)	C11	C12	C13	117.3(2)
N1	C1	C2	116.23(14)	C11	C12	C15	123.3(2)
C3	C2	C1	118.39(17)	C13	C12	C15	119.3(2)
C3	C2	C7	119.02(16)	C14	C13	C12	121.18(19)
C7	C2	C1	122.41(17)	C13	C14	C9	121.17(19)
C2	C3	C4	120.4(2)	C16	C15	C12	116.4(2)
C5	C4	C3	119.8(2)	O3	C17	N2	118.96(15)
C6	C5	C4	121.0(2)	O3	C17	C18	123.31(16)
C5	C6	C7	119.5(2)	N2	C17	C18	117.73(14)

| O2 C7 C6 | 118.95(17) | O4 C19 C20 | 124.21(18) |
| C6 C7 C2 | 120.25(19) | N1 C19 C20 | 116.42(16) |

Table 6 Hydrogen Atom Coordinates ($\text{Å}\times10^4$) and Isotropic Displacement Parameters ($\text{Å}^2\times10^3$) for (**4e**).

Atom	*x*	*y*	*z*	U(eq)
H3	8812	12982	4937	77
H4	7852	14733	4404	97
H5	5329	14308	2937	89
H6	3714	12158	2011	69
H8	4708	9264	765	50
H10	2908	8026	3001	62
H11	1436	5849	2721	74
H13	2936	4727	-479	77
H14	4405	6880	-214	72
H15A	122	3373	111	94
H15B	1819	3030	708	94
H16A	1042	3502	2609	171
H16B	-402	2359	1623	171
H16C	-674	3817	1995	171
H18A	10569	9817	1342	85
H18B	9994	8850	2137	85
H18C	10180	10393	2653	85
H20A	6870	6851	4664	104
H20B	6332	8219	5002	104
H20C	8310	8185	5282	104